# Technische Universität München

## Lehrstuhl für Entwicklungsgenetik

## Interrogating the *in vivo* significance of selenium-based catalysis of GPX4 for mammalian development and survival

### Irina Ingold

# Content

# Abbreviations

| | |
|---|---|
| °C | degree Celsius |
| α-Toc | α-Tocopherol |
| $\Delta\Psi_m$ | membrane potential |
| γGCS | γ-glutamyl-cysteine synthetase |
| µg | microgram |
| µl | microliter |
| µM | micromolar |
| µm | micrometer |
| AA | antimycin A |
| ACSL4 | acyl-CoA synthetase long chain family member 4 |
| ADP | adenosine diphosphate |
| Ala | alanine |
| Am | amnion |
| AMP | adenosine monophosphate |
| Amp | β-lactamase (ampicillin resistance) |
| ApoER2 | apolipoprotein E receptor 2 |
| ARF | acute renal failure |
| Asn | aspargine |
| ATP | adenosine triphosphate |
| a.u. | arbitrary units |
| bp | base pair |
| BS | pBluescript vector backbone |
| BSA | bovine serum albumin |
| BSO | L-buthionine sulfoximine |
| Cas | CRISPR associated |
| cDNA | complementary DNA |
| cGPX4 | cytosolic GPX4 |
| Ch | chorion |
| ChOOH | cholesterol hydroperoxide |
| Cre | Cre recombinase |
| CRISPR | clustered regularly interspaced short palindromic repeats |
| CypD | cyclophilin D |
| Cys | cysteine |
| DFO | deferoxamine |
| $dH_2O$ | distilled water |
| DAB | 3,3-diaminobenzidine |
| DIO | deiodinase |
| DMSO | dimethyl sulfoxide |

| | |
|---|---|
| DMT1 | divalent metal transporter 1 |
| DNA | deoxyribonucleic acid |
| dNTP | deoxynucleotides |
| Dox | doxycycline |
| DTNB | 5,5'-dithiobis (2-nitrobenzoicacid) |
| E | embryonic day |
| EC | ectoderm |
| EDTA | ethylendiaminetetraacetic acid |
| EFSec | Sec-specific elongation factor |
| EGFR | epidermal growth factor receptor |
| EGTA | ethyleneglycoltetraacetic acid |
| eIF4a3 | eukaryotic translation intiation factor 4a3 |
| EM | embryonic tissue |
| EN | endoderm |
| ER | endoplasmic reticulum |
| Erastin | eradicator of Ras and ST |
| ES cells | embryonic stem cells |
| ETC | electron transport chain |
| EX | extraembryonic tissue |
| F | filial generation |
| FAD | flavin adenine dinukleotide |
| Fer | ferrostatin-1 |
| FCCP | carbonyl cyanide-ρ-trifluoromethoxyphenylhydrazone |
| FCS | fetal calf serum |
| FIN | ferroptosis inducing agent |
| $Fe^{2+}$ | ferrous iron |
| $Fe^{3+}$ | ferric iron |
| flox | loxP flanked |
| Flpe | Flpe recombinase |
| FSH | FLAG-Strep-HA-tagged |
| fwd | forward |
| g | gravitational force/gram |
| GFAP | glial fibrillary acidic protein |
| GFP | green fluorescent protein |
| Gln | glutamine |
| Glu | glutamate |
| G/M | glutamate/malate |
| Gpx | glutathione peroxidase |
| GR | glutathione reductase |
| GS | glutathione synthase |
| GSH | reduced glutathione |

| | |
|---|---|
| GSSG | oxidized glutathione |
| h | hour |
| $H_2O_2$ | hydrogen peroxide |
| H&E | haematoxylin and eosin |
| HEK cells | human embryonic kidney cells |
| HCG | human chorionic gonadotropin |
| HCl | hydrochloric acid |
| HPRT | hypoxanthin-phosphoribosyl-transferase-1 |
| HRP | horseradish peroxidase |
| HTF | human tubal fluid |
| IbaI | ionized calcium-binding adapter molecule |
| i.p. | intraperitoneal |
| IRES | internal ribosomal entry site |
| IRI | ischemia/reperfusion injury |
| Kb | kilobase |
| KCl | potassium chloride |
| KCN | potassium cyanide |
| kDa | kilodalton |
| KEAP1 | kelch-like ECH-associated protein 1 |
| KO | knockout |
| L$^{\bullet}$ | lipid radical |
| LDH | lactate dehydrogenase |
| Liprox | liproxstatin-1 |
| LOO$^{\bullet}$ | lipid peroxyl radical |
| LOOH | lipid hydroperoxide |
| LOX | lipoxygenase |
| LPCAT3 | lysophosphatidylcholine acyltransferase 3 |
| M | molar |
| MCM | MerCreMer |
| ME | mesoderm |
| MEF | murine embryonic fibroblast |
| mGPX4 | mitochondrial GPX4 |
| mM | milimolar |
| mRNA | messenger RNA |
| ms | miliseconds |
| MSRB1 | methionine-R-sulfoxide reductase 1 |
| mt | mitochondrial |
| m/z | mass-to-charge ratio |
| NaCl | sodium chloride |
| NADPH | nicotinamide adenine dinucleotide phosphate |
| NAO | 10N-nonylacridine orange |

| | |
|---|---|
| NaOH | sodium hydroxide |
| NaSe | sodium selenite |
| NEM | N-Ethylmaleimide |
| neo | neomycin phosphotransferase resistance gene |
| ng | nanogram |
| nGPX4 | nuclear GPX4 |
| nm | nanometer |
| NMD | nonsense mRNA decay |
| NMDAR | glutamate-dependent N-methyl-D-aspartate receptor |
| NRF2 | nuclear factor (erythroid-derived 2)-like 2 |
| n.s. | not significant |
| OD | optical density |
| OH$^{\cdot}$ | hydroxyl radical |
| OCR | oxygen consumption rate |
| OMM | outer mitochondrial membrane rupture |
| P | postnatal day |
| PAO | phenylarsine oxide |
| PBS | phosphate buffered saline |
| PC | phosphatidylcholine |
| PCC | pump controlled cell rupture system |
| PCOOH | phosphatidylcholine hydroperoxide |
| PCR | polymerase chain reaction |
| PE | phosphatidylethanolamine |
| PFA | paraformaldehyde |
| PLOOH | phospholipid hydroperoxide |
| pmoles | picomolar |
| PMSG | pregnant mare serum gonadotropin |
| PPT | polypurine tract |
| PRE | post-transcriptional regulatory element |
| PRX | peroxiredoxin |
| PSTK | phosphoseryl-tRNA kinase |
| PTP1B | protein tyrosine phosphatase 1B |
| PUFA | polyunsaturated fatty acid |
| Puro | puromycin-acetyltransferase |
| PV | parvalbumin |
| qRT | quantitative real time |
| rev | reverse |
| Rh123 | Rhodamine 123 |
| RNA | ribonucleic acid |
| ROS | reactive oxygen species |
| Rot | rotenone |

| | |
|---|---|
| rpm | revolutions per minute |
| RSL3 | Ras selective lethal 3 |
| RSV | Rous sarcoma virus |
| SBP2 | SECIS binding protein 2 |
| SDS | sodium dodecyl sulfate |
| Se | selenium |
| Sec, (U) | selenocysteine |
| sec | seconds |
| SECIS | selenocysteine insertion sequence |
| SecS | selenocysteine synthase |
| SELENO | selenoportein |
| SEPHS2 | selenophosphate synthetase 2 |
| Ser | serine |
| SerS | seryl-tRNA synthetase |
| SFFV | spleen foci forming virus |
| sgRNA | single guide RNA |
| SIN | self-inactivating 3' LTR |
| SMCP | sperm mitochondria-associated cysteine-rich protein |
| SOD | superoxide dismutase |
| SSC | sidewards scatter |
| STEAP | six-transmembrane epithelial antigen of prostate 3 |
| $T_3$ | triiodothyronine |
| $T_4$ | thyroxine |
| TAM | 4-hydroxy tamoxifen |
| tBOOH | tertiary-butyl hydroperoxide |
| TCA | trichloroacetic acid |
| TFR1 | transferrin receptor 1 |
| TG | transgene |
| TGFβ1 | transforming growth factor β 1 |
| TK | thymidine kinase gene |
| $TNB^-$ | 2-nitro-5-thiobenzoate |
| TNFα | tumor necrosis factor α |
| Tris | trishydroxymethylaminomethan |
| tRNA | transfer-RNA |
| Trp | tryptophane |
| Txn | thioredoxin |
| Txnrd | thioredoxin reductase |
| TZN | thiaziolidinediones |
| U | units |
| UV | ultraviolet |
| V | voltage |

wt                                    wildtype

X

## Summary

Glutathione peroxidase 4 (GPX4), one of eight glutathione peroxidases in mammals, is expressed as a selenoprotein in mammals but exists as a cysteine-containing homolog in many other organisms. Yet, it has remained enigmatic why some organisms like mammals rely on the expression of selenoproteins, while others like plants and yeast express Cys-containing homologs. Recently, GPX4 has been identified as the master regulator of ferroptosis, a novel form of regulated necrotic cell death clearly distinct from other cell death modalities including apoptosis and necroptosis. As iron-dependent lipid peroxidation is a hallmark of ferroptosis and GPX4 is unique in efficiently scavenging hydroperoxides in lipid bilayers, proper control of lipid peroxide levels is of utmost importance to prevent ferroptotic cell death. To investigate the evolutionary advantage of selenothiol- versus thiol-based enzyme catalysis in one of the most important selenoenzymes in mammals, transgenic mouse lines have been generated and cell lines established thereof, where the catalytically important Sec of Gpx4 was replaced by Cys or Ser. Expectedly, the homozygous replacement of Sec by Ser did not allow animal survival as Ser is catalytically inactive. While mice with a homozygous expression of Ser die during early embryogenesis, heterozygous *Gpx4$^{wt/ser}$* animals were viable, although unexpectedly, the augmented expression of the Ser GPX4 protein conferred a dominant negative effect in male fertility. The expression of a Cys variant of GPX4 in mice showed that Sec in GPX4 is dispensable for adult animal survival but is essential for embryonic and postnatal development depending on the genetic background. While homozygous *Gpx4$^{cys/cys}$* animals on a *C57BL/6J* genetic background die during embryogenesis - but still remarkably later than *Gpx4$^{-/-}$* embryos - with malformations in brain and an impaired development of the cardiovascular system, homozygous animals on a mixed *129S6SvEvTac - C57BL/6J* genetic background showed pre-weaning lethality and epileptic seizures. The underlying reason for the latter was found to be a reduced number of parvalbumin-positive interneurons in the frontal cortex leading to the development of epileptic seizures. Thus, parvalbumin-positive interneurons emerge to be the limiting cell type, and thus selenium utilization, for survival of homozygous *Gpx4$^{cys/cys}$* animals. A detailed cellular and biochemical analysis of *Gpx4$^{cys/cys}$* and control murine embryonic fibroblasts revealed a yet unprecedented sensitivity of Cys-containing

GPX4 towards peroxide-induced overoxidation and ferroptotic cell death. The data presented here provide first evidence that Sec in GPX4 is evolutionary maintained to prevent peroxide-induced ferroptosis during developmental processes in mammals.

## Zusammenfassung

Glutathionperoxidase 4, eine von 8 Glutathionperoxidasen in Säugetieren, kommt als Selenoprotein in Säugetieren vor, wird aber in vielen anderen Organsimen als cysteinhaltiges, homologes Protein exprimiert. Es ist bis heute ein Rätsel, warum manche Organismen, wie Säugetiere, auf die Expression von Selenoproteinen angewiesen sind, während andere, wie beispielsweise höhere Pflanzen und Hefe, cysteinhaltige homologe Proteine exprimieren. Erst kürzlich konnte die GPX4 als Hauptregulationsprotein in der Ferroptose identifiziert werden, einer neuen Form des regulierten, nekrotischen Zelltods, der sich eindeutig von anderen Zelltodmodalitäten wie Apoptose und Necroptose unterscheidet. Da die eisenabhängige Lipidperoxidation ein zentrales Kennzeichen der Ferroptose darstellt, und die GPX4 als einziges Protein in der Lage ist Hydroperoxide in Lipiddoppelmembranen zu reduzieren, ist es von herausragender Bedeutung die Menge von Lipidperoxiden in der Zelle zu kontrollieren, um letztlich den ferroptotischen Zelltod zu verhindern. Um die Frage nach dem evolutionären Vorteil von selenothiolbasierter zu thiolbasierter Katalyse in einem der wichtigsten Selenoenzym der Säugetiere zu untersuchen, wurden zwei neue, transgene Mauslinien und entsprechende Zelllinien etabliert, bei denen das katalytisch wichtige Selenocystein der GPX4 entweder durch ein Cystein oder ein Serin ersetzt wurde. Wie erwartet starben Mäuse mit einer homozygoten Mutation des Selenocystein zu Serin in der GPX4 wie *Gpx4^-/-* Mäuse, was dafür spricht, dass zumindest ein Thiol oder Selenothiol essenziell für die katalytische Funktion der GPX4 ist. Im Gegensatz dazu waren heterozygote *Gpx4^wt/ser* Tiere zwar lebensfähig, jedoch übte die stark erhöhte Expression des Serin GPX4 Proteins unerwarteterweise einen dominant negativen Effekt auf die männliche Fertilität aus. Die anschließenden Studien mit Mäusen, die die Cysteinvariante der GPX4 exprimierten, zeigten, dass Selenocystein in GPX4 in adulten Tieren nicht essenziell ist, jedoch abhängig vom genetischen Hintergrund eine essenzielle Rolle während der Embryonalgenese bzw. in der postnatalen Entwicklung der Tiere spielt. Während homozygote *Gpx4^cys/cys* Tiere auf dem *C57BL/6J* Hintergrund schon während der Embryonalgenese starben, wenngleich wesentlich später als *Gpx4^-/-* Embryos, mit Anzeichen von Fehlbildungen in Hirn und einer gestörten Entwicklung des cardiovaskulären Systems, starben homoyzgote Tiere auf einem gemischten

genetischen *129S6SvEvTac - C57BL/6J* Hintergrund erst 2-3 wochen nach Geburt. Diese Mäuse zeigten Anzeichen für epileptische Anfälle, und die Entwicklung epileptischer Anfällen konnte dem Verlust von parvalbuminpositiven Interneuronen im Frontalcortex zugeschrieben werden. Somit konnten parvalbuminpositive Interneuronen als derjenige Zelltyp ausgemacht werden, der anhängig ist von Selen-haltiger GPX4, und der letztlich unabdingbar ist für das Überleben der *Gpx4^{cys/cys}* Tiere. Die umfassende zelluläre und biochemische Analyse homozygoter *Gpx4^{cys/cys}* Zellen und Kontrollzellen zeigte eine noch nie dagewesene Sensitivität der cysteinhaltigen GPX4 gegenüber einer peroxidinduzierten Überoxidierung des katalytischen Zentrums und des daraus resultierenden ferroptotischen Zelltods. Die hier vorgestellten Daten belegen eindeutig, dass Sec in GPX4 evolutionär konserviert wurde, um peroxidinduzierte Ferroptose während der Entwicklung von Säugetieren zu verhindern.

# 1    Introduction

## 1.1    Selenium as part of selenoproteins

The trace element selenium (Se) was discovered 200 years ago in 1817 by the Swedish chemist Jöns Jacob Berzelius, who named it after Selene, the Greek goddess of the moon (1). Being initially considered as a toxic compound, it was shown in 1957 - thanks to the work of Schwarz and Foltz - that Se also confers protective effects in organs, when Se inhibited liver necrosis in vitamin E-deficient rats (2). Due to these early studies, it is known today that Se can be toxic at high doses (400 µg- 700 µg/day (3)) causing hair loss, diarrhea and emesis in humans (4), whereas at low doses (~70 µg/day (5)) Se functions as an essential trace element with an enormous relevance for human health. In geographic regions with low Se status in the soil, such as rural areas of China and the eastern part of Russia, deficiency of Se has been previously associated with Keshan disease, a congestive cardiomyopathy, and Kashin-Beck disease, a chronic and endemic osteochrondopathy (6,7). Furthermore, Se deficiency was shown to have a negative impact on pathophysiological conditions including male infertility in humans and other mammals (8-10), childhood epilepsy (11-14) cancer, neurodegenerative disorders (15) and on the progression of HIV in infected patients (16,17). Since the identification of the first selenoprotein, rat glutathione peroxidase (Gpx) (18), in 1973, it has become clear that the amino acid residue selenocysteine (Sec) is the major biologically active form of Se in the cell, and that proteins containing Sec confer most, if not all, of the health benefits of Se in humans and other mammals (19).

After the identification of Sec being incorporated into proteins, the classical genetic code was reconsidered assigning TGA not only as a chain termination signal, but also as the codon for Sec (20). Sec itself is thus the 21st naturally occurring amino acid. Selenoproteins are characterized by having at least one Sec residue integrated in their polypeptide sequence, mostly forming the catalytic site at least of proteins catalyzing redox reactions (21). Therefore, most selenoproteins characterized so far act as oxidoreductases. Due to advent of high throughput sequencing of many genomes and great advances in their bioinformatical analyses, selenoproteins were identified in all three domains of life (Eukarya, Archaea, Bacteria) and viruses (22-25). Yet selenoproteins are not

expressed in all species among these kingdoms. The biggest variety of selenoproteins was found in eukaryotes ranging from a single selenoprotein in *C. elegans* to up to 59 in some brown algae (26). By contrast, yeast, fungi and higher plants completely lack selenoprotein expression and express cysteine (Cys)-containing homologs instead. This indicates that the expression of selenoproteins is independent from the complexity of the organism and the selenoprotein distribution within phyla. Thus, it still remains unknown why some organisms utilize and even depend on Se to a great extent, whereas others have lost the ability to utilize Sec during evolution expressing Cys-containing homologs instead. Interestingly, a high number of selenoproteins can be found in aquatic species, both animals and plants. Therefore, the prevailing concept nowadays is that the expression of Sec depends on the organisms` living environment and its access to water, since sessil organisms like higher plants or fungi with limited acces to water do not express selenoproteins. It is thus proposed that the change from an aquatic to a terrestrial habitat during evolution resulted in a reduced availability of Se and thereby shaped the selenoprotein evolution (22).

## 1.2    Advantage of selenothiol-based catalysis

As an analog of Cys (27) both amino acids - Sec and Cys - have similar chemicophysical properties and can undergo the same chemical reactions (28). Therefore, it is still under debate what the evolutionary advantage of Sec might be and why some organisms express selenoproteins instead of using the readily available Cys. Since most of the selenoproteins function as oxidoreductases, it is proposed that Sec might have better catalytic properties in redox reactions. Several *in vitro* studies indeed demonstrated that a naturally occurring Sec in proteins can be mutated to a Cys resulting in a dramatic reduction of the catalytic activity of the respective protein (29-32). In fact, Sec does have properties making it a better catalyst in redox reactions compared to Cys, namely a higher nucleophilicity, which increases the catalytic rates towards oxidative species, higher electrophilicity, which is important to break the selenylsulfide bond and prevents overoxidation, and a better leaving group ability (33). The nucleophilicity of an atom increases with its ionization state (34). Due to lower pKa (pKa = 5.4), Se is almost completely present in the ionized form, i.e. selenolate, at physiological pH (7.2-7.4), whereas sulfur under the same conditions is usually present in its protonated form as a thiol (pKa = 8.2) (33). Although *in vitro* mutant

studies have indicated that selenoproteins have a higher enzyme activity, it was shown that naturally occurring sulfur analogs in other organisms, e.g. thioredoxin reductases (TXNRD), may have similar activity (35) and the ability to lower their pKa by changing some important amino acids surrounding their active site (36). Furthermore, selenylsulfide was shown to be more electrophilic than its disulfide counterpart. The high polarizability and large atomic cloud makes selenium more accessible for a nucleophilic attack than sulfur, and is therefore easier to break the Se-S adduct (33). Additionally, overoxidation of Se is prevented by the high electrophilicity of the atom (37) and does only occur under denaturating conditions which might result in dehydroalanine formation and β-cleavage (38). In this context an *in vitro* study showed that the mutation of Sec to Cys in glutathione peroxidase (GPX4) of *Schistosoma mansoni* resulted immediately in an overoxidation of the sulfur atom and the formation of sulfonic acid (39). Taken together, these data indicate that Se is a better redox catalyst in scavenging peroxides and at the same time protects the enzyme from overoxidation and thus irreversible inactivation.

## 1.3   Selenoprotein biosynthesis

The discovery that Sec is encoded by UGA, which usually serves as one of the three translational stop codon in proteins (40-45), indicates that Sec synthesis and co-translational incorporation must be very complex and clearly distinct form that of other amino acids. Indeed, the Sec translation follows a noncanonical mechanism to decode UGA requiring two essential components, the selenocysteine insertion sequence (SECIS) element and its own Sec-specific tRNA (tRNA[Ser]Sec), which will be both described in more detail in the following chapters.

### 1.3.1   Sec synthesis

The key molecule of Sec synthesis is the Sec-specific tRNA, tRNA[Ser]Sec, encoded by the *Trsp* gene, which is comparable to other tRNAs in terms of size, shape, aminoacetylation and transcription. Yet it clearly discriminates from other tRNAs in two ways: (i) It is the only tRNA that controls the expression of a whole class of proteins (i.e. selenoproteins) and (ii) the amino acid is directly synthesized on its tRNA.

The synthesis of Sec in mammals starts with the aminoacetylation of tRNA[Ser]Sec with serine by seryl-tRNA synthetase (SerS) (Fig. 1). Then, the phosphoseryl-tRNA kinase (PSTK) phosphorylates Seryl-tRNA yielding pSer-tRNA (46). The last step is the conversion of pSer-tRNA[Ser]Sec to Sec. For this step, selenide first becomes phosphorylated to selenophosphate by selenophosphate synthetase 2 (SEPHS2). Then, selenocysteine synthase (SecS) catalyzes the substitution of the phosphate group of PSer-tRNA[Ser]Sec by the Se atom from selenophosphate (47,48). Selenide used for Sec synthesis derives from selenite from water and food which mammalian cells utilize as source for Se. Selenite gets reduced to selenide by the thioredoxin- and the glutaredoxin-dependent system (49,50), but can also be recycled from Sec and dietary selenomethionine.
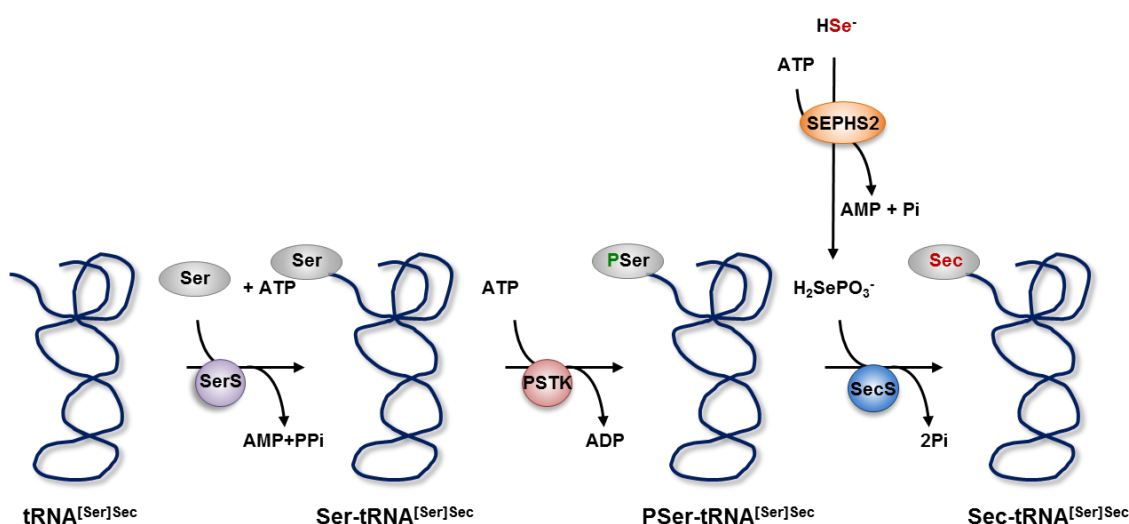


**Figure 1: Biosynthesis of selenocysteine-specific tRNA (Sec).** The synthesis of Sec occurs directly on its tRNA[Ser]Sec and commences with the loading of serine (Ser) to tRNA[Ser]Sec by seryl-tRNA synthetase (SerS). In the second step, Ser gets phosphorylated to PSer by phosphoseryl-tRNA kinase (PSTK) at the expense of one molecule ATP (46). Then, phosphoserine becomes converted to Sec by Sec synthase (SecS). Selenide used for Sec synthesis is phosphorylated to selenophosphate by selenophosphate synthetase 2 (SEPHS2) and selenocysteine synthase catalyzes the substitution of the phosphate group of phosphoserine tRNA[Ser]Sec by the Se atom from selenophosphate. Figure adapted from (7).

## 1.3.2  Sec incorporation into selenoproteins

Another element essential for decoding UGA as a Sec is the SECIS element, a stem-loop-stem-loop RNA motif consisting of ~100 nucleotides. Unlike in bacteria, the SECIS element in eukaryotes is located in the 3`-untranslated region

at least in a 50 nucleotides distance from the UGA codon (51). In bacteria, SECIS elements are located immediately downstream of Sec whitin the coding region of the gene (52).

The SECIS element is part of the selenoprotein synthesis machinery, because it serves as a dynamic platform for recruiting other components of the machinery and it controls the translation of the selenoprotein mRNA (Fig. 2). Selenoproteins containing several Sec residues, like selenoprotein P (SELENOP), require two SECIS elements for decoding up to 18 UGAs properly (53,54). Other components required for Sec incorporation are SECIS binding protein 2 (SBP2), Sec-specific elongation factor (EFSec), ribosomal protein eL30, eukaryotic translation intitiation factor (eIF4a3) and nucleolin. For a successful insertion of Sec into the nascent polypeptide chain in eukaryotes, EFsec builds a complex with tRNA[Ser]Sec which binds to a complex consisting of SECIS-SBP2 and the ribosome (52). Although the exact role of the factors eL30, eIF4a3 and nucleolin in this process remain unclear, it is proposed that they have a regulatory role in this mechanism (7) and might be involved in selenoprotein mRNA degradation under Se-deficient conditions.
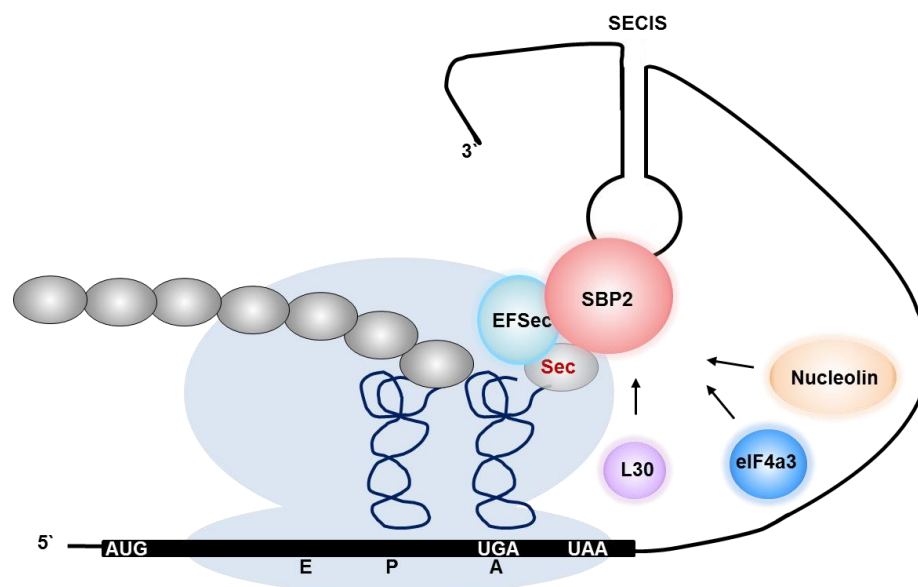


**Figure 2: Selenocysteine (Sec) incorporation into mammalian selenoproteins.** For the incorporation of Sec into the polypeptide chain, the selenocysteine insertion sequence (SECIS) element, which is located in the 3'-untranslated region of mammalian mRNAs, serves as a platform to recruit proteins important for the Sec insertion process. SECIS element forms a complex with SECIS binding protein 2 (SBP2) and Sec-specific elongation factor (EFSec) bound to Sec-tRNA[Ser]Sec at the ribosomal acceptor site (7,52) (A). The decoded Sec-tRNA[Ser]Sec is then transferred to the ribosomal peptidyl site (P), where it forms a peptide bond with the growing

polypeptide chain. Additional factors, such as eL30, nucleolin and eukaryotic translation initiation factor (eIF4a3) have a regulatory role during the incorporation process (7). Figure adapted from (7).

## 1.4    Mammalian selenoproteome

The human selenoproteome consists of 25 selenoproteins and shares 24 of them with rodents. Solely glutathione peroxidase 6 (GPX6) is a Cys containing homolog in rodents (22). As aforementioned, Sec is localized in the active site of most of the proteins and indeed half of the mammalian selenoproteome functions as oxidoreductases. At physiological pH, Sec is fully ionized and can thus act as a very efficient redox catalyst (55). Although the mammalian selenoproteome was completely identified, the function and role of some of the selenoproteins remains obscure. The expression of selenoproteins strongly depends on the Se availability in cells and tissues and follows a strict hierarchy (56-59). Therefore, selenoproteins can be divided into "stress-related" proteins, whose expression and activity decrease quickly under selenium-deficient conditions, e.g. GPX1, Methionine-R-sulfoxide reductase 1 (MSRB1), SELENOW and SELENOH, and "housekeeping" proteins, including GPX4, TXNRD1 and TXNRD2, whose expression remains stable even under prolonged Se deficiency. Yet under prolonged Se deficiency even housekeeping proteins will lose their activity and expression (60). Regulation of selenoprotein expression in dependence of Se status was shown to occur on the transcriptional level (57,61-63) resulting in the degradation of the mRNA. Although many hypotheses, including nonsense mRNA decay (NMD) (64,65), were proposed trying to explain the hierarchy of Se dependent mRNA degradation, the exact mechanisms remain to be fully understood.

### 1.4.1   Iodothyronine Deiodinases

The selenoprotein family of thyroid hormone deiodinases (DIO) consists of three paralogous proteins, namely DIO1, DIO2 and DIO3. As integral membrane proteins DIO1 and DIO3 are localized to the plasma membrane, whereas DIO2 was found in the ER membrane. The main function of DIOs is the regulation of thyroid hormone activity by reductive deiodination (19,66). The inactive prohormone of thyroid secreted by he thyroid gland, thyroxine ($T_4$), gets

converted in its active form 3,3`,5-triiodothyronine ($T_3$) by DIO1 and DIO2 (67). DIO3 catalyzes the reverse reaction from $T_3$ to $T_4$. DIOs are therefore very important for regulating the levels of thyroid hormones by both activating the prohormone $T_4$ and degrading the active form $T_3$ (19).

### 1.4.2 Thioredoxin reductases

*Three thioredoxin reductase* (*Txnrd*) genes were identified in mammalian cells and their products show different subcellular localization and tissue expression. TXNRD1 is mainly present in the cytosol and nucleus (68,69), TXNRD2 is mainly expressed in the mitochondrial matrix (70), and TXNRD3 (thioredoxin glutathione reductase) is a testis-specific protein (71). TXNRDs belong to the family of oxidoreductases containing FAD- and NADPH-binding domains and an interface domain (72). TXNRDs are present as homodimers consisting of two identical subunits that are arranged in a head-to-tail manner (72). Thereby, each homodimer forms two active sites consisting of a selenothiol of the C-terminal site of one monomer with an adjacent dithiol of the N-terminal site of the second monomer (32). The proposed mechanism for TXNRD involves an electron transfer from NADPH via FAD for the reduction of the disulfide bond at the N-terminus followed by a reduction of the selenylsulfide bond at the C-terminus of the opposite subunit. Finally, electrons are transferred from the active site Sec to the substrate (32,73). Due to its highly reactive catalytic center, TXNRDs have a wide range of substrates including selenite, lipid hydroperoxides and proteins, such as thioredoxin (TXN) and protein-disulfide isomerases (27). However, its main function is the reduction of oxidized TXN which provides electrons to ribonucleotide reductase, methionine sulfoxide reductase, peroxiredoxins (PRX) and transcription factors with critical redox-regulatory cysteins (74). By controlling the redox state of TXN, TXNRDs are involed in the regulation of most cellular process, such as proliferation, antioxidant defense and cell death. The significance of TXNRD1 and TXNRD2 for mammalian embryonic development was shown by knockout (KO) studies in mice, resulting in early embryonic lethal phenotypes (75-77). Due to its function to maintain redox homeostasis in cells, TXNRD1 was shown to promote and prevent cancer development. In a liver-specific mouse model of TXNRD1, the incidence of chemically induced liver tumors was strongly enhanced in TXNRD1-deficient mice compared to controls (78). On the other hand, TXNRD1 was found to be overexpressed in many

cancers and cancer cell lines to protect them from oxidative stress-induced cell death and to allow for fast proliferation (66).

### 1.4.3  Glutathione peroxidases

The glutathione peroxidase (GPX) family of proteins contains eight members, from which five (GPX1-4 and GPX6) are selenoproteins, whereas GPX5, GPX7 and GPX8 are Cys-containing proteins. As aforementioned (1.3) GPX6 is a Cys-containing homolog in rodents. Although GPXs can be found across all domains of life, Cys-containing homologs are predominantly expressed in bacteria, fungi, protozoa and terrestrial plants (19). This section focuses on all seleno-containing GPXs except for GPX4, which will be discussed in a separate chapter due to its outstanding role (1.5).

The GPX family is regarded as the main antioxidant system in the cell with substrate specificity for soluble, low-molecular weight hydroperoxides including hydrogen peroxide ($H_2O_2$) and fatty acid hydroperoxide (19). During detoxification of hydroperoxides to their corresponding alcohol or $H_2O_2$ to water, the active-site Sec becomes oxidized to selenenic acid which in the next step is reduced by one molecule of GSH resulting in an intermediate glutathionylated selenol, forming a selenylsulfide (Fig. 3). To complete the catalytic cycle, a second GSH molecule reacts with the intermediate to restore the catalytic activity of Sec, thereby forming an oxidized molecule of GSH (GSSG). GSSG is then reduced by glutathione reductase (GR) at the expense of NADPH/$H^+$. The catalytically active site of all GPXs was initially considered to be a triad, which is highly conserved within the GPX family even in Cys-containing homologs (79,80). Yet this paradigm was reconsidered showing that the catalytic site is in fact a tetrad consisting of Sec, glutamine (Gln), tryptophane (Trp) and aspargine (Asn) that accounts for the catalytic efficiency of this protein family (81). Due to the architecture of the active site, it is presumed that the selenothiol becomes activated by hydrogen bonding with the nitrogens of the Gln, Trp and Asn residues (81). GPX1-3 are homotetrameric proteins with subunits ranging from 22-25 kDa in size (82-85). Although GPXs share overlapping substrate specificities, they are not uniformly expressed across tissues and organs (60). The first described GPX protein and actually also the first identified selenoprotein (18,86,87), was GPX1, an ubiquitously expressed cytosolic protein with strong

expression in liver and kidney. GPX2 is mainly expressed in the epithelium of the gastrointestinal tract; GPX3 is expressed in the kidney, secreted into the blood stream and represents the major GPX form there. GPX6 expression is mainly confined to the olfactory bulb and expressed during embryogenesis (88). KO studies for *Gpx1* and *Gpx2* revealed that both proteins are dispensable for mouse development (89,90); however, under stress conditions like UV light or intoxication with toxic compounds KO mice appeared to be more sensitive than wt counterparts (91,92). Double KO mice for *Gpx1*/*Gpx2* are viable but develop spontaneous colitis and intestinal cancer (93).
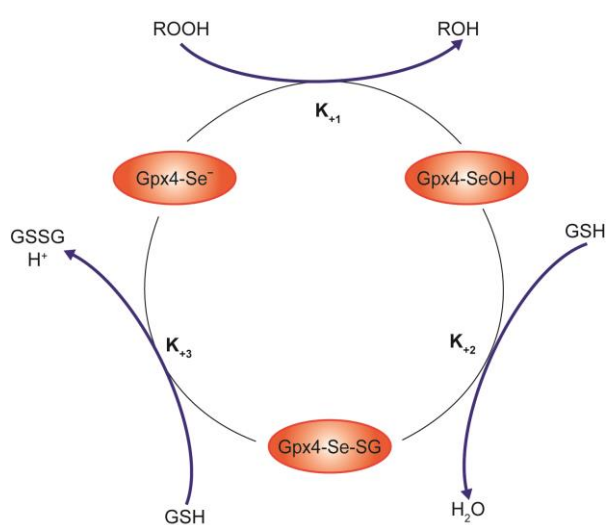


**Figure 3: Catalytic cycle of glutathione peroxidases (GPX).** GPX proteins detoxify lipid peroxides to the corresponding alcohol or hydrogen peroxide ($H_2O_2$) to water. During this reduction, Sec in the active site of GPX is oxidized to selenenic acid and reacts in the 2nd step with one molecule of glutathione (GSH) resulting in a glutathionylated selenol. To complete the catalytic cycle, GPX reacts with a second GSH molecule resulting in a fully reduced and active enzyme, thereby releasing one molecule of oxidized GSH (GSSG). GSSG is reduced by glutathione reductase (GR) at the expense of one molecule of NADPH.

### 1.4.4 Other selenoproteins

Unlike other selenoproteins, SELENOP contains up to 10 Sec residues in mammals, but the number of Sec residues in vertebrates vary from 7-18 residues depending on the species (94). SELENOP is responsible for the distribution of Se throughout the body, where it is utilized for *de novo* synthesis of selenoproteins. SELENOP is mainly expressed in liver, where Se ingested from food is used for the synthesis of this Se-rich protein (95). After being secreted

into the blood stream (95), it is distributed to other tissues, such as brain, testis and kidney (96,97), which take up SELENOP by receptor-mediated endocytosis or pinocytosis and catabolise it for selenoprotein synthesis (98,99). Impairment in SELENOP expression or distribution is associated with neurological disorders, such as Alzheimer`s (100-102) and Parkinson`s disease (103-105).

The previously mentioned (1.2.1) SEPHS2 protein has an essential role in selenoprotein synthesis (48) by converting selenide to selenophosphate. MSRB1, located in the cystosol and nucleus, functions as a reductant of oxidized methionine residues (106). 15 kDa Selenoprotein F (SELENOF) was found in the ER, where it controls protein folding (107). Further ER-associated proteins are SELENOK and SELENOS which are also predicted to play a role in the unfolded protein response (108-110), as well as SELENOM, SELENON and SELENOT whose exact functions are not elucidated yet (111). Selenoprotein SELENOH is associated with gene regulation due to its nuclear localization and its ability to bind DNA (112,113). SELENOI was proposed to function as an ethanolamine phosphotransferase responsible for the production of phosphatidylethanolamine (PE) in the membrane (114). The functions of SELENOW, SELENOV and SELENOO still remain unclear (25,88,115).

### 1.4.5 Unraveling selenoprotein functions by *Trsp*-specific KO

Since Sec is encoded by UGA, it requires several co-factors that are essential for a successful translation and incorporation of the amino acid into the polypeptide chain. A key molecule is the Sec-specific tRNA[Ser]Sec encoded by the *Trsp* gene. In order to elucidate the role of selenoproteins in mammalian development and health, numerous KO studies have been performed targeting the *Trsp* gene. The systemic KO of *Trsp* was shown to be embryonic lethal at the gastrulation stage (E6.5) (116,117) similar to the *Gpx4* KO (E7.5) (see 1.5.4), demonstrating the significance of selenoproteins for mammalian embryonic development in general and hinting towards an outstanding role of GPX4 among all selenoproteins.

To analyze functions of selenoproteins in adult and developing animals, conditional *Trsp* KO models have been developed using the loxP-Cre technology (117). Thereby, it could be shown that Se has an important role in the immune system as the *Trsp* KO in T cells and macrophages resulted in decreased T cell

maturation, antibody response and suppressed T cell proliferation after receptor stimulation (118). Macrophages showed enhanced oxidative stress and impaired invasiveness (119,120). *Trsp* deletion in the liver resulted in an early death of the animals between one and three months after birth due to hepatocellular degeneration (121). On the other hand, a liver-specific KO of *Gpx4* resulted in early death, shortly after birth, underlining the importance of that protein for hepatocelullar survival (122). Heart-specific *Trsp* KO led to death within the $2^{nd}$ week after birth due to cardiac failure (123). Endothelium-specific KO of *Trsp* caused embryonic death during midgestation (123). CamKIIα-Cre- and Tα1-Cre-mediated neuron-specific deletion of selenoproteins resulted in the death of the animals around two weeks after birth. The respective KO mice displayed seizures, generalized growth retardation, loss of parvalbumin (PV)-positive interneurons and Purkinje cells (124,125). Interestingly, using the same Cre lines conditional KO of just *Gpx4* very often phenocopied both phenotypes with seizures, loss of PV interneurons and cerebellar hypoplasia. This again highlights the outstanding importance of GPX4 among all selenoproteins (124,125). Targeted removal of *Trsp* in epidermis impaired proper skin function and development resulting in premature death of the animals 10 days after birth. Hair follicles were reduced in number and displayed growth retardation (126). In a model of epidermis-specific disruption of *Gpx4* a similar phenotype was observed, such as abnormal hair follicles, hyperplastic skin and growth retardation of the animals (127). Hence, *Trsp* KO models not only highlight the significance of all selenoproteins for mammalian health and development, they also helped to better understand the role and function of single selenoproteins in particular tissues and organs. Thereby, it is striking that the single KO of *Gpx4* very frequently phenocopied the KO of all selenoproteins in certain tissues.

## 1.5 GPX4

### 1.5.1 Cellular functions of GPX4

The GPX4 protein was initially purified from pig liver and identified as an inhibitor of lipid peroxidation by Ursini *et al.* (128). As part of the GPX family, GPX4 shares some common features with other members of the family (see. 1.4.3). But its biochemical functions, structural characteristics and its necessity for cell and mouse survival makes it a unique and outstanding member not only within the

GPX family, but also whithin all mammalian selenoproteins. Due to its ability to reduce not only $H_2O_2$ and other small hydroperoxides, but also peroxides in complex lipids such as phospholipid hydroperoxides (PLOOH), cholesterol ester hydroperoxides and cholesterol hydroperoxides (ChOOH), soluble or integrated within biomembranes and lipoproteins, GPX4 was previously referred to as phospholipid hydroperoxide glutathione peroxidase (PHGPx) (129). In contrast to GPX1-3, 5 and 6 GPX4 is monomeric and utillizes not only GSH as reductant, but also small molecular weight thiols (130,131) and protein thiols particularly under limiting GSH conditions, as physiologically evident during sperm maturation (132,133). Due to alternative transcription initiation, the *Gpx4* gene gives rise to three different isoforms referred to as mitochondrial (mGPX4), nuclear (nGPX4) and cytosolic (cGPX4) GPX4 that only differ in their 5`-ends (134,135) (Fig. 4). The *Gpx4* gene consists of 7 plus one alternative exons, whereas the alternative exon 1b, located between exon 1a and exon 2, harbors the translation start for the nuclear form of GPX4, which represents the biggest isoform (35 kDa) (136). The mitochondrial isoform has a size of 23 kDa and contains a mitochondrial leader sequence which gets truncated after entering mitochondria. Cytosolic GPX4 is the smallest isoform (19 kDa) that is ubiquitously expressed with a high prevelance in kidney, brain and testis, whereas the mitochondrial and nuclear isoforms are almost exclusively expressed in different spermatogenic cells. Transgenic studies performed in mice allowed to assign for each of the isoforms different functions and their individual significance for mammalian development and adult life.
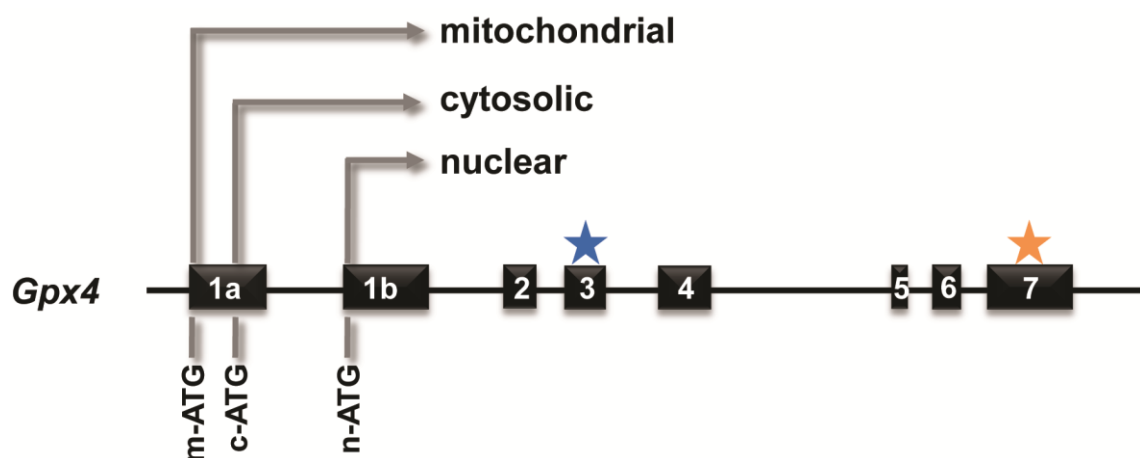


**Figure 4: Genomic arrangement of the *Gpx4* gene and transcription initiation sites of the different isoforms.** The *Gpx4* gene consists of 7 exons and one alternative exon 1b. Due to

alternative transcription initiation sites (depicted with arrows), the *Gpx4* gene gives rise to three different isoforms, namely mitochondrial GPX4 (mGPX4), cytosolic GPX4 (cGPX4) and nuclear GPX4 (nGPX4), that only vary in their 5`- termini (134,135). The translation of the mitochondrial and cytosolic isoform starts at exon 1a, whereas the translation start codon for nGPX4 is located in exon 1b. Translation start codons are depicted with an ATG. The blue asterisks marks the localisation of the catalytic site in exon 3 and the orange asterisks shows the localisation of the SECIS element in exon 7 (137). Figure adapted from (137).

### 1.5.2 Nuclear and mitochondrial isoforms and their role in spermatogenesis

To elucidate the specific function of each GPX4 isoform, mouse KO studies have been performed inserting a premature stop codon into the transcription start of the mitochondrial isoform (9) or by replacing exon 1b with an eGFP cassette gaining a KO of the nuclear isoform (138). In contrast to the short isoform, neither the mGPX4 nor nGPX4 isoforms are essential for mouse embryonic development or postnatal viability (9,138,139). Instead, both isoforms were shown to confer specific roles in sperm development. For many decades, Se is known to be indispensable for male fertility (140,141) and in 1999, by identifying GPX4 as a major component of sperm mitochondria capsule, it was shown that Se in form of GPX4 plays a pivotal role for sperm stability and function (133). Although initially considered to be the crucial isoform for sperm development, *nGpx4⁻ᐟ⁻* mice were found to be fully fertile with rather subtle defects in sperm chromatin compaction. Isolated sperm from these mice had giant heads (in response to treatment with detergents), delayed chromatin condensation and impairment in paternal chromatin decondensation (138,139). On the other hand, the KO of *mGpx4* resulted in male infertility and isolated sperm from *mGpx4⁻ᐟ⁻* animals phenocopied the morphological abnormalities of sperm isolated from rodents that were kept under selenium-deficient conditions, including bends in the midpiece, displaced heads and protrusion of outer dense fibers (142,143).

During final sperm maturation, when GSH becomes almost entirely deprived (144), GPX4 has a moonlighting function acting as an enzymatic inactive structural protein and as a thiol peroxidase. As such, mGPX4 oxidizes and polymerises proteins of the mitochondrial capsule to create a network of cross-linked proteinpolymers that stabilizes the midpiece of spermatozoa (9,132). During the polymerisation process, mGPX4 loses its enzymatic activity and

becomes an essential integral part of the protein network of the capsule due to a "dead-end" enzymatic cycle (133,145). Similarly, nGPX4 introduces disulfide bridges into protamine thiols to ensure a tightly packed chromatin (138,146).

### 1.5.3 Gpx4 and its role in cell death and survival

Only recently, in 2014, GPX4 was identified as a key player of a new regulated form of necrotic cell death designated as ferroptosis (147,148). Due to the special role of GPX4 in ferroptosis, this cell death pathway will be described in more detail in the next chapter (1.5.4). Long before GPX4 was shown to contribute to ferroptosis, numerous *in vivo* (149-151) and *in vitro* (152) studies assigned a protective involvement of GPX4 in cell death. Initially, GPX4 was considered to prevent apoptosis for instance induced by KCN induced lipid peroxidation, 2-deoxyglucose, staurosporine, UV radiation and actinomycin D and by suppressing cardiolipin peroxidation in cells overexpressing mitochondrial GPX4 (153-155). These findings led to the assumption that mGPX4 might contribute to the pro-survival function of GPX4 which was ruled out when mouse KO studies showed that *mGpx4* is predominantly expressed in testicular tissues (9) and that the cytosolic form is sufficient to allow normal development and adult life (151). Later, it was revealed that the inducible deletion of *Gpx4* caused cell death in a caspase-independent manner that was shown to involve 12/15 lipoxygenases (LOX, encoded by *Alox15*) (152).

Since GPX4 was identified as the key regulator of ferroptosis, lipid peroxidation was shown to be the critical event in this cell death paradigm. Despite intensive studies the exact process of lipid peroxidation, such as the localization and the initiation reaction during ferroptosis, is not yet fully understood (156). Yet the current consensus is that after initiation of lipid oxidation, most likely by highly reactive radicals, lipid peroxyl radicals (LOO$^{\bullet}$) further drive the oxidative chain reaction of adjacent lipids. By abstracting a hydrogen from another lipid molecule, lipid hydroperoxides (LOOH) and new lipid radicals (L$^{\bullet}$) are generated (157). While vitamin E is able to slow down the rate of peroxide formation by donating an electron to LOO$^{\bullet}$ generating LOOH, solely GPX4 and GSH are able to efficiently detoxify LOOH to their corresponding alcohol (158), thus breaking the oxidative chain reaction and preventing lipid peroxidation and consequently ferroptotic cell death.

## 1.5.4 Ferroptosis

The notion that apoptosis is the only form of regulated cell death was challenged when tumor necrosis factor α (TNFα) was shown to induce a form of regulated necrosis, which was later termed necroptosis (159). Since then, a myriad of novel forms of regulated necrotic cell death have been described including oxytosis, parthanatos, netosis, cyclophilin D-(CypD)–dependent necrosis and ferroptosis. Among them ferroptosis has gained special attention due to its impact in many pathophysiological conditions, such as cancer, neurodegeneration and ischemia/reperfusion injury (IRI) in liver, heart and kidney (147,148,160-162). The discovery of two small molecules able to induce cell death in tumor cells expressing an oncogenic Ras, named "eradicator of Ras and ST" (erastin) and "Ras Selective Lethal 3" (RSL3) (163,164) led to the identification of this new cell death pathway. Due to the fact that iron chelators inhibit this form of cell death, this pathway was then termed ferroptosis and described as an iron-dependent, non-apoptotic form of cell death (165). This cell death pathway was later shown to rely on glutathione metabolism for proper and unique function of GPX4 to detoxify lipid hydroperoxides (Fig. 5) (147,148). Since then, ferroptosis was intensively studied and new molecular players have been identified. The most upstream acting player in this pathway is the cystine/glutamate antiporter, system $x_c^-$, that takes up one extracellular molecule of cystine, the oxidized form of cysteine, and releases in exchange one molecule of glutamate (Glu) (166) (Fig. 5). The substrate-specificity conferring subunit SLC7A11 (xCT) of system $x_c^-$ is one of the proteins whose expression is regulated by the nuclear factor (erythroid-derived 2)-like 2-Kelch like ECH-associated protein 1 (NRF2-Keap1) pathway (167,168), which gets activated under conditions of oxidative (electrophilic) stress in cells (169,170). More recently, it was reported that one of the many tumor suppressor activites of p53 is to regulate system $x_c^-$ by direct inhibiton of SLC7A11 expression. Inhibition of SLC7A11 results in reduced cystine uptake thereby sensitizing tumor cells to ferroptosis (161). Cystine that is imported into the cell is reduced to Cys by GSH or TXNRD1 and is further utilized for protein and in particular for GSH synthesis (171,172). GSH represents the most abundant antioxidant molecule in the cell and acts as an important electron donor for many redox enzymes including GPX4. Pharmacological deprivation of GSH in the cell either by inhibiting cystine uptake or GSH synthesis was shown to

impair GPX4 activity thereby triggering ferroptosis. Therefore, compounds eliciting ferroptosis through GSH depletion were denominated as class I ferroptosis inducing agents (FINs). Compounds belonging to this class include glutamate, erastin, sulfasalazine and sorafenib which target system $x_c^-$, and buthionine sulfoximine (BSO) which targets γ-glutamyl-cysteine-synthase (γGCS) (148,152). In this context, it was recently demonstrated that sensitivity to system $x_c^-$ inhibition can be bypassed by activation of the transsulfuration pathway, which consumes methionine to increase the Cys pool (173). Alternatively, ferroptosis can also be induced by class II FINs. These compounds are classified as molecules acting downstream of GSH by targeting GPX4, such as (*1S,3R*)-RSL3 (147) and FIN56 (174). Since enhanced phospholipid oxidation represents a critical event in ferroptotic cell death, it is not surprising that the the lipophilic radical trapping antioxidants α-Tocopherol (α-Toc), ferrostatin-1, and liproxstatin-1 are able to block ferroptosis by preventing lipid peroxidation (148,165,175).

Nonetheless, the importance of polyunsaturated fatty acid (PUFA) oxidation in ferroptosis has been supported by recent discoveries. For instance, two genes, namely *acyl-CoA synthetase long-chain family member 4* (*ACSL4*) and *lysophosphatidylcholine acyltransferase 3* (*LPCAT3*), were identified by haploid screening as important players in ferroptotic cell death modality (176). Two independent functional screenings conducted in our laboratory could, however, only identify ACSL4 as a critical downstream component of the ferroptotic pathway not only in MEFs but also in a panel of triple negative breast cancer cell lines (177). *Acsl4* encodes for an enzyme that is involved in lipid metabolism and biosynthesis as it ligates HS-CoA to free, long-chain fatty acids converting them into acyl-CoA esters that become re-esterified by LPCAT3 into phospholipids (178-180). Its preference for long-chain polyunsaturated fatty acids, such as arachidonic and adrenic acid, and their incorporation into a specific class of phospholipids (i.e. phosphatidylethanolamine (PE)) increases the susceptibility of cells to lipid peroxidation, and thus identified oxidized PE containing arachidonic and adrenic acids as potential sources for the generation of the lethal ferroptotic signal (177,181). In this respect, Doll and colleagues showed that genetic deletion or pharmacological inhibition of ACSL4 using thiaziolidinediones (TZN) protected cells from undergoing ferroptosis upon *Gpx4* inactivation or

genetic deletion. Rosiglitazone (one of the TZN) treatment of mice was even able to delay mortality in animals suffering from ARF in a 4-OH-Tamoxifen (TAM)-inducible *Gpx4* KO mouse model (177).

Yet there is circumstantial evidence that lipid peroxidation is driven in an iron-dependent manner which is supported by the fact that iron chelators such as deferoxamine (DFO) and ciclopirox olamine efficiently inhibit ferroptotic cell death (165). Specifically, in ferroptosis-sensitive cells expressing onocogenic Ras expression of transferrin receptor 1 (TFR1) was found to be upregulated, whereas the iron-storage protein ferritin was downregulated compared to ferroptosis-resistant cells, indicating that iron loading is a strong contributor to ferroptosis (164). In this respect it was shown that ultrasmall nanoparticle induced ferroptosis in a mouse xenograft tumor by disrupting iron homeostasis (182).

Circulating ferric iron ($Fe^{3+}$) is bound by transferrin and gets internalized into the cell via endocytosis of transferrin bound to its receptor. After internalization, $Fe^{3+}$ is released into the endosome where it gets reduced by the ferrireductase activity of six-transmembrane epithelial antigen of prostate 3 (STEAP3) to ferrous iron ($Fe^{2+}$). Export of $Fe^{2+}$ to the cytoplasma in order to participate in different metabolic pathways occurs by iron transporters such as divalent metal transporter 1 (DMT1). Excessive iron in the cytoplasma is stored in form of a complex consisting of $Fe^{3+}$ bound to the iron storage protein ferritin (183,184). Ferritin consists of 24 subunits in a combination of ferritin heavy and ferritin light chains (185). The ferroxidase activity of the heavy chain subunits enables the conversion of the redox active $Fe^{2+}$ to $Fe^{3+}$. The release of stored iron involves an autophagic/lysosomal process of ferritin, named ferritinophagy, which contributes to ferroptosis since autophagy inhibitors were shown to prevent erastin and (*1S,3R*)-RSL3 triggered ferroptosis in human fibrosarcoma cells (HT1080) (183). Redox active $Fe^{2+}$, as part of the labile iron pool in the cell, can generate local ROS within the endosomes and the cytoplasma where it is able to promote or initiate lipid peroxidation by reacting for instance with $H_2O_2$ to highly reactive hydroxyl radicals (OH$^{\bullet}$) in a reaction known since the late 19th century as the Fenton reaction. Iron chelators may thus not only act on the labile iron pool to prevent ferroptosis but may also act on iron-containing proteins such as LOXs (186).
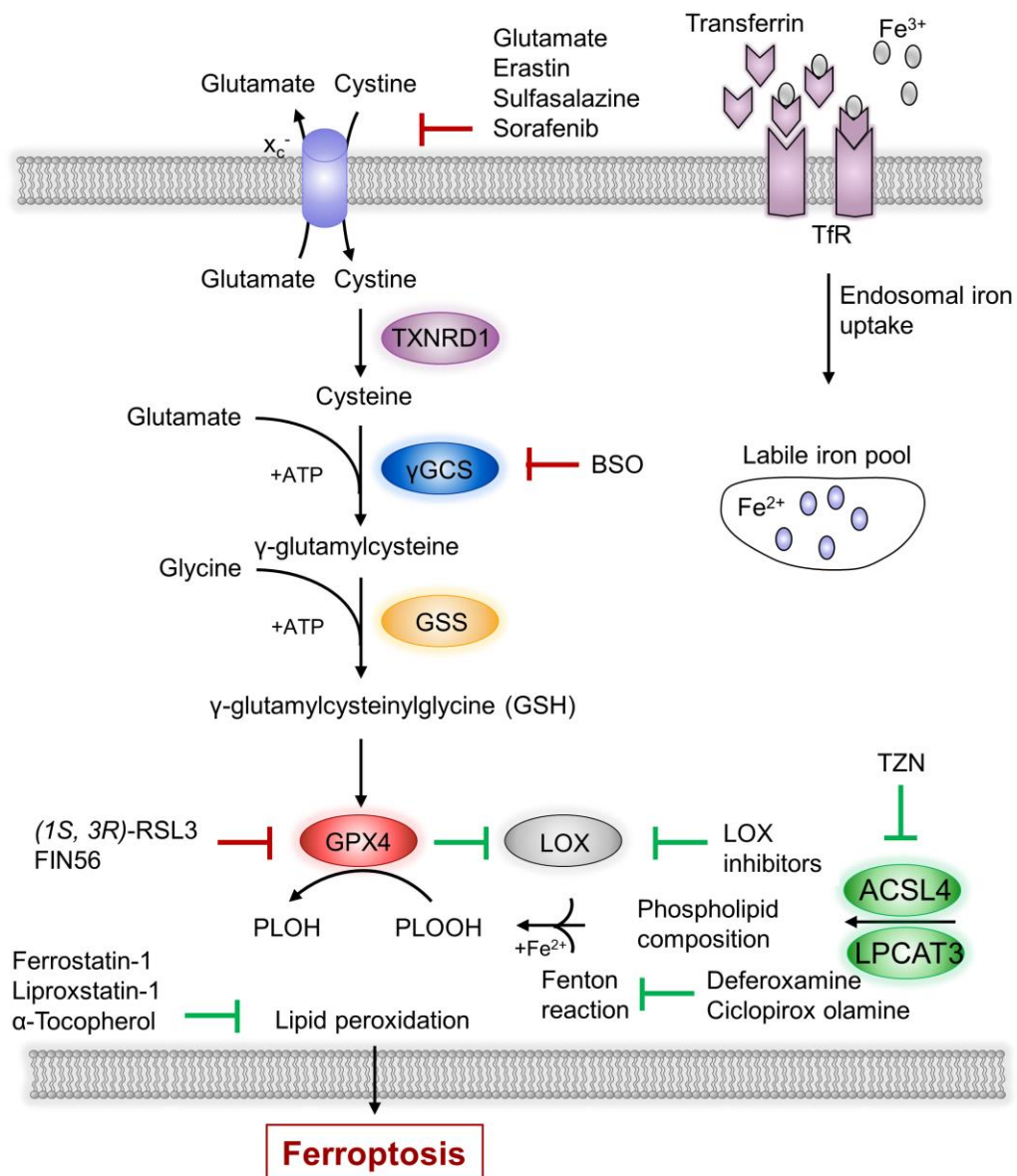
**Figure 5: Molecular events of ferroptosis.** The most upstream player in the ferroptotic pathway (at least in cells) is the cystine/glutamate (Glu) antiporter system $x_c^-$ that takes up one molecule of extracellular cystine (oxidized cysteine) and releases one molecule of Glu (166). The imported cystine becomes reduced in the cytosol by thioredoxin reducatse 1 (TXNRD1) or GSH and is further used for GSH synthesis (171,172). GSH is synthesized from cysteine in two steps by the enzymes γ-glutamylcysteine synthetase to γ-glutamylcysteine and by the enzyme glutathione synthetase to the final molecule γ-glutamylcysteinylglycine (GSH). GSH serves as electron donor for GPX4 which is essential in the cell to reduce phospholipid hydroperoxides (PLOOH) to the corresponding alcohols (128), thereby preventing lipid peroxidation and ferroptosis (147). Class I ferroptosis inducing agents (FINs) including glutamate, erastin, sulfasalazine, sorafenib and L-buthionine sulfoximine (BSO) decrease the GSH level in the cell by acting on system $x_c^-$ or by abrogating GSH synthesis through inhibition of γGCS (148,152). Class II FINs such as *(1S,3R)*-RSL3 and FIN56, directly impinge on GPX4. Lipid peroxidation might be promoted by ferrous iron ($Fe^{2+}$) via the Fenton reaction, where $Fe^{2+}$ reacts with $H_2O_2$ to form the highly toxic hydroxyl radicals (OH·) and by enzymes of the lipoxygenase family (LOX) (186). Therefore, iron chelators such as deferoxamine and ciclopirox olamine can inhibit ferroptotis. Ferric iron ($Fe^{3+}$) bound to

the iron carrier protein transferrin gets internalized via the transferrin receptor (TfR) into the cell forming the labile iron pool. ACSL4 is responsible for shaping the lipid membrane by activating preferrably long chain polyunsaturated fatty acids (PUFAs) that get incoporated into membrane phospholipids, which are then prone to undergo oxidation (176,177). Thus, ferroptosis can be prevented by lipophilic antioxidants including ferrostatin-1, liproxstatin-1 and α-tocopherol. ACSL4 can be pharmacologically inhibited by thiazolidinediones (TZN). Figure adapted from (187).

Except for radical-induced formation of LOOH, there is evidence of enzymatically formed LOOH by LOX that might be involved in driving lipid peroxidation during ferroptotic cell death (188). LOXs enhance lipid peroxidation by oxidizing PUFAs, such as arachidonic acid, linoleic acid or linolenic acid at different positions to their corresponding hydroperoxide (184,189); at the same time LOXs require a certain amount of LOOH that oxidize their catalytic iron to maintain the enzyme in an active state. Therefore, GPX4 does not only prevent ferroptosis by reducing LOOH but also indirectly by keeping LOXs in check. Despite the proposed contribution of LOXs in the ferroptosis cell death process (188), *in vivo* genetic proof of a single LOX as critical ferroptosis player is still missing. *Alox15* KO, the first LOX proposed to contribute to ferroptosis, could neither prevent embryonic lethality in mice expressing a catalytically inactive form of GPX4 (190) nor in a *Gpx4*$^{-/-}$ background and also failed to prevent acute renal failure (ARF) and lethality in adult TAM-inducible *Gpx4* KO animals (148). So far, efficient protection against ferroptosis by genetic deletion of *Aloxs* has only been shown to be effective *in vitro* (152,188).

Since ferroptosis is associated with different pathological conditions, such as IRI, neurodegeneration and cancer, genetic mouse studies as well as cell culture studies are indispensable to (i) further investigate the relevance of ferroptotic cell death in certain pathological settings, (ii) to find new targets for pharmacological treatment of certain diseases and (iii) to find new pharmacological compounds that modulate the ferroptosis process.

## 1.6 Mouse models targeting GPX4

Systemic KO of *Gpx4* leads to embryonic lethality during the gastrulation stage (E7.5) (149,150,152). Therefore, conditional and inducible KO approaches using the Cre-loxP technology have proven instrumental when studying the function and significance of GPX4 in different cell types and tissues (Fig. 6). Since no specific biomarkers for ferroptosis are available, genetic deletion of *Gpx4* as a

key regulator of this form of cell death has been mainly used to interrogate unsolved questions. Interestingly, a whole body KO of *γGCS*, the rate-limiting and essential enzyme for GSH synthesis, results in embryonic death at the same time point as *Gpx4* KO (191), suggesting that GPX4 is responsible for many of the cyto-protective functions of GSH (192).

The importance of GPX4 for neuronal cell survival was addressed by numerous KO studies targeting different types of neurons. In the first neuronal mouse model, *Gpx4* was deleted in glutamatergic neurons using CamKIIα-Cre mice. This resulted in ataxia, seizures, impaired differentiation and loss of PV-positive interneurons and pre-weaning lethality of KO animals, thus strongly resembling the phenotype of conditional *Trsp* KO mice (see 1.4.5) (124,152). Targeted deletion of *Gpx4* using Tα1-Cre mice caused early death of the animals displaying Purkinje cell loss and cerebellar hypoplasia, which was also seen in *Trsp* KO animals (see 1.4.5) (125). Inducible KO of *Gpx4* in motor neurons triggered rapid paralysis of the animals due to loss of motor neurons and muscle atrophy which led to death of animals eight days after tamoxifen induction (193). Loss of *Gpx4* in the forebrain showed ferroptotic cell death in the cerebral cortex and hippocampus causing diminished spatial learning capability and memory function. While vitamin E deficient diet accelerated the pathological phenotype, treatment with the ferroptosis inhibitor liproxstatin-1 slowed down neurodegeneration (194). These data show that GPX4 is crucial to protect neurons from cell death in developing embryos and adult animals. Transgenic mouse studies targeting other tissues exhibited an important role of GPX4 not only in neurons but also for photoreceptor development and maturation (195), hepatocellular survival (122), erythropoiesis (196) and skin function (see 1.4.5) (127). Interestingly, a keratinocyte-specific KO of *γGCS* presented a similar yet milder phenotype compared to KO of *Gpx4*. Animals displayed growth retardation and less elastic skin but no alterations in GPX4 expression, proving that GPX4 may utilize small molecule thiols and protein thiols other than GSH under limiting GSH conditions not only during sperm maturation (200).
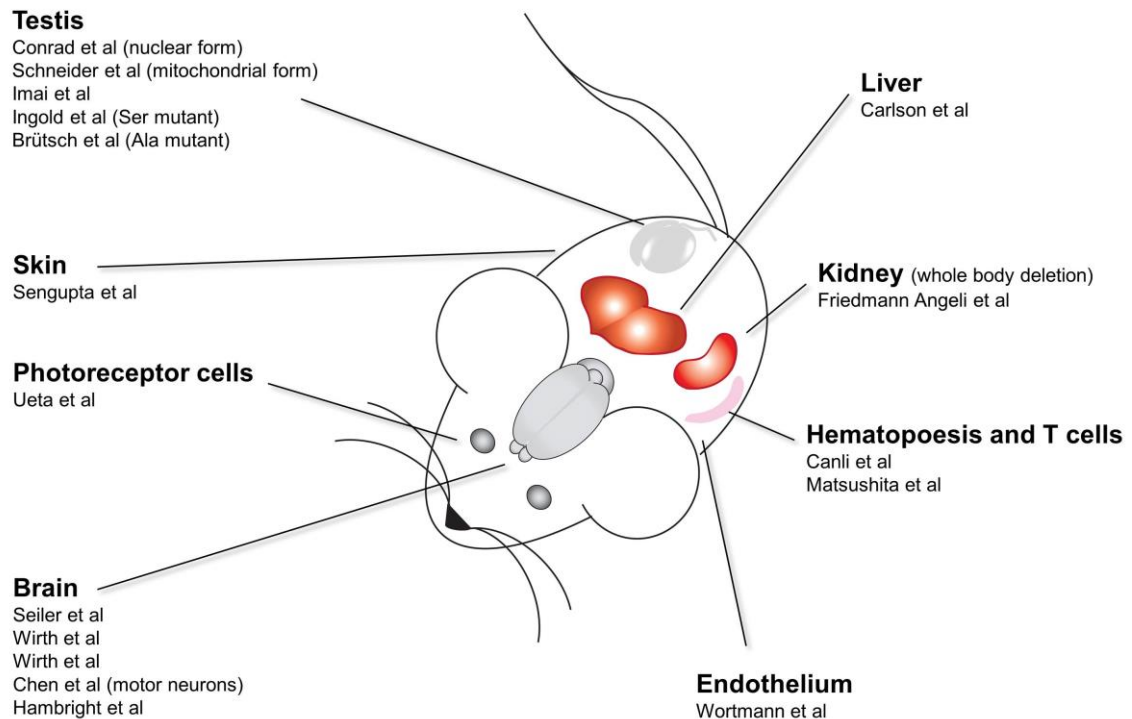
**Figure 6: Conditional KO mouse models targeting *Gpx4* in different cells and tissues.** Systemic ablation of *Gpx4* is embryonic lethal, therefore conditional and inducible *Gpx4* KO are used to study the function of GPX4 postnatally. Conditional KO of *Gpx4* in brain using either CamKIIα-Cre or Tα1-Cre leads to early death of newborn animals showing seizures, ataxia, loss of parvalbumin (PV)-positive interneurons and loss of Purkinje cells (124,125,152). *Gpx4* KO in motor neurons is lethal and results in paralysis and muscle atrophy (193). *Gpx4* KO in the forebrain causes deficits in spatial learning and memory (194). GPX4 is important for the development and maturation of photoreceptor cells (195), and essential for proper skin function (127). KO models targeting different isoform of *Gpx4* revealed an essential role of mGPX4 and Sec in the active site for male fertility (see also 4.2-4.3) (8,9,138,149,197). An essential role of GPX4 was identified for hepatocellular survival (122), proper kidney function and tubular cell survival (148), for hematopoiesis (196) and for immune cells during acute viral and parasite infections (198). An endothelium-specific KO of *Gpx4* showed thromboembolic events only under vitamin E deficient conditions resulting in heart failure, renal and splenic microinfarcts (199).

T cell-specific KO of *Gpx4* revealed an impairment in the expansion of CD8+ and CD4+ cells and protecting animals from acute virus and parasite infections, similar to what had been reported in a T cell-specific *Trsp* KO (see 1.4.5). Besides, CD8+ cells failed to maintain homeostatic balance in periphery (198). Moreover, an inducible whole body deletion of *Gpx4* (except brain) revealed an essential role for GPX4 in renal tubule cell survival (*Gpx4flox/flox;Rosa26CreERT2*, referred to as PZ mice) and showed for the first time *in vivo* that *Gpx4* deletion induces ferroptotic cell death in cells/tissues other than cancer cells. The

21

respective KO animals failed to survive beyond two weeks after tamoxifen induction due to ARF (148). Endothelium-specific KO of *Gpx4* did not show an overt phenotype unless animals were fed with vitamin E deprived diet. Vitamin E deficient conditions unmasked the phenotype of *Gpx4* KO in endothelium resulting in thromboembolic events and finally leading to heart failure, renal and splenic micro-infarctions (199). The numerous mouse studies described here (Fig. 6) thus highlight the cyto-protective and essential role of GPX4 in many organs, which, in certain organs, can be compensated to some extent by the antioxidant vitamin E.

## 1.7    Objectives

The selenoenzyme GPX4 emerges to be one of the most important redox enzymes in mammals. Apart from its unique function as a scavenger of phospholipid hydroperoxides in lipid bilayers, GPX4 has recently been assigned a key regulatory function in a novel, iron-dependent form of non-apoptotic cell death, named ferroptosis, a pathway that emerges to be linked to many pathophysiological conditions. The significance of GPX4 in embryogenesis and in adult tissues has been corroborated by a series of genetic mouse studies also showing that the nuclear and mitochondrial isoforms of GPX4 are only involved in proper sperm maturation. Since Sec is encoded by an opal codon, its synthesis and co-translational incorporation during protein synthesis require a number of proteins and co-factors, which is why it is energetically a very costly and inefficient process in contrast to other amino acids. GPX4 is one of 24 selenoproteins in mammals but exists as a Cys-containing homolog in many other organisms. Yet, it has remained largely unclear what the evolutionary advantage of Sec is and why some organisms including mammals rely on selenoproteins, while others like plants and yeast utilize the easy available Cys instead. Hence, the aim of this study was to interrogate the evolutionary advantage of selenothiol-based versus thiol-based catalysis for mammals in the model enzyme GPX4 *in vivo* and *in vitro*. To this end, two mouse lines and cell lines established thereof have been generated and thoroughly analysed in this work, harboring either a catalytically inactive serine (Ser) or Cys in the active site of GPX4 in place of Sec.

# 2 Material

## 2.1 Equipment

| Equipment | Company |
|---|---|
| Abiprism 7900-HT | Applied Biosystems, Darmstadt, Germany |
| Axiovert 40 CFL Microscope | Zeiss, Jena, Germany |
| AxioCam MRc | Zeiss, Jena, Germany |
| CB150 CO2 Incubator | Binder, Tuttlingen, Germany |
| Cell Homogenizer | Isobiotec, Heidelberg, Germany |
| Centrifuge 5424R | Eppendorf, Hamburg, Germany |
| ChemiDoc Imaging system™ | Bio-Rad, Munich, Germany |
| Consort EV series power supplies | Sigma-Aldrich GmbH, Taufkrichen, Germany |
| FACS Canto II | BD GmbH, Heidelberg, Germany |
| Fluorimeter Synergy 2 | Biotek, Bad-Friedrichshall, Germany |
| High Precision Pump | Harvard Aparatus, USA |
| Inverse Labmicroscope Leica DM IL LED | Leica, Wetzlar, Germany |
| Kryostat Microm HM 560 | Thermo Scientific, Bonn, Germany |
| Leica EG1160 Embedding Center, Dispenser + hot Plate | Leica, Wetzlar, Germany |
| 1 ml Luer Lock Gas Tight Syringe | SGE Supelco, USA |
| Luminometer Centro LB 960 | Berthold |
| Microscope Axioplan 2 Imaging | Zeiss, Jena, Germany |
| Mini-PROTEAN® Tetra electrophoresis chamber | Bio-Rad, Munich, Germany |
| New Brunswick™ Innova® 42/42R Incubation shaker | Eppendorf, Hamburg, Germany |
| Hemocytometer (Neubauer chamber) | Marienfeld, Lauda Königshofen, Germany |
| Olympus confocal microscope IX81 | Olympus, Münster, Germany |
| Photometer Bio | Eppendorf, Hamburg, Germany |
| Roller 10 D | IKA Labortechnik, Staufen, Germany |
| Rotary Microtom Mikrom HM355S | Thermo Fisher, Bonn, Germany |
| Rührwerk Eurostar RW16 | IKA Labortechnik, Staufen, Germany |
| Seahorse XFe 96 Extracellular Flux Analyzer | Seahorse Bioscience Inc., North Billerica, USA |
| Sharp-R-941-BK-W-Inverter-Microwave | Sharp |
| SpectraMax M5 Microplate Reader | Molecular Device GmbH, Biberach, Germany |
| Thermomixer® C | Eppendorf, Hamburg, Germany |
| Trans-Blot Turbo Transfer System™ | Bio-Rad, Munich, Germany |
| Ultracentrifuge L70 | Beckman, Brea, USA |
| Vortex Genie 2 | Scientific Industries, Bohemia, USA |
| Waterbath VWB 12 | VWR, Radnor, USA |
| Zeiss Libra 120 Plus | Carl Zeiss NTS GmbH, Oberkochen, Germany |

## 2.2    Disposables and Kits

| Disposables and Kit | Company | Catalog-No |
|---|---|---|
| Amplex Red | Life Technologies, Karlsruhe, Germany | A12222 |
| ApopTag Fluorescein In Situ Apoptosis Detection Kit | Merck-Millipore, Darmstadt, Germany | S7110 |
| ApopTag Peroxidase In Situ Apoptosis Detection Kit | Merck-Millipore, Darmstadt, Germany | S7100 |
| ATP Bioluminiscence Assay Kit CLS II | Roche, Mannheim, Germany | 11699695001 |
| BD Trucount Tubes | BD Biosciences, USA | 340334 |
| BODIPY 581/591 C11 | Invitrogen, Karlsruhe, Germany | D3861 |
| Clarity™ Western ECL Blotting Substrate | Bio-Rad, Munich, Germany | 170-5061 |
| Cytotoxicity Detection Kit (LDH) | Roche, Mannheim, Germany | 11644793001 |
| Disposable Vinyl Specimen Molds | Weckert Labortechnik, Kitzingen, Germany | 4557 |
| Fluoresbrite® YG Microspheres 0.94 µm | Polysciences, Warrington, USA | |
| GeneRuler 1 Kb Plus DNA Ladder | Fermentas Life Science, Bonn, Germany | SM1331 |
| Gibson Assembly® Master Mix | New England Biolabs GmbH, Frankfurt, Germany | E2611S |
| Millex GP Filter 0,22 µm | Millipore, Carrighwohill, Cork, Ireland | SLGP033RS |
| Mini-Protean® TGX™ Stain Free Gels | Bio-Rad, Munich, Germany | 456-8043 |
| Monobromobimane | Sigma-Aldrich GmbH, Taufkirchen, Germany | 69898 |
| 10N-nonylacridine orange (NAO) | Invitrogen, Karlsruhe, Germany | A-1372 |
| Parafilm M® | Pechiney Plastic Packaging Company | PM996 |
| PageRuler prestained protein ladder | Thermo Fisher, Bonn, Germany | 26616 |
| Pestles (1.5 ml) | Wilmbad Lab Glass | BP-7011-015 |
| Pierce BCA Protein Assay | Thermo Fisher, Bonn, Germany | 23227 |
| Pierce 660nm Protein Assay Reagent | Thermo Fisher, Bonn, Germany | |
| Plasmid Maxi Kit | Qiagen, Hilden, Germany | 12163 |
| Plasmid Mini Kit | Qiagen, Hilden, Germany | 12125 |
| QIAGEN® PCR cloning Kit | Qiagen, Hilden, Germany | 231124 |
| QIAmp DNA FFPE Tissue Kit | Qiagen, Hilden, Germany | 56404 |
| Rhodamine 123 | Invitrogen, Karlsruhe, Germany | R302 |
| Reverse Transcription system Kit | Promega, Mannheim, Germany | A3500 |
| RNeasy Kit | Qiagen, Hilden, Germany | 74104 |
| Sep-Pak C18 Cartridge | Waters GmbH, Eschborn, Germany | WAT051910 |
| Vectashield Hard Set with DAPI | Vector Laboratories Inc, Burlingame, USA | H-1500 |
| Vectastain ABC Kit | Vector Laboratories Inc, Burlingame, USA | PK-6100 |
| Vectastain DAB Kit | Vector Laboratories Inc, Burlingame, USA | SK-4100 |
| TaqMan® Gpx4 FAM | Applied Biosystems, Darmstadt, Germany | 4331182 |

| | | |
|---|---|---|
| TaqMan® Hprt VIC | Applied Biosystems, Darmstadt, Germany | 4448489 |
| TaqMan® MT-RNRN1 FAM | Applied Biosystems, Darmstadt, Germany | 4331182 |
| Tissue Tek® Compound Embedding Medium | Weckert Labortechnik, Kitzingen, Germany | 4583 |
| Trans-Blot® Turbo Transfer Pack, PVDF | Bio-Rad, Munich, Germany | 170-4156 |
| Wizard® SV Gel and PCR Clean-up System | Promega GmbH, Mannheim, Germany | A9282 |
| X-tremeGene HP DNA Transfection Reagent | Roche Diagnostics, Mannheim, Germany | 06366236001 |
| XF 96-Well cell culture plates | Seahorse Bioscience Inc., North Billerica, USA | 1101085004 |

## 2.3   Enzymes

| Enzymes | Company | Catalog-No |
|---|---|---|
| cOmplete™ Protease Inhibitor Cocktail | Roche Diagnostics, Mannheim, Germany | 1697498 |
| Glutathion Reductase | Sigma-Aldrich GmbH, Taufkirchen, Germany | G3664-100UN |
| Herculase II Fusion DNA Polymerase | Agilent, Santa Clara, USA | 600677 |
| Horseradish Peroxidase (HRP) | Sigma-Aldrich GmbH, Taufkirchen, Germany | P8125 |
| Lipoxidase from soy bean | Sigma-Aldrich GmbH, Taufkirchen, Germany | L6632-5MU |
| Phosphatase Inhibitor Cocktail | Roche Diagnostics, Mannheim, Germany | 04906845001 |
| Proteinase K | Carl Roth GmbH & Co, Karlsruhe, Germany | 7528.1 |
| Restriction Endonucleases | New England Biolabs GmbH, Frankfurt, Germany | various |
| Superoxide Dismutase (SOD) | Sigma-Aldrich GmbH, Taufkirchen, Germany | S5394 |
| Taq DNA Polymerase | Invitrogen, Karlsruhe, Germany | 18038-026 |

## 2.4   Chemicals

| Chemical | Company | Catalog-No |
|---|---|---|
| 0.5% Eosin Y | Carl Roth GmbH & Co, Karlsruhe, Germany | X883.2 |
| 3-Aminopropyltriethoxysilane | Sigma-Aldrich GmbH, Taufkirchen, Germany | A3648 |
| 4-Hydroxy-Tamoxifen | Sigma-Aldrich GmbH, Taufkirchen, Germany | H7954 |
| 5,5′-Dithiobis(2-nitrobenzoic acid) | Sigma-Aldrich GmbH, Taufkirchen, Germany | D8130 |
| Acetic acid | Merck KGaA, Darmstadt, Germany | 1000632500 |
| Acetonitrile | Carl Roth GmbH & Co, Karlsruhe, Germany | T907.1 |
| Adenosine diphosphate (ADP) | Sigma-Aldrich GmbH, Taufkirchen, Germany | A5285 |
| Adenosine diphosphate +$K_2$ (ADP) | Fluka Chemie GmbH, Buchs, Switzerland | 01899 |
| Agarose | Invitrogen, Karlsruhe, Germany | 15510-027 |
| Ammonia | Merck KGaA, Darmstadt, Germany | A3678 |

| | | |
|---|---|---|
| Ampicillin | Sigma-Aldrich GmbH, Taufkirchen, Germany | A9518 |
| Antimycin A | Sigma-Aldrich GmbH, Taufkirchen, Germany | A8674 |
| AquaBluer® Cell Viability Assay Solution | MultiTarget Pharmaceuticals LLC, Salt Lake City, USA | 6015 |
| Auranofin | Sigma-Aldrich GmbH, Taufkirchen, Germany | A6733 |
| α-Tocopherol | Sigma-Aldrich GmbH, Taufkirchen, Germany | T3251 |
| Blasticidin S hydrochloride | Sigma-Aldrich GmbH, Taufkirchen, Germany | 15205 |
| Bovine Serum Albumin (BSA) Fraction V | Carl Roth GmbH & Co, Karlsruhe, Germany | 0163.2 |
| Bromphenol blue | Sigma-Aldrich GmbH, Taufkirchen, Germany | B0126-25G |
| Calcium chloride ($CaCl_2$) | Sigma-Aldrich GmbH, Taufkirchen, Germany | C7902 |
| Carbonyl cyanide-$\rho$-trifluoromethoxyphenylhydrazone (FCCP) | Sigma-Aldrich GmbH, Taufkirchen, Germany | C2920 |
| CHAPS | Sigma-Aldrich GmbH, Taufkirchen, Germany | C9426 |
| Diethyl ether | Sigma-Aldrich GmbH, Taufkirchen, Germany | 296082 |
| Dimethyl sulfoxide (DMSO) | Sigma-Aldrich GmbH, Taufkirchen, Germany | D2650 |
| Sodium phosphate dibasic ($Na_2HPO_4$) | Sigma-Aldrich GmbH, Taufkirchen, Germany | 30412 |
| Dipotassium phosphate ($K_2HPO_4$) | Sigma-Aldrich GmbH, Taufkirchen, Germany | |
| DMEM (1×) | Thermo Fisher, Bonn, Germany | 21969-035 |
| DNA loading dye (6 ×) | Thermo Fisher, Bonn, Germany | R0611 |
| dNTP Mix 10 mM | Thermo Scientific, Regensburg, German | R0191 |
| Doxycycline hyclate | Sigma-Aldrich GmbH, Taufkirchen, Germany | D9891-1G |
| Epon | Merck KGaA, Darmstadt, Germany | |
| Erastin | Sigma-Aldrich GmbH, Taufkirchen, Germany | E7781 |
| Ethanol | Merck KGaA, Darmstadt, Germany | 1.00983.2500 |
| Ethylendiamintetraacetatic acid (EDTA) | Sigma-Aldrich GmbH, Taufkirchen, Germany | E9884 |
| Ethylene glycol-bis(β-aminoethyl ether)-N,N,N',N'-tetraacetic acid (EGTA) | Sigma-Aldrich GmbH, Taufkirchen, Germany | 03778 |
| Fetal Calf Serum (FCS) LOT41Q6942K | Thermo Fisher, Bonn, Germany | 10270 |
| Glacial acetic acid | Sigma-Aldrich GmbH, Taufkirchen, Germany | 1005706 |
| Glucose | Sigma-Aldrich GmbH, Taufkirchen, Germany | G-6152 |
| Gutamate | Sigma-Aldrich GmbH, Taufkirchen, Germany | 49621 |
| Glutaraldehyde (2.5%) | Science Services, Munich, Germany | 15960 |
| Glycerin | Sigma-Aldrich GmbH, Taufkirchen, Germany | G8773 |
| Glycine | Sigma-Aldrich GmbH, Taufkirchen, Germany | G8898-500G |
| Goat serum | New England Biolabs GmbH, Frankfurt, Germany | 5425 |
| HEPES | Invitrogen, Karlsruhe, Germany | 15630-080 |
| Hydrochloric acid (HCl) | Sigma-Aldrich GmbH, Taufkirchen, Germany | H1758 |
| Hydrogen peroxide ($H_2O_2$) | Carl Roth GmbH & Co., Karlsruhe, Germany | 8070.2 |
| Hygromycin B | Thermo Fisher, Bonn, Germany | HY067-L7 |
| Irinotecan | Sigma-Aldrich GmbH, Taufkirchen, Germany | I1406 |
| Isopropanol | Merck KGaA, Darmstadt, Germany | 1.09634.2511 |
| L-α-Phosphatidylcholine | Sigma-Aldrich GmbH, Taufkirchen, Germany | P7443 |
| L-Buthionine-sulfoximine (BSO) | Sigma-Aldrich GmbH, Taufkirchen, Germany | B2515 |
| L-Glutamine | Invitrogen, Karlsruhe, Germany | 25030 |
| L-Glutathione (reduced) | Sigma-Aldrich GmbH, Taufkirchen, Germany | G6013 |
| L-Sulforaphane | Sigma-Aldrich GmbH, Taufkirchen, Germany | S6317 |
| Magnesium chloride ($MgCl_2$) | Sigma-Aldrich GmbH, Taufkirchen, Germany | M2393 |

| | | |
|---|---|---|
| Magnesium sulfate (MgSO$_4$) | Sigma-Aldrich GmbH, Taufkirchen, Germany | M7774 |
| Malate | Merck KGaA, Darmstadt, Germany | 8208720025 |
| Mangan chloride (MnCl$_2$) | Sigma-Aldrich GmbH, Taufkirchen, Germany | M3634 |
| Mayer`s haematoxylin | Carl Roth GmbH & Co., Karlsruhe, Germany | T865 |
| Menadione | Sigma-Aldrich GmbH, Taufkirchen, Germany | M5625 |
| Methanol | Sigma-Aldrich GmbH, Taufkirchen, Germany | 322415 |
| Mitoxantron | Sigma-Aldrich GmbH, Taufkirchen, Germany | M6545 |
| Monopotassium phosphate (KH$_2$PO$_4$) | Sigma-Aldrich GmbH, Taufkirchen, Germany | P5655 |
| 4-Morpholinepropanesulfonic acid (MOPS) | Sigma-Aldrich GmbH, Taufkirchen, Germany | M1254 |
| Mygliol | ChemTik, Berlin, Germany | CTK5E4513 |
| Myxothiazol | Sigma-Aldrich GmbH, Taufkirchen, Germany | T5580 |
| β-Nicotinamide adenine dinucleotide 2′-phosphate reduced tetrasodium salt hydrate (NADPH) | Sigma-Aldrich GmbH, Taufkirchen, Germany | N1630 |
| Nocodazole | Sigma-Aldrich GmbH, Taufkirchen, Germany | M1404 |
| Nonidet-P40 | Fluka Chemie GmbH, Buchs, Switzerland | W401404 |
| Nycodenz® | Axis-Shield, Dundee, UK | 1002424 |
| Oligomycin A | Sigma-Aldrich GmbH, Taufkirchen, Germany | O4876 |
| Paraffin wax | Polysciences, Warminster, USA | 19652 |
| Paraformaldehyde (PFA) | Carl Roth GmbH & Co, Karlsruhe, Germany | 0335.3 |
| Penicillin/Streptomycin | Invitrogen, Karlsruhe, Germany | 15140-122 |
| Phenformin hydrochloride | Sigma-Aldrich GmbH, Taufkirchen, Germany | P7045 |
| Phenol/Chloroform/Isoamyl alcohol | Carl Roth GmbH & Co, Karlsruhe, Germany | A156.2 |
| Phenylarsine oxide (PAO) | Sigma-Aldrich GmbH, Taufkirchen, Germany | P3075 |
| Phosphoric acid (H$_3$PO$_4$) | Sigma-Aldrich GmbH, Taufkirchen, Germany | P5811-500G |
| Potassium chloride | Sigma-Aldrich GmbH, Taufkirchen, Germany | 4504 |
| Protamine sulfate salt from salmon | Sigma-Aldrich GmbH, Taufkirchen, Germany | P4020 |
| Puromycine dihydrochloride | Sigma-Aldrich GmbH, Taufkirchen, Germany | P7255 |
| Rotenone | Sigma-Aldrich GmbH, Taufkirchen, Germany | R8875 |
| Rothi-Histo Kit | Carl Roth GmbH & Co, Karlsruhe, Germany | 6638.1 |
| Skim Milk powder | Sigma-Aldrich GmbH, Taufkirchen, Germany | 70166 |
| Sodium acetate | Sigma-Aldrich GmbH, Taufkirchen, Germany | S8750 |
| Sodium bicarbonate | Sigma-Aldrich GmbH, Taufkirchen, Germany | S5761 |
| Sodium chloride (NaCl) | MP Biodemicals, Eschwege, Germany | 194848 |
| Sodium citrate | Sigma-Aldrich GmbH, Taufkirchen, Germany | W302600 |
| Sodium deoxycholate | Sigma-Aldrich GmbH, Taufkirchen, Germany | D6750 |
| Sodium dodecyl sulfate (SDS) | Carl Roth GmbH & Co, Karlsruhe, Germany | 2326.2 |
| Sodium hydroxide (NaOH) | Carl Roth GmbH & Co, Karlsruhe, Germany | 6771.1 |
| Sodium lactate | Sigma-Aldrich GmbH, Taufkirchen, Germany | L7900 |
| Sodium phosphate monobasic (NaH$_2$PO$_4$) | Sigma-Aldrich GmbH, Taufkirchen, Germany | 71505 |
| Sodium pyruvate | Sigma-Aldrich GmbH, Taufkirchen, Germany | P4562 |
| Sodium selenite | Sigma-Aldrich GmbH, Taufkirchen, Germany | S5261 |
| Succinate | Sigma-Aldrich GmbH, Taufkirchen, Germany | S3674-100G |
| Sucrose | Sigma-Aldrich GmbH, Taufkirchen, Germany | 84097 |
| SYBR® Safe DNA stain | Thermo Fisher, Bonn, Germany | S33102 |
| tertiary-butyl hydroperoxide (tBOOH) | Sigma-Aldrich GmbH, Taufkirchen, Germany | C6628 |
| Trichloroacetic acid (TCA) | Sigma-Aldrich GmbH, Taufkirchen, Germany | T6399 |

| | | |
|---|---|---|
| Trishydroxymethylaminomethan (Tris) | Merck KGaA, Darmstadt, Germany | 1.08382 |
| Triton X-100 | Sigma-Aldrich GmbH, Taufkirchen, Germany | X100 |
| Triton X-100 peroxide- and carbonyl-free | Sigma-Aldrich GmbH, Taufkirchen, Germany | X100PC |
| Trypsin-EDTA | Invitrogen, Karlsruhe, Germany | 25300 |
| Tween20 | Sigma-Aldrich GmbH, Taufkirchen, Germany | P5927 |
| Vinoblastine | Science Services, Munich, Germany | E22400 |
| XF Assay Medium Modified DMEM | Seahorse Bioscience Inc., North Billerica, USA | 102365-100 |
| Xylene | Carl Roth GmbH & Co, Karlsruhe, Germany | A538.1 |

(*1S*,*3R*)-RSL3 was kindly provided by Prof. Dr. Brent Stockwell, Columbia University, New York (165).

## 2.5 Bacteria

### Bacterial strain

| | |
|---|---|
| DH5α *E.coli* | F⁻ endA1 glnV44 thi-1 recA1 relA1 gyrA96 deoR nupG Φ80dlacZΔM15 Δ(lacZYA-argF)U169, hsdR17($r_K$- $m_K$+), λ⁻ |

## 2.6 Oligonucleotides

All oligonucleotides were synthesized by Life Technologies.

| Oligonucleotides | Sequence (5´- 3´) |
|---|---|

Genotyping

| | |
|---|---|
| Cre D | CACGACCAAGTGACAGCAATGCTG |
| Cre E | CAGGTAGTTATTCGGATCATCAGC |
| Gpx4_1 (fwd) | GTTTAAGGATGGTGGTGGTAACCTGCTAG |
| Gpx4_2 (fwd) | GTGGTATCATTCAGCTTTAGAAT |
| Gpx4_3 (rev) | ACTTAGCCCATAGTCCTAAGATCAC |
| Gpx4_4 (rev) | CTCCCCTACCCGGTAGAATTAGCTTG |
| Flpe S | CTAATGTTGTGGGAAATTGGAGC |
| Flpe AS | CTCGAGGATAACTTGTTTATTGC |
| TRNAsec (fwd) | GGCGCTATGCAAATGAAGCTAC |
| TRNASec (rev) | GAGCCGGAGTGAACAAATGAACA |

Gibson cloning

| | |
|---|---|
| Gpx4 cys p442 (fwd) | CCGGTCGAATCAAGCTTATCGATACCGTCGACGGATCCTTGGATCCACTAGTAACGGC |

| Gpx4 cys p442 (rev) | TACGTAACCGGTCTCGAGACGCGTTCTAGAGAATTCTTCGTCTAGAGC TAGCCTAGGC |
| Gpx4 cys pRTSI (fwd) | CCTCCGCGGCCCCGAATTCCTGCAGATTTAAATACTAGTGGATCCCC GCGGTTCGAAACTAGTAACGGCCGCCAGTG |
| Gpx4 cys pRTSI (rev) | CATGTCTGGATCCTCTAGAACTAGGTCGACAGATCTTCTAGAGCTAG CCTAGGC |

## Sequencing

| Gpx4_mut (fwd) | CATGGTCTGCCTGGATAAGTACAGGT |
| Gpx4_mut (rev) | CTTGGAAGATACACTACACTGTACACTG |

## Single guide RNA

| TRNAsec guide (fwd) | CACCGCTCTGTCGCTAAACAGCTACGT |
| TRNAsec guide (rev) | TAAAACGTAGCTGTTTAGCGACAGAGC |

## 2.7  Antibodies

| Primary | Species | Dilution | Company | Catalog-No |
|---|---|---|---|---|
| β-actin | mouse | 1:5000 | Sigma-Aldrich GmbH, Taufkirchen, Germany | A5441 |
| ACSL4 | mouse | 1:200 | Santa Cruz Biotechnology Inc. | sc-271800 |
| Calbindin | rabbit | 1:1000 | Swant, Bellinzona, Switzerland | CB-38a |
| Calretinin | rabbit | 1:2000 | Swant, Bellinzona, Switzerland | CR7697 |
| Caspase 3 (active) | rabbit | 1:200 | Cell Signaling Technologies, Danvers, USA | 9661 |
| Citrate synthase | rabbit | 1:1000 | Novus Biologicals | NBP2-13878 |
| Complex I-V | mouse | 1:1000 | Invitrogen, Karlsruhe, Germany | 458099 |
| Complex IV | rabbit | 1:1000 | Cell Signaling Technologies, Danvers, USA | 4844 |
| Dimedone | rabbit | 1:300 | Kind gift of the Molecular Proteomics Laboratory, Heinrich Heine University Düsseldorf, Germany | |
| GFAP | rabbit | 1:200 | Cell Signaling Technologies, Danvers, USA | 12389 |
| GPX4 | rabbit | WB: 1:1000 ICC: 1:100 IHC: 1:250 | Abcam, Cambridge, USA | 125066 |
| GPX1 | rabbit | 1:1000 | Abcam, Cambridge, USA | Ab22604 |
| HA-tag | rat | 1:5 | Dr. Elisabeth Kremmer, Helmholtz Zentrum München, Germany | |
| IBAI | rabbit | 1:500 | Genetex, USA | GTX10042 |
| Parvalbumin (PV) | mouse | 1:1000 | Swant, Bellinzona Switzerland | PV235 |
| PRX 1 | rabbit | 1:1000 | Dr. Christopher Lillig, University of Greifswald, Germany | |
| PRX 3 | rabbit | 1:2000 | Dr. Christopher Lillig, University of Greifswald, Germany | |
| TXNRD1 | rat | 1:3 | Dr. Elisabeth Kremmer, Helmholtz Zentrum München, Germany | |

| | | | | |
|---|---|---|---|---|
| TXNRD2 (1C4) | rat | 1:1 | Dr. Elisabeth Kremmer, Helmholtz Zentrum München, Germany | |
| **Secondary** | **Species** | **Dilution** | **Company** | **Catalog-No** |
| α-rabbit-bio | goat | 1:250 | Vector Laboratories Inc., Burlingame, USA | BA-1000 |
| α-mouse-bio | goat | 1:200 | Vector Laboratories Inc., Burlingame, USA | BA-9200 |
| α-rabbit-HRP | goat | 1:5000 | Santa Cruz Biotechnologies, Heidelberg, Germany | SC-2030 |
| α-mouse-HRP | goat | 1:5000 | Santa Cruz Biotechnologies, Heidelberg, Germany | SC-2031 |
| α-rat-HRP | goat | 1:5000 | Dianova GmbH, Hamburg, Germany | 90553 |
| Alexa-fluor 594 α-mouse | donkey | 1:500 | Life Technologies, Karlsruhe, Germany | A11058 |
| Alexa Fluor 488 α-rabbit | donkey | 1:500 | Life Technologies, Karlsruhe, Germany | A21206 |

## 2.8 Software

| | |
|---|---|
| Adobe Illustrator CS6 | Adobe Systems, San José USA |
| Adobe Photoshop | Adobe Systems, San José, USA |
| FlowJo | FlowJo LLC, Ashland, USA |
| GraphPad Prism 5.0 | GraphPad Software Inc., USA |
| Image Lab | Bio-Rad, Munich, Germany |
| iTEM Software | Olympus Soft Imaging Solutions, Münster, Germany |
| SDS Manager | Applied Biosystems |
| Wave XF$^e$ Analyzer | Seahorse Bioscience, Ann Arbor, USA |

## 2.9 Cloning vectors

Vector Map of the lentiviral vector 442-PL1-IRES puro is shown in Figure 7 and was a kind gift from Prof. Dr. Tim Schröder (ETH, Zurich). 442-PL1-IRES puro served as a backbone for cloning the FSH-tagged Cys-Gpx4 variant. Since this plasmid is replication incompetent, a co-transfection with the third generation packaging system consisting of the plasmids pEcoEnv-IRES puro, pMDLg_pRRE and pRSV_Rev is required (see 3.3.3). The lentiviral sgRNA expression plasmid pKLV-U6gRNA(BbsI)-PGKpuro2ABFP (Addgene #50946) and lentiCas9-Blast (Addgene #52962) were used for CRISPR/Cas9 cloning. The plasmid pKLV-U6gRNA(BbsI)-PGKpuro2ABFP was used as an expression plasmid for the single guide RNAs (sgRNA), whereas lentiCas9-Blast was utilized to transduce the target cell line with Cas9. The doxycycline dependent expression vector pRTS1 was used to express a doxycycline inducible wt and Cys-Gpx4 (201).
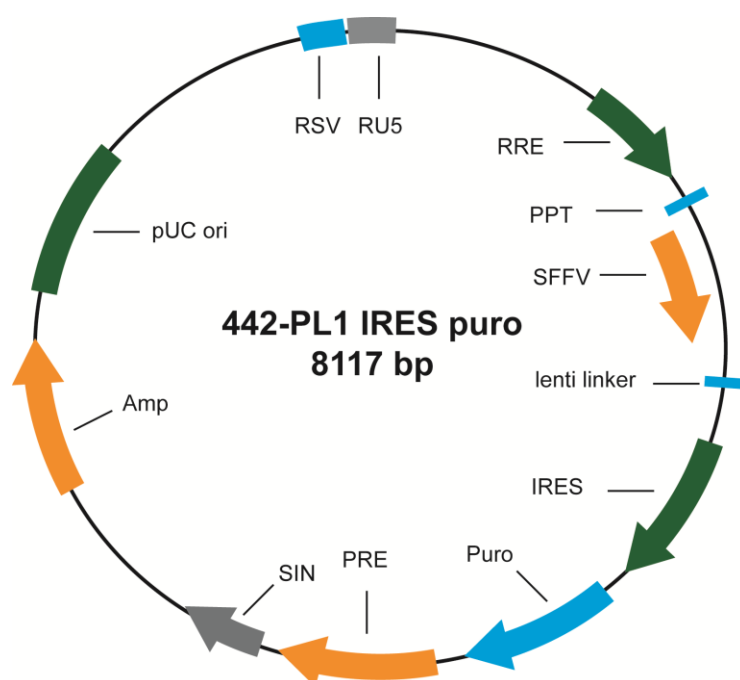
**Figure 7: Map of the transfer vector 442-PL1 IRES puro.** Based on the lentiviral HIV vector 442-PL1, the here displayed transfer vector consists of a modified and reduced viral genome, lacking the required proteins for infection and integration of the virus. The target cDNA is cloned into the lenti-linker and is expressed under the SFFV promotor after successful transduction. IRES: internal ribosomal entry site, RSV: rous sarcoma virus Promotor, RU5: RU5 LTR, RRE: rev-responsive element, PPT: polypurine tract, SFFV: spleen foci forming virus, Puro: puromycin-acetyltransferase (puromycin resistance), PRE: post-transcriptional regulatory element, SIN: self-inactivating 3' LTR, Amp: β-lactamase (ampicillin resistance), pUC ori: origin of replication.

## 2.10 Cell lines

<u>Mouse embryonic fibroblasts (MEFs):</u> MEFs were isolated from embryos from a breeding of *Gpx4^{wt/cys}* or *Gpx4^{wt/ser}* animals. The transgenic *Gpx4* allele contains a site-directed point mutation in the active site of the protein leading to the expression of a GPX4 with a serine (S, Ser) or cysteine (C, Cys) instead of a selenocysteine (U, Sec) in the active site (8).

<u>PFa1:</u> Tamoxifen-inducible *Gpx4^{flox/flox;MerCreMer}* fibroblasts, further referred to as PFa1 cells, were described before by Seiler et al. (152). Fibroblasts derived from a breeding of *Gpx4^{flox/flox}* animals carry the *Gpx4* alleles with two loxP sites flanking exons 5-7 of the gene. Cells were transfected with a pCAG-3SIP-MCM (MCM, MerCreMer) which consists of Cre recombinase and a mutated ligand binding domain of the human estrogen receptor ERT2. The stable expression of

pCAG-3SIP-MCM enables the deletion of the last three exons by TAM addition to the medium which results in a KO of the *Gpx4* gene.

FSH-tagged-Gpx4 addback: Exogenous expression of FLAG-Strep-Ha-tagged wt GPX4 in a PFa1 background further referred to as "Gpx4 addback" was described previously in Mannes *et al.* (29). PFa1 cells were transduced with a third generation lentiviral plasmid carrying the wt *Gpx4* cDNA furnished with N-terminal FLAG, Streptavidin and HA tags. Endogenous *Gpx4* was deleted by TAM administration.

Human Embryonic Kidney (HEK) 293 T cells: HEK293 T cells were utilized as packaging cell line for viral particles based on the third generation lentiviral plasmid 442-PL1 and were obtained from ATCC (293T (ATCC® CRL-3216™)).

## 2.11 Mouse lines

*Gpx4^{wt/ser}* and *Gpx4^{wt/cys}*: Mouse lines carrying a transgenic *Gpx4* allele with a site-directed mutation of Sec to either Ser (8) or Cys in the active site and a *neomycin phosphotransferase* resistance (*neo*) gene 1.5 Kbp downstream of the *Gpx4* gene. The *neo* gene is flanked by two FRT sites allowing Flpe recombinase-mediated deletion of the resistance gene. Both mouse lines were generated in the Conrad laboratory according to Ingold *et al.* (8). In brief, two vectors pPNT4.8 and pPNT4.10 (137,152) were digested with *Sal*I and *Sbf*I in order to clone the smaller fragment from pPNT4.8, containing the 5`wt sequence of the gene, into the backbone of pPNT4.10. Then, two independent PCRs were performed with one primer at a time carrying a mutation to introduce a Ser or Cys mutation in the active site of exon 3. The resulting PCR products that comprised either exon 2 and 3 or exon 3 and 4 were used for an overlapping PCR. The resulting PCR products carrying the respective point mutation were cloned into pDrive vector. DNA from the pDrive vector was transferred to a pPAF-1 yielding the targeting vector. pPAF-1 was linearized with *Sal*I and electroporated into the embryonic stem (ES) cell line IDG3.2-rosa26. ES cell clones positive for homologous insertion and the respective mutation were injected into blastocysts of *C57BL/6_DBA/2* F1 hybrid (BDF) mice and transferred into pseudo pregnant CD1 mice. Chimeric mice were backcrossed with *C57BL/6J* animals for germline transmission.

_Rosa26_Flpe_: Transgenic mouse line expressing a Flpe recombinase targeting FRT sites under the control of the Rosa26 promotor (202).

_Gpx4$^{flox/flox;Rosa26CreERT2}$_: Transgenic mouse line expressing a Tam-inducible CreERT2 recombinase targeting loxP sites flanking exons 5-7 of the _Gpx4_ gene under the control of the ROSA26 promotor (148).

# 3 Methods

## 3.1 Cell culture

### 3.1.1 Murine embryonic fibroblasts (MEFs)

Male and female mice both heterozygous for $Gpx4^{wt/cys}$ or $Gpx4^{wt/ser}$ were mated and female animals were daily checked for vaginal mucous plug. Plug-positive females were sacrificed at day 13.5 of embryonic development to establish MEFs (76). The uterus containing the embryos was removed and transferred in PBS. Single embryos were dissected from the uterus under sterile conditions. After dissecting the placenta, embryos were washed in PBS to remove maternal blood. The head and visceral organs were removed and the body trunk was minced with a scalpel in 6 cm plates. The tissue pieces were incubated with 0.05% trypsin-EDTA for 10 min at 37°C, homogenized by pipetting and centrifuged at 135 × g for 5 min. The cell pellet was resuspended with standard DMEM and plated on 6 cm plates defined as passage 0. Primary MEFs were cultured at 5% $O_2$, 5% $CO_2$ and 37°C in Standard DMEM until passage 15 as described (204). From passage 15 onwards primary MEFs were defined as immortalized and were then cultured at 20% $O_2$, 5% $CO_2$ and 37°C in Standard DMEM. Cells were split 1:3 (primary) or 1:5 (immortalized) when they reached confluency approximately every 3rd day. Subsequent *in vitro* experiments were first performed with primary cells and then repeated with immortalized ones. Genetic manipulation of cells was only performed with immortalized cells as they are easier to manipulate genetically.

PFa1 and HEK293T cell lines were cultured like immortalized MEFs at 20% $O_2$, 5% $CO_2$ and 37°C in Standard DMEM.

**Standard DMEM**: DMEM, 10% FCS, 50 µg/ml streptomycin, 50 U/ml penicillin, 1% L – glutamine

### 3.1.2 Determination of cell number

Cells were washed twice with PBS, harvested by trypsinization with 0.05% Trypsin-EDTA and resuspended with Standard DMEM. The cell suspension was collected by centrifugation at 135 × g for 5 min and the cell pellet was resuspended in 5 ml Standard DMEM. 10 µl of the cell suspension was used to determine cell number using the Neubauer chamber.

### 3.1.3 Cryoconservation and thawing of cells

For longtime storage of cell lines, cells were stored in liquid nitrogen. Cells were harvested by trypsinization when they reached approximately 80% confluency. After centrifugation the cell pellet was resuspended in Standard DMEM containing 10% DMSO and transferred to cryo vials which were stored overnight at -80°C before they were transferred to liquid nitrogen.

For thawing cells cryo-vials were placed in a waterbath at 37°C and the cell suspension was immediately transferred in 10 ml Standard DMEM after being defrosted. After centrifugation cells were seeded on 10 cm cell culture plates in Standard DMEM.

### 3.2 Methods working with DNA

### 3.2.1 Isolation of genomic DNA from mouse ear punches and MEFs

Cell pellets from harvested MEFs or ear punches from mice were lysed overnight in 250 µl lysis buffer containing 50 µg/ml proteinase K in a thermo shaker at 55°C. To separate the DNA fraction from the protein fraction, 250 µl of phenol/chloroform/isoamylalcohol was added to the lysed solution and centrifuged for 10 min at 18,400 × g at room temperature giving two phases. After centrifugation the upper aqueous phase containing the DNA was transferred into a new tube and DNA was precipitated by adding 500 µl of 100% ethanol containing 75 mM NaCl. Precipitated DNA was collected by centrifugation at 18,400 × g for 10 min at 4°C, followed by a washing step with 70% ethanol. Finally, the DNA pellet was allowed to dry at room temperature and resuspended in 100 µl TE buffer.

**Lysis buffer I**: 10 mM Tris (pH 7.6), 10 mM EDTA, 0.5% SDS, 10 mM NaCl
**Proteinase K buffer**: 50 mM Tris (pH 7.6), 5 mM EDTA (pH 8), 10 mg/ml proteinase K
**TE buffer**: 10 mM Tris, 1 mM EDTA (pH 8)

### 3.2.2 Isolation of genomic DNA from paraffin-embedded mouse embryos

For genotyping of paraffin-embedded embryos, decidua containing the embryos were collected from plug-positive heterozygous $Gpx4^{wt/ser}$ or $Gpx4^{wt/cys}$ females at different embryonic stages that were mated with heterozygous males. Paraffin

embedding and sectioning of the decidua was performed as described in chapter 3.16.2. For DNA isolation, 6-8 sections of decidua were used to scrape out embryonic tissue. The pooled material was collected in a microcentrifuge tube and 50 µl xylene was added to remove the paraffin. DNA was isolated using the QIAmp DNA FFPE Tissue Kit (Qiagen) according to manufacturer`s instructions.

### 3.2.3  Isolation of genomic DNA from mouse embryos

For genotyping embryos were collected at different embryonic stages from plug-positive heterozygous $Gpx4^{wt/ser}$ or $Gpx4^{wt/cys}$ females that were mated with heterozygous males. Freshly dissected embryos were washed twice in ice-cold PBS and transferred into a microcentrifuge tube with 40 µl lysis buffer containing 200 µg/ml proteinase K. Samples were digested for 3-4 h at 55°C in a thermo shaker followed by a heating step at 95°C for 10 min to inactivate proteinase K. Samples were briefly centrifugated and were directly used for genotyping by PCR.

**Lysis buffer II**: 20 mM Tris (pH 8.3), 50 mM KCl, 0.45% Nonidet-P40, 0.45% Tween 20, 200 µg/ml proteinase K

### 3.2.4  Isolating DNA from bacterial colonies

DNA from bacterial colonies transformed with plasmid DNA was isolated using either a Plasmid Mini or Maxi Kit (Qiagen) according to manufacturer's instructions. DNA concentration was determined using a spectrophotometer (Eppendorf).

### 3.2.5  Ligation of DNA Fragments by Gibson Cloning

Gibson cloning is a method that enables the ligation of blunt-end inserts with at least 40 bp overlapping sequence to a linearized vector (205). Digested vectors were separated by agarose gel electrophoresis and purified using the Wizard® SV Gel and PCR clean up system (Promega). To achieve overhang sequences, the fragments were amplified with specific primers in a 50 µl reaction mix containing 2 µl DNA, 0.5 µM of the respective primer, 5 × reaction buffer, 0.2 mM dNTP, 8% DMSO and Herculase II Fusion polymerase. PCR products were purified using the Wizard® SV Gel and PCR clean up system (Promega). DNA concentration was assessed by a spectrophotometer (Eppendorf). For the

ligation reaction, 100 ng of vector was used together with a 2-fold molar excess of the desired insert and 10 µl of the Gibson Assembly® Master Mix (NEB) in a total volume of 20 µl. The DNA fragments were assembled at 50°C for 15 min in a thermo cycler. 5 µl of the ligation reaction was further used for bacteria transformation.

**PCR program**: Initial denaturation: 95°C – 5 min, 9 cycles: denaturation: 95°C – 30 sec, annealing: 68°C – 1 min; -1°C/cycle, elongation: 72° - 1 min; 25 cycles: denaturation: 95°C – 30 sec, annealing: 59°C – 1 min, elongation: 72°C – 1 min, final elongation: 75° - 5 min; PCR product: 1 kb

### 3.2.6   Ligation of DNA fragments into the pDrive vector

For cloning DNA fragments into the pDrive vector the QIAGEN® PCR cloning kit (Qiagen) was used according to manufacturer`s protocol.

### 3.2.7   PCR protocol for mouse genotyping

The method of enzymatic DNA amplification was used to detect wildtype (wt) or transgenic (tg) alleles. For each mouse strain specific oligonucleotides were designed that give small PCR products of different sizes allowing the determination of the different genotypes. PCR reactions were set up in 25 µl containing 1 µl gDNA isolated from ear clips or embryos (see 3.2.1-3.2.3), 10 × PCR buffer, 1.5 mM MgCl$_2$, 0.2 mM dNTP mix, 0.5 µM of the specific primers and recombinant Taq polymerase. PCR reactions were performed in a G-Storm thermo cycler and DNA was amplified for 35 cycles. As different oligonucleotides require different annealing and elongation temperatures, the exact PCR programs with the corresponding mouse strains and primers are listed below. The resulting PCR products were separated on a 2% agarose gel (see 3.2.10).

*Gpx4*$^{wt/cys}$; *Gpx4*$^{wt/ser}$ **tg**: Primer Gpx4_2 and Gpx4_4; initial denaturation: 95°C – 5 min, denaturation: 95°C – 30 sec, annealing: 58°C - 30 sec, elongation: 72° - 30 sec, final elongation: 75° - 5 min; tg: 203 bp, wt: no product

*Gpx4*$^{wt/cys}$; *Gpx4*$^{wt/ser}$ **wt**: Primer Gpx4_1 and Gpx4_3; initial denaturation: 95°C – 5 min, denaturation: 95°C – 30 sec, annealing: 60°C - 30 sec, elongation: 72° - 30 sec, final elongation: 75° - 5 min; wt: 256 bp; tg: no product

**Gpx4 Cys flpe; Gpx4 Ser flpe**: Primer Gpx4_1 and Gpx4_3; inital denaturation: 95°C – 5 min, denaturation: 95°C – 30 sec, annealing: 60°C - 30

sec, elongation: 72° - 30 sec, final elongation:75° - 5 min; tg: 310 bp, wt: 256 bp

***Gpx4^{cys/fl}***; ***Gpx4^{ser/fl}***: Primer Gpx4_1 and Gpx4_3; inital denaturation: 95°C – 5 min, denaturation: 95°C – 30 sec, annealing : 60°C - 30 sec, elongation: 72° - 30 sec, final elongation: 75° - 5 min; tg/floxed: 310 bp, wt: 256 bp

**Flpe**: Primer: Flpe S and Flpe AS; initial denaturation: 95°C – 5 min, denaturation: 95°C – 30 sec, annealing: 59°C - 30 sec, elongation: 72° - 1 min, final elongation: 75° - 5 min; product:~500 bp

**Rosa26CreERT2**: Primer CreD and CreE; initial denaturation: 95°C – 5 min, denaturation: 95°C – 30 sec, annealing: 63°C - 30 sec, elongation: 72° - 30 sec, final elongation: 75° - 5 min; product: ~500 bp

### 3.2.8   PCR for sequencing

PCR products that were used for sequencing required amplification with a proof reading polymerase and a scale-up PCR reaction mix. Therefore, the PCR reaction was set up in 50 µl containing 3 µl DNA, 0.5 µM of the respective primers, 5 × reaction buffer, 0.2 mM dNTP, 8% DMSO and Herculase II Fusion polymerase. PCR products were purified using the Wizard® SV Gel and PCR clean up kit (Promega) according to manufacturer's instructions.

**PCR program**: Primer: Gpx4_mut (fwd) and (rev); initial denaturation: 95°C – 5 min, denaturation: 95°C – 30 sec, annealing: 61°C – 30sec, elongation: 72°C – 45 sec, final elongation: 72°C – 5 min; product: 350 bp

### 3.2.9   Restriction digestion

Restriction enzymes were obtained from New England Biolabs GmbH and were used to prepare DNA for cloning. Restriction reactions were set up in 20 – 50 µl according to manufacturer`s instructions. Digested DNA was analysed by agarose gel electrophoresis, isolated with a scalpel from the gels and purified using Wizard® SV Gel and PCR Clean-Up System (Promega). DNA concentration was assessed using a spectrophotometer (Eppendorf).

### 3.2.10 Agarose gel electrophoresis

Agarose gel electrophoresis is a general method to separate DNA fragments according to their size. Depending on the size of the DNA fragments a 0.8%, 1% or 2% agarose gel was prepared of agarose in 1 × TAE buffer containing SYBR®

Safe DNA stain in a ratio of 1:10000. The gel was placed in a gel running chamber filled with 1 × TAE buffer. DNA samples were mixed with 6 × DNA loading dye and pipetted into gel pockets. An electric field was applied to enable the separation of the DNA fragments. The ChemiDoc™ UV transilluminator (Bio-Rad) was used for the visualization of the DNA fragments in the gel.

**TAE buffer (10 ×)**: 200 mM Tris, 100 mM sodium acetate, 6 mM EDTA (pH 7.5)

### 3.2.11 Cloning of new vectors

Cloning *cys-Gpx4* into 442-PL1-IRES-puro viral expressing vector: The third generation viral plasmid 442-PL1-IRES-puro (a kind gift from Prof. Dr. Timm Schröder, ETH Zurich) was used to express a Flag-Strep-HA-tagged Cys variant of Gpx4 (further referred to as U46C) using Gibson cloning (see 3.2.5). Therefore, 442-PL1-IRES-puro plasmid was first digested with *Xba*I at 37°C for 1 h, then *Bstb*I was added and the temperature was raised to 65°C for another hour. The tagged *Gpx4* cDNA with a mutation of the Sec to Cys codon was obtained as a GeneArt® String™ from Invitrogen (see Sequence in supplementary fig. 1). The DNA sequence was codon-optimized for protein production and flanked by B*stb*I and X*ba*I restriction sites. The gene string was amplified with primers to add ~40 bp homology to each end of the digested 442-L1-IRES-puro vector.

Cloning *cys-Gpx4* into pRTSI: For a doxycycline-inducible expression of cys-Gpx4 the plasmid pRTSI (201) was digested with *Swa*I at 25°C for 1 h, then *Bgl*II was added and temperature was raised to 37°C for another hour. To perform Gibson cloning (see 3.2.5), the cys-Gpx4 was amplified to gain a ~40 bp overlapping sequence to each end of the linearized vector backbone.

Cloning *n-TUtca2* (*Trsp*) guide into single guide (sg) RNA plasmid: For the generation of cell lines with a stable expression of sgRNAs, the lentiviral pKLV-U6gRNA(BbsI)-PGKpuro2ABFP vector (Addgene) was used. To clone the guide sequence (~20-21 bp) that represents the CRISPR target into the vector, pKLV-U6gRNA(BbsI)-PGKpuro2ABFP was digested with the restriction enzyme *Bbs*I. Therefore, 5 µg vector DNA was linearized with *Bbs*I for 1.5 h at 37°C in a 100 µl reaction mix. The digested vector was separated on a 1% agarose gel, extracted from the gel using Wizard® SV Gel and PCR clean up system (Promega) and DNA concentration was determined using the spectrophotometer (Eppendorf).

New CRISPR guides were designed with the help of the platform *http://www.crisprscan.org/*. To clone the guide into the linearized vector, two oligos per guide (forward and reverse) were ordered consisting the guide sequence (20 bp) and overhangs (red) matching the digested backbone at the restriction site:

Forward oligo: CACC(G)N20GT

Reverse oligo: TAAAACN20(complementary to forward oligo)(C)

Lyophilized oligos were dissolved in $dH_2O$ at a final concentration of 100 µM. To gain small fragments of double stranded oligos that can be ligated with the digested vector, 1 µM of the forward and reverse oligo stock was added to 100 µl of 1 × TE buffer and heated to 100°C for 5 min. Oligos were allowed to anneal by cooling down to room temperature before using them in a ligation reaction with pKLV-U6gRNA(BbsI)-PGKpuro2ABFP yielding a pKLV-U6gRNA(guide)-PGKpuro2ABFP vector. For the ligation, 50 ng linearized vector was mixed with 4 µl oligos in 15 µl reactions at 4°C overnight.

## 3.3 Gene transfer methods

### 3.3.1 Transformation of chemically competent bacteria

For bacterial transformation the *E.coli* strain DH5α was used. Bacteria were stored at -80°C and thawed on ice when needed. 50 µl of thawed cells were mixed with 2 µl plasmid DNA and incubated on ice for 15 min. Heat shock (42°C) was applied for 2 min to enhance the uptake of the plasmid, and then bacterial cell suspension was immediately placed on ice. After adding 750 µl of LB medium, bacteria were incubated for 20 min at 37°C. Next, bacterial cells were centrifugated (210 × g, 1 min), supernatant was removed, cell pellet was resuspended in the residual medium and cells were seeded on a LB agar plate containing the corresponding antibiotics for selection.

**LB Agar**: 20 mM $MgSO_4$, 10 mM KCl, 1% (w/v) Trypton, 0.5% (w/v) bacto yeast extract, 0.5% (w/v) NaCl, 1.2 % bacto agar

### 3.3.2 Lipofection

Transfection of doxycycline-dependent pRTSI vector containing the *cys-Gpx4* cDNA into immortalized MEFs was conducted via lipofection using the X-tremeGene HP DNA Transfection Reagent. To this end, $5 \times 10^4$ cells were seeded on a 6-well plate and were allowed to attach overnight. On the next day, 200 µl of FCS-free DMEM was mixed with 2 µg plasmid DNA and X-tremeGene HP DNA Transfection Reagent in a ratio of 1:3 (DNA:reagent). The solution was incubated for 15 min at room temperature and applied dropwise to the cells after medium change. MEFs were incubated for 72 h before initiating the selection with hygromycin (250 µg/ml final) on a 15 cm cell culture plate.

PFa1 cells transfected with pRTSI-cys-Gpx4 were selected with hygromycin (250 µg/ml) and TAM (1 µM) in the presence of 1 µg/ml doxycycline. Expression of the GPX4 protein was checked by immunoblot analysis.

### 3.3.3 Viral transduction

Viral transduction was performed using third generation lentiviral vectors (lentiCas9-Blast, 442-PL1-IRES-puro and pKLV-U6gRNA(BbsI)-PGKpuro2ABFP based vectors) together with the third generation packaging system containing pEcoEnv-IRES-puro (ecotropic envelope and glycoprotein), pMDLg_pRRE (structural protein Gag and enzyme cluster Pol) and pRSV_Rev (post-transcriptional regulation protein Rev). HEK293T cells were used to produce replication-incompetent viral particles which can only infect rodent cells due to their ecotropic envelope proteins. To this end, HEK293T cells were seeded to reach 70% confluency after overnight incubation. Cells were co-transfected with the transfer vector and the vectors from the packaging system in a fixed molar ratio (5:2:10:5) by lipofection (3.3.2). 72 h after transfection supernatant containing viral particles was collected from the HEK293T cells and sterile filtered using a 45 µm low protein binding syringe filter. Target cells were trypsinized and seeded on 6-well plates containing a 1:1 dilution of the infectious supernatant supplemented with 8 µg/ml protamine sulfate to enhance viral transduction. Selection with the corresponding antibiotics started 48 h after transduction.

## 3.4    RNA-relevant methods

### 3.4.1   RNA isolation

Approximately 80% confluent cell culture plates were trypsinized and collected by centrifugation. Cell pellets were lysed for RNA isolation using the RNeasy Mini Kit (Qiagen) as described in the manufacturer's protocol.

### 3.4.2   cDNA synthesis

Isolated RNA was quantified by spectrophotometry (Eppendorf). 2 µgRNA were used for cDNA synthesis utilizing the Reverse Transcription System Kit (Promga) according to manufacturer`s instructions.

### 3.4.3   Quantitative real time PCR

For the determination of *Gpx4* mRNA levels and mitochondrial RNA (mtRNA) in MEFs, quantitative real-time (qRT) PCR was performed using the TaqMan® gene expression assay according to manufacturer`s instructions (Applied Biosystems). To be able to include the target cDNA and the housekeeping control *hypoxanthin-phosphoribosyl-transferase-1* (HPRT) in the same PCR reaction, different dye-labeled probes were used together with the cDNA, cDNA-specific primers and the TaqMan® Master Mix in a 20 µl reaction mix. Quantitative real-time PCR was conducted in triplicates at the Abiprism 7900-HT sequence detective system (Applied Biosystems). Data analysis was performed using the software SDS RQ Manager (Applied Biosystems).

## 3.5    Protein-related methods

### 3.5.1   Protein purification from MEFs and tissues

For protein extraction whole cells were directly lysed with LCW lysis buffer in the presence of proteinase and phosphatase inhibitors (both Roche) on cell culture plates using cell scrapers. Lysed cell homogenate was mixed by vortexing and incubated on ice (30 min). Freshly dissected tissues were frozen in liquid nitrogen and stored at -80°C until required. For protein extraction, tissue was transferred in 1 ml LCW lysis buffer, homogenized using the Eurostar RW16 (IKA-Labortechnik) and incubated on ice for 30 min. Cell debris and nucleus were removed by centrifugation (18,400 × g, 4°C, 30 min). The supernatant was transferred to a new tube and used for protein quantification using the Pierce

BCA Protein Assay Kit (Thermo Scientific) according to manufacturer`s instructions. 6 × loading buffer was added to 20 µg of the protein samples stored at -20°C.

**LCW lysis buffer**: 0.5% TritonX-100, 0.5% sodium deoxycholate salt, 150 mM NaCl, 20 mM Tris, 10 mM EDTA, 30 mM sodium pyrophosphate, 1% phosphatase inhibitor, 1% protease inhibitor cocktail

**6 × loading buffer**: 375 mM Tris, pH 6.8, 9% SDS, 50% glycerol, 9% β-mercaptoethanol, 0.03% bromophenol blue

### 3.5.2 Sodium dodecyl sulfate (SDS) polyacrylamide gel electrophoresis (PAGE)

Protein samples were boiled for 5 min at 95°C, applied to precast 12% SDS Mini-PROTEAN® TGX™ Stain-Free Protein Gels (Bio-Rad) and separated by size at 100V. Proteins were allowed to separate for ~1.5 h in a Mini-PROTEAN® Tetra (Bio-Rad) electrophoresis chamber in the presence of 1 × running buffer. Protein ladder (Prestained Protein Page Ruler) was used along with the protein samples to determine the size of the proteins. After gel electrophoresis SDS gel was removed from the plastic scaffold and transferred on a Trans-Blot® Turbo™ PVDF (polyvinylidene difluoride) membrane (Bio-Rad) to perform western blot analysis.

**Running buffer (10 ×)**: 250 mM Tris-HCl, 2.5 M Glycine, 1% SDS

### 3.5.3 Western blot analysis

For immunoblot analysis the SDS gel was transferred to a ready to use Trans-Blot® Turbo™ PVDF membranes (Bio-Rad) and protein transfer was conducted using the standard program (30 min, 25 V, 1 A) in the semi-dry Trans-Blot® Turbo™ Transfer System (Bio-Rad). Afterwards, membranes were blocked in blocking solution (depending on antibody requirements) for ~1 h under constant shaking at room temperature. Next, primary antibody was applied to membranes diluted according to manufacturer`s protocol in the corresponding blocking solution for an overnight incubation at 4°C. Then, primary antibody was removed and membranes were washed 3 times (~10 min) with TBST before applying horseradish peroxidase (HRP)-conjugated secondary antibody for ~1.5 h diluted in the corresponding blocking solution. Membranes were washed again 3 times

with TBST before antibody signal was visualized by application of Clarity™ Western ECL Blotting Substrate (Bio-Rad) using the ChemiDoc™ Imaging system (Bio-Rad) for visualization. If required membranes were washed with TBST and antibody binding was resolved by applying 0.5 M NaOH to the membrane for 7 min to allow binding and detection of different antibodies. If necessary protein bands were quantified using the ImageLab software (Bio-Rad).

**TBS (10 ×)**: 1.5 M NaCl, 250 mM Tris, (pH 7.4)
**TBST**: 1 × TBS, 0.1% Tween, 900 ml dH$_2$O
**Blocking buffer**: TBST, 5% BSA/ 5% skim milk/ 1% BSA + 5% skim milk

## 3.6    CRISPR/Cas9 technology

To knockout specific genes using the CRISPR/Cas9 technology, CRISPR guides were first cloned into the lentiviral pKLV-U6gRNA-PGKpuro2ABFP vector as aforementioned (see 3.2.11). Before transducing MEFs with the pKLV-U6gRNA-PGKpuro2ABFP vector carrying the CRISPR target sequence, immortalized MEFs were first transduced with lentiviral particles carrying Cas9-Blast (Addgene) (see 3.3.3). Two days after transduction cells were selected for two weeks with 10 µg/ml blasticidin. Cas9-positive cells were then utilized for further transduction with pKLV-U6gRNA-PGKpuro2ABFP vector carrying the CRISPR guide of interest. Two days after transduction selection for positive cells was started using 2.5 µg/ml puromycin. After selection cells were seeded at a very low density (~100 cells/15 cm plate) and single cell colonies were allowed to form. Single cell clones were picked and analysed for CRISPR/Cas9 mediated changes in the targeted gene by PCR and sequence validation. For the detection of CRISPR/Cas9-mediated deletion/insertion, the online tool TIDE (Tracking of Indels by DEcomposition (www.tide.nki.nl)) was used. Positive cell clones with a KO in the gene of interest were additionally confirmed by immunoblot analysis with and without sodium selenite supplementation (100 nM).

## 3.7    Flow Cytometry

### 3.7.1   Quantification of protein thiols in sperm

Freshly collected spermatozoa from caput epididymis, cauda epididymis and vas deferens (see 3.16.1) were collected by centrifugation (5,000 × g, 10 min, 4°C)

and resuspended in 1 ml PBS. For free protein thiol staining, 1 mM monobromobimane was added to the cells and incubated for 30 min in the dark (room temperature). Labeled cell suspension was washed twice with PBS and resuspended in 1 ml PBS. Free thiols were assessed by measuring the fluorescent signal of labeled sperm by flow cytometry using the 452 nm laser and BD FACS Canto II (BD Bioscience). Data analysis was conducted using FlowJo software.

### 3.7.2 Assessment of lipid peroxidation

$1 \times 10^5$ cells were seeded on 10 cm plates and were allowed to attach overnight. The following day cells were either treated with $H_2O_2$ alone (1 h) or after pre-incubation with liproxstatin-1 for 30 min at the indicated concentrations. C11-BODIPY (581/591) (1 µM) was applied to the cells for 15 min. Afterwards, cells were harvested by trypsinization, washed twice with PBS and resuspended in 500 µl PBS for flow cytometry analysis. Lipid peroxidation was assessed by monitoring a fluorescence change of the fluorophore C11-BODIPY (581/591) using the 488 nm laser of the flow cytometer BD FACS Canto II (BD Bioscience). For data analysis with the FlowJo Software at least 10,000 cells were measured per sample.

## 3.8    Cell viability assays

### 3.8.1    AquaBluer® method

To test the sensitivity of MEFs towards cytotoxic and genotoxic compounds, cells were seeded in a 96-well plate (2000 cells/well) and incubated overnight. The following day, cells were treated with increasing concentrations of different compounds including (*1S*,*3R*)-RSL3, tertiary-butyl hydroperoxide (tBOOH), cholersterol hydroperoxide (ChOOH), hydrogen peroxide ($H_2O_{2)}$, menadione, antimycin A, rotenone, phenformin, myxothiazol, Carbonyl cyanide-ρ-trifluoromethoxyphenylhydrazone    (FCCP),    irinotecan,    vinoblastine, mitoxantrone, phenylarsine oxide (PAO), sulforaphane, auranofin, erastin and BSO. For treatment with cell death inhibitors, cells were pre-incubated for 2 h with different cell death inhibitors (necrostatin-1(S), ferrostatin-1, liproxstatin-1, ciclopirox olamine, α-Toc and Z-VAD-FMK) before cell death was elicited using the aforementioned compounds. To determine cell viability, AquaBluer® was

added to the cells 48-72 h after treatment (1:100) and fluorescence of the reagent was measured at 562 nm using the SpectraMax microplate reader (Molecular Device GmbH). Due to its characteristics as a redox-sensitive probe, AquaBluer® enters the cells in an oxidized state and gets reduced by electrons such as NADPH and $FADH_2$ derived from active mitochondria resulting in a color change of the medium from blue to pink. Therefore, AquaBluer® is solely an indicator for cell viability (actually metabolism) and not a direct approach to determine cell death.

### 3.8.2  Lactate dehydrogenase (LDH) release method

For a direct assessment of cell death LDH release was measured in cells treated with $H_2O_2$ and rotenone for given times using the Cytotoxicity Detection (LDH) Kit (Roche Diagnostics) according to manufacturer`s instructions. Therefore, MEFs were seeded ($5 \times 10^4$) in 6-well plates and treated with 100 µM $H_2O_2$ and 1 µM rotenone for given times. Aliquots of the cell culture medium were taken after certain time points and cell death was determined by measuring LDH content. For normalization, cells were additionally treated with Triton X-100, to release LDH from all cells.

### 3.9  Labeling of cells with $^{75}$Se

### 3.9.1  Labeling primary MEFs with $^{75}$Se

This experiment was conducted by the group of Prof. Elias Arnèr (Karolinska Institutet, Sweden). Labeling of cells with $^{75}$Se-radioisotope was performed as described previously (206), with minor modifications. Cells were seeded and incubated with 1 µCi/ml $^{75}$Se-labeled selenite (Research Reactor Center) for 48 h. Proteins of clarified supernatants of cell lysates were subsequently fractionated on reducing SDS-PAGE (buffers, gel and equipment from Invitrogen) and transferred onto nitrocellulose membrane using iBlot Dry Blotting System (Thermo Fisher Scientific). Ponceau S staining was performed to ensure equal loading. The membrane was thereafter exposed to a phosphor screen and autoradiography was finally visualized with a Typhoon FLA 7000 (GE Healthcare Life Sciences).

### 3.9.2  Labeling MEFs with induced *Trsp* KO with $^{75}$Se

The following experiment was performed by the group of Prof. Ulrich Schweizer (University of Bonn). Confluent cell plates, seeded the day before, were labeled overnight using 10 µCi/plate of $^{75}$Se. After labeling, medium was removed and plates were washed twice with cold 1 × PBS. Cell lysates were collected in RIPA buffer and quantified using the BCA method. 25 µg of protein extract were separated on a SDS-PAGE gel. The gel was stained with Comassie brilliant blue to show equal loading. After drying, the gel was exposed for one day to a Phosphoimager screen, which was developed by a BAS-1800 II Phosphoimager (Fujifilm).

**RIPA buffer**: 50 mM Tris-HCl pH 7.5, 150 mM NaCl, 1% NP-40, 0.25% sodium deoxycholate, 1 mM DTT and protease inhibitors.

### 3.10   Detection of the redox state of GPX4

Experiments addressing the detection of the redox state of GPX4 were conducted by Drs. Carsten Berndt and Gereon Poschman (University of Düsseldorf).

### 3.10.1 Preparing samples

For Western blot-based detection of sulfenic acid, 70% confluent cells expressing GPX4 addback or GPX4 U46C were either only treated with 5 mM dimedone for 120 min or with 100 µM $H_2O_2$ for 180 min and addition of 5 mM dimedone 120 min after $H_2O_2$ challenge. For detection of sulfonic acid by mass spectrometry, cells were seeded at a density of 70 %, incubated overnight and treated the following day with 100 µM $H_2O_2$ for 180 min. Cells were washed in washing buffer and treated with lysis buffer for protein purification. GPX4 was isolated using 200 µg of anti-flag M2 magnetic beads. SDS-PAGE and Western transfer was performed as described previously (see 3.5.2 and 3.5.3). Dimedone and GPX4 (HA-antibody) were visualized by using secondary antibodies conjugated with infrared fluorescent dyes and an Odyssey infrared scanner (Li-Cor). Intensity of signals was quantified using Image J.

**Washing buffer**: PBS containing 100 mM N-ethyl-maleimide (NEM)
**Lysis buffer**: 50 mM Tris (pH 7.4), 150 mM NaCl, 0.5% Nonidet-P40, 100 mM NEM and protease inhibitor

## 3.10.2 Mass spectrometry of isolated protein samples

For mass spectrometry GPX4 containing bands were excised and processed with a few modifications as described recently (207). Three samples per group were individually processed and measured. Briefly, samples were washed, alkylated as a control for yet unreacted cysteines with 55 mM iodoacetamide in a 50 mM ammonium hydrogen carbonate containing aqueous solution, and digested with 0.066 µg trypsin (Serva) in a 100 mM ammonium hydrogen carbonate containing aqueous solution overnight at 37°C. Resulting peptides were extracted from the gel with 1:1 (v/v) 0.1 % trifluoroacetic acid (TFA)/acetonitrile. After vacuum concentration peptides were resuspended in 34 µl 0.1% TFA and analysed with liquid chromatography coupled electrospray ionization mass spectrometry. Here, peptides were separated on an UltiMate 3000 RSLCnano chromatography system (Thermo Fisher Scientific). Initially, peptides were pre-concentrated on a 2 cm long trap column (Acclaim PepMap100, 3 µm C18 particle size, 100 Å pore size, 75 µm inner diameter, Thermo Fisher Scientific) for 10 min at a flow rate of 6 µl/min with

0.1% (v/v) TFA as mobile phase and subsequently separated on a 25 cm long analytical column (Acclaim PepMapRSLC, 2 µm C18 particle size, 100 Å pore size, 75 µm inner diameter, Thermo Fisher Scientific) at 60°C using a 54 min gradient from 4 to 40% solvent B at a flow rate of 300 nl/min. The amount of solvent B was increased to 95% within one minute and held at 95% for an additional 4 min. Separated peptides were analysed with a Q Exactive plus hybrid quadrupole-orbitrap mass spectrometer (Thermo Fisher Scientific) coupled to the liquid-chromatography system via a nano electrospray ionization source equipped with distal coated SilicaTip emitters (New Objective). The instrument was operated data dependently in positive mode, the spray voltage was between 1.4 and 1.8 kV and the capillary temperature between 250 and 275°C. First, survey scans were recorded in the orbitrap in profile mode over a mass range from 200 – 2000 m/z at a resolution of 70000 (at 400 m/z) with the target value for automatic gain control set to 3000000 and the maximum ion time to 50 ms. Second, up to twenty > 1 charged precursor ions were selected within an 4 m/z isolation window, fragmented by higher-energy collisional dissociation (HCD) in the HCD cell of the instrument and MS/MS spectra recorded within the orbitrap analyzer over an available scan range of 200 to 2,000 m/z at a resolution of

17,500 (at 400 m/z) in profile mode. The target value for automatic gain control was 100,000 and the maximum ion time 50 ms; already fragmented ions were excluded from further fragmentation for 10 sec. Mass spectra were further processed within the Proteome Discoverer framework (version 1.4.1.14, Thermo Fisher Scientific) with standard parameters for spectrum selection. Searches were carried out in a modified version (in entries O70325 and Q91XR9 U converted into C) of the mouse SwissProt database (downloaded on 21$^{st}$ October 2015 from UniProt KB, containing 15660 entries) using the embedded Mascot search engine (version 2.4.1, Matrix Science) with following parameters: tryptic cleavage specificity, maximal one missed cleavage site, 10 ppm precursor mass tolerance, 10 mmu fragment mass tolerance. Methionine oxidation and following modifications at cysteines were considered as variable modifications: dioxidation, trioxidation, glutathione, N-ethylmaleimide and carbamidomethyl. Identifications were accepted at a false discovery rate of 1% using the 'fixed value PSM validator' node. Precursor ion quantification of modified variants of the peptide GFVCIVTNVASQCGK was subsequently carried out in Skyline (version 3.5.0.9.3.1.9, MacCoss Lab, University of Washington) and resulting peak areas from doubly and triply charged precursor ions normalized to signals from the three unmodified GPX4 peptides TDVNYTQLVDLHAR, EFAAGYNVK and FLIDK.

**Solvent A**: 0.1% (v/v) formic acid in water

**Solvent B**: 0.1% (v/v) formic acid, 84% (v/v) acetonitrile in water

## 3.11  GPX4-specific enzyme activity

### 3.11.1 Substrate preparation

Phosphatidylcholine hydroperoxide (PCOOH) was used as a specific substrate for GPX4 activity measurements. For the generation of the substrate, phosphatidylcholine (PC) was oxygenated by the enzyme lipoxidase in the presence of deoxycholate. To this end, L-α-phophatidylcholine from soy bean was dissolved in 0.2 M Tris (pH 8.8) containing 0.2 M sodium deoxycholate salt. For the oxygenation step, 5 mM PC and 13000 U/ml lipoxidase were incubated for 45 min under constant stirring at room temperature in a substrate solution. For substrate purification, the whole solution was loaded on reverse phase Sep-Pak

C18 cartridges (Waters GmbH). Prior to loading the cartridge was equilibrated with elution buffer consisting of 90% methanol and 10% acetonitrile, followed by a washing step with 10 ml $dH_2O$. After substrate was loaded on the cartridge, it was washed again with $dH_2O$ and finally eluted in 1.5 ml elution buffer. PCOOH was stored at -20°C in a glassware tube where it is stable for several months. During storage a white precipitate may appear. This is residual deoxycholate, which was not removed during the purification steps but can be eliminated from the substrate solution by centrifugation.

**Substrate solution**: 0.2 M Tris (pH 8.8), 5 mM sodium deoxycholate salt

**Elution buffer**: 90% methanol, 10% acetonitrile

### 3.11.2 Activity measurements

GPX4 activity was assessed using a GPX4-specific substrate in an enzymatically coupled test in crude whole cell lysates as described in (208). To this end, cells were seeded on 15 cm plates and were allowed to gain ~80% confluency before they were harvested by trypsinization. Cell pellets were washed twice with PBS and stored at -80°C to preserve enzymatic activity. Freshly dissected tissue was snap frozen in liquid nitrogen and stored at -80°C. Cell pellets were resuspended in 100 µl lysis buffer and tissue was transferred in 300 µl lysis buffer followed by homogenization with 50 pestle strokes. After 15 min incubation in lysis buffer on ice, homogenate was centrifuged (4°C, 10 min, 18400 × g) and supernatant was transferred to a new tube. For activity measurement, 50 µl of protein supernatant from cells and 10 µl from tissue were added to a reaction mix consisting of 1 ml assay buffer, NADPH, 3 mM GSH, 0.6 U/ml glutathione reductase and 20-30 µM phosphatidylcholine hydroperoxide (PCOOH). GPX4 activity is determined by measuring the spectrometric decrease of 200 µM NADPH at 340 nm min after being oxidized by glutathione reductase to allow the recovery of oxidized GSH which gets oxidized by GPX4 after substrate reduction. For normalization, protein concentration of the samples was measured using the Pierce 660 nm Protein Assay Reagent (Thermo Fisher) according to manufacturer`s instructions. Both measurements were conducted at the SpectraMax microplate reader (Molecular Device GmbH).

**Protein lysis buffer**: 100 mM $KH_2PO_4/K_2HPO_4$ (pH7.4), 150 mM KCl, 0.05% CHAPS, 2 mM β-mercaptoethanol, 1% protease inhibitors cocktail.

**Assay buffer**: 100 mM Tris (pH 7.8), 5 mM EDTA, 0.1% Triton X-100 (peroxide free), 3 mM GSH

## 3.12    Determination of total intracellular GSH level

Cells were seeded on 6-well plates ($1 \times 10^5$) and incubated overnight. On the next day, cell culture medium was discarded and cells were washed twice with ice-cold PBS. 5% trichloroacetic acid (TCA) was applied to the cells to allow permeabilization of the membrane and the release of small molecules, such as GSH. Solution was collected in a tube and treated with ether to remove TCA. The assessment of total GSH level is based on the catalytic activity of GSH to reduce 5,5'-dithiobis(2-nitrobenzoic acid) (DTNB) to 2-nitro-5-thiobenzoate ($TNB^-$) at the expense of NADPH (209). To this end, 500 µl GSH sample was mixed with 1.2 ml assay buffer, 4 mg/ml DNTP, 1 IU GR and 3.62 mg/ml NADPH. GSH content is defined by the intensity of color change from DTNB to $TNB^-$ within a period of 5 min at 412 nm absorbance. To calculate GSH content per mg protein, cells were treated after TCA extraction with 0.5 M NaOH overnight for cell membrane destruction and protein release. Proteins quantification was performed using the Pierce BCA Protein Assay Kit (Thermo Scientific) as described in manufacturer's protocol.

**GSH assay buffer**: 0.2 M $K_2HPO_4$, 0.2 M $KH_2PO_4$, 10 mM EDTA, (pH 7.2)

## 3.13    Mitochondria-related techniques

### 3.13.1 Isolation of mitochondria from cultured MEFs

$20-25 \times 10^6$ MEFs were trypsinized and collected by centrifugation. The cell pellet was resuspended in isolation buffer given a concentration of ~$5 \times 10^6$ cell/ml. Cell homogenization was conducted using the pump controlled cell rupture system (PCC) that allows a speed rate-controlled isolation of mitochondria through a defined clearance by using a tungsten carbide ball of defined diameter (210). Cell suspension was pumped through the homogenizer with a clearance of 6 µm with 7 strokes at a speed rate of 700 µl/min. To remove cell debris and nuclei, homogenate was centrifuged at 800 × g (5 min, 4°C). Mitochondria were collected

at 9000 × g (10 min, 4°C) and resuspended in fresh isolation buffer. For further purification of the mitochondrial fractions, mitochondria were loaded on a 12%/24% Nycodenz® gradient and centrifuged in an ultracentrifuge (Beckman, SW55Ti; 30000 rpm, 15 min, 4°C). Mitochondria were collected from the interphase and washed once with isolation buffer (9000 × g, 10 min, 4°C). Concentration was determined by quantifying mitochondrial protein concentration using the Bradford assay. Isolated and purified mitochondria were either used for further functional studies or for immunoblotting.

**Isolation buffer**: 300 mM sucrose, 5 mM TES, 200 µM ethyleneglycoltetraacetic acid (EGTA), (pH 7.2)

### 3.13.2 Determining the number of mitochondria by flow cytometry

Determining the number of mitochondria by flow cytometry requires staining of mitochondria and two internal standards that can be distinguished from stained mitochondria by fluorescence and sidewards scatter (SSC) (211). Therefore, TruCOUNT™ beads and Fluoresbrite® microspheres (diameter 0.94 µm) were used for the measurement. Mitochondria were isolated from cultured cells and purified on a Nycodenz® gradient (see 3.13.1). Mitochondrial suspension was diluted to 0.1 µg/ml and stained with 10 nM (final concentration) N-nonyl acridine orange (NAO). 500 µl of stained mitochondria were mixed with a defined number of TruCOUNT™ beads and 20 µl of premixed Fluoresbrite® microspheres. Then, a first measurement determined the concentration of Fluoresbrite® microspheres in a defined volume by the number of TruCOUNT™ beads. The second measurement analysed the number of stained mitochondria by the number of Fluoresbrite® microspheres. Data analysis was conducted using FlowJo software and calculated the number of mitochondria per mg protein.

### 3.13.3 Assessing mitochondrial integrity

Mitochondrial integrity is defined by a functional membrane potential ($\Delta\Psi_m$) and mitochondrial swelling (212). Using the plate reader Fluorimeter Synergy (Biotek) it is possible to measure both parameters in parallel. Therefore, 50 µg of isolated mitochondria were diluted with swelling assay containing either 500 nM Rhodamine 123 (Rh123) or additionally 500 nM FCCP (for $\Delta\Psi_m$) or 100 µM CaCl$_2$ (swelling) as negative control. Intact mitochondria are able to maintain membrane

potential over a period of at least 1 h and thereby quenching the fluorescent signal of Rh123 that accumulates in the mitochondria due to proton transfer across the inner membrane. Fluorescence was measured every 90 sec (excitation: 485/20 nm; emission: 528/20 nm). Mitochondrial swelling was monitored at 540 nm.

**Swelling assay buffer**: 0.2 M sucrose, 10 mM MOPS-Tris, 5 mM succinate, 1 mM Pi [$H_3PO_4$], 10 µM EGTA

### 3.13.4 Determination of $H_2O_2$ generation

In order to determine $H_2O_2$ generated by mitochondria, isolated mitochondria (50 µg) were mixed with assay buffer containing different inductors (glutamate/malate [G/M, 20 mM], G/M and ADP [12.8 mM], G/M and rotenone [20 µM]) as well as an enzyme mix consisting of Amplex Red (320 µM), superoxide dismutase (SOD, 60 U/ml) and horseradish peroxidase (HRP) (2 U/ml). The fluorescent change of Amplex Red (excitation: 540/20 nm; emission: 620/40 nm) over a period of 1 h (every 90 sec; plate reader Fluorimeter Synergy; Biotek) in the samples was used to determine the generation of $H_2O_2$. The standard curve with defined $H_2O_2$ concentrations was utilized to calculate generation of pmol $H_2O_2$ per min/mg protein under different inductors.

**Assay buffer**: 125 mM KCl, 10 mM HEPES, 5 mM $MgCl_2$, 2 mM $K_2HPO_4$, 5 µM $MnCl_2$

### 3.13.5 Measuring ATP production of isolated mitochondria

ATP generation of isolated mitochondria was measured by adding glutamate (12.5 mM) / malate (12.5 mM) as substrates for complex I in a bioluminescence-based assay using ATP Bioluminiszenz Assay Kit CLS II (Roche) according to manufacturer's instructions. Therefore, 10 µg of mitochondrial suspension were mixed with 160 µM ADP (final concentration) and the substrate solution was incubated for 30 min at room temperature. The negative control additionally contained 2 mM KCN (final concentration). Reaction mix was then heated up to 95°C for 5 min and afterwards placed on ice for another 5 min. Samples were centrifuged for 2 min and 10 µl of the supernatant was diluted with $H_2O$ (1:100). 50 µl of the diluted supernatant was mixed with 50 µl of the luciferase reagent and samples were measured in duplicates. ATP content in the samples was

assessed by measuring the luminescence of samples along with the standard curve containing defined ATP concentrations using the Luminometer Centro LB 960 (Berthold).

**Assay buffer**: 1 mM EGTA, 30 mM $K_2HPO_4$ (pH 7.4), 15 mM KCl, 5 mM $MgCl_2$, Sucrose

## 3.14 Measurement of oxygen consumption

MEFs ($2 \times 10^4$) were seeded onto 96-well plates and incubated overnight at 37°C. The following day, cell culture medium was discarded, cells were washed twice with PBS, XF assay medium was applied and cells were incubated for 1 h at 37°C. In order to the measure oxygen consumption rate (OCR) under the influence of different mitochondrial complex inhibitors, the cell culture plate was placed in an XFe96 Extracellular Flux Analyzer (Seahorse) and oligomycin A (1 µg/µL), FCCP (0.5 µM), antimycin A (2 µM) and rotenone (5 µM) were injected sequentially. After the measurement, DNA was isolated for normalization.

**XF Standard Medium**: XF Modified Assay Medium, 10% FCS, 40 mM sodium bicarbonate, 25 mM glucose

## 3.15 Ultrastructural analysis

Ultrastrucutral analysis of samples was conducted by Dr. Michaela Aichler (Helmholtz Zentrum München).

### 3.15.1 Transmission electron microscopy

Freshly dissected tissues or cell pellets were fixed in 2.5% electron microscopy grade glutaraldehyde (Science Services), post-fixed in 2% aqueous osmium tetraoxide, dehydrated in gradual steps of Ethanol (30-100%) and propylene oxide, embedded in Epon (Merck), and cured for 24 h (60°C). Ultrathin sections (50 nm) were collected onto 200 mesh copper grids, stained with uranyl acetate and lead citrate before analysed by transmission electron microscopy (Zeiss). Pictures were taken using Slow Scan CCD-camera and iTEM software (Olympus)

### 3.15.2 Scanning electron microscopy

Freshly isolated spermatozoa from cauda and caput epidiymis were washed twice in Soerensen buffer, fixed in (para)formaldeyde/glutaraldehyde, 3% each in 0.1 M sodiumcacodylate buffer, pH 7.4 (Electron Microscopy Sciences) overnight at 4°C. On the next day, spermatozoa were washed again and centrifuged onto slides coated with 3-aminopropylene-ethoxysilane. Then, sperm samples were dehydrated in an ascending ethanol series and dried by the critical-point method using $CO_2$ as the transitional fluid (Polaron Critical Point Dryer). Specimens were sputter-coated with a thin layer of 7-nm platinum bya sputtering device and observed by scanning electron microscopy (JSM-6510LV; JEOL,) equipped with a LaB6-emitter (8).

**Soerensen buffer**: 0.07 M $KH_2PO_4$, 0.07 M $Na_2HPO_4$-$2H_2O$ (pH 7.4)

### 3.16    Histology

### 3.16.1 Tissue dissection

Embryo preparation: Female animals from heterozygous *Gpx4^wt/ser* or *Gpx4^wt/cys* breedings were daily checked for vaginal mucous plug. Plug-positive animals were sacrificed at various embryonic stages (E7.5- E12.5) for the isolation of decidua from the uterus.

Isolation of epididymal sperm: Fresh sperm from cauda epididymis, caput epididymis and vas deferens was isolated from 3-8 month old *Gpx4^wt/ser* animals as described before (9). After dissection, tissue was briefly washed in 0.09% NaCl and transferred in human tubal fluid (HTF) medium. Epididymis and vas deferens was carefully dissected with a few cuts and sperm was allowed to swim out for 10 min at 37°C while gently shaking the plate.

**HTF Medium**: 100 mM NaCl, 4.7 mM KCl, 200 µM $MgSO_4$, 400 µM $KH_2PO_4$, 5 mM $CaCl_2$, 25 mM $NaHCO_3$, 3 mM glucose, 30 µM sodium lactate, 330 µM sodium pyruvate, 200 µM Penicillin G, 70 µM Streptomycin, 400 mg/100 ml BSA

Collecting tissues from pre-weaning aged and adult animals: Animals were sacrificed either by decapitation or cervical dislocation and organs like brain,

thymus, heart, lung, spleen, kidney, liver, testis, caput and cauda epididymis were dissected and briefly washed in PBS when necessary.

## 3.16.2 Paraffin-embedded sections

Freshly dissected tissue was fixed in 4% paraformaldehyde (PFA) overnight at 4°C following dehydration in an ascending series of ethanol (70% - overnight, 80% - 1 h, 95% - 2 h, 100% - 2 h) and 2 h in xylene. Tissue was incubated overnight in paraffin at 60°C and embedded in paraffin in disposable vinyl specimen molds the following day. Brain and decidua were cut at the rotary microtom HM355S (Thermo Fischer) in 8-µm-thick serial sections, whereas other tissue was cut in 10-µm-thick sections.

**PFA**: 4% paraformaldehyde in PBS
**Ethanol series**: 100% ethanol diluted in $dH_2O_2$

## 3.16.3 Cryosections

Freshly dissected brain tissue was fixed overnight in 4% PFA at 4°C followed by an overnight incubation in 20% sucrose in PBS at 4°C. Then, brain tissue was transferred into disposable vinyl specimen molds filled with Tissue Tek® medium and placed on dry ice until Tissue Tek® medium was completely frozen. Tissue embedded in Tissue Tek® medium was stored at -80°C until sectioning of the tissue was performed. Brain tissue was cut in 20-µm-thick serial sections at a cryostat (Microm HM 60).

## 3.16.4 Hematoxylin & Eosin (H&E) staining

Paraffin-embedded sections were deparaffinized in three steps of xylene and hydrated in a descending series of ethanol (100% 2 × 5 min, 95% 2 × 5 min, 80% 2 × 5 min). Then, sections were stained for 7 min in Mayer`s hematoxylin followed by a washing step in $dH_2O$ and a 5 min washing step under tab water. After another washing step in $dH_2O$, sections were stained for 3 min in 0.5% eosin Y containing gacial acid and washed again briefly in $dH_2O$. Finally, sections were dehydrated briefly in a graded series of ethanol (70%, 80%, 95%, 100%) and xylene before they were mounted with Rothi-Histo Kit. Staining was analysed at microscope Axioplan2 Imaging (Zeiss) and pictures were taken with the camera AxioCam MRc and the software AxioVision (both Zeiss).

**Eosin Y**: one drop of glacial acid per 100 ml 0.05% eosin Y

### 3.16.5 Immunohistochemistry of paraffin-embedded sections

Paraffin-embedded sections were deparaffinized as described before (3.16.4). Then, sections were incubated in hot citrate buffer for 20 min, washed in $dH_2O$, treated for 5 min in 3% $H_2O_2$, washed again with $dH_2O$ and incubated for 1 h with a blocking solution. Sections were incubated overnight at 4°C with GPX4-, active Caspase-3-, calretinin-, calbindin-, parvalbumin (PV)-, glial fibrillary acidic protein (GFAP)-, ionized calcium-binding adapter molecule 1 (IBAI)- specific antibodies diluted in blocking solution according to manufacturer`s instructions. Primary antibody binding detection was achieved with a biotinylated secondary antibody IgG diluted in washing buffer and an avidin-biotin-peroxidase complex for enhancing the signal. 3,3-Diaminobenzidine (DAB) solution was used to visualize the staining. Staining was analysed using the microscope Axioplan 2 Imaging and pictures were taken using the camera AxioCam Mrc together with the software AxioVision (all Zeiss).

**Citrate buffer**: 10 mM citrate buffer (pH 6)
**3% $H_2O_2$**: 30% $H_2O_2$ in PBS
**Washing buffer**: 1 × TBS (pH 7.6), 0.1% Tween-20
**Blocking solution**: 1 × TBS (pH 7.6), 0.1% Tween-20, 5% goat serum

### 3.16.6 Immunohistochemistry of cryosections

Cryosections stored at -80°C were allowed to thaw for 15 min at room temperature, fixed in 1% PFA for 10 min, washed twice with PBS and fixed in a second step in 100% ethanol containing acetic acid (2:1) for 10 min at -20°C. Sections were washed again twice in PBS and incubated for 1 h in blocking solution before they were incubated overnight at 4°C with PV-, GFAP- or IbaI-specific primary antibodies diluted in blocking solution according to manufacturer`s instructions. On the next day, sections were washed three times with PBS and incubated for 2 h with fluorescence-conjugated secondary antibody diluted in secondary antibody solution. After another washing step with PBS, sections were mounted with Vectashield Hard Set containing DAPI for nuclei counterstaining and stored at -20°C. Antibody staining was visualized and

captured at the Olympus confocal microscope IX81 (Olympus) using the laser 405 nm, 488 nm and 595 nm.

**Blocking solution**: PBS, 5% goat serum, 0.3% Triton X-100
**Secondary antibody solution**: PBS, 1% BSA, 0.3% Triton X-100

### 3.16.7 Immunocytochemistry of isolated spermatozoa

Freshly collected spermatozoa were spread on a glass slide and allowed to dry. Glass slides with the sperm cells were heated for 1 min at 70°C and fixed in 2% PFA for 10 min at room temperature. Permeabilization of the cells was achieved by treatment with 0.15% Triton X-100 for 5 min three times followed by incubation of the cells in blocking solution for 1 h. Cells were then incubated with the primary GPX4-specific antibody diluted in blocking solution according to manufacturer`s instructions overnight at 4°C. Then, cells were washed with PBS for 5 min and with 0.15% Triton X-100 for 10 min and blocked again for 7 min in blocking solution. Spermatozoa were treated for 45 min with a fluorescence-conjugated secondary antibody (Alexa Fluor 488 anti-rabbit) diluted in blocking solution. After two washing steps in 0.15% Triton X100 for 5 min and two washing steps in PBS, spermatozoa was mounted in Vectashield mounting medium containing DAPI and stored at 4°C in the dark. Antibody staining was visualized and captured at the Olympus confocal microscope IX81 (Olympus) using the laser 405 nm and 488 nm.

**Blocking solution**: PBS, 1% BSA, 0.15% glycine

### 3.16.8 Terminal Deoxynucleotideyltransferase dUTP Nick End labeling (TUNEL)

For the detection of dead cells, TUNEL staining was performed using either the ApopTag® Peroxidase in situ Apoptosis Detection Kit (Millipore) for PFA fixed sections embedded in paraffin or ApopTag® Fluorescein in situ Apoptosis Detection Kit (Millipore) for cryosections according to manufacturer`s instructions. For paraffin-embedded sections, staining was achieved with an anti-digoxigenin peroxidase conjugate that was visualized by a DAB solution. Cryosections were incubated with anti-digoxigenin fluoresceine conjugate and mounted in Vectashield mounting medium containing DAPI for counterstaining of the nuclei. Staining was analysed as described before in 3.16.4 and 3.16.6.

## 3.17 Animal husbandry

### 3.17.1 Animals facility

Mice were kept in the animal facility of the Helmholtz Zentrum München under standard conditions with water and food *ad libitum* and in a controlled environment (22 ± 2°C, 55 ± 5% humidity, 12 h light/dark cycle). Cages were supplied with nesting material and houses in case of breeding cages. 2-5 animals were grouped per cage. Offspring was separated from the mothers between days 19-21 after birth and marked by ear punch for identification and genotyping. All experiments conducted on the animals were in compliance with the German Animal Welfare Law and have been approved by the institutional committee on animal experimentation and the government of Upper Bavaria.

### 3.17.2 Cross-breeding of *Gpx4$^{cys/wt}$* and *Gpx4$^{ser/wt}$* mice with Flpe recombinase transgenic and Tamoxifen-inducible CreERT2 transgenic mice

*Gpx4$^{cys/wt}$* and *Gpx4$^{ser/wt}$* mice (the latter described in (8)) were first cross-bred with Flpe recombinase expressing transgenic *Rosa26_Flpe* animals (202) to delete the frt-flanked *neo* gene of the transgenic *Gpx4* allele. Animals that were negative for the *neo* gene and positive for the insertion of the *Flpe* allele were further mated with *C57BL/6J* animals to remove Flpe. In the final cross-breeding step, only animals that were positive for the deletion of the *neo* gene and negative for the insertion of the *Flpe* recombinase gene were mated with TAM-inducible *Gpx4$^{flox/flox;Rosa26CreERT2}$* mice (148), yielding *Gpx4$^{cys/flox;Rosa26CreERT2}$* and *Gpx4$^{ser/flox;Rosa26CreERT2}$* mice among the control mice.

### 3.17.3 TAM application

To induce the disruption of the loxP-flanked *Gpx4* allele in the adult whole body (except brain), animals (females and males) older than 8 weeks of age expressing the *ROSA26CreERT2* allele were injected twice intraperitoneally (i.p.) with 0.5 mg TAM dissolved in Miglyol. Survival analysis was conducted using the software GraphPad Prism 5.0.

### 3.17.4 Mating assay

Wt (n = 5) and heterozygous *Gpx4$^{wt/ser}$* (n = 5) male mice (3-8 months old) were mated with *C57BL/6J* female mice. Females were daily checked vaginal mucous

plug and separated from males when positive. At least five plug positive females were collected per male and observed for offspring.

### 3.17.5 *In vitro* fertilization

*In vitro* fertilization assay was conducted by Adriane Tasdemir (Helmholtz Zentrum München). 4 µl of freshly isolated sperm suspension (see 3.16.1) from *Gpx4*[wt/wt] and *Gpx4*[wt/ser] males was added to a drop (500 µl) of HTF medium covered by mineral oil and incubated (45 min, 37°C, 5% $CO_2$) to allow capacitation of the spermatozoa. 8 weeks-old *C57BL/6J* females were used as oocyte donors. Therefore, all females were superovulated by i.p. hormone injections using Pregnant mare serum gonadotropin (PMSG) (5 IU) followed by human chorionic gonadotropin (HCG) (5 IU) 48-50 h later. In order to collect both oviduct and oocyte cumulus complexes, animals were sacrificed 14 h after HCG injection by cervical dislocation. 80 oocytes were applied to the capacitated sperm from *Gpx4*[wt/wt] and *Gpx4*[wt/ser] and incubated for 4-6 h (37°C, 5% $CO_2$). Subsequently, oocytes were washed four times with mouse embryo media KSOM and cultured overnight in a 100 µl drop of KSOM covered in mineral oil (37°C, 5% $CO_2$). Then, the number of 2-cell stage embryos and blastocysts were determined.

### 3.17.6 Sperm quality analysis

To determine sperm motility, sperm progressivity and concentration of sperm, 1 µl of freshly dissected sperm suspension (see 3.16.1) from *Gpx4*[wt/wt] and *Gpx4*[wt/ser] animals was added in a drop of HTF medium covered in mineral oil and incubated for 15 min (37°C, 5% $CO_2$). Afterwards, 15 µl of sperm were applied to a sperm analysis chamber (2X-Cel, height 80 µm) and analysed using the IVOS sperm analyzer (Hamilton Thorne Research).

### 3.18   Statistical analysis and data presentation

Statistical analysis was conducted using GraphPad Prism 5.0 software. Data are presented as mean ± s.d. unless stated otherwise.

# 4 Results

## 4.1 Generation of mouse lines expressing the Ser or Cys variant of GPX4

In order to interrogate the evolutionary advantage of selenothiol- versus thiol-based catalysis in GPX4, one of the most important selenoproteins, two mouse lines have been generated in the Conrad laboratory carrying point mutations in the active site of GPX4 yielding either a Ser or Cys in place of Sec (Fig. 8). The analysis of these mouse lines should help in addressing the question why Sec particularly in GPX4 is essential for mammalian development and possibly survival and if it can be substituted by Ser or its analogon Cys both *in vivo* and *in vitro*.
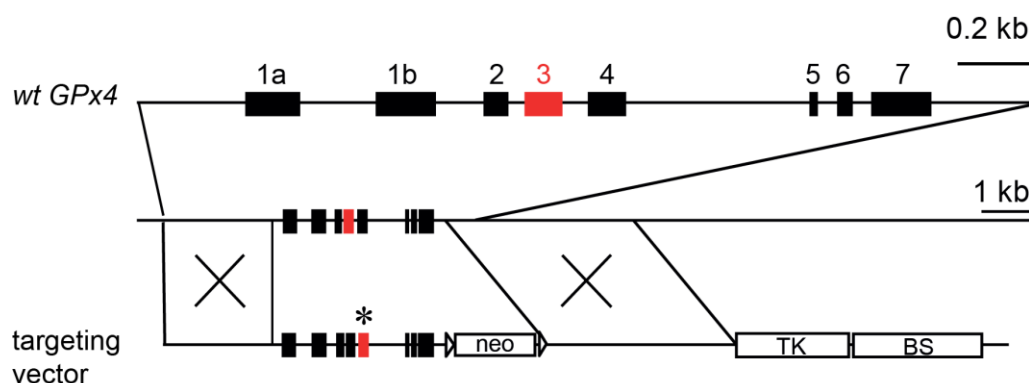


**Figure 8: Gene targeting strategy for Sec replacement by Ser or Cys in GPX4.** The upper line presents the wt allele of *Gpx4* consisting of 7 "classical" exons and one alternative exon (1b). The active site of *Gpx4* is encoded by exon 3 that is highlighted in red. The lower line depicts the targeting vector which was used for the generation of the two mouse lines carrying a point mutation in the active site. The *neomycin phosphotranferase gene* (neo), flanked by two frt sites, was used for the positive selection of transfected embryonic stem (ES) cells. Downstream of the 3`arm for homologous recombination, the thymidine kinase gene (TK) is located which was used for negative selection. BS = pBluescript vector backbone. Figure adapted from (8).

## 4.2 Analysis of animals expressing the Ser variant of GPX4

### 4.2.1 Mice homozygous for the Ser variant of GPX4 die during embryogenesis

To generate transgenic mice that carry a Ser in the active site of GPX4, a targeting vector (Fig. 8) was cloned containing two point mutations in exon 3 yielding a Ser (AGC) instead of a Sec (UGA). Positive offspring was confirmed by PCR and verified by sequencing exon 3, where the catalytic site of *Gpx4* is located (Fig. 9A).
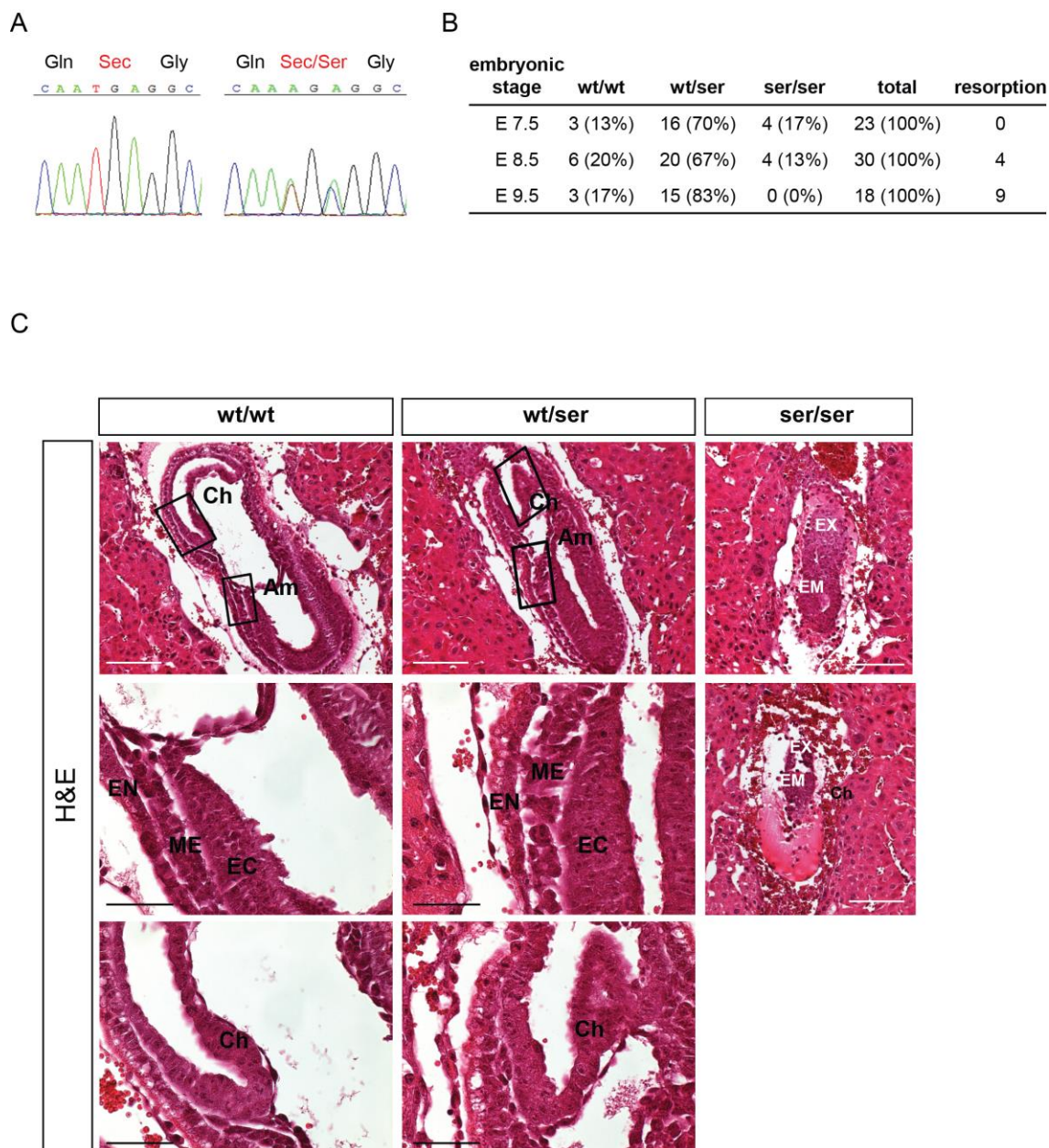
A

Gln  Sec  Gly
C A A T G A G G C

Gln  Sec/Ser  Gly
C A A A G A G G C

B

| embryonic stage | wt/wt | wt/ser | ser/ser | total | resorption |
|---|---|---|---|---|---|
| E 7.5 | 3 (13%) | 16 (70%) | 4 (17%) | 23 (100%) | 0 |
| E 8.5 | 6 (20%) | 20 (67%) | 4 (13%) | 30 (100%) | 4 |
| E 9.5 | 3 (17%) | 15 (83%) | 0 (0%) | 18 (100%) | 9 |

C



**Figure 9: Histopathological analysis of embryos obtained from heterozygous *Gpx4^wt/ser* mating.** (A) PCR amplification and sequencing of a region spanning exon 3, where the active site of *Gpx4* is located, confimed the targeted mutation changing Sec (TGA) to Ser (AGC). AGA is shown for Ser since the second A, derived from the wt allele, appears to be more prominent in the sequencing than C. (B) *Gpx4^ser/ser* (ser/ser) embryos were easily detected at E7.5. The number of intrauterine resorptions increased at E8.5 and intrauterine resorptions were frequently detected at E9.5, when *Gpx4^ser/ser* embryos were no longer detectable. (C) H&E staining of decidua containing embryos did not show morphological abnormalitiers between *Gpx4^wt/wt* and *Gpx4^wt/ser* embryos. On the contrary in *Gpx4^ser/ser* embryos intrauterine resorption was evident and a determination of the three embryonic layers, a sign for proper embryonic development, was not possible. Am = amnion, Ch = chorion, EC = ectoderm, EM = embryonic tissue, EN = endoderm, EX = extraembryonic tissue, ME = mesoderm. Scale bars: white 100 µm; black 50 µm). Figure adapted from (8).

Since homozygous animals have never been obtained from heterozygous *Gpx4^{wt/ser}* breeding, embryo analysis was conducted to check for embryonic lethality as previously reported for *Gpx4^{-/-}* (149,150,152). Therefore, female animals from heterozygous *Gpx4^{wt/ser}* breeding were daily checked for vaginal mucous plug and pregnant mice were sacrificed at day E7.5, E8.5 and E9.5 of embryogenesis to determine the genotype and the phenotype of the embryos. Genotyping of the embryos revealed that embryonic death occurs during gastrulation stage (between E7.5 - E8.5) (Fig. 9B). At E9.5 homozygous *Gpx4^{ser/ser}* embryos were no longer detectable, instead an increased number of intrauterine resorptions and empty descidua were frequently observed (Fig. 9B). Histopathological analysis showed normal development of *Gpx4^{wt/ser}* embryos, but *Gpx4^{ser/ser}* embryos revealed widespread resorptions and structural abnormalities (Fig. 9C). A clear determination of the three embryonic germ layers, indicative for proper gastrulation and embryonic development, was not possible in homozygous embryos and phenocopied that of *Gpx4^{-/-}* mice as reported much earlier (Fig. 9C) (150,152). This data suggested that homozygous Sec replacement by Ser does not allow proper embryonic development and survival of the animals.

### 4.2.2  GPX4 protein expression is elevated in heterozygous *Gpx4^{wt/ser}* mice

Unlike homozygous *Gpx4^{ser/ser}* embryos, one wt allele seems to be sufficient for the viability of the animals as heterozygous *Gpx4^{wt/ser}* animals are fully viable and histopathological analysis of somatic tissue (heart, lung, kidney and liver) from adult *Gpx4^{wt/ser}* mice did not show any morphological aberrations (Fig. 10A). Immunoblot analysis of organs (heart, brain, kidney, lung, thymus, liver and spleen) revealed a strongly increased expression of the GPX4 protein in heterozygous *Gpx4^{wt/ser}* samples (Fig. 10B), although GPX4-specific activity was found to be unaltered in tissues such as kidney, brain, heart and liver (Fig. 10C). For *in vitro* studies, MEFs were then established from breedings of heterozygous *Gpx4^{wt/ser}* and *C57BL/6J* animals (Fig. 10D). According to what was observed in different somatic tissues, GPX4 protein level was significantly higher in heterozygous *Gpx4^{wt/ser}* MEFs (Fig. 10F), whereas GPX4-specific activity measured in wt and heterozygous MEFs did not show any significant differences (Fig. 10G). In order to define whether the upregulation of the GPX4 protein occurs

on a transcriptional or translational level, RNA was isolated from MEFs and qRT PCR analysis was performed. As depicted in Figure 10H, *Gpx4* mRNA levels were not different in heterozygous compared to wt MEFs. From this data it can be concluded that an increased GPX4 protein expression in *Gpx4^wt/ser^* samples most likely results from an easier insertion of a readily available Ser compared to a less efficient incorporation of Sec (see 1.3) as also previously reported for bacterial selenoproteins (213).
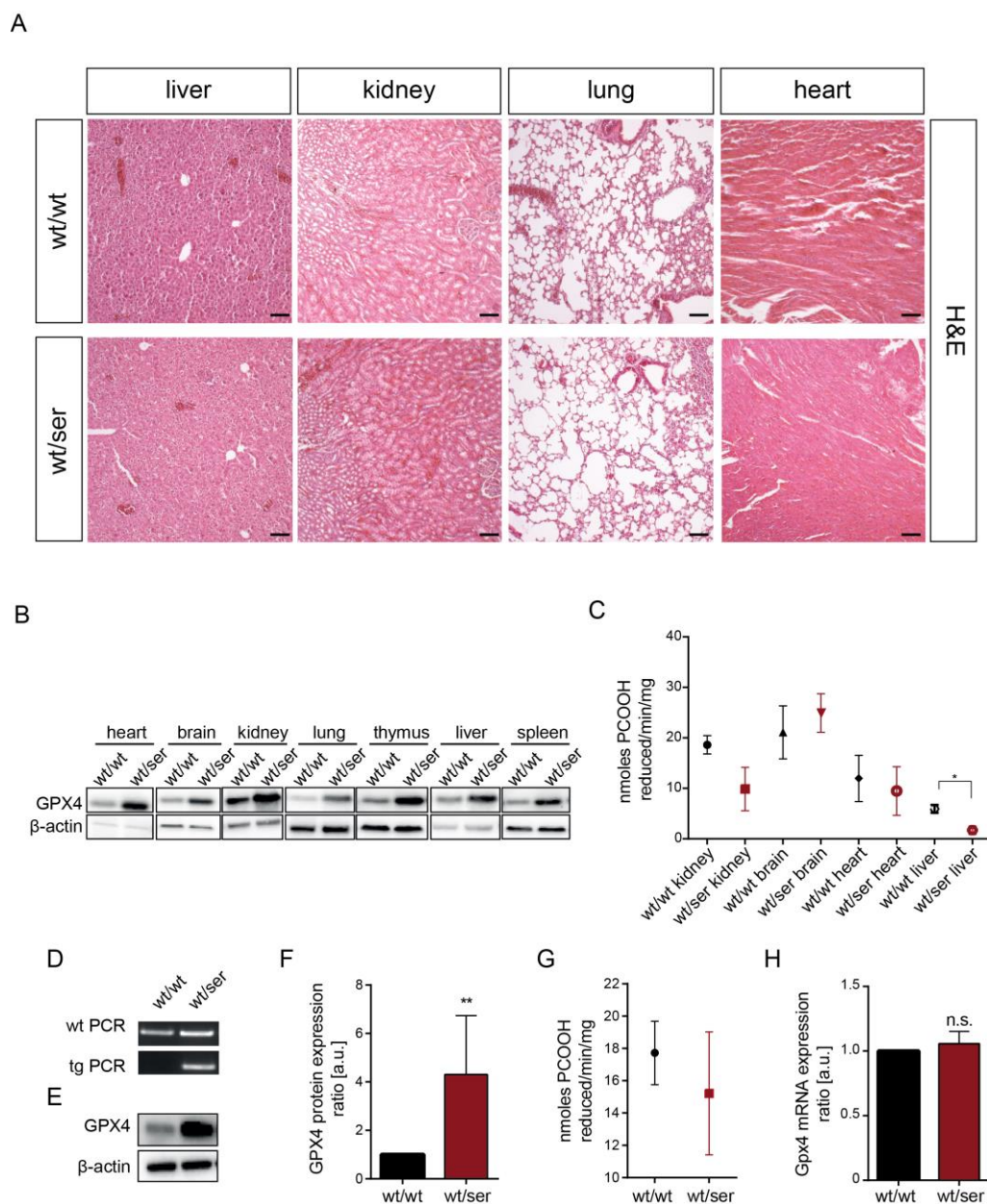


**Figure 10: GPX4 protein level is elevated in somatic tissues and cells heterozygous for the Ser variant of GPX4.** (A) Histological analysis of somatic tissues by H&E staining showed no overt abnormalities in *Gpx4^wt/ser^* animals compared to *Gpx4^wt/wt^*. (B) GPX4 protein expression was found to be increased in all tissues analysed. (C) GPX4-specific activity was significantly decreased in liver samples derived from *Gpx4^wt/ser^* animals, whereas in kidney, brain and heart

samples no difference was detectable. Data was kindly provided by Dr. Antonella Roveri (University of Padova). (D) MEFs isolated from embryos were genotyped by two independent PCRs amplifiying a product of 256 bp for the wt and 203 bp for the heterozygous (transgene = tg) allele. (E and F) GPX4 expression was significantly higher in $Gpx4^{wt/ser}$ cells. (G) Despite increased GPX4 expression in $Gpx4^{wt/ser}$ cells, GPX4-specific activity remained unaltered as was observed for the $Gpx4$ mRNA levels (H). (Statistical analysis was performed using the t test, $\rho < 0.05$ (*), $\rho < 0.001$ (**). n.s. = not significant, a.u. = arbitrary units. Scale bars = 100 µm). Figure adapted from (8).

### 4.2.3 Male $Gpx4^{wt/ser}$ mice are subfertile

When heteroyzgous breedings were set up for vaginal mucous plugs, it was striking that $Gpx4^{wt/ser}$ female animals were frequently found not to be pregnant despite positive plugs. As aforementioned (see 1.5.2) numerous previous studies reported that GPX4 confers crucial and versatile functions in sperm maturation (9,133,138). Therefore, it was hypothesized that the upregulated expression of a catalytically inactive form of GPX4 might lead to an impairment of the function of the wt protein due to a dominant-negative effect. To investigate this, test breedings of heterozygous $Gpx4^{wt/ser}$ males with $C57BL/6J$ females and $Gpx4^{wt/wt}$ males with $C57BL/6J$ females as controls were set up. Females were daily checked for vaginal mucous plug and 25 plug-positive $C57BL/6J$ females were collected for 5 $Gpx4^{wt/ser}$ and 5 $Gpx4^{wt/wt}$ males. Although there was no difference between both groups regarding the time period when the breeding was started and positive plug, a great variance was observed in the number of offspring. While in the control group 17 out of 25 plug-positive females gave birth to 119 pups, only 11 offspring with 70 pups were obtained from the heterozygous group (Fig. 11A). The litter size in the control group ranged from 1 to 11 pups which was similar to the heterozygous group where 2 to 10 pups per litter were born (Fig. 11A). To further analyze the ability of heterozygous $Gpx4^{wt/ser}$ sperm to fertilize oocytes and generate blastocysts *in vitro*, *in vitro* fertilization assays were performed. Therefore, sperm from 3 heterozygous $Gpx4^{wt/ser}$ and 3 $Gpx4^{wt/wt}$ males were collected and incubated for three days with 80 oocytes isolated from $C57BL/6J$ females. The incubated oocytes were daily checked for their embryonic stages and survival. In the control group, 105 2-cell stage embryos developed into 20 blastocysts, but the heterozygous group contained only 16 2-cell stage embryos that developed into 2 blastocysts (Fig. 11B). The *in vivo* and *in vitro* fertilization data stongly suggested that the function of GPX4 is perturbed

in *Gpx4^{wt/ser}* sperm resulting in reduced fertilization ability. Since sperm quality is defined by specific parameters, such as sperm concentration, motility and progressivity, sperm was isolated from heterozygous *Gpx4^{wt/ser}* (n = 17) and *Gpx4^{wt/wt}* (n = 9) males for evaluation of those parameters and in a computer-assisted semen analysis system. Although no difference was assessed in sperm concentration and motility, the analysis showed that *Gpx4^{wt/ser}* sperm was significantly less progressive than their wt counterparts (Fig. 11C). As one of the key features for good sperm quality, progressivity is defined as the capability of rapid and directed movement of sperm which serves as a strong indicator for the fertilization potential of sperm.
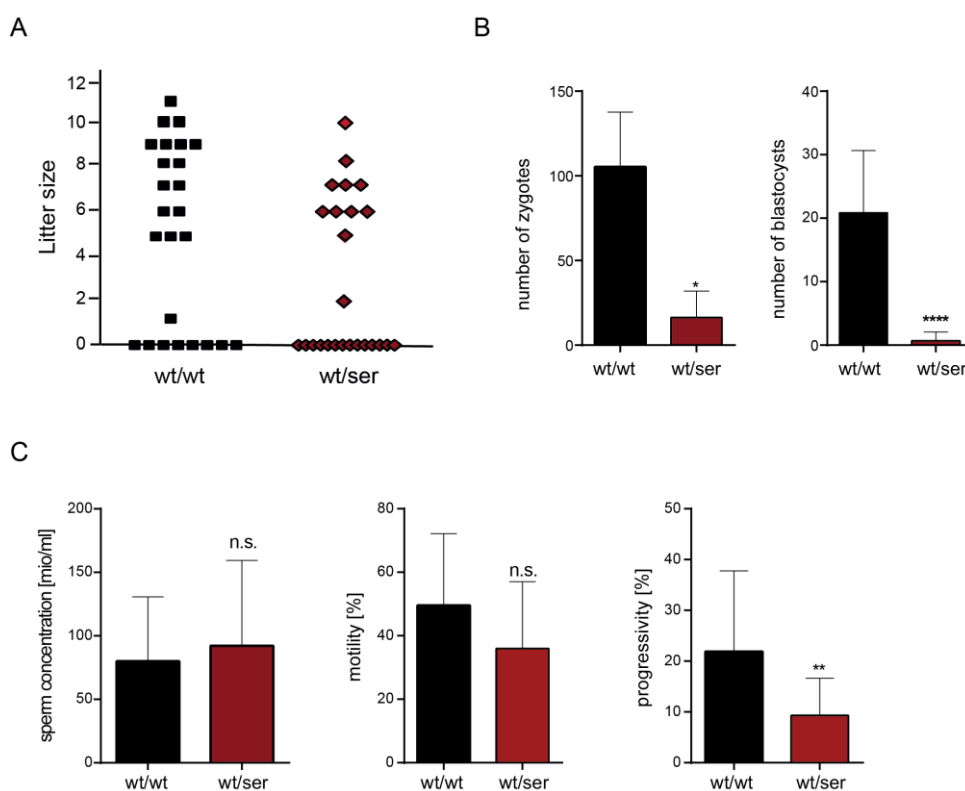


**Figure 11: *Gpx4^{wt/ser}* males are subfertile.** (A) Test breedings of *Gpx4^{wt/wt}* and *Gpx4^{wt/ser}* males with *C57BL/6J* females resulted in 17 litters and a total number of 119 offspring in the wt group. The heterozygous group yielded 11 litter with a total of 70 animals (n = 5 males per genotype). (B) *In vitro* fertilization performed with sperm isolated from *Gpx4^{wt/wt}* and *Gpx4^{wt/ser}* males (n = 3 each genotype) showed a significantly lower number of zygotes and blastocysts in the heterozygous *Gpx4^{wt/ser}* group. (C) Assessment of sperm quality by analysis of sperm concentration, motility and progressivity showed no difference in sperm concentration and motility, but a significantly lower progressivity of sperm isolated from *Gpx4^{wt/ser}* males (n = 9 wt/wt; n = 17 wt/ser). (Statistical analysis was conducted using the two-tailed t test, $p < 0.05$ (*), $p < 0.001$ (**), $p < 0.00001$ (****), n.s. = not significant). Figure adapted from (8). *In vitro* fertilization data was kindly provided by Adriane Tasdemir (Helmholtz Zentrum München).

### 4.2.4  Analysis of testicular and epididymal tissue of *Gpx4^{wt/ser}* animals

In a histopathological analysis of testicular and epididymal tissue no overt morphological changes could be detected in heterozygous *Gpx4^{wt/ser}* animals that could explain the functional impairment observed in their spermatozoa (Fig. 12A).
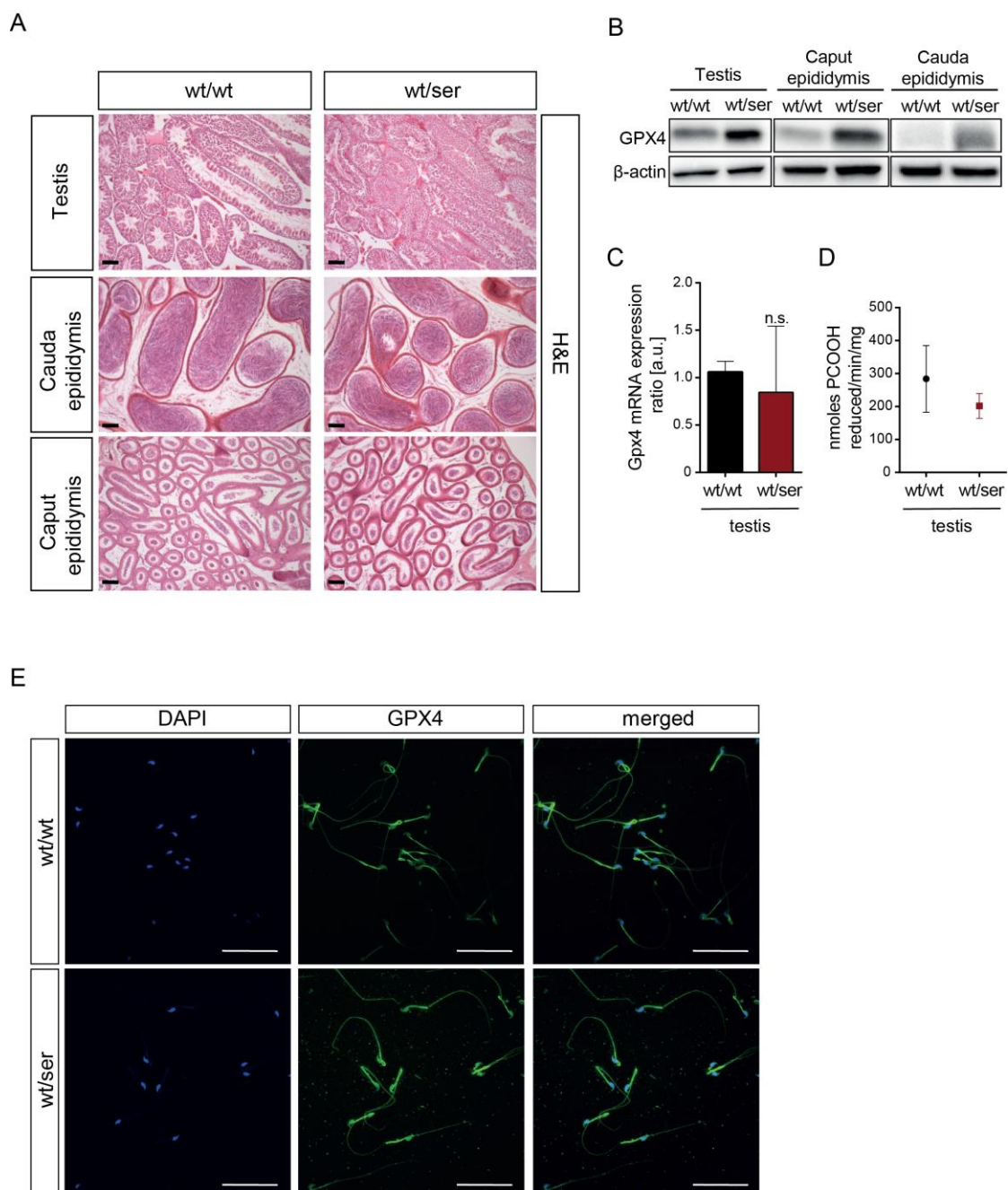


**Figure 12: Immunohistological analysis of testicular tissue and isolated spermatozoa.** (A) Histological analysis of testis and caput and cauda epididymis by H&E staining showed no morphological abnormalities in *Gpx4^{wt/ser}* males compared to *Gpx4^{wt/wt}* mice (scale bars = 100 μm). (B) As monitored in somatic tissue by immunoblot analysis, GPX4 protein expression was increased in testis and epididymal tissue of *Gpx4^{wt/ser}* males , whereas (C) *Gpx4* mRNA level and (D) GPX4-specific activity remained unaltered (statistics was assessed by two-tailed t test, n.s. = not significant; a.u. = arbitrary unit). (E) Immunocytochemical analysis of isolated epididymal

spermatozoa by whole mount staining detected increased GPX4 expression (green) in spermatozoa derived from *Gpx4^(wt/ser)* males, which was mainly restricted to the midpiece and the head-region of sperm. Sperm nuclei were counterstained with DAPI (scale bars = 50 µm). Figure adapted from (8).

When determining protein expression by Western blot (Fig. 12B), GPX4 was found to be upregulated in heterozygous testicular and epididymal tissue without alterations in their mRNA level (Fig. 12C) or GPX4-specific activity (Fig. 12D), which is in line with what had been observed in somatic tissues and MEFs (see Fig. 10A and E). Immunohistochemical whole-mount staining of isolated spermatozoa using GPX4-specific antibody detected an increased expression of the GPX4 protein in the sperm midpiece and the head of spermatozoa, where the mitochondrial and nuclear isoforms of GPX4 are located, respectively (9,146) (Fig. 12E).

### 4.2.5 Ultrastructural analyses of spermatozoa derived from *Gpx4^(wt/ser)* animals reveal severe structural abnormalities

When isolated spermatozoa were analysed by immunohistochemical staining (see Fig. 12E), morphological alterations were frequently noticed in sperm obtained from *Gpx4^(wt/ser)* males, which was mainly confined to the midpiece of spermatozoa. To investigate this in more detail, ultrastructural analyses of testicular tissue and spermatozoa from epididymis were performed. Transmission electron microscopy analysis demonstrated that mitochondria surrounding the axoneme in late stage spermatids (testis) and spermatozoa (epididymis) were swollen in samples derived from *Gpx4^(wt/ser)* males (Fig. 13A). Scanning electron microscopy analysis revealed that structural alterations were mainly restricted to the midpiece and midpice-principal piece junction including bends at the junction of midpiece and midpiece-principal piece, extrusions of outer dense fibers and also irregularly aligned spermatozoa (Fig. 13B). Interestingly, the same structural abnormalities had been reported previously in animals that were kept under selenium-deficient conditions (142,143), or in animals lacking mGPX4 (9).
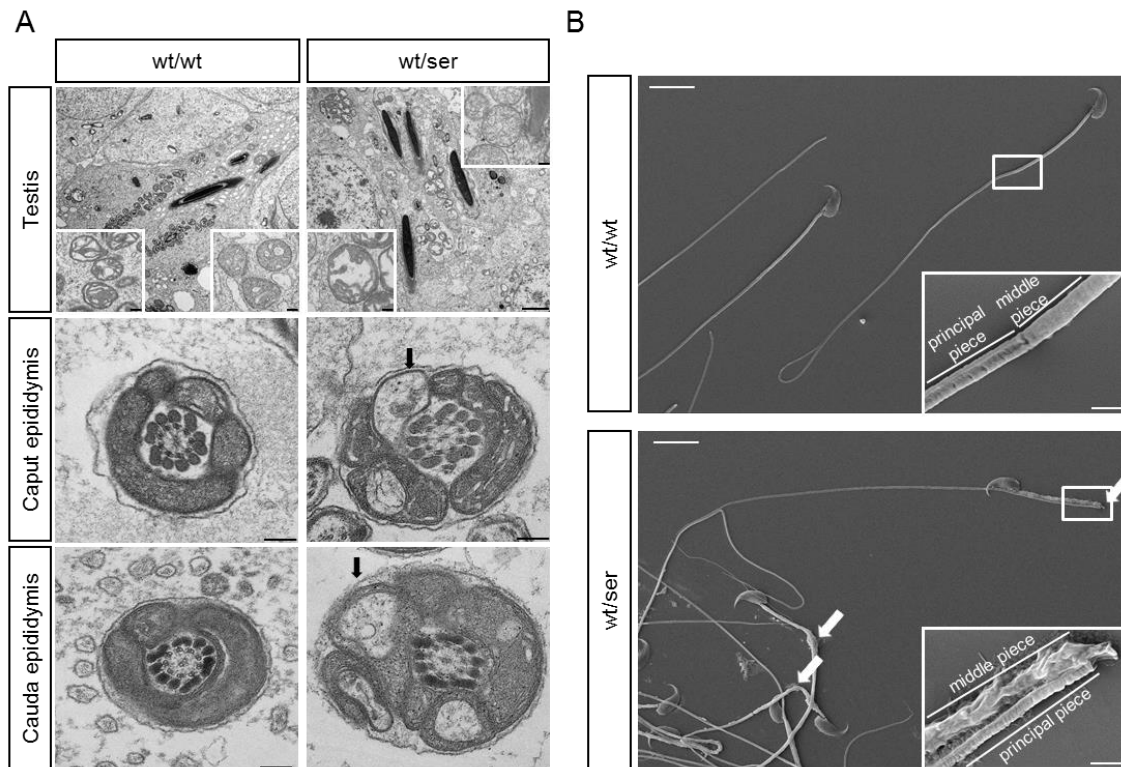
**Figure 13: Developing and mature spermatozoa from *Gpx4^{wt/ser}* males show severe structural malformations.** (A) Ultrastructural analysis of testicular and epididymal tissue revealed an increased number of swollen mitochondria in late spermatids (testis) and epididymal spermatozoa (arrows) (scale bar = 2 μm; insets = 200 nm). (B) Scanning electron microscopy of isolated spermatozoa detected severe morphological changes, such as bends and extrusions of outer dense fibers mainly present at the midpiece and the junction of midpiece and principal piece of spermatozoa (scale bar = 10 μm; insets = 1μm). Figure adapted from (8). Data was kindly provided by Dr. Michaela Aichler (Hemholtz Zentrum München).

## 4.2.6 Spermatozoa isolated from *Gpx4^{wt/ser}* animals show higher levels of free thiols

Reportedly, one of the main functions of GPX4 during sperm development is the introduction of disulfide bridges into capsular proteins of the mitochondria surrounding the spermatozoan midpiece in order to ensure a full spermatozoan stability (132). As GPX4 was previously found to constitute up to 50% of mitochondrial capsular proteins cross-linked via disulfide bridges in an enzymatically inactive form (133), it was also hypothesized that high expression of dysfunctional GPX4 (*Gpx4^{wt/ser}*) may confer a dominant-negative effect in the oxidative cross-linking steps of sperm caspsular proteins conferred by the protein thiol peroxidase function of wt GPX4. To this end, monobromobimane staining

was used for free thiol labeling of spermatozoa isolated from *Gpx4^{wt/ser}* (n = 9) and *Gpx4^{wt/wt}* animals (n = 9).
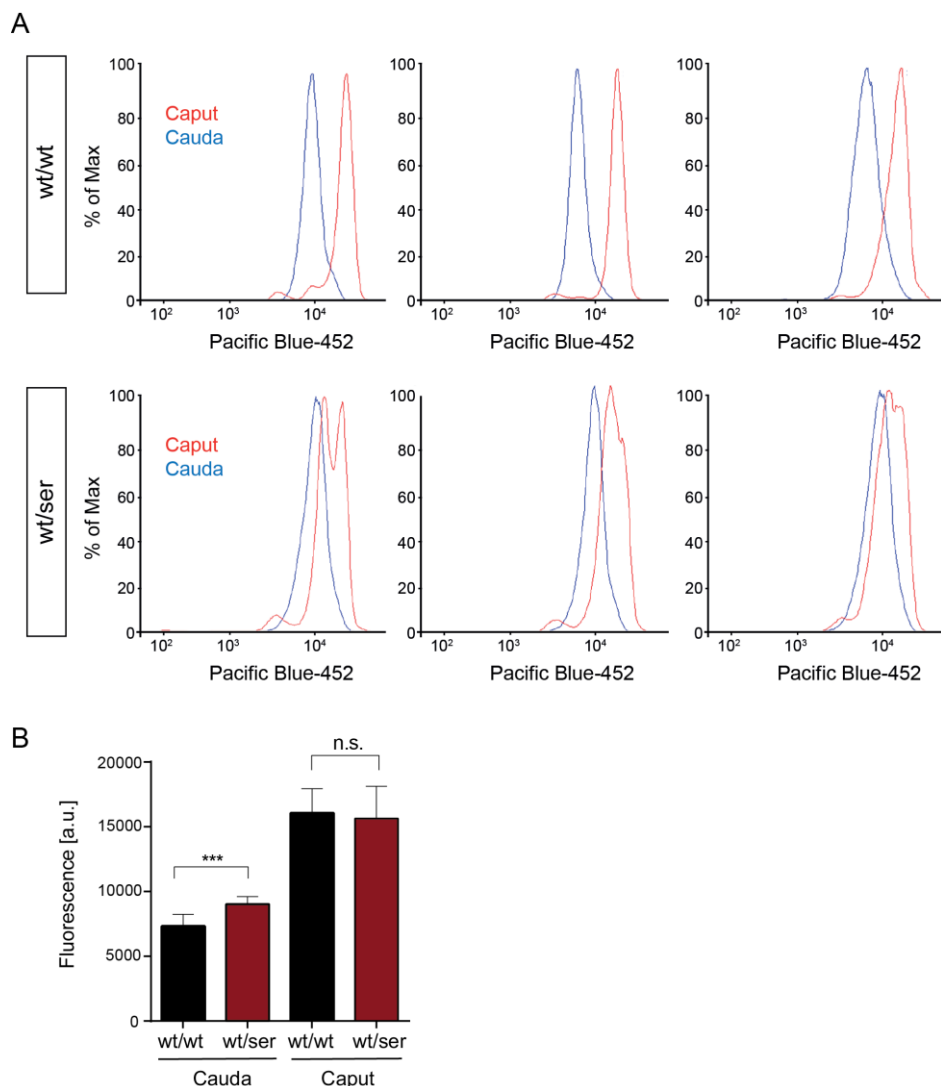


**Figure 14: Spermatozoa isolated from *Gpx4^{wt/ser}* animals contain higher levels of free thiols.** (A) Monobromobimane-labeling of spermatozoa isolated from caput and cauda epididymis was assessed by flow-cytometry. Statistical evaluation of the flow-cytometry data showed a significantly higher level of free thiols in heterozygous spermatozoa of cauda epididymis, whereas no difference was detected in free thiol content of spermatozoa derived from caput epididymis of both genotypes (n = 9 each genotype). Statistical evaluation was performed using two-tailed t test ($p<0.001$ (***); a.u. = arbitrary units; n.s. = not significant). Figure adapted from (8).

By monobromobimane labeling the overall content of free thiols in spermatozoa derived from cauda epididymis in comparison to caput epididymis was determined. Flow cytometry analysis revealed an increased fluorescence signal in spermatozoa derived from cauda epididymis of *Gpx4^{wt/ser}* animals compared to their wt counterparts (Fig. 14A). Statistical analysis confirmed that spermatozoa derived from cauda epididymis of G*px4^{wt/ser}* animals contained significantly more

free thiols (Fig. 14B). These data indicate that protein thiols in *Gpx4^{wt/ser}* animals are present in a more reduced state and are therefore not able to yield properly formed mitochondrial capsules.

## 4.3 Analysis of animals expressing the Cys variant of GPX4

### 4.3.1 The Cys variant of GPX4 is sufficient to allow normal embryogenesis on a mixed *129S6SvEvTac-C57BL/6J* genetic background

To address the *in vivo* relevance of Sec vs Cys based catalysis of GPX4, a mouse line was generated using a targeting vector (Fig. 8) that contained a targeted point mutation in the UGA codon which results in the insertion of a Cys (UGC) instead of a Sec (UGA) in the mutant protein. After successful germline transmission of the targeted allele, heterozygous *Gpx4^{wt/cys}* animals were cross-bred in order to interrogate whether Cys in GPX4 allows proper embryogenesis. Genotyping and sequencing of the obtained offspring (Fig. 15A) revealed that homozygous *Gpx4^{cys/cys}* animals were born at Mendelian ratio (Fig. 15B). Unlike systemic *Gpx4^{-/-}* (149,150,152) or *Gpx4^{ser/ser}* mice (8) (Fig. 9), which die during gastrulation stage ~E7.5, this data showed that the Cys variant of GPX4 is sufficient for normal embryonic development. Although *Gpx4^{cys/cys}* animals were obtained from heterozygous *Gpx4^{wt/cys}* breeding, homozygous animals showed reduction in body weight at P14 - P16 (P = postnatal day) (Fig. 15C). Furthermore, homozygous animals were hyperexcitable when touched by the experimenter or littermates (Supplementry video file) and developed severe spontaneous seizures. Therefore, homozygous mice had to be sacrificed by P18 (Fig. 15D). Since heterozygous *Gpx4^{wt/cys}* animals were viable like the wt and no abnormalities were observed, further studies were performed with *Gpx4^{wt/wt}* and *Gpx4^{cys/cys}* animals.
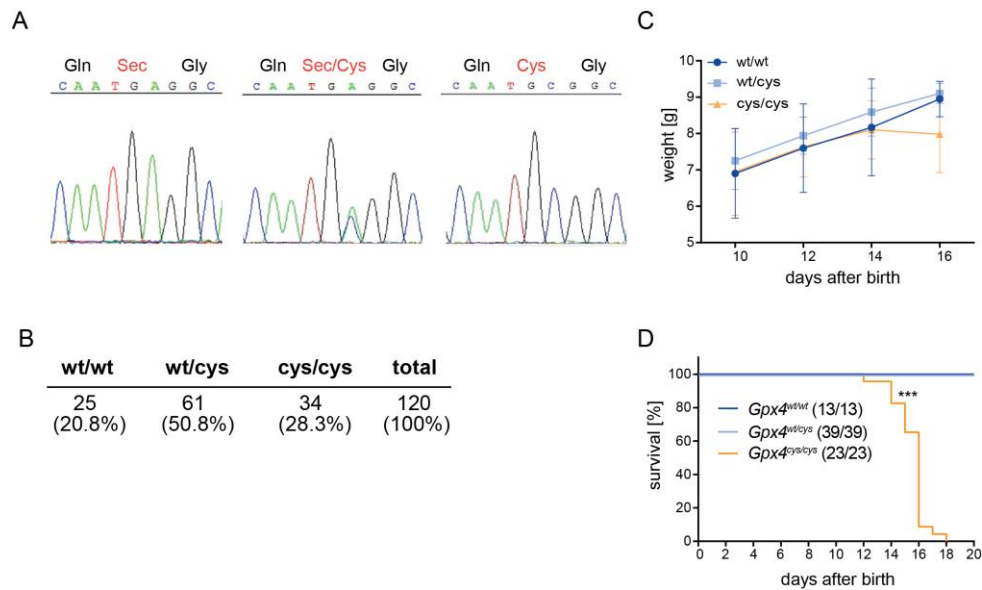
**Figure 15:** *Gpx4$^{cys/cys}$* **animals survive during embryogenesis but die at pre-weaning age.** (A) Amplifying and sequencing a region covering the critical exon 3 confirmed the targeted point mutation of Sec (UGA) to Cys (UGC) codon in offspring heterozygous and homozygous for the *Gpx4* Cys allele. (B) Offspring derived from a *Gpx4$^{wt/cys}$* breeding were born according to Mendelian ratio. (C) *Gpx4$^{cys/cys}$* animals survived embryogenesis, but showed reduced body weight between P14 - 16 (P = postnatal day). (D) As *Gpx4$^{cys/cys}$* animals developed severe spontaneous seizures they had to be sacrificed lately by P18. Statistical analysis was performed using Mantel Cox test ρ< 0.0001 (****).

Since the behavioral phenotype of the homozygous *Gpx4$^{cys/cys}$* animals pointed to an impairment of neuronal function, an (immuno)histopathological study was conducted on animals at the age of P16 using different neuronal markers (Fig. 16A). Epileptic seizures occur due to an imbalance of the network and function of inhibitory interneurons (GABAergic) and excitatory neurons (glutamatergic) (214). Although GABAergic interneurons represent only 10% - 20% of all neurons in the brain, any abnormalities or impairment of GABAergic interneuron function may disrupt the regulation of local excitatory circuits causing hyperexcitability thereby contributing to the development of epilepsy (214,215). Among all GABAergic interneurons, PV+ are considered to be the dominant interneuron cell type in rodents (214) and are strongly associated with controlling and regulating seizure activity (216,217). Therefore, stainings were performed to detect PV+ interneurons in brain slices of *Gpx4$^{wt/wt}$* and *Gpx4$^{cys/cys}$* animals. This analysis revealed a dramatic loss of PV+ interneurons in the cortex of homozygous *Gpx4$^{cys/cys}$* animals (Fig. 16A). Further immunohistochemical analyses showed that the decrease of PV+ interneurons was accompanied by increased TUNEL-positive cells.
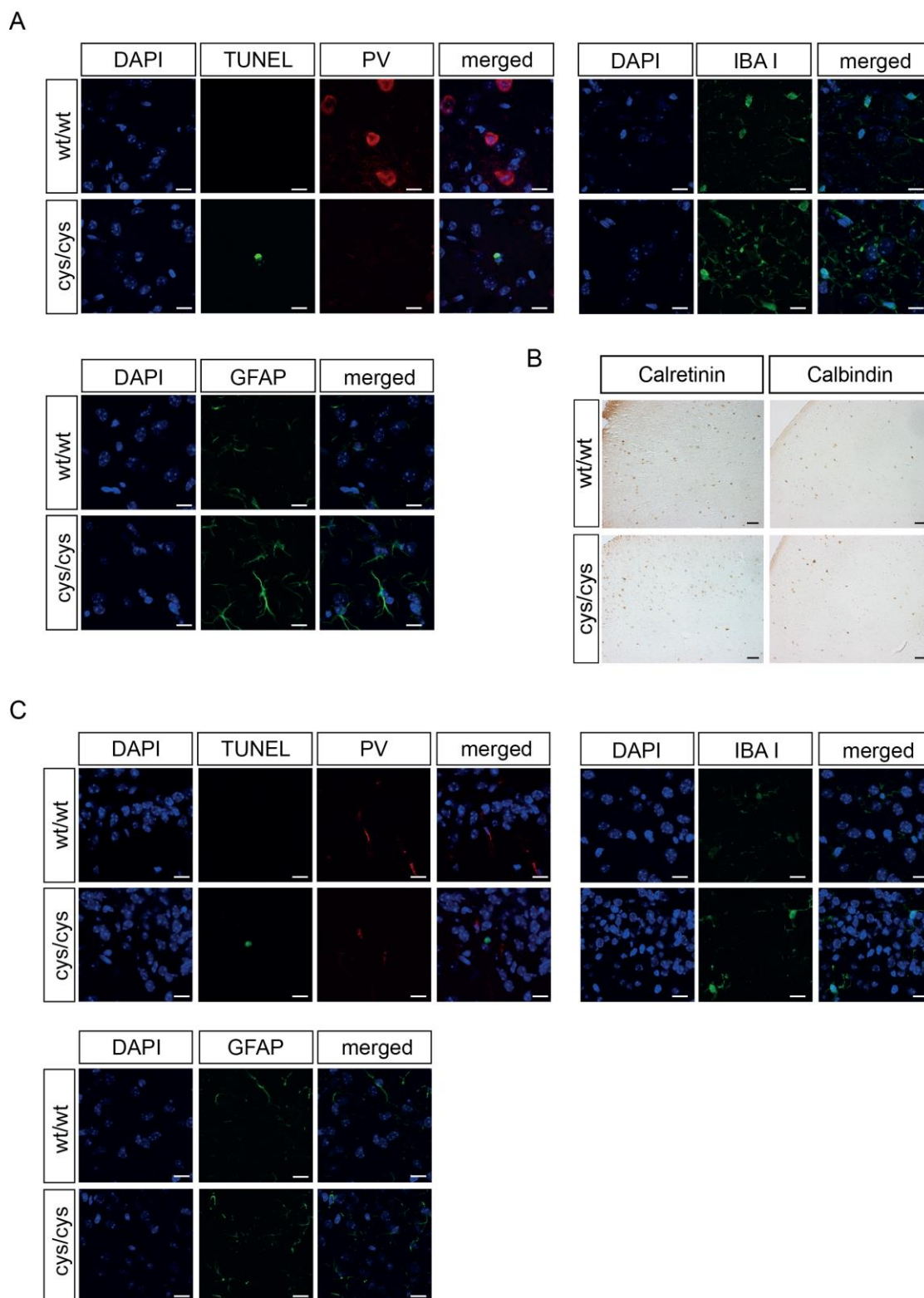
A



B



C



**Figure 16: *Gpx4cys/cys* animals show loss of parvalbumin-positive interneurons in the cortex.** (A) Immunohistochemical analysis of the brain revealed a reduced number of parvalbumin positive (PV+) interneurons (red) in the cortex of homozygous *Gpx4cys/cys* animals at P16. TUNEL-positive cells (green) were solely detected in the brain of *Gpx4cys/cys* animals. Additionally, augmented expression of glial fribrillary acidic protein (GFAP) and ionized calcium binding adaptor molecule 1 (IBA1) was observed in the cortex of *Gpx4cys/cys* animals (n = 5 each genotype; scale bars = 10 µm). (B) No difference was detected in the expression of other interneuron markers such as calretinin and calbindin (n = 5 each genotype; scale bars = 100 µm).

(C) At earlier days of postnatal development (P10), no differences were observed in the expression of PV+ interneurons, GFAP and Iba1 in the cortex of both genotypes. Yet, TUNEL-positive cells were already detectable in the cortex of $Gpx4^{cys/cys}$ animals (n = 5 each genotype; scale bars = 10 μm).

Besides, elevated expression of glial fibrillary acidic protein (GFAP) and ionized calcium binding adaptor molecule 1 (IBA1) was detected in the cortex of homozygous $Gpx4^{cys/cys}$ animals indicating reactive astrogliosis and neuroinflammation due to the loss of neurons (Fig. 16A). On the contrary, the expression of other markers of GABAergic interneurons, such as calbindin- and calretinin-positive neurons, remained unaltered (Fig. 16B). Since PV+ interneurons develop between P8 and P16, immunohistochemical staining of PV was conducted on animals at P10. Although no difference was detected regarding PV expression in homozygous and wt animals at P10 (Fig. 16C), TUNEL positive cells were already detectable in $Gpx4^{cys/cys}$ cortex. These findings suggest that PV+ interneurons fail to develop to fully mature neurons in homozygous $Gpx4^{cys/cys}$ animals. Remarkably, the phenotype of $Gpx4^{cys/cys}$ mice strongly resembled the phenotype of animals lacking $Gpx4$ specifically in glutamatergic neurons, which also suffered from spontaneous seizures and showed loss of PV+ interneurons (124,152).

## 4.3.2 Histopathological and immunoblot analysis of tissues derived from $Gpx4^{cys/cys}$ animals

Immunoblot analysis of different somatic organs (brain, lung, heart, spleen, liver, kidney) derived from $Gpx4^{wt/wt}$ and $Gpx4^{cys/cys}$ animals showed a profound increase in GPX4 expression (Fig. 17A), which is in line with what had been already observed in $Gpx4^{wt/ser}$ animals (see 4.2.1) (8), and might be likely explained by a faciliated insertion of Cys compared to Sec. Although GPX4 expression in somatic tissue was strongly increased, GPX4-specific activity using PCOOH as a substrate was not detectable in tissue samples obtained from homozygous $Gpx4^{cys/cys}$ animals (Fig. 17B). Since a complete loss of GPX4 activity would not allow animal survival and embryonic development, as already demonstrated in systemic $Gpx4^{-/-}$ (149-151), $Gpx4^{ala/ala}$ (190) and $Gpx4^{ser/ser}$ mice (8), it is more likely that the Cys variant of GPX4 preserved partial activity in intact cells and tissue that is no longer detectable using the classical GPX4-specific enzyme activity assay upon lysis of cells and tissues. Although the immunohistochemical data of the brain strongly suggested that pre-weaning

lethality of homozygous *Gpx4cys/cys* animals was caused by severe seizures, a histopathological analysis of other somatic tissue was performed to rule out morphological aberrations in other tissues that could result in pre-weaning lethality. Conditional *Gpx4* KO models performed previously revealed a vital role of GPX4 for proper cell function and survival not only in brain (124,125,152,193), but also in liver (122) and kidney (148). Therefore, H&E staining was performed with organs including liver, lung, heart and kidney derived from 15 days old *Gpx4wt/wt* and *Gpx4cys/cys* animals. Morphological abnormalities were, however, not detected in any tissues isolated from *Gpx4cys/cys* animals (Fig. 17C) strongly suggesting that pre-weaning lethality of homozygous *Gpx4cys/cys* mice is due to severe spontaneous seizures rather than impaired function of other vital organs, such as liver, heart and kidney.
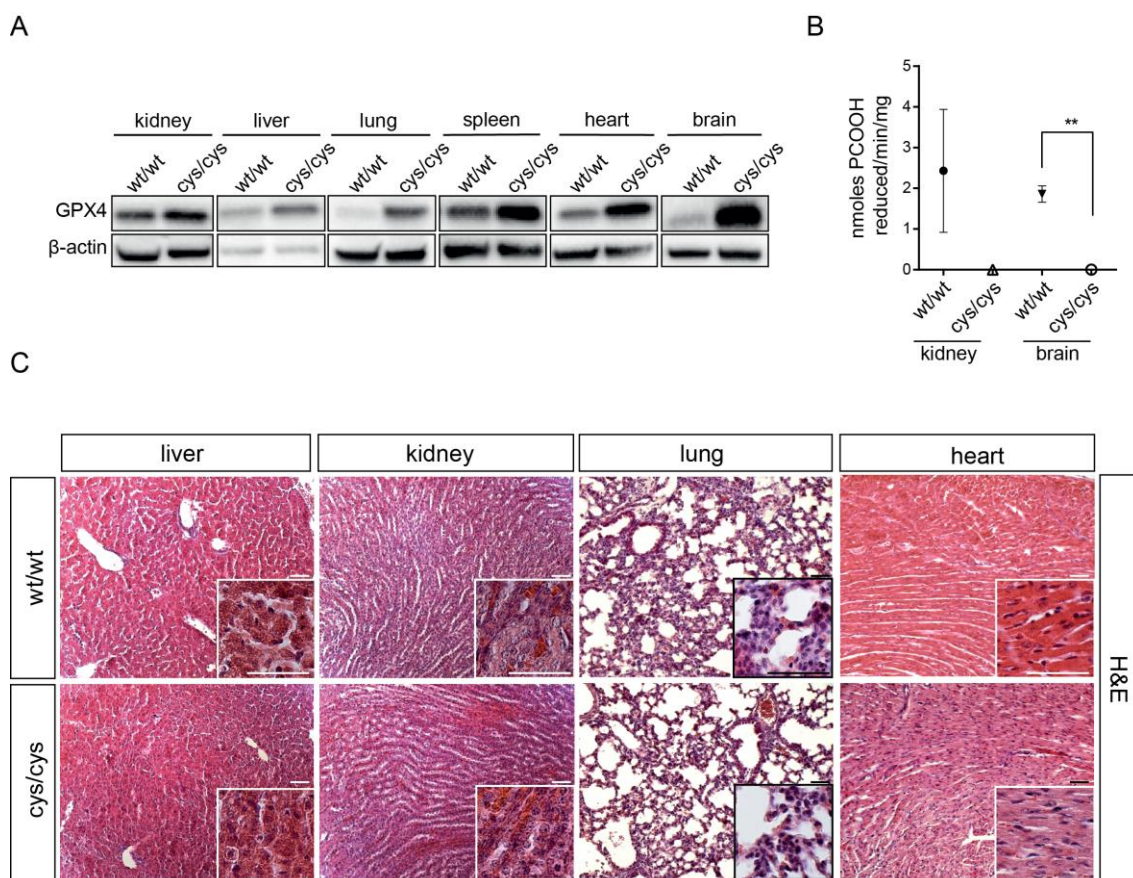


**Figure 17: *Gpx4cys/cys* mice show augmented expression of the GPX4 protein and normal development of somatic tissue.** (A) Immunoblot analysis of GPX4 in somatic tissue revealed an increased expression of the Cys variant of GPX4 in homozygous animals. (B) No GPX4-specific enzyme activity using PCOOH as substrate was detectable in kidney and brain samples derived from *Gpx4cys/cys* animals (n = 3 samples per tissue; statistical analysis was conducted using two-tailed t test $p<0.01$ (**)). Data was provided by Dr. Antonella Roveri (University of Padova). (C) H&E staining of somatic tissue did not reveal any overt morphological abberations (scale bars = 50 µm, insets = 20 µm).

### 4.3.3 Animals expressing the Cys variant of GPX4 on a *C57BL/6J* genetic background die during embryogenenesis at E10.5 – E11.5

For the generation of the mouse line expressing the Cys variant of GPX4, the ES cell line IDG3.2-rosa26 was used for the transfection of the targeting vector. Since the IDG3.2-rosa26 cell line is an F1 hybrid ES cell line established from (*C57BL/6J × 129S6SvEvTac*)-$F_1$ blastocyst (218), *Gpx4$^{wt/cys}$* mice were backcrossed with *C57BL/6J* mice during the course of the thesis to obtain a *C57BL/6J* genetic background of the original mouse strain. During the backcrossing and subsequent intercrosses of heterozygous mice it was, however, found that the phenotype of homozygous *Gpx4$^{cys/cys}$* mice dramatically changed. After the 7$^{th}$ - 8$^{th}$ generation heterozygous *Gpx4$^{wt/cys}$* matings no longer yielded homozygous *Gpx4$^{cys/cys}$* offspring, strongly suggesting embryonic lethality of homozygous mice (74% *Gpx4$^{wt/cys}$*, 26% *Gpx4$^{wt/wt}$*). Therefore, embryonic analysis was performed to determine the time and the reason of lethality of homozygous embryos. Female mice from heterozygous *Gpx4$^{wt/cys}$* breeding were daily checked for vaginal mucous plug and pregnant females were sacrificed at different times of gestation (E9.5 - E12.5). Embryos at E9.5 and E10.5 were collected with the expected Mendelian ratio of genotypes (Fig. 18A). While homozygous *Gpx4$^{cys/cys}$* embryos at E9.5 were morphologically normal and were phenotypically indistinguishable from their wt or heterozygous littermates (Fig. 18B), homozygous embryos at E10.5 showed signs of malformations including growth retardation, open neural tube (arrows) and hemorrhages (arrows) around the head indicating defects in the integrity of the vascular system (Fig. 18B). At E11.5, severe malformations such as growth retardation, pericardial edema (arrows) and paleness were observed in homozygous *Gpx4$^{cys/cys}$* embryos (Fig. 18B). At E12.5, increased resorption of embryos was detected, indicating that the time of embryonic lethality of *Gpx4$^{cys/cys}$* embryos must lie between E10.5 and E11.5 (Fig. 18B). In order to determine the reason of lethality, immunohistochemical and histological analysis was performed on paraffin-embedded embryo sections isolated at E9.5 - E11.5 of embryogenesis (Fig. 18C and D). H&E confirmed the presence of pericardial edema, which is visible at E10.5 and E11.5 from the dilatation of the pericardial sac in homozygous embryos (Fig. 18C, arrows).

A

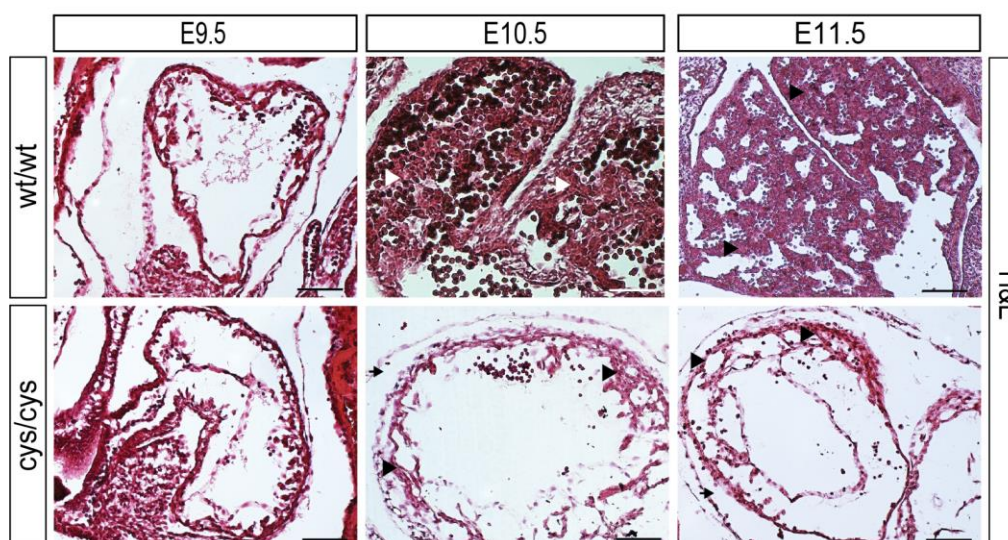| Embryonic stage | wt/wt | wt/cys | cys/cys | total | resorption |
|---|---|---|---|---|---|
| E9.5 | 5 (21.7%) | 14 (61.9%) | 4 (17.4%) | 23 (100%) | 0 |
| E10.5 | 9 (33.3%) | 13 (48.3%) | 5 (18.4%) | 27 (100%) | 1 |
| E11.5 | 8 (28.6%) | 16 (57.1%) | 4 (14.3%) | 28 (100%) | 3 |
| E12.5 | 2 (25%) | 5 (62.5%) | 1 (12.5%) | 8 (100%) | 2 |

B
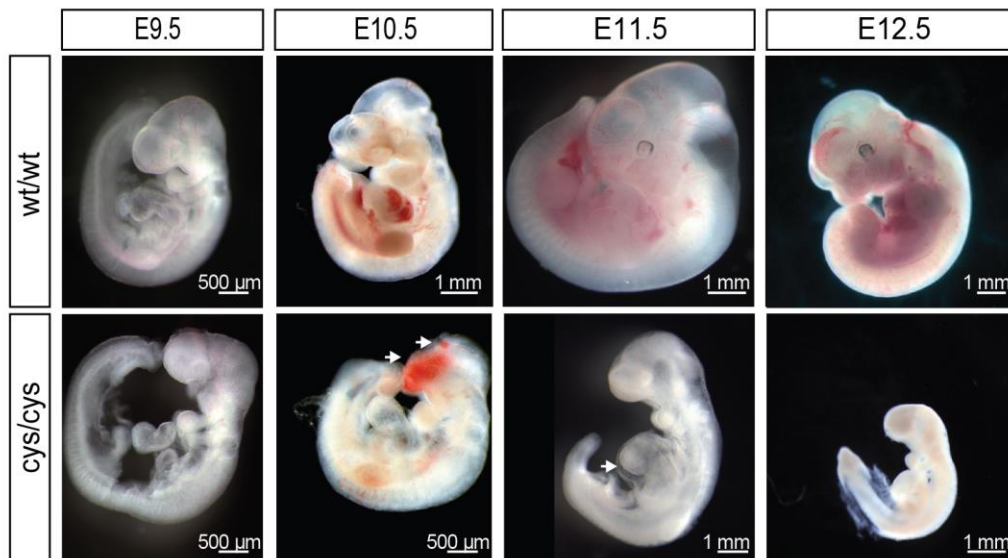


C



**Figure 18: *Gpx4<sup>cys/cys</sup>* mice on a *C57BL/6J* genetic background fail to survive embryogenesis.** (A) Genotyping of embryos from *Gpx4<sup>wt/cys</sup>* breeding isolated at various embryonic stages (E9.5 - E12.5) showed Mendelian distribution of genotypes at E9.5 and E10.5. At E11.5 the number of intrauterine resoprotion increased and by E12.5 homoyzgous *Gpx4<sup>cys/cys</sup>* embryos were no longer detectable by PCR. (B) At E9.5, homozygous *Gpx4<sup>cys/cys</sup>* embryos appeared normal and were mostly indistinguishable from their wt and heterozygous littermates.

At E10.5, malformations were observed in mutant homozygous embryos including growth retardation, hemorrhages in the head (arrow) and open neural tube (arrow). Homozygous *Gpx4^{cys/cys}* embryos showerd severe malformations by E11.5 and 12.5 including massive growth retardation, paleness and pericardial edema (arrow). (C) H&E staining of embryo sections confirmed pericardial edema (arrow) and revealed decreased myocardial trabeculation (arrow heads) in homozygous mutant embryos at E10.5 and E11.5. (Scale bars 18C = 100 µm).

Furthermore, the myocardial trabeculation in the heart ventricle was found to be dramatically decreased in mutant compared to wt embryos (Fig. 18C, arrow heads). Taken together the analysis of the homozygous *Gpx4^{cys/cys}* embryos points to an impaired heart development.

### 4.3.4 MEFs as a cellular tool to investigate the mechanistic functions of Sec in GPX4

In order to explain the underlying cellular and biochemical mechanisms for the above-described phenotypes, MEF cell lines were established from embryos derived from heterozygous *Gpx4^{wt/cys}* breedings. The genotype of the embryos was assessed by two independent PCRs that identified either the wt or the mutant allele (Fig. 19A). Cell lines of the three different genotypes were viable *in vitro*, and the proliferation rate between the different cell lines was indistinguishable (Fig. 19A). Immunoblotting against GPX4 in MEFs revealed a significant increase of the expression levels in *Gpx4^{wt/cys}* and *Gpx4^{cys/cys}* MEFs (Fig. 19B) without alterations in their mRNA levels (Fig. 19C). These data are in line with what was already observed in MEFs and tissue derived from *Gpx4^{wt/ser}* animals (see Fig. 10 and 12) (8), again suggesting that decoding and insertion of Cys is by far easier than the complex co-translational Sec incorporation mechanism. As already observed in tissue samples derived from *Gpx4^{cys/cys}* mice (Fig. 17B), GPX4-specific activity in homozygous *Gpx4^{cys/cys}* MEFs dramatically dropped despite an almost 15-fold increased expression of the mutant GPX4 protein (Fig. 19D). These findings imply that the Sec → Cys conversion either dramatically affects the activity of the enzyme, or its sensitivity towards oxidation upon cell and tissue rupture.

Labeling of cells with $^{75}$Se radioisotope ruled out that homozygous *Gpx4^{cys/cys}* cells incorporate Se unspecifically in the mutant protein (Fig. 19E). Furthermore, heterozygous *Gpx4^{wt/ser}* and *Gpx4^{wt/cys}* demonstrated a reduced incorporation of Se in the mutant GPX4 protein (Fig. 19E), indicating gene-dosage effects. Immunoblot analysis of other important selenoproteins (TXNRD1, TXNRD2) and

related redox enzymes (i.e. PRX1-3) expressed in cultured cells only showed a slight increase of mitochondrial PRX3 expression (Fig. 19F). Since no differences were evidenced between *Gpx4^{wt/wt}* and *Gpx4^{wt/cys}* cells, the following studies were performed with wt and homozygous mutant cells.
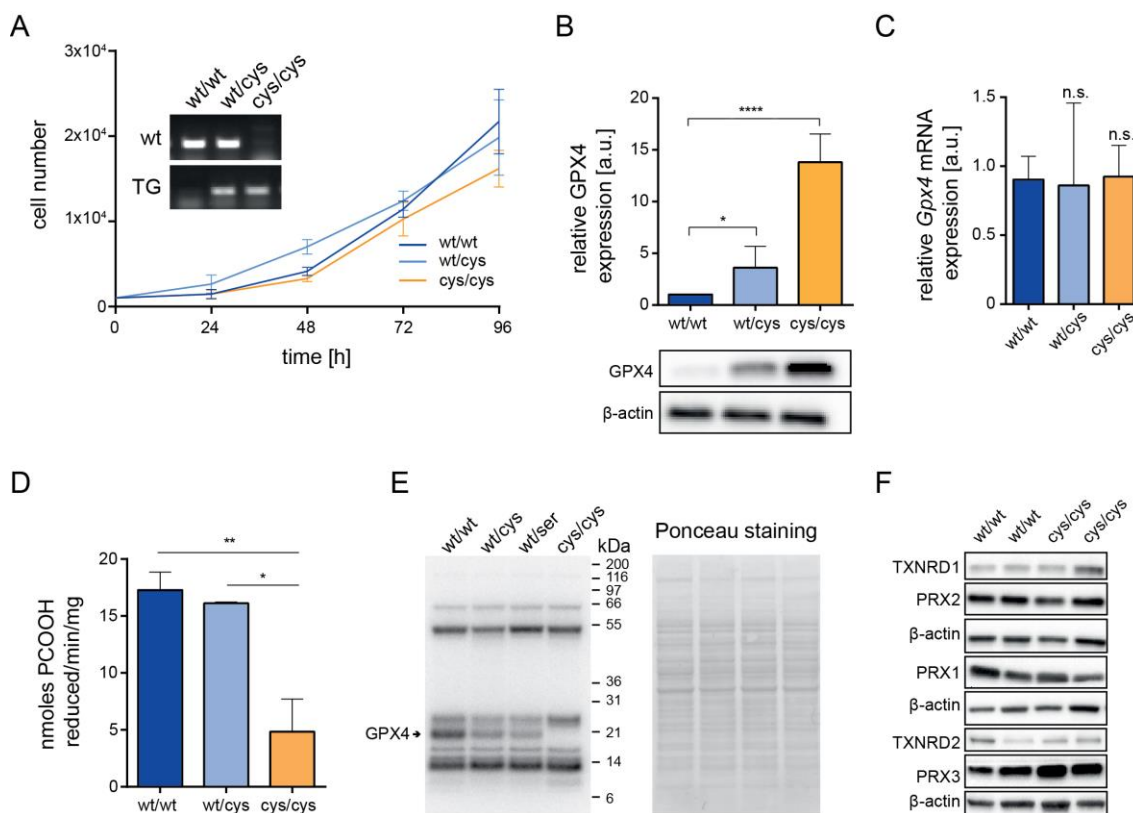


**Figure 19: *Gpx4^{cys/cys}* MEFs are viable *in vitro* and show highly increased GPX4 protein levels.** (A) MEFs derived from heterozygous *Gpx4^{wt/cys}* breeding were viable *in vitro* and showed no differences in their proliferation rates. The genotype of the established cells lines was assessed by two independent PCRs identifying the wt allele (256 bp) or the Cys (tg) allele (203 bp). (B-C) GPX4 protein expression was found to be significantly increased in *Gpx4^{wt/cys}* and *Gpx4^{cys/cys}* MEFs without any alteration of *Gpx4* mRNA levels (statistical analysis was conducted using the two-tailed t test $\rho<0.05$ (*); $\rho<0.0001$ (****); n.s. = not significant; a.u. = arbitrary units). (D) Despite increased GPX4 protein levels, GPX4-specific activity was dramatically decreased in *Gpx4^{cys/cys}* MEFs (statistical analysis was conducted using the two-tailed t test $\rho<0.05$ (*); $\rho<0.01$ (**)). (E) Cell labeling with radioisotope $^{75}$Se confirmed that *Gpx4^{cys/cys}* MEFs do not unspecifically incorporate Se in GPX4. Decreased levels of Se are incorporated in Gpx4 of *Gpx4^{wt/ser}* and *Gpx4^{wt/cys}* MEFs, indicating a gene-dosage effect. Ponceau staining of the gel confirmed equal loading of the proteins (Data was kindly provided by Dr. Xiao Xiao Peng, Karolinska Institutet, Sweden). (F) Immunoblot analysis of different important redox enzymes revealed only a slight increase of peroxiredoxin 3 (PRX3) expression (F).

### 4.3.5 Hydroperoxide-induced cell death in *Gpx4^{cys/cys}* MEFs shows classical hallmarks of ferroptosis

Since *Gpx4^{cys/cys}* MEFs were viable *in vitro* and no difference was evident under basal conditions to *Gpx4^{wt/wt}* MEFs (Fig. 19A), both cell lines were treated with

different cytotoxic compounds to assess their response to these lethal stimuli. Surprisingly, *Gpx4*$^{cys/cys}$ MEFs demonstrated an unforeseen sensitivity against hydroperoxide-induced cell death using hydrogen peroxide ($H_2O_2$), tBOOH and cholesterol hydroperoxide (ChOOH) (Fig. 20A). Additionally, inducers of superoxide and hence $H_2O_2$ formation, such as mitochondrial complex I inhibitors rotenone and phenformin, provoked similar toxic effects in *Gpx4*$^{cys/cys}$ MEFs like the aforementioned hydroperoxides (Fig. 20B). For a direct assesement of cell toxicity, lactate dehydrogenase (LDH) release was measured. LDH release assays confirmed that low concentrations of hydroperoxides and complex I inhibitor indeed induce profound cell death within a 6-12 h after treatment (Fig. 20C). By stark contrast, mutant cells were equally resistant towards other cytotoxic compounds, such as FCCP, menadione, vinoblastine, irinotecan, mitoxantron, nocodazole, PAO and sulforaphane (Fig. 20D). Although *Gpx4*$^{cys/cys}$ cells were slightly sensitiver towards the Complex III inhibitors antimycin A and myxothiazol, a cytotoxic dosis effect was not observed (Fig. 20D), indicating that in *Gpx4*$^{cys/cys}$ cells the site of ROS formation in the mitochondrial respiratory chain might play a role for the sensitivity towards mitochondrial complex inhibitors.

Intriguingly, homozygous *Gpx4*$^{cys/cys}$ cells were more resistant towards ferroptosis-inducing agents (FIN) including *(1S,3R)*-RSL3, erastin and the γGCS inihibitor BSO (Fig. 21A). One of the hallmarks of ferroptotic cell death is the loss of GPX4 expression/activity. While *(1S,3R)*-RSL3 is supposedly a direct inhibitor of GPX4 by alkylation of the selenolate thus inactivating GPX4, erastin and BSO impair GPX4 activity indirectly by decreasing the GSH level in the cell (148,152,156). Determination of the GSH level in the MEFs revealed that homozygous *Gpx4*$^{cys/cys}$ cells contained significantly more total GSH than their wt counterparts (Fig. 21B), explaining why they required a higher concentration of the GSH inhibitors BSO and erastin to induce cell death.
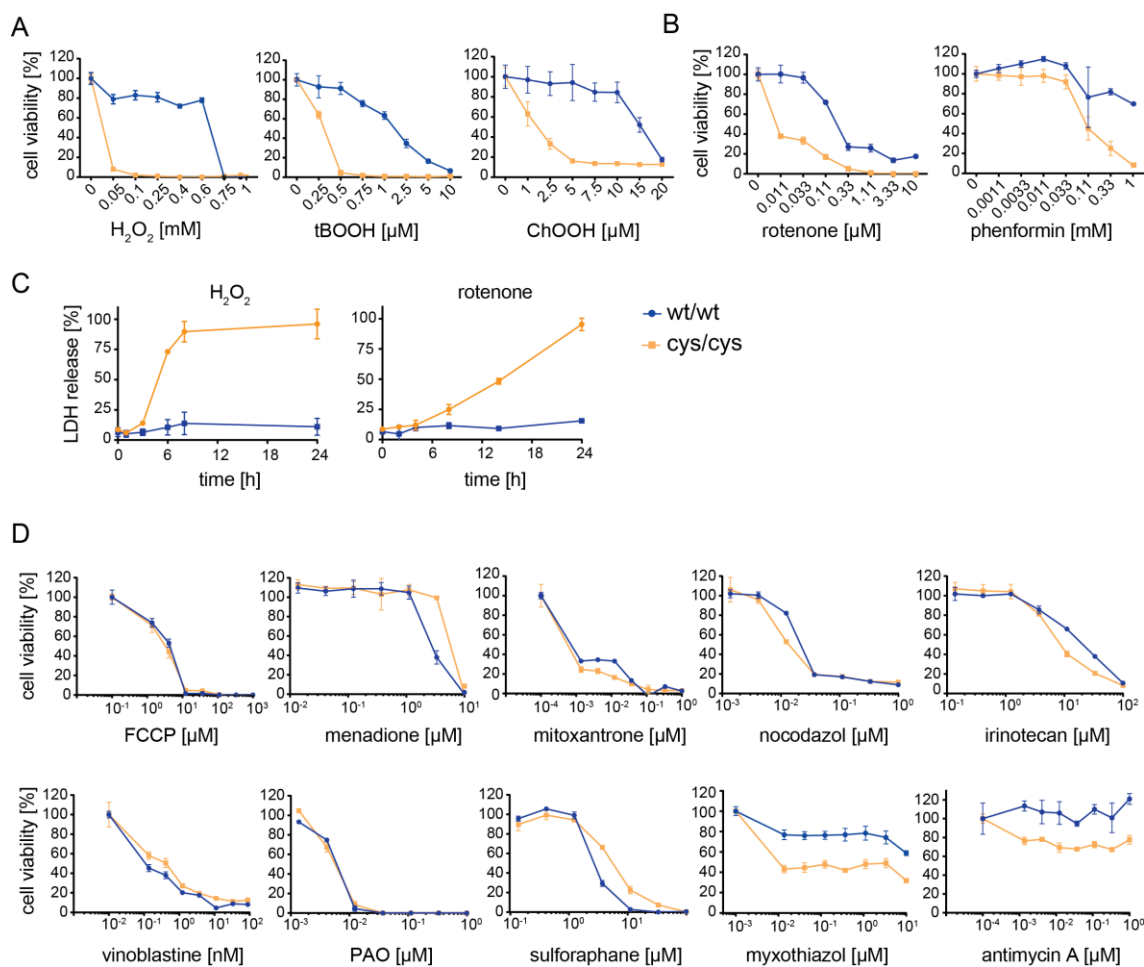
**Figure 20: *Gpx4^{cys/cys}* MEFs are highly sensitive towards hydroperoxide-induced cell death.** (A) Homozygous cells expressing the Cys variant of GPX4 showed a profoundly increased sensitivity towards hydroperoxide-induced cell death triggered by $H_2O_2$, tBOOH and ChOOH compared to wt cells. (B) A similar toxic effect was observed using the complex I inhibitors rotenone and phenformin. (C) For a direct asssessement of cell toxicity lactate dehydrogenase (LDH) release was measured under hydrogen peroxide ($H_2O_2$) and complex I inhibitor (rotenone) treatment. LDH release measurement showed that cell death occurred within 6 h ($H_2O_2$) and 12 h (rotenone) in *Gpx4^{cys/cys}* cells. (D) This increased sensitivity to cell death inducers appeared to be specific for hydroperoxides as no difference was detected upon treatment with other cytotoxic compounds including FCCP, menadione, mitoxantrone, nocodazol, irinotecan, vinoblastine, PAO and sulforaphane. *Gpx4^{cys/cys}* cells were more sensitive toward treatment with the complex III inhibitors antimycin A and myxothiazol, although dosis dependent effects were not evident.

Although *(1S,3R)*-RSL3 was shown to specifically interact with Sec of GPX4 (188), cells were generated with a doxycycline (Dox)-dependent expression of wt or Cys variant of GPX4 in order to investigate if elevated expression of the mutant protein might also impact on the resistance of the protein. Therefore, two cell lines were generated expressing either a doxycycline (Dox) dependent wt or Cys variant of GPX4 in a PFa1 background which are further referred to as "Dox addback" and "Dox U46C", allowing a regulated expression of both variants of GPX4. In order to find a concentration which induces a similar expression level,

both cell lines were supplemented with different concentrations of doxycycline and tested for GPX4 portein levels (Fig. 21C). For the *(1S,3R)*-RSL3 treatment cells were supplemented with 10 µg/ml (Dox addback) or 1 µg/ml (Dox U46C) doxycycline to achieve comparable protein expression levels of GPX4 in both cell lines (Fig. 21D). As illustrated in Figure 21D, *(1S,3R)*-RSL3 indeed has a much higher affinity for Sec in the active site of wt GPX4 as previously published (188), but not with the Cys residue as the cells were much more resistant towards *(1S,3R)*-RSL3 induced cell death despite an equal expression wt and Cys containing GPX4 protein.

In order to explore in more detail the cell death modality that is triggered upon hydroperoxide treatment in homozygous mutant MEFs, *Gpx4^{wt/wt}* and *Gpx4^{cys/cys}* cells were treated with different cell death inhibitors before cell death was elicited using the aforementioned hydroperoxides. As depicted in Figure 21E-H, the ferroptosis inhibitors ferrostatin-1, liproxstatin-1, ciclopirox olamine and α-Tocopherol (α-Toc) were able to rescue hydroperoxide-induced cell death in *Gpx4^{cys/cys}* cells. By contrast, apoptosis (Z-VAD-FMK) and necroptosis (necrostatin-1(S)) inhibitors failed to rescue hydroperoxide-induced cell death in homozygous mutant cells, strongly suggesting that hydroperoxide-induced death is indeed ferroptotic. Noteworthy, hydrogen peroxide-induced cell death in *Gpx4^{wt/wt}* could not be prevented with any of the aforementioned cell death inhibitors, indicating that they probabaly undergo a necrotic ("explosive") type of cell death.
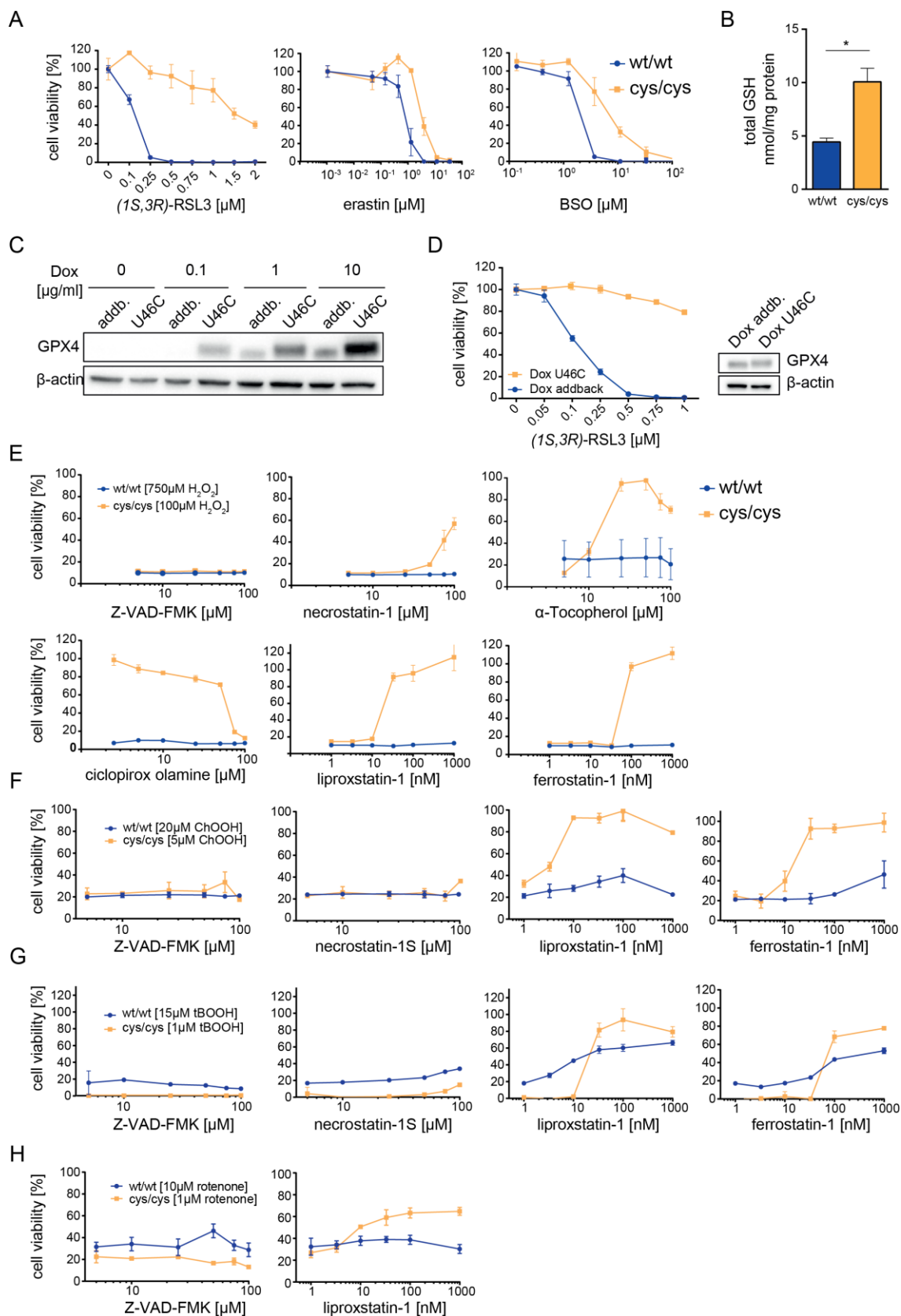
**Figure 21: Hydroperoxide-induced cell death in *Gpx4^cys/cys* cells can be prevented by ferroptosis inhibitors.** (A) Homozygous cells expressing the Cys variant of GPX4 were more resistant towards ferroptosis inducers *(1S,3R)*-RSL3, erastin and BSO than the wt control cells. (B) Assessment of total GSH in the cell revealed that *Gpx4^cys/cys* cells contain a significantly higher level of total GSH than wt cells. (C) Doxycyclin-dependent expression of GPX4 performed in "Dox

addback" and "Dox U46C" cells using increasing concentrations of Dox. (D) *(1S,3R)*-RSL3 treatments performed on cells with equal GPX4 expression showed that *(1S,3R)*-RSL3 has a much higher affinity for Sec than Cys leading to an increased resistance of *Gpx4$^{cys/cys}$* cells towards *(1S,3R)*-RSL3-induced cell death. Equal GPX4 protein expression was achieved by supplementing different amounts of Dox to the cell culture medium (10 µg/ml Dox for wt and 1 µg/ml Dox for Cys). (E) Hydroperoxide-induced cell death using lethal concentrations of $H_2O_2$ could be prevented by ferroptosis inhibitors including ferrostatin-1 (fer-1), liproxstatin-1 (liprox-1), ciclopirox olamine and α-Tocopherol (α-Toc) only in *Gpx4$^{cys/cys}$* but not in wt cells, whereas the apoptosis inhibitor Z-VAD-FMK and the necroptosis inhibitor Necrostatin-1(S) failed to rescue. $H_2O_2$ induced cell death in wt cells could not be rescued with any of the tested cell death inhibitors, indicating that wt cells undergo an unregulated form of necrotic cell death. (F) Likewise, cell death induced by ChOOH (F), tBOOH (G) and rotenone (H) could only be inhibited by ferroptosis inhibtors in *Gpx4$^{cys/cys}$* but not in *Gpx4$^{wt/wt}$* cells.

Previous studies showed that genetic or pharmacological inactivation of GPX4 causes lipid peroxidation, a hallmark of ferroptosis that can be fully blunted by ferroptosis inhibitors (148). Therefore, lipid peroxidation was assessed in *Gpx4$^{wt/wt}$* and *Gpx4$^{cys/cys}$* cells using the lipid peroxidation sensitive dye BODIPY 581/591 C11. While *Gpx4$^{cys/cys}$* cells treated with $H_2O_2$ showed a dramatic increase of lipid peroxidation that could be blocked by liproxstatin-1, *Gpx4$^{wt/wt}$* cells presented only a marginal increase in dye oxidation even at very high concentrations of $H_2O_2$ (750 µM) (Fig. 22A).

To further interrogate the striking sensitivity of the Cys variant of GPX4 towards hydroperoxide-induced cell death, a mass spectrometry analysis of FLAG-Strep-tagged cys-GPX4 expressed in the PFa1 background (further referred to as U46C) was conducted. Prior to protein isolation, U46C cells were exposed to lethal concentrations of $H_2O_2$ for 3 h and lysed well before cells undergo cell death. Mass spectrometry analysis performed on the isolated mutant protein identified the critical Cys (C46) to be readily overoxidized yielding sulfonic acid ($SO_3H$), however solely under hydroperoxide-treated conditions (Fig. 22B).
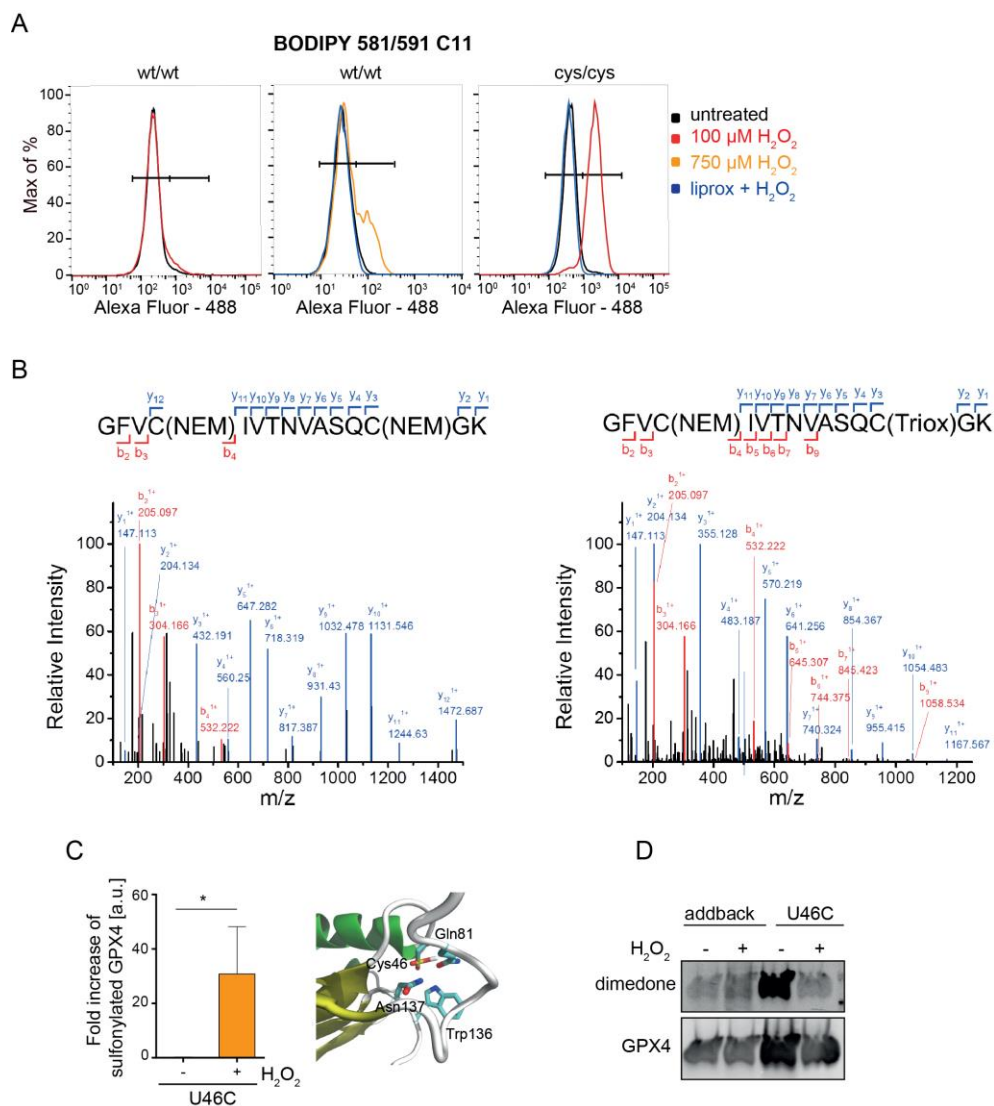
**Figure 22: Hydroperoxide treatment of *Gpx4^cys/cys* cells causes ferroptosis by irreversible overoxidation of GPX4 in intact cells.** (A) Lipid peroxidation using the fluorophoric probe BODIPY 581/591 C11 was not detectable in wt cells treated with low (100 µM) and only marginal at exceeding lethal concentrations (750 µM) of $H_2O_2$. *Gpx4^cys/cys* cells showed increased probe oxidation already at very low $H_2O_2$ concentrations which could be blocked by liproxstatin-1. (B) Prior to cell lysis, cells expressing exogenous FLAG-Strep-tagged Cys variant of GPX4 were treated with N-ethylmaleinimide (NEM) for irreversible protein thiol alkylation. Mass spectrometry analysis detected the peptide containing the critical Cys46 with alkylated thiols by NEM under basal conditions (left; presented spectrum: precursor charge: 2+, Monoisotopic m/z: 888.426, precursor mass deviation: -0.11ppm, Mascot Ionscore: 88) and with oxidative modification of the critical Cys under $H_2O_2$ treated conditions (right; Triox; presented spectrum: precursor charge: 2+, Monoisotopic m/z: 849.895, precursor mass deviation: -0.22ppm, Mascot Ionscore: 93). (C) Oxidative modification of the critical Cys46 embedded in the catalytic tetrade is depicted in a crystallographic modell. Modification of the critical Cys46 to a sulfonic acid ($SO_3H$) was significantly increased under $H_2O_2$ treated conditions (in 3 independent replicates; statistical analysis was conducted using two-tailed t test, $p < 0.05$ (*)). (D) Immunoblot detection of sulfenic acid (SOH) using an antibody against dimedone-labeled GPX4 showed no difference of the dimedone labeling after $H_2O_2$ treatment in addback (wt) cells. U46C cells showed decreased dimedone labeling of the Cys variant of GPX4 after $H_2O_2$ treatment. Mass spectrometry data and analysis of Cys modification were kindly provided by Dr. Carsten Berndt and Dr. Gereon Poschmann (University of Düsseldorf).

Under $H_2O_2$ treated conditions the oxidative modification of C46 was significantly increased compared to basal conditions where thiols were found to be alkylated by NEM (Fig. 22C). A crystallographic modell of the oxidized C46 embedded in the catalytic tetrade is depicted in Figure 22C. To rule out that the oxidation to - $SO_3H$ in C46 was unspecific due to cell lysis, an immunoblot-based detection of sulfenic acid (SOH) was performed. Therefore, FLAG-Strep-tagged wt GPX4 (further referred to as addback) and U46C cells were either treated with dimedone alone (dimedone specifically traps sulfenic acids (219)) or with $H_2O_2$ (100 µM) for 3 h followed by additional dimedone treatment. After FLAG-mediated precipitation, the tagged GPX4 protein was blotted against dimedone and GPX4 (using an HA-specific antibody) showing that after $H_2O_2$ treatment reduced amount of dimedone was bound to the mutant GPX4 protein in the U46C cell line compared to untreated cells (Fig. 22D). On the contrary, wt GPX4 protein showed no alteration of dimedone modified GPX4 protein after hydroperoxide treatment. Taken together these results provide compelling evidence that the (irreversible) oxidation of the catalytically active Cys in GPX4 protein is due to hydroperoxide treatment and not secondary to cell lysis.

Only recently, acyl-CoA synthetase long chain family member 4 (ACSL4) was identified as an important downstream player in the ferroptotic death pathway (176). ACSL4 is involved in lipid metabolism and biosynthesis by ligating HS-CoA to free long chain fatty acids converting them to acyl-CoA esters. Due to its preference for PUFAs, it is believed that ACSL4 shapes the phospholipid composition of lipid bilayers in the cell (177) and thereby raises its sensitivity towards oxidative modification and ferroptosis. In this context it was shown that PE containing oxigenated arachidonic and adrenic acid might be a potential source for the generation of a lethal ferroptotic signal (177). Genetic deletion of *Acsl4* was recently shown to confer an unprecedented inhibitory effect on ferroptosis induction in response to GPX4 inhibition or genetic deletion (177) (see 1.5.4). Therefore, ACSL4 expression level was evaluated by immunoblot analysis in *Gpx4^{wt/wt}* and *Gpx4^{cys/cys}* cells. As illustrated in Figure 23A, a strong decrease of ACSL4 protein level was detected in *Gpx4^{cys/cys}* MEFs, which may point to a compensatory mechanism to lower the sensitivity of *Gpx4^{cys/cys}* cells to ferroptosis induction. Accordingly, CRISPR/Cas9 mediated KO of *Acsl4* in U46C cells

rendered them even more resistant towards hydroperoxide-induced cell death compared to the parental cell line (Fig. 23B).
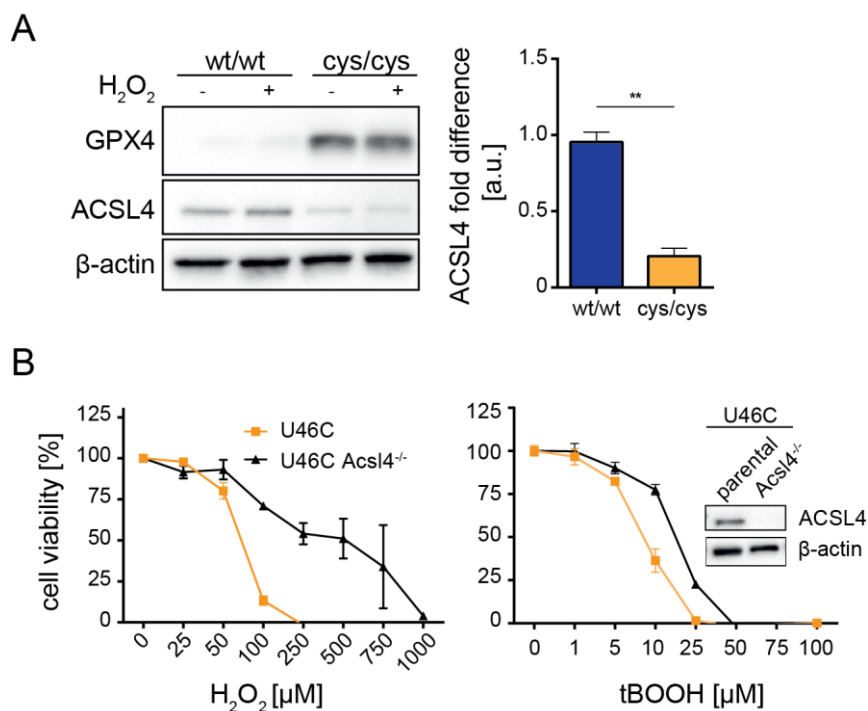


**Figure 23: ACSL4 expression is strongly reduced in *Gpx4cys/cys* cells**. (A) Immunoblot analysis revealed significantly decreased expression of acyl-CoA synthetase long chain family member 4 (ACSL4) in *Gpx4cys/cys* cells (statistical analysis was performed by two-tailed t test $p<0.01$ (**)). (B) CRISPR/Cas9 mediated KO of *Acsl4* in *Gpx4cys/cys* cells increased their resistance upon hydroperoxide-induced cell death compared to the parental cell line.

For a better understanding of the hydroperoxide-induced cell death process in homozygous mutant cells, ultrastructural analysis was then performed. The same hallmarks of structural changes in homozygous mutant cells that were already observed before in wt cells exposed to GPX4 inhibitors (148,177) i.e. outer mitochondrial membrane rupture (OMM) and shrinkage of mitochondrial matrix was manifested in *Gpx4cys/cys* cells treated with $H_2O_2$ and rotenone (Fig. 24).

Conclusively, hydroperoxide-induced cell death in *Gpx4cys/cys* cells reveals all hallmarks of ferroptosis pointing to an inactivation of GPX4 activity by hydroperoxides due to an irreversible oxidation of the Cys residue in the active site, which would be otherwise prevented in the wt protein due to the presence of the Sec residue.
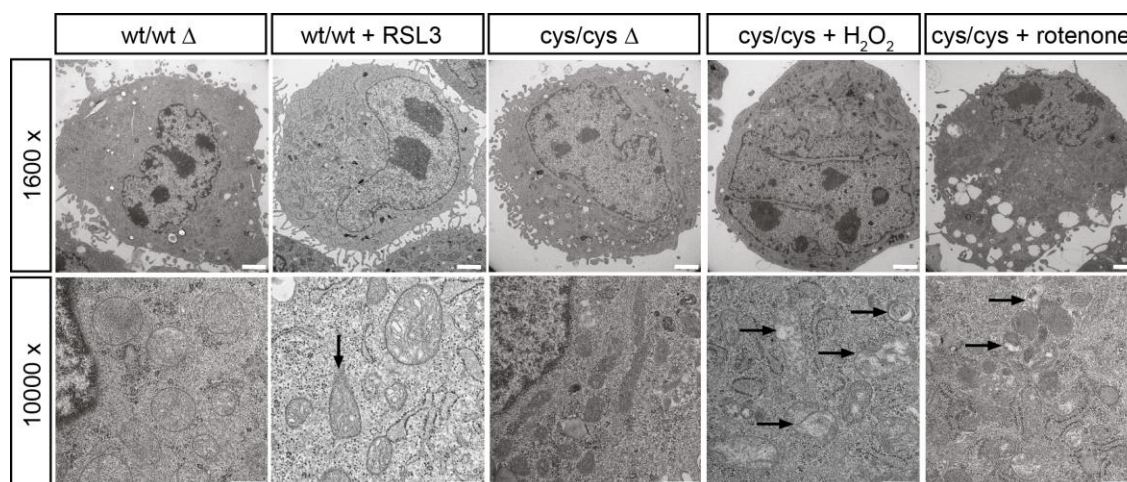
**Figure 24: Hydroperoxides induce structural damage of mitochondria of *Gpx4^cys/cys^* cells.** Structural analysis of whole cells by electron microscopy revealed that *Gpx4^cys/cys^* cells contained long mitochondria with a very dense mitochondrial matrix. Upon $H_2O_2$ (100 µM) and rotenone (1 µM) treatment, severe structural alterations of mitochondria (arrows) were detected including outer mitochondrial membrane rupture (OMM) and shrinkage of mitochondrial matrix. OMM can also be observed in wt cells treated with *(1S, 3R)*-RSL3 (148,177). (Scale bars upper lane = 2 µM; lower lane = 500 nm). Electron microscopy data was kindly provided by Dr. Michaela Aichler (Helmholtz Zentrum München).

## 4.3.6  Mitochondria are fully functional in *Gpx4^cys/cys^* MEFs

Previous reports indictated that GPX4 plays an important role in mitochondria by preventing oxidative damage in mitochondria and decreasing cardiolipin peroxidation, a highly unsaturated phospholipid exclusively present in the inner membrane of mitochondria (153,220). The increased sensitivity towards hydroperoxides and complex I inhibitors, as seen in *Gpx4^cys/cys^* cells (see Fig. 20B), raised the question if the Cys variant of GPX4 might have a negative impact on mitochondrial function since GPX4 is located in the intermembrane space and on the outer leaflet of the mitochondrial inner membrane. To investigate this in more detail, mitochondrial integrity was assessed on whole cell level and on isolated mitochondria derived from *Gpx4^wt/wt^* and *Gpx4^cys/cys^* cells. Determination of the basic functional parameters, such as number of mitochondria, mitochondrial swelling and mitochondrial membrane potential ($\Delta\Psi_m$), revealed that *Gpx4^cys/cys^* cells tend to contain larger mitochondria than wt cells yet with stable $\Delta\Psi_m$ (Fig. 25A-C). In order to evaluate the functionality of the mitochondrial electron transport chain (ETC) in wt and mutants cells, oxygen consumption rate (OCR) was measured using the seahorse XF extracellular flux analyzer. The

sequential injection of different compounds targeting the ETC, namely oligomycin A (ATP synthase inhibitor), FCCP (uncoupler of respiratory chain) and rotenone (complex I inhibitor) together with antimycin A (complex III inhibitor) allows a detailed characterization of the key parameters of metabolic function including basal respiration (1), ATP-linked respiration (2), non-mitochondrial respiration (3) and maximal respiration (4) (221).
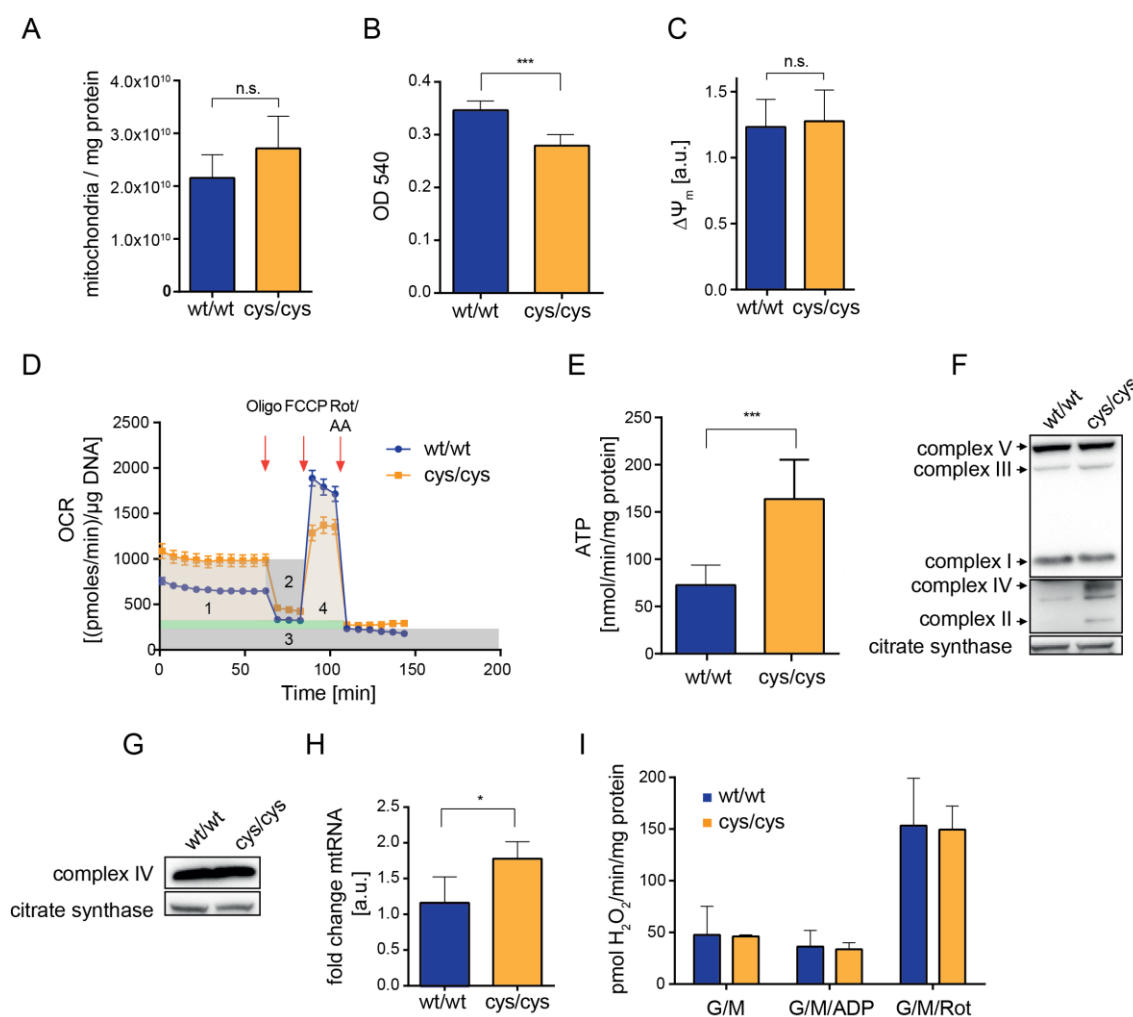


**Figure 25: Mitochondria of *Gpx4cys/cys* cells are functional and even show higher ATP production than *Gpx4wt/wt* cells.** (A, B) Assessment of basal functional parameters of mitochondria revealed that *Gpx4cys/cys* cells tend to have larger mitochondria, but do not show any impairment of their membrane potential (statistical analysis was performed by the two-tailed t test $\rho<0.001$ (***); n.s. = not significant) (C). (D) Measurement of oxygen consumption on whole cells performed by seahorse XF extracellular flux analyzer revealed that *Gpx4cys/cys* cells consume more oxygen due to a higher basal respiration, but fail to reach the same maximal respiration rate as *Gpx4wt/wt* cells (1 = basal respiration; 2 = ATP-linked respiration; 3 = non-mitochondrial respiration; 4 = maximal respiration). (E) ATP production measurements of isolated mitochondria revealed that *Gpx4cys/cys* cells generate significantly more ATP than wt counterparts (statistical analysis was conducted using two-tailed t test $\rho<0.001$ (***)). (F) Analysis of the expression of mitochondrial complexes revealed an increased expression of a mitochondrial encoded subunit of complex IV in *Gpx4cys/cys* mitochondria using an antibody that recognizes the mitochondrially

encoded subunit. (G) No difference in Complex IV expression was detected with an antibody recognizing a nuclear encoded subunit. (H) Abundance of mitochondrial (mt) RNA measured by qRT-PCR was significantly increased in $Gpx4^{cys/cys}$ cells (statistical analysis was conducted using two-tailed t test $\rho < 0.05$ (*); a.u. = arbitrary units). (I) No difference was detected when $H_2O_2$ release was measured on isolated mitochondria using Amplex Red under basal (G/M and G/M/ADP) and stress conditions (G/M/Rot) in $Gpx4^{wt/wt}$ and $Gpx4^{cys/cys}$ cells (oligo = oligomycin; Rot/AA = rotenone/antimycin A; G = glutamate; M = malate).

Interestingly, $Gpx4^{cys/cys}$ cells showed higher basal and ATP-linked respiration than $Gpx4^{wt/wt}$ cells (Fig. 25D). On the contrary, maximal respiration rate was higher in $Gpx4^{wt/wt}$ cells raising the question if maximal respiration might be impaired in $Gpx4^{cys/cys}$ cells (Fig. 25D). To challenge some of the results gained from the OCR measurement, ATP generation and the expression of mitochondrial respiratory chain complexes were analysed in isolated mitochondria. ATP generation was assessed by a bioluminescence-based assay that confirmed a significantly higher ATP generation in $Gpx4^{cys/cys}$ mitochondria (Fig. 25E). An immunoblot analysis of mitochondrial respiratory chain complexes revealed an unexpected increased expression of complex IV (cytochrome c oxidase) in $Gpx4^{cys/cys}$ mitochondria (Fig. 25F). Since the antibody used for the immunoblot analysis recognizes the mitochondrially encoded subunit I of Complex IV, qRT-PCR was performed to quantify the abundance of mitochondrial (mt) RNA in $Gpx4^{wt/wt}$ and $Gpx4^{cys/cys}$ cells. Quantification of mtRNA revealed a significantly higher mtRNA level in $Gpx4^{cys/cys}$ samples likely explaining the difference in complex IV subunit I expression (Fig. 25H). Accordingly, an immunoblot analysis using a different antibody recognizing a nuclear encoded subunit did not reveal any difference in the expression of complex IV (Fig. 25G).

Next, $H_2O_2$ release was determined to investigate electron leakage under different conditons such as glutamate/malate (G/M), G/M/ADP and G/M/rotenone in isolated mitochondria. Glutamate and malate serve as substrates for complex I, the addition of ADP increases the activity of ATP-synthase that results in a faster electron flux through the ETC and thus allows drawing conclusions about the activity of ATP-synthase activity. Surprisingly, no difference was detected regarding $H_2O_2$ release in wt and mutant mitochondria (Fig. 25I). Even under the G/M/rotenone condition, $Gpx4^{cys/cys}$ mitochondria did not show elevated $H_2O_2$ release compared to wt samples (Fig. 25I). This indicates that the sensitivity of $Gpx4^{cys/cys}$ cells towards complex I inhibitors (see Fig. 19B) is not due to increased $H_2O_2$ release but rather due to the site of $H_2O_2$ formation that is

generated upon this treatment, namely where GPX4 is located. These data collectively show that mitochondria of $Gpx4^{cys/cys}$ cells are fully functional and that their sensitivity towards complex I inhibitors is not due to elevated $H_2O_2$ release. It is notable, however, that $Gpx4^{cys/cys}$ cells seem to have a higher ATP demand since ATP generation and expression of mitochondrial proteins were found to be increased.

### 4.3.7 Cys variant of GPX4 can substitute for the loss of all selenoproteins in MEFs

Rodents express 24 selenoproteins of which four proteins, namely GPX4, TXNRD1, TXNRD2 and SELENOT are essential for embryonic development and survival *in vivo* (76,77,149,222), while just GPX4 was shown to be absolutely vital for cell survival *in vitro* (152). As aforementioned (see 1.5.5), it is striking that the KO of *Gpx4* alone in certain murine tissues phenocopies the loss of all selenoproteins by targeted deletion of Sec-specific tRNA[Ser]Sec, pointing to GPX4 as perhaps the most important selenoprotein at least in cells. Therefore, it was next asked whether the Cys GPX4 variant is sufficient to sustain cell viability and proliferation even when all selenoproteins are simultaneously deleted in MEFs. To challenge this idea, CRISPR/Cas9 mediated KO of the *Trsp* gene was conducted in $Gpx4^{wt/wt}$ and $Gpx4^{cys/cys}$ cells. The sgRNAs were designed to target the acceptor arm of the tRNA[Ser]Sec. PCR analysis of 180 single cell colonies revealed three potential *Trsp* KO clones on a wt *Gpx4* genetic background (further referred to as $Gpx4^{wt/wt}:Trsp^{mut/mut}$) and seven potential clones out of 90 picked colonies on a mutant *Gpx4* genetic background (further referred to as $Gpx4^{cys/cys}:Trsp^{mut/mut}$). In order to determine the CRISPR/Cas9 mediated genetic modification in the *Trsp* gene, DNA of the positive clones was isolated and amplified for sequencing. Genetic modifications found in $Gpx4^{wt/wt}:Trsp^{mut/mut}$ cells contained a 30 bp deletion on one allele and 1 base insertion on the other allele (Fig. 26A).
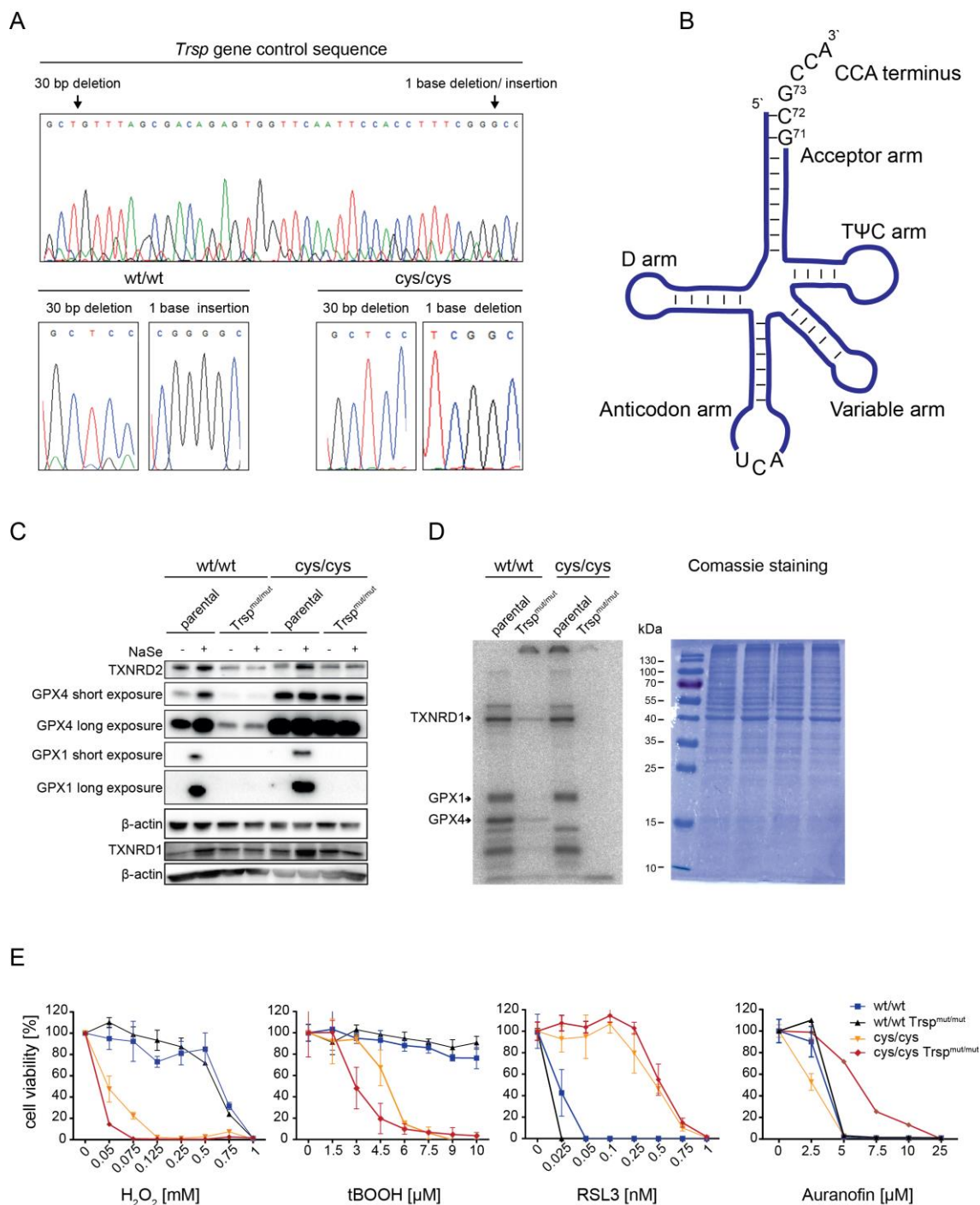
**Figure 26: CRISPR/Cas9 mediated KO of Sec-specific tRNA (*Trsp*) is only possible in *Gpx4cys/cys* cells**. (A) Chromatogram showing the CRISPR/Cas9 mediated modifications in the *Trsp* gene of *Gpx4* wt and homozygous mutant cells. (B) Cloverleaf model of murine tRNA[Sec]Ser. (C) Immunoblot analysis of single cell clones after CRISPR/Cas9 mediated KO of the *Trsp* gene (further referred to as *Gpx4wt/wt:Trspmut/mut* and *Gpx4cys/cys:Trspmut/mut* ) and their parental cell lines, cultured with and without sodium selenite (NaSe) supplementation, showed a loss of GPX1 expression and a strong decrease of TXNRD1, TXNRD2 and GPX4 protein expression. (D) Labeling of cells with radioactive ^{75}Se revealed the complete absence of selenoprotein expression in *Gpx4cys/cys:Trspmut/mut* cells. In *Gpx4wt/wt:Trspmut/mut* cells, a decreased incorporation of Se was still detectable in TXNRD1 and GPX4. Comassie staining shows equal loading of proteins. Data was kindly provided by Dr. Noelia Fradejas-Villar and Prof. Ulrich Schweizer (University of Bonn). (E) Challenging *Trsp* KO and parental cells with hydroperoxides, revealed an increased sensitivity

92

of *Gpx4cys/cys:Trspmut/mut* upon tBOOH and $H_2O_2$ treatment. Although selenoprotein expression in *Gpx4wt/wt:Trspmut/mut* cells was decreased, their sensitivity upon hydroperoxide treatment was unaltered compared to the parental wt cell line. RSL3 treatment showed increased sensitivity of *Gpx4wt/wt:Trspmut/mut* cells due to reduced GPX4 expression. *Gpx4cys/cys:Trspmut/mut* clls were resistant towards the TXNRD inhibitor auranofin.

In the *Gpx4cys/cys:Trspmut/mut* cells also a 30 bp deletion was detected as well as 1 base deletion (Fig. 26A). Since the sgRNA targeted the acceptor arm, the 30 bp deletion affected the ´3-terminus of the tRNA removing the entire acceptor arm and the TψC arm (Fig. 26B). The one base deletion found in *Gpx4cys/cys:Trspmut/mut* cells removed $G^{71}$ in the acceptor arm, while in *Gpx4wt/wt:Trspmut/mut* cells an additional G was found to be inserted at the same position (Fig. 26B).

For a further validation of the expression pattern of the four prominent selenoproteins in cells, immunoblot analysis was performed against TXNRD1, TXNRD2, GPX1 and GPX4 with and without sodium selenite supplementation (Fig. 26C). Although GPX1 expression was lost in *Gpx4wt/wt:Trspmut/mut* cells, a residual protein expression of GPX4, TXNRD1 and 2 was still detectable. Since Sec is located at the C terminus of TXNRD1 and 2, the protein detected by immunoblot might represent a truncated form or a variant with Cys incorporation at the UGA codon (223). Specifically, previous studies showed a Cys incorporation at the active site of TXNRD1 under conditions of severe selenium deficieny, which might account for this residual expression (223). However, the residual expression of GPX4 in the *Gpx4wt/wt:Trspmut/mut* cell clone pointed to an incomplete KO of the *Trsp* gene. The *Gpx4cys/cys:Trspmut/mut* cells showed no GPX1 expression but TXNRD1 and 2 expression was still detectable. GPX4 expression in the *Gpx4cys/cys:Trspmut/mut* cells was found to be unaltered as expected.

Next, parental cell lines (*Gpx4wt/wt* and *Gpx4cys/cys*) and *Trsp* KO cell lines (*Gpx4wt/wt:Trspmut/mut* and *Gpx4cys/cys:Trspmut/mut*) were labeled with $^{75}$Se radioisotope to analyse if the proteins detected by immunoblot show any Se incorporation (Fig. 26D). Remarkably, no Se incorporation was detected in *Gpx4cys/cys:Trspmut/mut* cells indiacating a full KO of the *Trsp* gene. By contrast, *Gpx4wt/wt:Trspmut/mut* cells showed residual Se incorporation in TXNRD1 and GPX4 after $^{75}$Se labeling (Fig. 26D), hinting towards the presence of a hypomorphic allele of the *Trsp* gene.

Challenging the cells with tBOOH and $H_2O_2$ revealed an increased sensitivity of *Gpx4$^{cys/cys}$:Trsp$^{mut/mut}$* cells when all other selenium-containing proteins were simultaneously deleted (Fig. 26E). In contrast to that no increased sensitivity was observed in *Gpx4$^{wt/wt}$:Trsp$^{mut/mut}$* cells (Fig. 26E). Upon RSL3 treatment *Gpx4$^{wt/wt}$:Trsp$^{mut/mut}$* cells showed increased sensitivity due to its reduced GPX4 expression level (Fig. 26E). Treatment of the cells with the electrophilic TXNRD inhibitor auranofin (224) revealed an increased resistance of the *Gpx4$^{cys/cys}$:Trsp$^{mut/mut}$* cells likely accounting for the absence of Sec incorporation into TXNRD (Fig. 26E). Notwithstanding, it is intriguing that despite the loss of all selenoproteins Trsp KO *Gpx4$^{cys/cys}$* cells were fully viable in cell culture without any additional antioxidant supplementation, indicating that cell survival and proliferation just requires residual GPX4 activity.

## 4.4    Generation and analysis of an inducible Gpx4 Cys and Ser variant

In order to address whether the Cys and Ser variants are able to sustain viability in adult mice, both lines (*Gpx4$^{wt/cys}$* and *Gpx4$^{wt/ser}$* (8)) were then cross-bred with TAM-inducible Rosa26CreERT2 mice (*Gpx4$^{flox/flox;Rosa26CreERT2}$* referred to as PZ (148)). This strategy would thus allow to bypass the early death of *Gpx4$^{cys/cys}$* mice and to perform studies in adult animals. First, the frt-flanked *neomycin phosphotransferase* gene was removed from the transgenic alleles by mating *Gpx4$^{wt/cys}$* (F3) and *Gpx4$^{wt/ser}$* (F5) mice with *Rosa26_Flpe* animals expressing Flpe recombinase (Fig. 27A). Positive animals were backcrossed with *C57BL/6J* animals and finally mated with *Gpx4$^{flox/flox;Rosa26CreERT2}$* mice yielding *Gpx4$^{flox/cys;Rosa26CreERT2}$*, *Gpx4$^{flox/ser;Rosa26CreERT2}$* and *Gpx4$^{flox/wt;Rosa26CreERT}$*, mice, respectively (further referred to as *Gpx4$^{fl/cys}$*, *Gpx4$^{fl/ser}$*, *Gpx4$^{fl/wt}$*). At the age of two months, CreERT2-mediated deletion of the loxP-flanked *Gpx4* allele was induced by TAM-injection. Reportedly, induced PZ animals died around two weeks after TAM-injection due to massive kidney proximal tubular cell death and acute renal failure (ARF) (148).
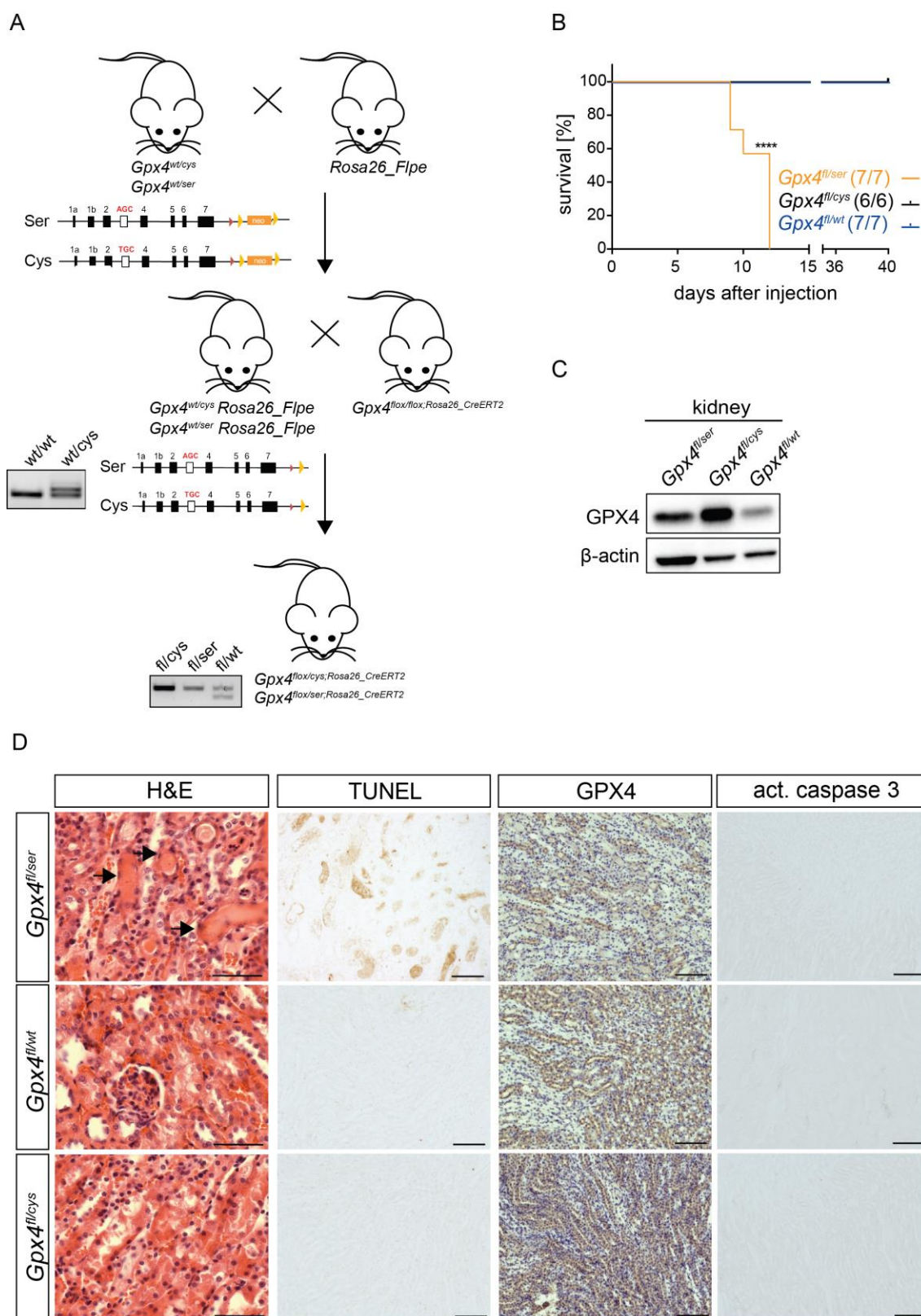
**Figure 27: Adult animals survive expressing only a Cys *Gpx4* allele.** (A) Breeding scheme describing the mating steps of *Gpx4^{wt/ser}* or *Gpx4^{wt/cys}* with a mouse strain expressing Flpe recombinase under the control of the *Rosa26* promotor in order to remove the *neomycin phosphotransferase* gene (neo). Genotyping of positive animals was performed with a PCR that detects the wt region yielding either a product of 256 bp (wt) or two products of 256 bp and 310 bp (tg). In the final breeding step, *Gpx4^{wt/ser}* or *Gpx4^{wt/cys}* animals with a successful removal of the *neo* gene were mated with a strain expressing a loxP-flanked *Gpx4* allele and an inducible Cre

recombinase under the control of the Rosa26 promotor yielding $Gpx4^{flox/flox;Rosa26CreERT2}$, $Gpx4^{flox/cys;Rosa26CreERT2}$, $Gpx4^{flox/ser;Rosa26CreERT2}$ and $Gpx4^{flox/wt;Rosa26CreERT}$, mice, respectively (further referred to as $Gpx4^{fl/cys}$, $Gpx4^{fl/ser}$, $Gpx4^{fl/wt}$). Animals were genotyped by a PCR yielding one band with 310 bp (fl/cys or fl/ser) or two bands with 256 bp and 310 bp (fl/wt) (Yellow triangle = Frt site; red triangle = loxP site). (B) A Kaplan-Meier survival analysis showed that $Gpx4^{fl/ser}$ animals died between 12-14 days after TAM injections, whereas $Gpx4^{fl/cys}$ animals survive like the wt controls (Statistical analysis was assessed using Mantel-cox test ****$P$<0.0001). (C) Immunoblot analysis of kidney tissue derived from Tam-induced $Gpx4^{wt/ser}$, $Gpx4^{wt/wt}$ or $Gpx4^{wt/cys}$ animals showed a loss of GPX4 expression in $Gpx4^{wt/ser}$ compared to $Gpx4^{wt/cys}$ mice. (D) Immunohistochemical and histopathological analysis of kidneys derived from TAM injected animals showed signs of ARF only in $Gpx4^{fl/ser}$ animals. H&E staining revealed proteinacous casts in renal tubular cells (arrows). Besides massive increase of TUNEL-positivety was present while the same sections were negative for active caspase 3 (act. caspase 3) staining. Partial loss of GPX4 expression was detected in kidneys isolated from $Gpx4^{fl/ser}$ mice (Scale bars left panel = 20 µm; other panels = 100 µm).

While induced $Gpx4^{fl/ser}$ mice resembled the phenoptye of PZ mice including proteinaceous casts in tubular cells and widespread cell death of tubular renal cells, the mice had to be sacrificed around 12-14 days after TAM-injection (Fig. 27 B,D). By stark contrast, $Gpx4^{fl/cys}$ mice survived throughout the entire observation period of 40 days without any signs of ARF (Fig. 27B,D). Western blot analysis of GPX4 expression in kidney samples derived from Tam-induced $Gpx4^{fl/ser}$, $Gpx4^{fl/cys}$ $Gpx4^{fl/wt}$ animals revealed a decrease in GPX4 expression in $Gpx4^{fl/ser}$ animals compared to $Gpx4^{fl/cys}$ mice (Fig. 27C), which is in line with the immunostainings, where reduced levels of GPX4 were observed in the kidney of $Gpx4^{fl/ser}$ animals (Fig. 27D). These findings demonstrate that the Cys GPX4 mutant form allows mouse survival and can substitute for wt GPX4 in in adult kidney, an organ that is otherwise the most sensitive organ requiring GPX4 expression (148)

# 5    Discussion

The trace element Se was discovered by Jöns Jacob Berzelius 200 years ago (1). First suspected to be a toxic compound in the sixties of last century, it was then later recognized as an essential trace element for mammals (2,5). Meanwhile, it is widely accepted that Se exerts its main function in biological systems as an integral part of the 21st amino acid Sec (19). Both, the biosynthesis and the decoding mechanism of Sec are now known to be highly complex and energetically very costly. On one hand, Sec first needs to be synthesized in several consecutive steps on its cognate tRNA[Ser]Sec, and on the other hand the decoding at the opal codon UGA necessitates a series of co-factors acting in cis and trans to allow for a successful co-translational incorporation of Sec in the nascent polypeptide chain (7).

Despite the recognition that Se in form of Sec is essential for mammalian life (116), the question concerning the actual advantage of selenothiol over thiol-based catalysis of many selenoenzymes has remained unanswered to large extent. Moreover, it is still unclear why many organisms, such as some eu- and archaebacteria, protozoon, nematodes, fly, birds, mammals and fish express selenoproteins, whereas other including yeast and higher plants use cysteine-containing homologs instead. In addition, it is still unknown why some organisms, including mammals, rely on selenoenzymes for proper embryogenesis, fertility, tissue development and protection of somatic tissues from cell death, whereas others including nematodes and flies apparently do not depend on selenoproteins for basic life. Among the 24 (25) selenoproteins expressed in mammals four of them have been identified to be of vital importance for murine embryonic development and survival. These are TXNRD1, TXNRD2, SELENOT and GPX4. *SelenoT* KO mice die during early embryogenesis (222) for unknown reasons and *Txnrd1* and *Txnrd2* KO mice die during early embryogenesis at E8.5 - E9.5 and around midgestation (E13.5), respectively (76,77). Systemic KO of *Gpx4* (E7.5) (149,150,152) causes embryonic lethality almost at the same stage as the simultaneous loss of all selenoproteins due to a KO of the Sec-specific tRNA gene *Trsp* (E6.5) (116), suggesting that GPX4 might represent the most important and limiting selenoprotein in mammals. Although the mechanism of embryonic death of *Gpx4*^{-/-} mice is still not elucidated, it is well accepted that

GPX4 protects cells from ferroptosis *in vivo* and *in vitro* by controlling specific lipid oxidation events (147,148).

## 5.1 Homozygous expression of the Ser variant of GPX4 leads to embryonic death

To dissect the role and relevance of Sec-based catalysis in GPX4, mice were generated and analysed in this work, which express a targeted mutation in the catalytically active Sec to Ser of GPX4. As shown here, mice homozygous for the Ser variant of *Gpx4* die during early embryogenesis. Like previously reported for the genetic deletion of *Gpx4* (149,150,152), embryonic lethality of *Gpx4*<sup>ser/ser</sup> embryos occurred at the gastrulation stage (E7.5) as manifested by an increased number of intrauterine resorpotions at E8.5 and E9.5 (Fig. 9) (8). These data are in line with a recently published study (190) using a mouse line expressing alanine (Ala) instead of Sec in the active site of GPX4, resulting in embryonic death at the same stage as reported here for *Gpx4*<sup>ser/ser</sup> and *Gpx4*<sup>-/-</sup> mice. The finding that a catalytically inactive form of GPX4 is embryonic lethal is not really surprising because it was previously shown that an ectopic expression of a Ser variant of GPX4 on a Tam-inducible PFa1 background fails to prevent cell death induced by genetic deletion of *Gpx4* (29). Transgenic mouse models expressing a catalytically inactive form of GPX4, like *Gpx4*<sup>ser/ser</sup> or *Gpx4*<sup>ala/ala</sup>, thus highlight the protective and essential function of GPX4 for murine development and survival of mice. This data unequivocally demonstrates that the essential role conferred by GPX4 relies on its peroxidase-mediated activity and not by possibly other functions such as by acting as a structural protein (133).

## 5.2 Augmented expression of Ser variant of GPX4 confers a dominant-negative effect in male fertility of *Gpx4*<sup>wt/ser</sup> mice

While it was shown in this work that *Gpx4*<sup>ser/ser</sup> animals do not survive beyond gastrulation stage, heterozygous *Gpx4*<sup>wt/ser</sup> mice develop normally and do not reveal any overt phenotype which accords with the histopathological analysis of important organs.

Analysis of the GPX4 protein levels examined in somatic and germline tissues as well as MEFs uncovered a robust increase in all samples analysed. Despite the augmented protein expression, *Gpx4* mRNA levels and GPX4 specific activity

remained unaltered in the respective tissues. A previous report by Suppmann and colleagues indicated that the efficiency and kinetics of UGA decoding in *Escherichia coli* is in the range of 3-5% compared to Ser incorporation (213). Therefore, data presented here strongly suggests that a facilitated translation mechanism of Ser instead of Sec allows much higher protein levels of the mutated GPX4 variant, which is in stark contrast to the wt protein with Sec in the active site that requires a co-translational decoding mechanism of the UGA codon.

Although heterozygous *Gpx4*<sup>wt/ser</sup> animals develop normally and are fully viable, an impairment of fertility was observed in male mice during the course of this thesis. This was evidenced by a reduced number of litters, a strongly decreased capability of *in vitro* fertilization, decreased sperm progressivity, and many structural abnormalities particularly evident in the midpiece of spermatozoa, such as bends and extrusions of outer dense fibers, pointed to an impairment in sperm function of heterozygous *Gpx4*<sup>wt/ser</sup> male mice. The same phenotype was later reported in male mice expressing an Ala variant of GPX4 (*Gpx4*<sup>wt/ala</sup>) (197). A similar but more pronounced phenotype as described here for *Gpx4*<sup>wt/ser</sup> male mice was earlier detected in *mGpx4* KO males (9), and in rodents kept for several generations under selenium-deprived conditions (142,143). It had been known for decades that Se has a strong impact on male fertility in rodents (140,141). In a landmark study by Ursini and colleagues published in 1999 (133), the essential role of Se in male fertility could be assigned to GPX4 which was identified as the most abundant selenoprotein in sperm mitochondrial capsules. A KO study by the Conrad laboratory later identified *mGPX4* as the essential GPX4 isoform for male gametogenesis as *mGpx4* KO mice were fully viable while male mice were infertile (9). Severe structural abnormalities were detected in the midpiece of *mGpx4* KO spermatozoa, where the mitochondrial capsule is located (9). The mitochondrial capsule is a keratin-like structure that is formed around the elongated mitochondria in the midpiece of mature spermatozoa and which is essential for sperm midpiece stability. Here, mGPX4 fulfills a moonlighting function as a thiol peroxidase and as a major structural protein interacting with other capsular proteins, including sperm mitochondria-associated cysteine-rich protein (SMCP) and different types of keratin proteins (224). As the abundance of GSH becomes limited during late sperm maturation stages, mGPX4 adopts a

thiol peroxidase function by cross-linking capsular proteins via disulfide bridges, thus giving sperm full midpiece stability (225). Once free thiols are no longer present GPX4 itself becomes cross-linked via its selenocysteine and cysteine residues to other proteins resulting in a "dead-end" enzymatic reaction (132). It was therefore hypothesized that the augmented expression of the catalytically inactive form of GPX4 in epididymis has a dominant-negative effect on mitochondrial capsule formation in male *Gpx4*<sup>wt/ser</sup> mice by interfering with the thiol peroxidase activity of the wt protein (8). This notion was indeed supported by the measurement of free thiols of sperm derived from *Gpx4*<sup>wt/ser</sup> mice using monobromobimane staining. Monobromobimane staining revealed a significant increase of free reduced thiols in sperm derived from cauda epididymis of *Gpx4*<sup>wt/ser</sup> males compared to their wt counterpart. Although the Ser variant of GPX4 contains eight remaining Cys residues that can be used by the wt protein for cross-linking itself with other mitochondrial capsular proteins, a tightly controlled balance of expression of wt GPX4 appears to be crucial, suggesting a complex network of proteins to be polymerized during capsule formation. Otherwise capsular proteins are only partially oxidized as shown by monobromobimane staining, resulting in an incomplete polymerization and causing instability of the spermatozoan midpiece (8). Taken together these data underline the importance of a well-balanced expression of a functional GPX4 and the necessity of Sec to ensure full male fertility.

## 5.3 Sec in GPX4 prevents peroxide-induced ferroptosis

To interrogate the still enigmatic role of Se for mammalian health, a mouse line has been generated with a targeted mutation of the catalytically active site Sec to Cys in GPX4. Mouse embryonic fibroblast cell lines isolated thereof were used as a cellular tool to study the advantage of selenothiol- over thiol-based catalysis *in vitro*. The data presented in this work provide strong evidence that Sec-mediated catalysis in GPX4 was evolutionary maintained in mammalian cells to protect them from ferroptotic cell death. Although homozygous *Gpx4*<sup>cys/cys</sup> cells were fully viable under routine cell culture conditions, a strongly increased sensitivity was observed when cells were treated with hydroperoxides including $H_2O_2$, tBOOH, and ChOOH (Fig. 20A). Analysis of the cell death modality showed that hydroperoxides - the actual substrates of GPX4 - induce ferroptotic cell death

in *Gpx4$^{cys/cys}$* cells but not in *Gpx4$^{wt/wt}$* cells, which was supported by increased lipid peroxidation upon $H_2O_2$ treatment of *Gpx4$^{cys/cys}$* cells and the capability to prevent hydroperoxide-induced cell death by ferroptosis inhibitors and not by inhibitors targeting other cell death paradigms, such as apoptosis and necroptosis. In this context is it notable that in response to a hydrogen peroxide challenge wt cells die in a rather necrotic ("unspecific") manner as this form of death could not be inhibited by known cell death inhibitors, hinting to a more specific physiological function of wt GPX4 in preventing hydroperoxide-induced ferroptosis.

Since the replacement of Sec by Cys in recombinant GPX4 was shown to dramatically reduce the velocity of the catalytic cycle particularly during the steps 2 and 3 (79) (Fig. 3) when oxidized GPX4 is normally reduced to its ground state, it was hypothesized that a prolonged period in the sulfenic acid state makes the Cys variant of GPX4 highly susceptible to irreversible overoxidation. To address this notion, *Gpx4$^{cys/cys}$* cells were analysed by mass spectrometry under basal and hydroperoxide-treated conditions. Mass spectrometric analysis indeed showed that $H_2O_2$ treatment of homozygous mutant cells led to a direct and fast impairment of the activity of the Cys variant of GPX4 by an irreversible overoxidation of the critical C46 to sulfonic acid (-$SO_3H$). The very similar findings were made by Orian and colleagues in a quantum mechanics-based mass spectrometric analysis of wt and a recombinant Cys variant of GPX4 in the presence of $H_2O_2$ yet under limiting GSH concentrations (38). In their work, the C46 of the mutant GPX4 enzyme was also shown to become overoxidized in the presence of $H_2O_2$ to -$SO_3H$ as described here in intact cells, while the wt GPX4 protein showed a reversible protective mechanism to prevent overoxidation under limiting concentrations of the reducing substrate. The formation of an 8-membered ring, where Se forms a selenenylamide with an N-bond (Gly47-Lys48) of the protein backbone protects the enzyme from inactivation due to overoxidation and from β-elimination of Se due to dehydroalanine formation (38). An analogous sulfenylamide formation was already observed before in a crystallographic analysis of oxidized protein tyrosine phosphatase 1B (PTP1B), where the active Cys binds to the N-chain of the adjacent Ser residue (226,227) but never in Cys-containing GPXs (38). Instead, typical 2-Cys-PRXs and 2-Cys-GPXs form as a self-protecting mechanism from overoxidation a stable disulfide

bond between the catalytic and resolving Cys after sulfenic acid formation (38,228). These results underline the sensitivity of the Cys variant of GPX4 towards overoxidation not only in the test tube but also in cells. Therefore, it is well conceivable that GPX4-specific activity was undetectable or dramatically reduced in samples derived from homozygous $Gpx4^{cys/cys}$ cells or tissues respectively, although GPX4 protein levels were found to be strongly increased. (Irreversible) Overoxidation of the mutant protein most likely occurs during cell lysis and/or by the substrate itself (i.e. PCOOH) used in the classical GPX4 activity assay. From these findings one may infer that the classical GPX4-specific activity assay cannot be used to assess GPX4 enzyme activity of the mutant protein. Like shown for cells and tissues from $Gpx4^{wt/ser}$ mice, the expression of the Cys variant of GPX4 was also strongly increased in samples derived from $Gpx4^{cys/cys}$ tissues and $Gpx4^{cys/cys}$ MEFs. Since $Gpx4$ mRNA level remained unchanged, increased protein expression levels of mutant protein most likely results again from a facilitated incorporation of Cys compared to Sec as already described for $Gpx4^{wt/ser}$ animals (see 5.2) (8,213).

Increased sensitivity towards hydroperoxide-induced cell death was not only observed when cells were directly challenged with hydroperoxides, but also when intracellular $H_2O_2$ formation was induced by treatment with complex I inhibitors rotenone and phenformin. Rotenone and phenformin, which inhibit the electron transfer from complex I to complex II in the mitochondrial respiratory chain, induce an increased formation of superoxide and consequently $H_2O_2$ predominantly into the intermembrane space due to electron leckage, whereas complex III inhibitors lead to electron leckage into the mitochondrial matrix (229). This implies that augmented $H_2O_2$ formation in the intermembrane space, where GPX4 is located, impairs GPX4 activity causing ferroptotic cell death. A link between mitochondria and ferroptosis was made when structural alterations of mitochondria - i.e. matrix shrinkage and outer mitochondrial membrane rupture - were detected upon ferroptosis induction in wt cells *in vitro* (148,177), which is now considered to be another trait of ferroptosis.

In this context, it was previously shown that GPX4 activity is important to maintain proper mitochondrial function (230,231) by regulating and maintaining the redox state in mitochondria (230). In previous studies downregulation of *Gpx4 in vitro*

induced changes in the expression of mitochondrial respiratory chain complexes and decreased mitochondrial ATP generation (230). On the contrary, overexpression of *Gpx4 in vivo* protected mitochondrial ATP production upon increased oxidative stress (231). In order to examine whether the expression of a Cys variant of GPX4 has an impact on mitochondrial function and integrity during basal conditions, a detailed analysis was performed in this thesis on isolated mitochondria derived from $Gpx4^{wt/wt}$ and $Gpx4^{cys/cys}$ cells. The results gained from the mitochondrial analysis showed that mitochondria derived from $Gpx4^{cys/cys}$ cells are fully functional and do not show any impairment in their mitochondrial ATP generation. The observed functional and morphological changes of $Gpx4^{cys/cys}$ mitochondria, such as larger mitochondria and an elevated expression of mitochondrial proteins (i.e. subunit of complex IV), are present to achieve a higher ATP production rate, which was detected in both intact cells and isolated mitochondria. As 30% of generated ATP in the cell is utilized for protein synthesis, one reason for elevated ATP generation might be increased protein synthesis due to potential oxidative damage and a higher protein turnover in mutant cells, which needs to be addressed in further studies. Along this line, the expression of the redox protein PRX3 was found to be elevated $Gpx4^{cys/cys}$ cells, which might represent a protective mechanism in order to compensate the sensitivity of the Cys variant of GPX4 towards the metabolic by-product $H_2O_2$.

As an intriguing finding the protein level of ACSL4, a recently identified downstream player of GPX4 in ferroptotic cell death cascade (176,177), was found to be strongly decreased in $Gpx4^{cys/cys}$ compared to $Gpx4^{wt/wt}$ cells (Fig. 23A). ACSL4 shapes the phospholipid composition of lipid bilayers by esterifying PUFAs with coenzyme A, and thereby senses cells for the induction of ferroptosis. Since the KO and pharmacological inhibition of *Acsl4* prevents from ferroptosis (177,181), it is reasonable to assume that the downregulation of ACSL4 in $Gpx4^{cys/cys}$ cells might represent an intrinsic compensatory mechanism to decrease the sensitivity of the homozygous mutant cells towards ferroptosis induction. Consequently, CRISPR/Cas9 mediated KO of *Acsl4* in $Gpx4^{cys/cys}$ cells increased their resistance towards hydroperoxide-induced ferroptosis (Fig. 23B).

Taken together this set of data demonstrates that Sec utilization in GPX4 was evolutionary maintained to prevent mammalian cells from undergoing ferroptosis

in response to increased hydroperoxide levels. Thereby, the decisive advantage of Se versus sulfur utilization in the active site of GPX4 appears to be the resistance of Sec towards inactivation via irreversible overoxidation under conditions of increased/sustained hydroperoxide levels and/or limiting GSH concentrations. While other self-protective mechanisms can be observed in 2-Cys-GPXs, it it still under debate how 1-Cys-GPXs, such as GPX5 and GPX7, stabilize their active sites to protect them from irreversible inactivation.

## 5.4    GPX4 emerges to be the most important selenoprotein in cells

The targeted loss of all selenoproteins induced by *Trsp* deletion causes early embryonic death (E6.5) (116), and tissue specific KO of *Trsp* using loxP-Cre technology revealed a major role for selenoproteins in various tissues as introduced in 1.4.5. Nevertheless, the fact that the deletion of *Gpx4* alone often leads to phenotypes that strongly resemble the loss of all selenoproteins (e.g. as observed in neurons (124,125), whole body (116,149,150), epidermis (126,127) and T cells (198,232)), it is reasonable to assume that GPX4 might represent the most essential selenoprotein in mammals due to its unique function to act as the master regulator of ferroptosis (147,148) mediated through its capability to detoxify PLOOH. In order to challenge this hypothesis, CRISPR/Cas9 mediated KO of the *Trsp* gene which encodes for the Sec-specific tRNA was performed in MEFs expressing either a wt or Cys variant of GPX4. Remarkably, *Trsp* deletion was only successful in *Gpx4^{cys/cys}* cells since Se incorporation was not detectable in these cells (Fig. 26). Despite the lack of expression of any Sec-containing protein, *Gpx4^{cys/cys}:Trsp^{mut/mut}* cells were fully viable and their proliferation did not require antioxidant supplementation. This unequivocally shows that a minimum of GPX4 activity is sufficient for cells *in vitro* to survive even under selenoprotein-deficient conditions, reasonably arguing for the assumption that GPX4 is indeed the most essential selenoprotein in mammals.

Although *Gpx4^{wt/wt}:Trsp^{mut/mut}* and *Gpx4^{cys/cys}:Trsp^{mut/mut}* cells showed almost the same CRISPR/Cas9 edited modification in the Trsp gene, *Gpx4^{wt/wt}:Trsp^{mut/mut}* cells presented residual Se incorporation for housekeeping selenoproteins, such as GPX4 and TXNRD1. In both, *Gpx4^{wt/wt}:Trsp^{mut/mut}* and *Gpx4^{cys/cys}:Trsp^{mut/mut}* cells a deletion of approximately 30 nucleotides was observed on one allele, while the other allele of *Gpx4^{cys/cys}:Trsp^{mut/mut}* cells showed a deletion of 1 nucleotide

lacking G71 in the acceptor stem, and in *Gpx4^{wt/wt}:Trsp^{mut/mut}* cells an insertion of a G at position C72 was present. G71, located in the acceptor stem, is part of a highly conserved sequence (23) and was shown to be important in archaea for the recognition by the phosphoseryl-tRNA-kinase (PSTK) (233). Although it remains to be shown in eukaryotes whether G71 of the tRNA[Sec]Ser is essential for PSTK recognition, this alteration in the acceptor arm may reason why Sec incorporation in *Gpx4^{cys/cys}:Trsp^{mut/mut}* cells in fact does not occur. Since Sec is the only amino acid synthesized on its cognate tRNA, special secondary structural features are required in tRNA[Sec]Ser compared to canonical tRNAs. Thereby, it appears to be important that in case of the eukaryotic tRNA[Sec]Ser the acceptor stem consists of 9 bp and the T stem of 4 bp (9/4) (234,235). The deletion of only 1 bp in the mammalian acceptor stem was shown to significantly slow down the Sec-tRNA synthesis by 3-5 fold (236,237). By contrast, the classical tRNAs have a 7/5 secondary structure (238). Furthermore, a functional study identified base G73 as an important determinant for the serylation of the tRNA. Ser loading of the tRNA is therefore impaired when G73 is mutated to a C73 or A73 (239,240). In case of the *Gpx4^{cys/cys}:Trsp^{mut/mut}* cells the deletion of G71 not only removes a highly conserved base but also results in a switch from G73 to C73, thus preventing serylation and selenoprotein expression. In *Gpx4^{wt/wt}:Trsp^{mut/mut}* cells the insertion of a G at position 72 also leads to a mutation of G73 to C73, yet low expression of some selenoproteins is still detectable. From this data one may speculate whether a one-base insertion at this position indeed inhibits Sec synthesis or whether the Sec incorporation occurs unspecifically because the survival pressure is too strong. The fact that selenoprotein expression does not increase under NaSe supplementation argues for an unspecific Sec incorporation. To elucidate whether the C73 mutation of the tRNA[Sec]Ser is still (at least partially) functional, generation of a tRNA containing the same mutation as found in *Gpx4^{wt/wt}* cells, *in vitro* serylation and selenocysteylation experiments would be required.

## 5.5 Sec in GPX4 is evolutionary maintained to prevent ferroptosis in mammals

### 5.5.1 Sec in GPX4 is required for proper neuronal development

In stark contrast to $Gpx4^{ser/ser}$ (Fig. 9) (8) and $Gpx4^{ala/ala}$ mice (190), homozygous $Gpx4^{cys/cys}$ mice on a mixed *129S6SvEvTac-C57BL/6J* genetic background develop normally during embryogenesis and are born according to the expected Mendelian ratio. Yet, just before weaning $Gpx4^{cys/cys}$ mice had to be sacrificed as they suffered from severe spontaneous seizures and/or status epilepticus. The reason for this severe phenotype was unraveled to be the loss or perturbed maturation of GABAergic PV+ interneurons. A very similar phenotype was actually previously reported in mice with glutamatergic neuron-specific deletion of *Gpx4* alone or all selenoproteins by *Trsp* KO. Here, loss of PV+ interneurons in the cortex and hippocampus, severe epileptic seizures and pre-weaning lethality was described (124,152). Although it is not exactly clear why specifically PV+ interneurons react so sensitively to loss of or dysfunctional G*px4* (as shown here), it was previously reported that this subtype of interneurons has an intrinsic sensitivity towards cellular redox perturbations (241-243). This might be due to the fact that all PV+ interneurons are fast-spiking interneurons and therefore have an exceptionally high energy demand which they accomodate by increased ATP generation (244). Thereby, ATP generation via oxidative phosphorylation appears to be their prime source of energy. In fact, PV+ interneurons contain not only a higher number of mitochondria in their dendrites, presynaptic terminals and somata compared to other subtypes of interneurons but those mitochondria are also bigger in size and enriched with proteins that are important for the mitochondrial respiratory chain (245-247). It is therefore not surprising that a well-balanced redox balance in PV+ interneurons is of utmost importance and that the loss or dysfunction of an important redox protein, such as GPX4, is critical for proper cell functioning and survival. Increased oxidative stress in PV+ interneurons is believed to cause impairment in the glutamate-dependent N-methyl-D-aspartate receptor (NMDAR) function and is hypothesized to contribute to PV+ interneuronal dysfunction and the development of various neuronal disorders including epilepsy and schizophrenia (248,249). Remarkably, a similar phenotype was obtained in mice with a genetic deletion of *Selenop* that showed a decreased number of PV+ interneurons in the inferior collicus and increased

oxidative stress in this region (250). SELENOP is synthesized in the liver as a selenoprotein with up to 10 Sec residues and its prime function is to distribute Se for selenoprotein synthesis throughout the whole body. In the brain, SELENOP binds to its cognate receptor, apolipoprotein receptor 2 (ApoER2), which internalizes SELENOP into neuronal cells by endocytosis (251). It was shown that ApoER2 is highly expressed in PV+ interneurons but not in other GABAergic interneurons, such as calretinin and calbindin interneurons (250). Therefore, based on the data presented here and on existing literature, the following hypothesis is proposed regarding the loss of PV+ interneurons in $Gpx4^{cys/cys}$ mice: PV+ interneurons appear to be highly dependent on the redox activity of selenoproteins (250), and particularly that of GPX4 (124) to protect themselves from oxidative stress that also occurs during maturation, migration and firing processes. Since the Cys variant of GPX4 is prone overoxidation by the metabolic by-product $H_2O_2$ and other hydroperoxides, its inactivation in PV+ interneurons results in a fatal cascade of events including increased oxidative stress due to GPX4 inactivation followed by a decrease of PV+ expression and development of seizures that induce even more neuronal damage due to glutamate induced excitotoxicity. Conclusively, Sec utilization of GPX4 is required to allow proper development and function of PV+ interneurons, which has been discovered in this thesis as the limiting factor for the survival of $Gpx4^{cys/cys}$ mice and protect them from hydroperoxide-induced ferroptosis.

### 5.5.2  Sec in GPX4 is maintained to allow proper embryogenesis

During backcrossing on a congenic genetic background (i.e. *C57BL/6J*) and subsequent intercross of heterozygous mutant mice, homozygous expression of the Cys variant of GPX4 surprisingly failed to allow proper embryogenesis. Homozygous mutant embryos died during embryonic development (~E11.5) showing signs of strongly impaired brain and heart development, paleness, severe malformation and growth retardation of the homozygous mutant embryos. Until E9.5 when GPX4 is expressed throughout the whole embryo, but with a more prominent expression in mesenchymal structures and the heart tube primordium (252), $Gpx4^{cys/cys}$ mice develop normally without any signs of morphological abnormalities. Severe malformation was mainly observed at E10.5 - E12.5 when GPX4 showed strong expression e.g. in the neural tissue, the developing eye, branchial arches, developing tail and the ventricle of the heart

(252). Conditional KO studies with targeted deletion of *Gpx4* revealed a major role for GPX4 for postnatal neuronal development (124,253) and neuronal development during late embryogenesis (125,254). A hematopoeiesis-specific deletion of *Gpx4* in adult mice prevented erythropoesis due to impaired reticulocyte maturation (196). Furthermore, tissue specific deletion of *Trsp* showed that selenoproteins had a major impact on skeletal development (255) and a proper development of the vascular system (123). In the latter case, the *Tie2Cre:Trsp^{fl/fl}* embryos resembled the phenotype observed in homozygous *Gpx4^{cys/cys}* mice to some extent showing growth retardation and malformation of the embryo, paleness and perturbed brain and vascular development. Since GPX4 dysfunction is not restricted to endothelial progenitor cells, the phenotype presented in homozygous *Gpx4^{cys/cys}* mice appears to be more severe and to affect the whole embryo. Based on the results gained from the embryo analysis and taking the existing literature in consideration it seems that the reason for embryonic death in homozygous *Gpx4^{cys/cys}* mice is an impaired development of the cardiovascular system. During embryogenesis, the formation of the cardiovascular system is one of the most critical events (256,257). The vascularisation of the embryo starts at E6.0 by the differentiation from the mesodermal cells to endothelial cells (258) but blood circulation commences only at E8.5 (257) which is required for the transport of metabolic products and nutrient supply of the embryo. At E9.5, when cardiomyocyte differentiation starts at the same time mitochondrial maturation is initiated to allow a switch in the embryonic energy supply from anaerobic glycolysis to oxidative metabolism (259,260). The switch from glycolysis to oxidative phosphorylation can cause metabolic stress and increased formation of the by-product $H_2O_2$ resulting in GPX4 inactivation. An impaired development of this essential organ thus prevents future developmental steps thereby leading to embryonic death (258).

Because *Gpx4^{-/-}* embryos die after gastrulation at E7.5 (149,150), just a little later than KO of all selenoproteins (E6.5) (116), little is known regarding the role of GPX4 for embryonic development in mice beyond E7.5. Although the exact reason for embryonic lethality in *Gpx4^{cys/cys}* mice on a *C57BL/6J* background remains unclear and requires future investigation, this transgenic mouse model may help to decipher the role of GPX4 and Se during midgestational embryogenesis. Interestingly, single reported cases of patients carrying

mutations in *GPX4* resulting in a truncated protein cause Sedaghatian-type spondylometaphyseal dysplasia. This phenotype displays a combination of both phenotypes of homozygous *Gpx4^{cys/cys}* mice described in this work namely skeletal dysformation, severe cerebellar hypoplasia, seizures, cardiorespiratory insufficiency and early death within days after birth (261,262).

The stark discrepancy observed between pre-weaning lethality and embryonic death around midgestation on the mixed background and the *C57BL/6J* background, respectively, most likely results from an incomplete penetrance of the mutated gene due to modifier genes that are expressed in the 1*29S6SvEvTac* strain (263). This is not an unknown phenomenon as a number of reports have shown this in previous KO studies, such as for *fibronectin* (264), *keratin-8* (265,266), *epidermal growth factor receptor (EGFR)* (267) and *transforming growth factor β1 (TGFβ1)* (263). To proove this, *Gpx4^{wt/cys}* animals were crossed again on a mixed F1 background followed by intercross of heterozygous mice. As expected the phenotype of homozygous *Gpx4^{cys/cys}* mice was regained showing seizures and postnatal lethality.

### 5.5.3 Sec in GPX4 is dispensable for adult animal survival

Despite the lethal phenotypes either at the embryonic or preweaning stage of homozygous mutant mice, it was still possible to interrogate the relevance of mutant GPX4 in the adult setting. This was possible by having both the mutant Cys *Gpx4* allele and the floxed *Gpx4* mice at hand. To this end, *Gpx4^{wt/cys}* mice were cross-bred with PZ animals (148) to allow Cre-mediated deletion of the loxP-flanked *Gpx4* allele after Tam injection. Surprisingly, adult animals expressing only the Cys variant of GPX4 survived like the wt animals. No signs of kidney damage were observed, although kidney failure was previously shown to be the limiting survival factor upon *Gpx4* deletion in adult animals (148). By contrast, *Gpx4^{fl/ser}* animals on a PZ background died within 2 weeks after Tam injection phenocopying the PZ phenotype (148). This was not surprising since the Ser variant of GPX4 lacks any catalytic activity as previously reported (see 5.1) (8). ARF in PZ and *Gpx4^{fl/ser}* animals was induced by proximal tubule cell death, a cell type located in the renal cortex as well as the outer stripe of the outer medulla (OSOM) whose main function is to reabsorb amino acids, low molecular protein and solutes filtered by glomeruli in order to maintain electrolyte, fluid and

nutrient homeostasis (268). To accomplish this, these cells have a high demand for ATP as it is of utmost importance to drive the ATPase dependent sodium-potassium pump. This pump generates an electrical gradient across the proximal tubular epithelium thereby creating a negative membrane potential and thereby facilitating reabsorption processes (269). While NaCl can be absorbed by the proximal tubule in an isotonic manner, the uptake of other solutes is mediated either via $Na^+$-dependent anti- and co-transporter using the energy of the gradient or $Na^+$-independent co-transporter (270). Impaired function of proximal tubule cells causes loss of amino acids, proteins, electrolytes and glucose which results in severe renal pathophysiology. It is therefore not surprising that proper mitochondrial function is essential for this cell type and that a lack of *Gpx4* might promote mitochondrial dysfunction due to cardiolipin oxidation and cell death (148), respectively.

Proper mitochondrial function appears to be the limiting survival factor for adult *Gpx4* KO animals. Data presented in this work clearly show that the Cys variant of GPX4 does not impair mitochondrial function thus allowing survival of the animals expressing only the Cys allele of *Gpx4*. As a consequence Sec in GPX4 seems to be dispensable in adult mice when all developmental processes are completed, whereby one should take in consideration that the *Rosa26* driven Cre-line used in this study does not induce gene excision in the brain. In order to analyze if Sec can be replaced by Cys even in neurons of adult animals, *Gpx4*$^{fl/cys}$ mice should be cross-bred with a Cre-line driven by a neuron-specific promotor. Furthermore it would be interesting to monitor survival of *Gpx4*$^{fl/cys}$ mice under different stress-induced conditions, such as IRI in the kidney and liver, where GPX4 is highly expressed, or in a model of ischemic stroke.

The findings presented in this work regarding the *in vivo* results clearly show that Sec in GPX4 is essential during developmental processes such as embryogenesis and postnatal development but can be replaced by Cys in adulthood at least under non-stressed conditions.

## 5.6    Concluding remarks

In conclusion, the *in vivo* data shown here corroborate the necessity of selenothiol-based catalysis in GPX4 for mammals to allow proper developmental

processes during embryogenesis and postnatally which are strongly compromised in mice expressing the Cys variant of GPX4. The cellular and biochemical data presented here strongly suggest that the underlying reason for the requirement of Se is that the mutated GPX4 protein reveals marked sensitivity to overoxidation. Once oxidized by a hydroperoxide to a sulfenic acid and an impaired reduction to its ground state leads to swift overoxidation to sulfinic and sulfonic acid resulting in an irreversibly overoxidized enzyme (79). Consequently, PLOOH can accumulate and form proximate signals as triggers of ferroptotic cell death. An interesting finding thereby is that the protein level of ACSL4, an enzyme involved in lipid biosynthesis (178) and identified as important player in the ferroptosis pathway (176,177), was found to be robustly reduced in homozygous *Gpx4*<sup>cys/cys</sup> cells. As a likely compensatory mechanism to a lowered activity of the mutant GPX4 protein, diminished expression of ACSL4 would decrease the amount of activated PUFAs in lipid bilayers thus reducing the risk of becoming oxygenated as only PUFAs with a conjugated diene are prone to undergo peroxidation. Mammalian cells contain up to 62% unsaturated fatty acids of which 35% are PUFAs (271) that are highly susceptible towards oxidation. In order to address whether the lipid composition is indeed different in *Gpx4*<sup>wt/wt</sup> compared to *Gpx4*<sup>cys/cys</sup> cells due to reduced ACSL4 expression, mass spectrometric analysis of the lipid fraction would be required. The predominant form of membrane lipids in eukaryotic cells are phospholipids (272-274), which consists of 60-85% of phosphatidylcholine (PC) and phosphatidylethanolamine (PE) (275). In this context, oxidized arachidonic and adrenic acid in PE have been identified as a potential source for the lethal ferroptotic signal occurring in mammalian cells (177,181). Based on the findings presented here and in existing literature, one may infer that the evolutionary pressure of a Sec-containing GPX4 protein correlates with an organism`s phospholipid composition and the level of unsaturation in order to prevent ferroptosis. In fact, Sec utilization in GPX4 is mainly preserved in vertebrates, including mammals, fish, birds and reptiles (Fig. 28), which predominantly esterify long chain PUFAs in their lipid bilayers (276), while invertebrates, including insects and worms, mainly insert monounsaturated and saturated fatty acids in their lipid bilayers (277,278). Various studies performed in different vertebrate groups indicated a correlation between tissue-specific lipid unsaturation and GPX4 activity (279). PUFAs, which are particularly

enriched in brain, liver, testes and kidney tissues (148,194), are essential for cellular and physiological functions such as membrane fluidity, plasticity, neuronal network development, migration and neurotransmitter release (280), cold adaptation (281), mitochondrial ATP generation (282) and pathogen defense (276). The same tissues contain very high levels of GPX4 and, more importantly, retain GPX4 biosynthesis even under selenium-deprived conditions (60). On the contrary, PUFA residues of phospholipids are very susceptible to oxidative damage compared to monounsaturated or saturated fatty acids, leading to the formation of PLOOH which require sustained surveillance conferred by GPX4. The fact that Cys-containing GPX4 homologs are only expressed in insects, parasites, viruses, higher plants and algae (Fig. 28) further supports this concept. Nontheless, Sec-containing GPX4 was found in certain non-vertebrates such as avian *Fowlpox virus* (283) and *Schistosoma mansoni* (39). Sec encoding *Gpx4* gene found in the avian *F. virus* was identified as a host-derived gene adopted by the virus (283). The parasite *S. mansoni* persists most of its life time in a (vertebrate) host where it requires efficient detoxification mechansism to withstand the oxidative stress induced by the host as an inflammatory response to the parasitic infection (284). It is therefore not surprising that the highest expression of this selenoenzyme is found in the tegmentum and gut epithelium of adult worms, which display the most exposed interfaces of the parasite towards the host (285).

The presented data in this work and the identification of GPX4 as the master regulator of a new regulated form of cell death, termed ferroptosis, underlines the unique characteristics of GPX4 among all selenoproteins. As ferroptotic cell death may contribute to a number of different pathophysiological conditions, it is reasonable to conclude that Sec in GPX4 was evolutionary maintained in vertebrates to keep in check lipid peroxidation and associated ferroptotic cell death.

**Figure 28: GPX4 protein sequence alignment of different species.** GPX4 sequence alignment of *Homo sapiens* (*H. sapiens*, P36969), *Mus musculus* (*M. musculus*, O70325), *Seriola lalandi* (*S. lalandi*, F8UV59**)**, *Gallus gallus* (*G. gallus*, Q8QG67), *Canarypox virus* (*C. virus*, Q6VZR0), *Trypanosoma brucei brucei* (*T. brucei brucei*, D6XK30), *Arabidopsis thaliana* (*A. thaliana*, Q8L910), *Caenorhabditis elegans* (*C. elegans*, Q9N2X2). The active site, which is marked in red with an asterisk, consists of a Sec in vertebrates, while virus, higher plants and invertebrates contain a Cys instead. The amino acids Gln, Trp and Asn that are part of the catalytic tetrad are marked in blue and are highly conserved across all the listed species.

# 6 References

1. Berzelius, J. J. (1818) Undersökning af en ny Mineral-kropp, funnen i de orenare sorterna af det i Falun tillverkade svaflet. *Afhandlingar i fysik, kemi och mineralogi* **6:42**

2. Schwarz, K., and Foltz, C. M. (1958) Factor 3 activity of selenium compounds. *The Journal of biological chemistry* **233**, 245-251

3. Kieliszek, M., and Blazejak, S. (2013) Selenium: Significance, and outlook for supplementation. *Nutrition* **29**, 713-718

4. Fordyce, F. (2007) Selenium geochemistry and health. *Ambio* **36**, 94-97

5. Rayman, M. P. (2000) The importance of selenium to human health. *Lancet* **356**, 233-241

6. Kieliszek, M., and Blazejak, S. (2016) Current Knowledge on the Importance of Selenium in Food for Living Organisms: A Review. *Molecules* **21**

7. Hatfield, D. L., Tsuji, P. A., Carlson, B. A., and Gladyshev, V. N. (2014) Selenium and selenocysteine: roles in cancer, health, and development. *Trends in biochemical sciences* **39**, 112-120

8. Ingold, I., Aichler, M., Yefremova, E., Roveri, A., Buday, K., Doll, S., Tasdemir, A., Hoffard, N., Wurst, W., Walch, A., Ursini, F., Friedmann Angeli, J. P., and Conrad, M. (2015) Expression of a Catalytically Inactive Mutant Form of Glutathione Peroxidase 4 (Gpx4) Confers a Dominant-negative Effect in Male Fertility. *The Journal of biological chemistry* **290**, 14668-14678

9. Schneider, M., Forster, H., Boersma, A., Seiler, A., Wehnes, H., Sinowatz, F., Neumuller, C., Deutsch, M. J., Walch, A., Hrabe de Angelis, M., Wurst, W., Ursini, F., Roveri, A., Maleszewski, M., Maiorino, M., and Conrad, M. (2009) Mitochondrial glutathione peroxidase 4 disruption causes male infertility. *FASEB journal : official publication of the Federation of American Societies for Experimental Biology* **23**, 3233-3242

10. Olson, G. E., Winfrey, V. P., Hill, K. E., and Burk, R. F. (2004) Sequential development of flagellar defects in spermatids and epididymal spermatozoa of selenium-deficient rats. *Reproduction* **127**, 335-342

11. Weber, G. F., Maertens, P., Meng, X. Z., and Pippenger, C. E. (1991) Glutathione peroxidase deficiency and childhood seizures. *Lancet* **337**, 1443-1444

12. Ramaekers, V. T., Calomme, M., Vanden Berghe, D., and Makropoulos, W. (1994) Selenium deficiency triggering intractable seizures. *Neuropediatrics* **25**, 217-223

13. Volpe, S. L., Schall, J. I., Gallagher, P. R., Stallings, V. A., and Bergqvist, A. G. (2007) Nutrient intake of children with intractable epilepsy compared with healthy children. *J Am Diet Assoc* **107**, 1014-1018

14. Ashrafi, M. R., Shams, S., Nouri, M., Mohseni, M., Shabanian, R., Yekaninejad, M. S., Chegini, N., Khodadad, A., and Safaralizadeh, R. (2007) A probable causative factor for an old problem: selenium and glutathione peroxidase appear to play important roles in epilepsy pathogenesis. *Epilepsia* **48**, 1750-1755

15. Zhang, S., Rocourt, C., and Cheng, W. H. (2010) Selenoproteins and the aging brain. *Mech Ageing Dev* **131**, 253-260

16. Look, M. P., Rockstroh, J. K., Rao, G. S., Kreuzer, K. A., Spengler, U., and Sauerbruch, T. (1997) Serum selenium versus lymphocyte subsets and markers of disease progression and inflammatory response in human immunodeficiency virus-1 infection. *Biol Trace Elem Res* **56**, 31-41

17. Hori, K., Hatfield, D., Maldarelli, F., Lee, B. J., and Clouse, K. A. (1997) Selenium supplementation suppresses tumor necrosis factor alpha-induced human immunodeficiency virus type 1 replication in vitro. *AIDS Res Hum Retroviruses* **13**, 1325-1332

18. Flohe, L., Gunzler, W. A., and Schock, H. H. (1973) Glutathione peroxidase: a selenoenzyme. *FEBS Lett* **32**, 132-134

19. Labunskyy, V. M., Hatfield, D. L., and Gladyshev, V. N. (2014) Selenoproteins: molecular pathways and physiological roles. *Physiol Rev* **94**, 739-777

20. Chambers, I., Frampton, J., Goldfarb, P., Affara, N., McBain, W., and Harrison, P. R. (1986) The structure of the mouse glutathione peroxidase gene: the selenocysteine in the active site is encoded by the 'termination' codon, TGA. *EMBO J* **5**, 1221-1227

21. Brigelius-Flohe, R. (2015) The evolving versatility of selenium in biology. *Antioxidants & redox signaling* **23**, 757-760

22. Lobanov, A. V., Hatfield, D. L., and Gladyshev, V. N. (2009) Eukaryotic selenoproteins and selenoproteomes. *Biochimica et biophysica acta* **1790**, 1424-1428

23. Lobanov, A. V., Fomenko, D. E., Zhang, Y., Sengupta, A., Hatfield, D. L., and Gladyshev, V. N. (2007) Evolutionary dynamics of eukaryotic selenoproteomes: large selenoproteomes may associate with aquatic life and small with terrestrial life. *Genome biology* **8**, R198

24. Kryukov, G. V., and Gladyshev, V. N. (2004) The prokaryotic selenoproteome. *EMBO Rep* **5**, 538-543

25. Zhang, Y., Fomenko, D. E., and Gladyshev, V. N. (2005) The microbial selenoproteome of the Sargasso Sea. *Genome biology* **6**, R37

26. Gobler, C. J., Lobanov, A. V., Tang, Y. Z., Turanov, A. A., Zhang, Y., Doblin, M., Taylor, G. T., Sanudo-Wilhelmy, S. A., Grigoriev, I. V., and Gladyshev, V. N. (2013) The central role of selenium in the biochemistry and ecology of the harmful pelagophyte, Aureococcus anophagefferens. *ISME J* **7**, 1333-1343

27. Papp, L. V., Lu, J., Holmgren, A., and Khanna, K. K. (2007) From selenium to selenoproteins: synthesis, identity, and their role in human health. *Antioxidants & redox signaling* **9**, 775-806

28. Wessjohann, L. A., Schneider, A., Abbas, M., and Brandt, W. (2007) Selenium in chemistry and biochemistry in comparison to sulfur. *Biological chemistry* **388**, 997-1006

29. Mannes, A. M., Seiler, A., Bosello, V., Maiorino, M., and Conrad, M. (2011) Cysteine mutant of mammalian GPx4 rescues cell death induced by disruption of the wild-type selenoenzyme. *FASEB journal : official publication of the Federation of American Societies for Experimental Biology* **25**, 2135-2144

30. Rocher, C., Lalanne, J. L., and Chaudiere, J. (1992) Purification and properties of a recombinant sulfur analog of murine selenium-glutathione peroxidase. *Eur J Biochem* **205**, 955-960

31. Berry, M. J., Maia, A. L., Kieffer, J. D., Harney, J. W., and Larsen, P. R. (1992) Substitution of cysteine for selenocysteine in type I iodothyronine deiodinase reduces the catalytic efficiency of the protein but enhances its translation. *Endocrinology* **131**, 1848-1852

32. Zhong, L., and Holmgren, A. (2000) Essential role of selenium in the catalytic activities of mammalian thioredoxin reductase revealed by characterization of recombinant enzymes with selenocysteine mutations. *The Journal of biological chemistry* **275**, 18121-18128

33. Saccoccia, F., Angelucci, F., Boumis, G., Desiato, G., Miele, A. E., and Bellelli, A. (2014) Selenocysteine robustness versus cysteine versatility: a hypothesis on the evolution of the moonlighting behaviour of peroxiredoxins. *Biochemical Society transactions* **42**, 1768-1772

34. Hondal, R. J., Marino, S. M., and Gladyshev, V. N. (2013) Selenocysteine in thiol/disulfide-like exchange reactions. *Antioxidants & redox signaling* **18**, 1675-1689

35. Gromer, S., Johansson, L., Bauer, H., Arscott, L. D., Rauch, S., Ballou, D. P., Williams, C. H., Jr., Schirmer, R. H., and Arner, E. S. (2003) Active sites of

thioredoxin reductases: why selenoproteins? *Proc. Natl. Acad. Sci. U. S. A.* **100**, 12618-12623

36. Kanzok, S. M., Fechner, A., Bauer, H., Ulschmid, J. K., Muller, H. M., Botella-Munoz, J., Schneuwly, S., Schirmer, R., and Becker, K. (2001) Substitution of the thioredoxin system for glutathione reductase in Drosophila melanogaster. *Science* **291**, 643-646

37. Steinmann, D., Nauser, T., and Koppenol, W. H. (2010) Selenium and sulfur in exchange reactions: a comparative study. *J Org Chem* **75**, 6696-6699

38. Orian, L., Mauri, P., Roveri, A., Toppo, S., Benazzi, L., Bosello-Travain, V., De Palma, A., Maiorino, M., Miotto, G., Zaccarin, M., Polimeno, A., Flohe, L., and Ursini, F. (2015) Selenocysteine oxidation in glutathione peroxidase catalysis: an MS-supported quantum mechanics study. *Free radical biology & medicine* **87**, 1-14

39. Dimastrogiovanni, D., Anselmi, M., Miele, A. E., Boumis, G., Petersson, L., Angelucci, F., Nola, A. D., Brunori, M., and Bellelli, A. (2010) Combining crystallography and molecular dynamics: the case of Schistosoma mansoni phospholipid glutathione peroxidase. *Proteins* **78**, 259-270

40. Allmang, C., Wurth, L., and Krol, A. (2009) The selenium to selenoprotein pathway in eukaryotes: more molecular partners than anticipated. *Biochimica et biophysica acta* **1790**, 1415-1423

41. Donovan, J., and Copeland, P. R. (2010) The efficiency of selenocysteine incorporation is regulated by translation initiation factors. *J Mol Biol* **400**, 659-664

42. Driscoll, D. M., and Copeland, P. R. (2003) Mechanism and regulation of selenoprotein synthesis. *Annu Rev Nutr* **23**, 17-40

43. Lee, B. C., Lobanov, A. V., Marino, S. M., Kaya, A., Seravalli, J., Hatfield, D. L., and Gladyshev, V. N. (2011) A 4-selenocysteine, 2-selenocysteine insertion sequence (SECIS) element methionine sulfoxide reductase from Metridium senile reveals a non-catalytic function of selenocysteines. *The Journal of biological chemistry* **286**, 18747-18755

44. Hatfield, D. L., and Gladyshev, V. N. (2002) How selenium has altered our understanding of the genetic code. *Molecular and cellular biology* **22**, 3565-3576

45. Squires, J. E., and Berry, M. J. (2008) Eukaryotic selenoprotein synthesis: mechanistic insight incorporating new factors and new functions for old factors. *IUBMB Life* **60**, 232-235

46. Xu, X. M., Carlson, B. A., Mix, H., Zhang, Y., Saira, K., Glass, R. S., Berry, M. J., Gladyshev, V. N., and Hatfield, D. L. (2007) Biosynthesis of selenocysteine on its tRNA in eukaryotes. *PLoS Biol* **5**, e4

47. Low, S. C., Harney, J. W., and Berry, M. J. (1995) Cloning and functional characterization of human selenophosphate synthetase, an essential component of selenoprotein synthesis. *The Journal of biological chemistry* **270**, 21659-21664

48. Xu, X. M., Carlson, B. A., Irons, R., Mix, H., Zhong, N., Gladyshev, V. N., and Hatfield, D. L. (2007) Selenophosphate synthetase 2 is essential for selenoprotein biosynthesis. *The Biochemical journal* **404**, 115-120

49. Kumar, S., Bjornstedt, M., and Holmgren, A. (1992) Selenite is a substrate for calf thymus thioredoxin reductase and thioredoxin and elicits a large non-stoichiometric oxidation of NADPH in the presence of oxygen. *Eur J Biochem* **207**, 435-439

50. Bjornstedt, M., Kumar, S., and Holmgren, A. (1992) Selenodiglutathione is a highly efficient oxidant of reduced thioredoxin and a substrate for mammalian thioredoxin reductase. *The Journal of biological chemistry* **267**, 8030-8034

51. Martin, G. W., 3rd, Harney, J. W., and Berry, M. J. (1996) Selenocysteine incorporation in eukaryotes: insights into mechanism and efficiency from

sequence, structure, and spacing proximity studies of the type 1 deiodinase SECIS element. *RNA* **2**, 171-182

52. Seeher, S., Mahdi, Y., and Schweizer, U. (2012) Post-transcriptional control of selenoprotein biosynthesis. *Curr Protein Pept Sci* **13**, 337-346

53. Berry, M. J., Banu, L., Harney, J. W., and Larsen, P. R. (1993) Functional characterization of the eukaryotic SECIS elements which direct selenocysteine insertion at UGA codons. *EMBO J* **12**, 3315-3322

54. Kryukov, G. V., and Gladyshev, V. N. (2000) Selenium metabolism in zebrafish: multiplicity of selenoprotein genes and expression of a protein containing 17 selenocysteine residues. *Genes Cells* **5**, 1049-1060

55. McKenzie, R. C., Arthur, J. R., and Beckett, G. J. (2002) Selenium and the regulation of cell signaling, growth, and survival: molecular and mechanistic aspects. *Antioxidants & redox signaling* **4**, 339-351

56. Hill, K. E., Lyons, P. R., and Burk, R. F. (1992) Differential regulation of rat liver selenoprotein mRNAs in selenium deficiency. *Biochem Biophys Res Commun* **185**, 260-263

57. Lei, X. G., Evenson, J. K., Thompson, K. M., and Sunde, R. A. (1995) Glutathione peroxidase and phospholipid hydroperoxide glutathione peroxidase are differentially regulated in rats by dietary selenium. *J Nutr* **125**, 1438-1446

58. Schomburg, L., and Schweizer, U. (2009) Hierarchical regulation of selenoprotein expression and sex-specific effects of selenium. *Biochimica et biophysica acta* **1790**, 1453-1462

59. Sunde, R. A., and Raines, A. M. (2011) Selenium regulation of the selenoprotein and nonselenoprotein transcriptomes in rodents. *Adv Nutr* **2**, 138-150

60. Brigelius-Flohe, R. (1999) Tissue-specific functions of individual glutathione peroxidases. *Free radical biology & medicine* **27**, 951-965

61. Saedi, M. S., Smith, C. G., Frampton, J., Chambers, I., Harrison, P. R., and Sunde, R. A. (1988) Effect of selenium status on mRNA levels for glutathione peroxidase in rat liver. *Biochem Biophys Res Commun* **153**, 855-861

62. Weiss, S. L., Evenson, J. K., Thompson, K. M., and Sunde, R. A. (1997) Dietary selenium regulation of glutathione peroxidase mRNA and other selenium-dependent parameters in male rats. *J Nutr Biochem* **8**, 85-91

63. Sunde, R. A., Evenson, J. K., Thompson, K. M., and Sachdev, S. W. (2005) Dietary selenium requirements based on glutathione peroxidase-1 activity and mRNA levels and other Se-dependent parameters are not increased by pregnancy and lactation in rats. *J Nutr* **135**, 2144-2150

64. Weiss, S. L., and Sunde, R. A. (1998) Cis-acting elements are required for selenium regulation of glutathione peroxidase-1 mRNA levels. *RNA* **4**, 816-827

65. Moriarty, P. M., Reddy, C. C., and Maquat, L. E. (1998) Selenium deficiency reduces the abundance of mRNA for Se-dependent glutathione peroxidase 1 by a UGA-dependent mechanism likely to be nonsense codon-mediated decay of cytoplasmic mRNA. *Molecular and cellular biology* **18**, 2932-2939

66. Lu, J., and Holmgren, A. (2009) Selenoproteins. *The Journal of biological chemistry* **284**, 723-727

67. Bianco, A. C., Salvatore, D., Gereben, B., Berry, M. J., and Larsen, P. R. (2002) Biochemistry, cellular and molecular biology, and physiological roles of the iodothyronine selenodeiodinases. *Endocr Rev* **23**, 38-89

68. Zhong, L., Arner, E. S., Ljung, J., Aslund, F., and Holmgren, A. (1998) Rat and calf thioredoxin reductase are homologous to glutathione reductase with a carboxyl-terminal elongation containing a conserved catalytically active penultimate selenocysteine residue. *The Journal of biological chemistry* **273**, 8581-8591

69. Gladyshev, V. N., Jeang, K. T., and Stadtman, T. C. (1996) Selenocysteine, identified as the penultimate C-terminal residue in human T-cell thioredoxin

reductase, corresponds to TGA in the human placental gene. *Proc. Natl. Acad. Sci. U. S. A.* **93**, 6146-6151

70. Biterova, E. I., Turanov, A. A., Gladyshev, V. N., and Barycki, J. J. (2005) Crystal structures of oxidized and reduced mitochondrial thioredoxin reductase provide molecular details of the reaction mechanism. *Proc. Natl. Acad. Sci. U. S. A.* **102**, 15018-15023

71. Sun, Q. A., Kirnarsky, L., Sherman, S., and Gladyshev, V. N. (2001) Selenoprotein oxidoreductase with specificity for thioredoxin and glutathione systems. *Proc. Natl. Acad. Sci. U. S. A.* **98**, 3673-3678

72. Sandalova, T., Zhong, L., Lindqvist, Y., Holmgren, A., and Schneider, G. (2001) Three-dimensional structure of a mammalian thioredoxin reductase: implications for mechanism and evolution of a selenocysteine-dependent enzyme. *Proc. Natl. Acad. Sci. U. S. A.* **98**, 9533-9538

73. Zhong, L., Arner, E. S., and Holmgren, A. (2000) Structure and mechanism of mammalian thioredoxin reductase: the active site is a redox-active selenolthiol/selenenylsulfide formed from the conserved cysteine-selenocysteine sequence. *Proc. Natl. Acad. Sci. U. S. A.* **97**, 5854-5859

74. Lillig, C. H., and Holmgren, A. (2007) Thioredoxin and related molecules--from biology to health and disease. *Antioxidants & redox signaling* **9**, 25-47

75. Bondareva, A. A., Capecchi, M. R., Iverson, S. V., Li, Y., Lopez, N. I., Lucas, O., Merrill, G. F., Prigge, J. R., Siders, A. M., Wakamiya, M., Wallin, S. L., and Schmidt, E. E. (2007) Effects of thioredoxin reductase-1 deletion on embryogenesis and transcriptome. *Free radical biology & medicine* **43**, 911-923

76. Conrad, M., Jakupoglu, C., Moreno, S. G., Lippl, S., Banjac, A., Schneider, M., Beck, H., Hatzopoulos, A. K., Just, U., Sinowatz, F., Schmahl, W., Chien, K. R., Wurst, W., Bornkamm, G. W., and Brielmeier, M. (2004) Essential role for mitochondrial thioredoxin reductase in hematopoiesis, heart development, and heart function. *Molecular and cellular biology* **24**, 9414-9423

77. Jakupoglu, C., Przemeck, G. K., Schneider, M., Moreno, S. G., Mayr, N., Hatzopoulos, A. K., de Angelis, M. H., Wurst, W., Bornkamm, G. W., Brielmeier, M., and Conrad, M. (2005) Cytoplasmic thioredoxin reductase is essential for embryogenesis but dispensable for cardiac development. *Molecular and cellular biology* **25**, 1980-1988

78. Carlson, B. A., Yoo, M. H., Tobe, R., Mueller, C., Naranjo-Suarez, S., Hoffmann, V. J., Gladyshev, V. N., and Hatfield, D. L. (2012) Thioredoxin reductase 1 protects against chemically induced hepatocarcinogenesis via control of cellular redox homeostasis. *Carcinogenesis* **33**, 1806-1813

79. Maiorino, M., Aumann, K. D., Brigelius-Flohe, R., Doria, D., van den Heuvel, J., McCarthy, J., Roveri, A., Ursini, F., and Flohe, L. (1995) Probing the presumed catalytic triad of selenium-containing peroxidases by mutational analysis of phospholipid hydroperoxide glutathione peroxidase (PHGPx). *Biol Chem Hoppe Seyler* **376**, 651-660

80. Schlecker, T., Comini, M. A., Melchers, J., Ruppert, T., and Krauth-Siegel, R. L. (2007) Catalytic mechanism of the glutathione peroxidase-type tryparedoxin peroxidase of Trypanosoma brucei. *The Biochemical journal* **405**, 445-454

81. Tosatto, S. C., Bosello, V., Fogolari, F., Mauri, P., Roveri, A., Toppo, S., Flohe, L., Ursini, F., and Maiorino, M. (2008) The catalytic site of glutathione peroxidases. *Antioxidants & redox signaling* **10**, 1515-1526

82. Ladenstein, R., Epp, O., Bartels, K., Jones, A., Huber, R., and Wendel, A. (1979) Structure analysis and molecular model of the selenoenzyme glutathione peroxidase at 2.8 A resolution. *J Mol Biol* **134**, 199-218

83. Flohe, L., Eisele, B., and Wendel, A. (1971) [Glutathion peroxidase. I. Isolation and determinations of molecular weight]. *Hoppe Seylers Z Physiol Chem* **352**, 151-158

84. Ren, B., Huang, W., Akesson, B., and Ladenstein, R. (1997) The crystal structure of seleno-glutathione peroxidase from human plasma at 2.9 A resolution. *J Mol Biol* **268**, 869-885

85. Scheerer, P., Borchert, A., Krauss, N., Wessner, H., Gerth, C., Hohne, W., and Kuhn, H. (2007) Structural basis for catalytic activity and enzyme polymerization of phospholipid hydroperoxide glutathione peroxidase-4 (GPx4). *Biochemistry* **46**, 9041-9049

86. Rotruck, J. T., Pope, A. L., Ganther, H. E., Swanson, A. B., Hafeman, D. G., and Hoekstra, W. G. (1973) Selenium: biochemical role as a component of glutathione peroxidase. *Science* **179**, 588-590

87. Mills, G. C. (1957) Hemoglobin catabolism. I. Glutathione peroxidase, an erythrocyte enzyme which protects hemoglobin from oxidative breakdown. *The Journal of biological chemistry* **229**, 189-197

88. Kryukov, G. V., Castellano, S., Novoselov, S. V., Lobanov, A. V., Zehtab, O., Guigo, R., and Gladyshev, V. N. (2003) Characterization of mammalian selenoproteomes. *Science* **300**, 1439-1443

89. Esworthy, R. S., Mann, J. R., Sam, M., and Chu, F. F. (2000) Low glutathione peroxidase activity in Gpx1 knockout mice protects jejunum crypts from gamma-irradiation damage. *Am J Physiol Gastrointest Liver Physiol* **279**, G426-436

90. Ho, Y. S., Magnenat, J. L., Bronson, R. T., Cao, J., Gargano, M., Sugawara, M., and Funk, C. D. (1997) Mice deficient in cellular glutathione peroxidase develop normally and show no increased sensitivity to hyperoxia. *The Journal of biological chemistry* **272**, 16644-16651

91. Walshe, J., Serewko-Auret, M. M., Teakle, N., Cameron, S., Minto, K., Smith, L., Burcham, P. C., Russell, T., Strutton, G., Griffin, A., Chu, F. F., Esworthy, S., Reeve, V., and Saunders, N. A. (2007) Inactivation of glutathione peroxidase activity contributes to UV-induced squamous cell carcinoma formation. *Cancer Res* **67**, 4751-4758

92. Cheng, W. H., Ho, Y. S., Valentine, B. A., Ross, D. A., Combs, G. F., Jr., and Lei, X. G. (1998) Cellular glutathione peroxidase is the mediator of body selenium to protect against paraquat lethality in transgenic mice. *J Nutr* **128**, 1070-1076

93. Chu, F. F., Esworthy, R. S., Chu, P. G., Longmate, J. A., Huycke, M. M., Wilczynski, S., and Doroshow, J. H. (2004) Bacteria-induced intestinal cancer in mice with disrupted Gpx1 and Gpx2 genes. *Cancer Res* **64**, 962-968

94. Lobanov, A. V., Hatfield, D. L., and Gladyshev, V. N. (2008) Reduced reliance on the trace element selenium during evolution of mammals. *Genome biology* **9**, R62

95. Kato, T., Read, R., Rozga, J., and Burk, R. F. (1992) Evidence for intestinal release of absorbed selenium in a form with high hepatic extraction. *Am J Physiol* **262**, G854-858

96. Renko, K., Werner, M., Renner-Muller, I., Cooper, T. G., Yeung, C. H., Hollenbach, B., Scharpf, M., Kohrle, J., Schomburg, L., and Schweizer, U. (2008) Hepatic selenoprotein P (SePP) expression restores selenium transport and prevents infertility and motor-incoordination in Sepp-knockout mice. *The Biochemical journal* **409**, 741-749

97. Burk, R. F., and Hill, K. E. (2015) Regulation of Selenium Metabolism and Transport. *Annu Rev Nutr* **35**, 109-134

98. Burk, R. F., and Hill, K. E. (2009) Selenoprotein P-expression, functions, and roles in mammals. *Biochimica et biophysica acta* **1790**, 1441-1447

99. Burk, R. F., Olson, G. E., Hill, K. E., Winfrey, V. P., Motley, A. K., and Kurokawa, S. (2013) Maternal-fetal transfer of selenium in the mouse. *FASEB journal : official publication of the Federation of American Societies for Experimental Biology* **27**, 3249-3256

100. Bellinger, F. P., He, Q. P., Bellinger, M. T., Lin, Y., Raman, A. V., White, L. R., and Berry, M. J. (2008) Association of selenoprotein p with Alzheimer's pathology in human cortex. *J Alzheimers Dis* **15**, 465-472

101. Peters, M. M., Hill, K. E., Burk, R. F., and Weeber, E. J. (2006) Altered hippocampus synaptic function in selenoprotein P deficient mice. *Mol Neurodegener* **1**, 12

102. Takemoto, A. S., Berry, M. J., and Bellinger, F. P. (2010) Role of selenoprotein P in Alzheimer's disease. *Ethn Dis* **20**, S1-92-95

103. Bellinger, F. P., Raman, A. V., Rueli, R. H., Bellinger, M. T., Dewing, A. S., Seale, L. A., Andres, M. A., Uyehara-Lock, J. H., White, L. R., Ross, G. W., and Berry, M. J. (2012) Changes in selenoprotein P in substantia nigra and putamen in Parkinson's disease. *J Parkinsons Dis* **2**, 115-126

104. Perry, T. L., Godin, D. V., and Hansen, S. (1982) Parkinson's disease: a disorder due to nigral glutathione deficiency? *Neurosci Lett* **33**, 305-310

105. Perry, T. L., and Yong, V. W. (1986) Idiopathic Parkinson's disease, progressive supranuclear palsy and glutathione metabolism in the substantia nigra of patients. *Neurosci Lett* **67**, 269-274

106. Kim, H. Y., and Gladyshev, V. N. (2004) Characterization of mouse endoplasmic reticulum methionine-R-sulfoxide reductase. *Biochem Biophys Res Commun* **320**, 1277-1283

107. Korotkov, K. V., Kumaraswamy, E., Zhou, Y., Hatfield, D. L., and Gladyshev, V. N. (2001) Association between the 15-kDa selenoprotein and UDP-glucose:glycoprotein glucosyltransferase in the endoplasmic reticulum of mammalian cells. *The Journal of biological chemistry* **276**, 15330-15336

108. Shchedrina, V. A., Everley, R. A., Zhang, Y., Gygi, S. P., Hatfield, D. L., and Gladyshev, V. N. (2011) Selenoprotein K binds multiprotein complexes and is involved in the regulation of endoplasmic reticulum homeostasis. *The Journal of biological chemistry* **286**, 42937-42948

109. Xia, L., Nordman, T., Olsson, J. M., Damdimopoulos, A., Bjorkhem-Bergman, L., Nalvarte, I., Eriksson, L. C., Arner, E. S., Spyrou, G., and Bjornstedt, M. (2003) The mammalian cytosolic selenoenzyme thioredoxin reductase reduces ubiquinone. A novel mechanism for defense against oxidative stress. *The Journal of biological chemistry* **278**, 2141-2146

110. Labunskyy, V. M., Yoo, M. H., Hatfield, D. L., and Gladyshev, V. N. (2009) Sep15, a thioredoxin-like selenoprotein, is involved in the unfolded protein response and differentially regulated by adaptive and acute ER stresses. *Biochemistry* **48**, 8458-8465

111. Shchedrina, V. A., Zhang, Y., Labunskyy, V. M., Hatfield, D. L., and Gladyshev, V. N. (2010) Structure-function relations, physiological roles, and evolution of mammalian ER-resident selenoproteins. *Antioxidants & redox signaling* **12**, 839-849

112. Novoselov, S. V., Kryukov, G. V., Xu, X. M., Carlson, B. A., Hatfield, D. L., and Gladyshev, V. N. (2007) Selenoprotein H is a nucleolar thioredoxin-like protein with a unique expression pattern. *The Journal of biological chemistry* **282**, 11960-11968

113. Panee, J., Stoytcheva, Z. R., Liu, W., and Berry, M. J. (2007) Selenoprotein H is a redox-sensing high mobility group family DNA-binding protein that up-regulates genes involved in glutathione synthesis and phase II detoxification. *The Journal of biological chemistry* **282**, 23759-23765

114. Horibata, Y., and Hirabayashi, Y. (2007) Identification and characterization of human ethanolaminephosphotransferase1. *J Lipid Res* **48**, 503-508

115. Bellinger, F. P., Raman, A. V., Reeves, M. A., and Berry, M. J. (2009) Regulation and function of selenoproteins in human disease. *The Biochemical journal* **422**, 11-22

116. Bosl, M. R., Takaku, K., Oshima, M., Nishimura, S., and Taketo, M. M. (1997) Early embryonic lethality caused by targeted disruption of the mouse selenocysteine tRNA gene (Trsp). *Proc. Natl. Acad. Sci. U. S. A.* **94**, 5531-5534

117. Kumaraswamy, E., Carlson, B. A., Morgan, F., Miyoshi, K., Robinson, G. W., Su, D., Wang, S., Southon, E., Tessarollo, L., Lee, B. J., Gladyshev, V. N., Hennighausen, L., and Hatfield, D. L. (2003) Selective removal of the selenocysteine tRNA [Ser]Sec gene (Trsp) in mouse mammary epithelium. *Molecular and cellular biology* **23**, 1477-1488

118. Shrimali, R. K., Lobanov, A. V., Xu, X. M., Rao, M., Carlson, B. A., Mahadeo, D. C., Parent, C. A., Gladyshev, V. N., and Hatfield, D. L. (2005) Selenocysteine tRNA identification in the model organisms Dictyostelium discoideum and Tetrahymena thermophila. *Biochem Biophys Res Commun* **329**, 147-151

119. Suzuki, T., Kelly, V. P., Motohashi, H., Nakajima, O., Takahashi, S., Nishimura, S., and Yamamoto, M. (2008) Deletion of the selenocysteine tRNA gene in macrophages and liver results in compensatory gene induction of cytoprotective enzymes by Nrf2. *The Journal of biological chemistry* **283**, 2021-2030

120. Carlson, B. A., Yoo, M. H., Sano, Y., Sengupta, A., Kim, J. Y., Irons, R., Gladyshev, V. N., Hatfield, D. L., and Park, J. M. (2009) Selenoproteins regulate macrophage invasiveness and extracellular matrix-related gene expression. *BMC Immunol* **10**, 57

121. Carlson, B. A., Novoselov, S. V., Kumaraswamy, E., Lee, B. J., Anver, M. R., Gladyshev, V. N., and Hatfield, D. L. (2004) Specific excision of the selenocysteine tRNA[Ser]Sec (Trsp) gene in mouse liver demonstrates an essential role of selenoproteins in liver function. *The Journal of biological chemistry* **279**, 8011-8017

122. Carlson, B. A., Tobe, R., Yefremova, E., Tsuji, P. A., Hoffmann, V. J., Schweizer, U., Gladyshev, V. N., Hatfield, D. L., and Conrad, M. (2016) Glutathione peroxidase 4 and vitamin E cooperatively prevent hepatocellular degeneration. *Redox Biol* **9**, 22-31

123. Shrimali, R. K., Weaver, J. A., Miller, G. F., Starost, M. F., Carlson, B. A., Novoselov, S. V., Kumaraswamy, E., Gladyshev, V. N., and Hatfield, D. L. (2007) Selenoprotein expression is essential in endothelial cell development and cardiac muscle function. *Neuromuscul Disord* **17**, 135-142

124. Wirth, E. K., Conrad, M., Winterer, J., Wozny, C., Carlson, B. A., Roth, S., Schmitz, D., Bornkamm, G. W., Coppola, V., Tessarollo, L., Schomburg, L., Kohrle, J., Hatfield, D. L., and Schweizer, U. (2010) Neuronal selenoprotein expression is required for interneuron development and prevents seizures and neurodegeneration. *FASEB journal : official publication of the Federation of American Societies for Experimental Biology* **24**, 844-852

125. Wirth, E. K., Bharathi, B. S., Hatfield, D., Conrad, M., Brielmeier, M., and Schweizer, U. (2014) Cerebellar hypoplasia in mice lacking selenoprotein biosynthesis in neurons. *Biol Trace Elem Res* **158**, 203-210

126. Sengupta, A., Lichti, U. F., Carlson, B. A., Ryscavage, A. O., Gladyshev, V. N., Yuspa, S. H., and Hatfield, D. L. (2010) Selenoproteins are essential for proper keratinocyte function and skin development. *PLoS One* **5**, e12249

127. Sengupta, A., Lichti, U. F., Carlson, B. A., Cataisson, C., Ryscavage, A. O., Mikulec, C., Conrad, M., Fischer, S. M., Hatfield, D. L., and Yuspa, S. H. (2013) Targeted disruption of glutathione peroxidase 4 in mouse skin epithelial cells impairs postnatal hair follicle morphogenesis that is partially rescued through inhibition of COX-2. *J Invest Dermatol* **133**, 1731-1741

128. Ursini, F., Maiorino, M., Valente, M., Ferri, L., and Gregolin, C. (1982) Purification from pig liver of a protein which protects liposomes and biomembranes from peroxidative degradation and exhibits glutathione peroxidase activity on phosphatidylcholine hydroperoxides. *Biochimica et biophysica acta* **710**, 197-211

129. Thomas, J. P., Geiger, P. G., Maiorino, M., Ursini, F., and Girotti, A. W. (1990) Enzymatic reduction of phospholipid and cholesterol hydroperoxides in artificial bilayers and lipoproteins. *Biochimica et biophysica acta* **1045**, 252-260

130. Roveri, A., Maiorino, M., Nisii, C., and Ursini, F. (1994) Purification and characterization of phospholipid hydroperoxide glutathione peroxidase from rat testis mitochondrial membranes. *Biochimica et biophysica acta* **1208**, 211-221

131. Ursini, F., Maiorino, M., Brigelius-Flohe, R., Aumann, K. D., Roveri, A., Schomburg, D., and Flohe, L. (1995) Diversity of glutathione peroxidases. *Methods Enzymol* **252**, 38-53

132. Maiorino, M., Roveri, A., Benazzi, L., Bosello, V., Mauri, P., Toppo, S., Tosatto, S. C., and Ursini, F. (2005) Functional interaction of phospholipid hydroperoxide glutathione peroxidase with sperm mitochondrion-associated cysteine-rich protein discloses the adjacent cysteine motif as a new substrate of the selenoperoxidase. *The Journal of biological chemistry* **280**, 38395-38402

133. Ursini, F., Heim, S., Kiess, M., Maiorino, M., Roveri, A., Wissing, J., and Flohe, L. (1999) Dual function of the selenoprotein PHGPx during sperm maturation. *Science* **285**, 1393-1396

134. Brigelius-Flohe, R., Aumann, K. D., Blocker, H., Gross, G., Kiess, M., Kloppel, K. D., Maiorino, M., Roveri, A., Schuckelt, R., Usani, F., and et al. (1994) Phospholipid-hydroperoxide glutathione peroxidase. Genomic DNA, cDNA, and deduced amino acid sequence. *The Journal of biological chemistry* **269**, 7342-7348

135. Moreno, S. G., Laux, G., Brielmeier, M., Bornkamm, G. W., and Conrad, M. (2003) Testis-specific expression of the nuclear form of phospholipid hydroperoxide glutathione peroxidase (PHGPx). *Biological chemistry* **384**, 635-643

136. Maiorino, M., Scapin, M., Ursini, F., Biasolo, M., Bosello, V., and Flohe, L. (2003) Distinct promoters determine alternative transcription of gpx-4 into phospholipid-hydroperoxide glutathione peroxidase variants. *The Journal of biological chemistry* **278**, 34286-34290

137. Conrad, M., Schneider, M., Seiler, A., and Bornkamm, G. W. (2007) Physiological role of phospholipid hydroperoxide glutathione peroxidase in mammals. *Biological chemistry* **388**, 1019-1025

138. Conrad, M., Moreno, S. G., Sinowatz, F., Ursini, F., Kolle, S., Roveri, A., Brielmeier, M., Wurst, W., Maiorino, M., and Bornkamm, G. W. (2005) The nuclear form of phospholipid hydroperoxide glutathione peroxidase is a protein thiol peroxidase contributing to sperm chromatin stability. *Molecular and cellular biology* **25**, 7637-7644

139. Puglisi, R., Maccari, I., Pipolo, S., Conrad, M., Mangia, F., and Boitani, C. (2012) The nuclear form of glutathione peroxidase 4 is associated with sperm nuclear matrix and is required for proper paternal chromatin decondensation at fertilization. *J Cell Physiol* **227**, 1420-1427

140. Jacobsson, S. O., and Hansson, E. (1965) Distribution of selenium in mice studied by whole-body autoradiography after injection ff SE-75-sodium selenite. *Acta Vet Scand* **6**, 287-298

141. Gunn, S. A., Gould, T. C., and Anderson, W. A. (1967) Incorporation of selenium into spermatogenic pathway in mice. *Proc Soc Exp Biol Med* **124**, 1260-1263

142. Wu, S. H., Oldfield, J. E., Whanger, P. D., and Weswig, P. H. (1973) Effect of selenium, vitamin E, and antioxidants on testicular function in rats. *Biol Reprod* **8**, 625-629

143. Watanabe, T., and Endo, A. (1991) Effects of selenium deficiency on sperm morphology and spermatocyte chromosomes in mice. *Mutat Res* **262**, 93-99

144. Bauche, F., Fouchard, M. H., and Jegou, B. (1994) Antioxidant system in rat testicular cells. *FEBS Lett* **349**, 392-396

145. Mauri, P., Benazzi, L., Flohe, L., Maiorino, M., Pietta, P. G., Pilawa, S., Roveri, A., and Ursini, F. (2003) Versatility of selenium catalysis in PHGPx unraveled by LC/ESI-MS/MS. *Biological chemistry* **384**, 575-588

146. Pfeifer, H., Conrad, M., Roethlein, D., Kyriakopoulos, A., Brielmeier, M., Bornkamm, G. W., and Behne, D. (2001) Identification of a specific sperm nuclei selenoenzyme necessary for protamine thiol cross-linking during sperm maturation. *FASEB journal : official publication of the Federation of American Societies for Experimental Biology* **15**, 1236-1238

147. Yang, W. S., SriRamaratnam, R., Welsch, M. E., Shimada, K., Skouta, R., Viswanathan, V. S., Cheah, J. H., Clemons, P. A., Shamji, A. F., Clish, C. B., Brown, L. M., Girotti, A. W., Cornish, V. W., Schreiber, S. L., and Stockwell, B. R. (2014) Regulation of ferroptotic cancer cell death by GPX4. *Cell* **156**, 317-331

148. Friedmann Angeli, J. P., Schneider, M., Proneth, B., Tyurina, Y. Y., Tyurin, V. A., Hammond, V. J., Herbach, N., Aichler, M., Walch, A., Eggenhofer, E., Basavarajappa, D., Radmark, O., Kobayashi, S., Seibt, T., Beck, H., Neff, F., Esposito, I., Wanke, R., Forster, H., Yefremova, O., Heinrichmeyer, M., Bornkamm, G. W., Geissler, E. K., Thomas, S. B., Stockwell, B. R., O'Donnell, V. B., Kagan, V. E., Schick, J. A., and Conrad, M. (2014) Inactivation of the ferroptosis regulator Gpx4 triggers acute renal failure in mice. *Nat Cell Biol* **16**, 1180-1191

149. Imai, H., Hirao, F., Sakamoto, T., Sekine, K., Mizukura, Y., Saito, M., Kitamoto, T., Hayasaka, M., Hanaoka, K., and Nakagawa, Y. (2003) Early embryonic lethality caused by targeted disruption of the mouse PHGPx gene. *Biochem Biophys Res Commun* **305**, 278-286

150. Yant, L. J., Ran, Q., Rao, L., Van Remmen, H., Shibatani, T., Belter, J. G., Motta, L., Richardson, A., and Prolla, T. A. (2003) The selenoprotein GPX4 is essential for mouse development and protects from radiation and oxidative damage insults. *Free Radical Biology and Medicine* **34**, 496-502

151. Liang, H., Yoo, S. E., Na, R., Walter, C. A., Richardson, A., and Ran, Q. (2009) Short form glutathione peroxidase 4 is the essential isoform required for survival and somatic mitochondrial functions. *The Journal of biological chemistry* **284**, 30836-30844

152. Seiler, A., Schneider, M., Forster, H., Roth, S., Wirth, E. K., Culmsee, C., Plesnila, N., Kremmer, E., Radmark, O., Wurst, W., Bornkamm, G. W., Schweizer, U., and Conrad, M. (2008) Glutathione peroxidase 4 senses and translates oxidative stress into 12/15-lipoxygenase dependent- and AIF-mediated cell death. *Cell metabolism* **8**, 237-248

153. Nomura, K., Imai, H., Koumura, T., Kobayashi, T., and Nakagawa, Y. (2000) Mitochondrial phospholipid hydroperoxide glutathione peroxidase inhibits the release of cytochrome c from mitochondria by suppressing the peroxidation of cardiolipin in hypoglycaemia-induced apoptosis. *The Biochemical journal* **351**, 183-193

154. Arai, M., Imai, H., Koumura, T., Yoshida, M., Emoto, K., Umeda, M., Chiba, N., and Nakagawa, Y. (1999) Mitochondrial phospholipid hydroperoxide glutathione peroxidase plays a major role in preventing oxidative injury to cells. *The Journal of biological chemistry* **274**, 4924-4933

155. Nomura, K., Imai, H., Koumura, T., Arai, M., and Nakagawa, Y. (1999) Mitochondrial phospholipid hydroperoxide glutathione peroxidase suppresses apoptosis mediated by a mitochondrial death pathway. *The Journal of biological chemistry* **274**, 29294-29302

156. Yang, W. S., and Stockwell, B. R. (2016) Ferroptosis: Death by Lipid Peroxidation. *Trends Cell Biol* **26**, 165-176

157. Ayala, A., Munoz, M. F., and Arguelles, S. (2014) Lipid peroxidation: production, metabolism, and signaling mechanisms of malondialdehyde and 4-hydroxy-2-nonenal. *Oxid Med Cell Longev* **2014**, 360438

158. Maiorino, M., Coassin, M., Roveri, A., and Ursini, F. (1989) Microsomal lipid peroxidation: effect of vitamin E and its functional interaction with phospholipid hydroperoxide glutathione peroxidase. *Lipids* **24**, 721-726

159. Laster, S. M., Wood, J. G., and Gooding, L. R. (1988) Tumor necrosis factor can induce both apoptic and necrotic forms of cell lysis. *J Immunol* **141**, 2629-2634

160. Linkermann, A., Skouta, R., Himmerkus, N., Mulay, S. R., Dewitz, C., De Zen, F., Prokai, A., Zuchtriegel, G., Krombach, F., Welz, P. S., Weinlich, R., Vanden Berghe, T., Vandenabeele, P., Pasparakis, M., Bleich, M., Weinberg, J. M., Reichel, C. A., Brasen, J. H., Kunzendorf, U., Anders, H. J., Stockwell, B. R., Green, D. R., and Krautwald, S. (2014) Synchronized renal tubular cell death involves ferroptosis. *Proc. Natl. Acad. Sci. U. S. A.* **111**, 16836-16841

161. Jiang, L., Kon, N., Li, T., Wang, S. J., Su, T., Hibshoosh, H., Baer, R., and Gu, W. (2015) Ferroptosis as a p53-mediated activity during tumour suppression. *Nature* **520**, 57-62

162. Gao, M., Monian, P., Quadri, N., Ramasamy, R., and Jiang, X. (2015) Glutaminolysis and Transferrin Regulate Ferroptosis. *Mol Cell* **59**, 298-308

163. Dolma, S., Lessnick, S. L., Hahn, W. C., and Stockwell, B. R. (2003) Identification of genotype-selective antitumor agents using synthetic lethal chemical screening in engineered human tumor cells. *Cancer Cell* **3**, 285-296

164. Yang, W. S., and Stockwell, B. R. (2008) Synthetic lethal screening identifies compounds activating iron-dependent, nonapoptotic cell death in oncogenic-RAS-harboring cancer cells. *Chem Biol* **15**, 234-245

165. Dixon, S. J., Lemberg, K. M., Lamprecht, M. R., Skouta, R., Zaitsev, E. M., Gleason, C. E., Patel, D. N., Bauer, A. J., Cantley, A. M., Yang, W. S., Morrison, B., 3rd, and Stockwell, B. R. (2012) Ferroptosis: an iron-dependent form of nonapoptotic cell death. *Cell* **149**, 1060-1072

166. Bannai, S., and Kitamura, E. (1980) Transport interaction of L-cystine and L-glutamate in human diploid fibroblasts in culture. *The Journal of biological chemistry* **255**, 2372-2376

167. Itoh, K., Tong, K. I., and Yamamoto, M. (2004) Molecular mechanism activating Nrf2-Keap1 pathway in regulation of adaptive response to electrophiles. *Free radical biology & medicine* **36**, 1208-1213

168. Sasaki, H., Sato, H., Kuriyama-Matsumura, K., Sato, K., Maebara, K., Wang, H., Tamba, M., Itoh, K., Yamamoto, M., and Bannai, S. (2002) Electrophile response element-mediated induction of the cystine/glutamate exchange transporter gene expression. *The Journal of biological chemistry* **277**, 44765-44771

169. Bannai, S., Sato, H., Ishii, T., and Taketani, S. (1991) Enhancement of glutathione levels in mouse peritoneal macrophages by sodium arsenite, cadmium chloride and glucose/glucose oxidase. *Biochimica et biophysica acta* **1092**, 175-179

170. Bannai, S., Sato, H., Ishii, T., and Sugita, Y. (1989) Induction of cystine transport activity in human fibroblasts by oxygen. *The Journal of biological chemistry* **264**, 18480-18484

171. Mandal, P. K., Seiler, A., Perisic, T., Kolle, P., Banjac Canak, A., Forster, H., Weiss, N., Kremmer, E., Lieberman, M. W., Bannai, S., Kuhlencordt, P., Sato, H., Bornkamm, G. W., and Conrad, M. (2010) System x(c)- and thioredoxin reductase 1 cooperatively rescue glutathione deficiency. *The Journal of biological chemistry* **285**, 22244-22253

172. Bannai, S. (1986) Exchange of cystine and glutamate across plasma membrane of human fibroblasts. *The Journal of biological chemistry* **261**, 2256-2263

173. Hayano, M., Yang, W. S., Corn, C. K., Pagano, N. C., and Stockwell, B. R. (2016) Loss of cysteinyl-tRNA synthetase (CARS) induces the transsulfuration

pathway and inhibits ferroptosis induced by cystine deprivation. *Cell Death Differ* **23**, 270-278

174. Shimada, K., Skouta, R., Kaplan, A., Yang, W. S., Hayano, M., Dixon, S. J., Brown, L. M., Valenzuela, C. A., Wolpaw, A. J., and Stockwell, B. R. (2016) Global survey of cell death mechanisms reveals metabolic regulation of ferroptosis. *Nature chemical biology* **12**, 497-503

175. Skouta, R., Dixon, S. J., Wang, J., Dunn, D. E., Orman, M., Shimada, K., Rosenberg, P. A., Lo, D. C., Weinberg, J. M., Linkermann, A., and Stockwell, B. R. (2014) Ferrostatins inhibit oxidative lipid damage and cell death in diverse disease models. *J Am Chem Soc* **136**, 4551-4556

176. Dixon, S. J., Winter, G. E., Musavi, L. S., Lee, E. D., Snijder, B., Rebsamen, M., Superti-Furga, G., and Stockwell, B. R. (2015) Human Haploid Cell Genetics Reveals Roles for Lipid Metabolism Genes in Nonapoptotic Cell Death. *ACS Chem Biol* **10**, 1604-1609

177. Doll, S., Proneth, B., Tyurina, Y. Y., Panzilius, E., Kobayashi, S., Ingold, I., Irmler, M., Beckers, J., Aichler, M., Walch, A., Prokisch, H., Trumbach, D., Mao, G., Qu, F., Bayir, H., Fullekrug, J., Scheel, C. H., Wurst, W., Schick, J. A., Kagan, V. E., Angeli, J. P., and Conrad, M. (2016) ACSL4 dictates ferroptosis sensitivity by shaping cellular lipid composition. *Nature chemical biology*

178. Tuohetahuntila, M., Spee, B., Kruitwagen, H. S., Wubbolts, R., Brouwers, J. F., van de Lest, C. H., Molenaar, M. R., Houweling, M., Helms, J. B., and Vaandrager, A. B. (2015) Role of long-chain acyl-CoA synthetase 4 in formation of polyunsaturated lipid species in hepatic stellate cells. *Biochimica et biophysica acta* **1851**, 220-230

179. Soupene, E., and Kuypers, F. A. (2008) Mammalian long-chain acyl-CoA synthetases. *Exp Biol Med (Maywood)* **233**, 507-521

180. Shindou, H., and Shimizu, T. (2009) Acyl-CoA:lysophospholipid acyltransferases. *The Journal of biological chemistry* **284**, 1-5

181. Kagan, V. E., Mao, G., Qu, F., Angeli, J. P., Doll, S., Croix, C. S., Dar, H. H., Liu, B., Tyurin, V. A., Ritov, V. B., Kapralov, A. A., Amoscato, A. A., Jiang, J., Anthonymuthu, T., Mohammadyani, D., Yang, Q., Proneth, B., Klein-Seetharaman, J., Watkins, S., Bahar, I., Greenberger, J., Mallampalli, R. K., Stockwell, B. R., Tyurina, Y. Y., Conrad, M., and Bayir, H. (2016) Oxidized arachidonic and adrenic PEs navigate cells to ferroptosis. *Nature chemical biology*

182. Kim, S. E., Zhang, L., Ma, K., Riegman, M., Chen, F., Ingold, I., Conrad, M., Turker, M. Z., Gao, M., Jiang, X., Monette, S., Pauliah, M., Gonen, M., Zanzonico, P., Quinn, T., Wiesner, U., Bradbury, M. S., and Overholtzer, M. (2016) Ultrasmall nanoparticles induce ferroptosis in nutrient-deprived cancer cells and suppress tumour growth. *Nat Nanotechnol* **11**, 977-985

183. Torii, S., Shintoku, R., Kubota, C., Yaegashi, M., Torii, R., Sasaki, M., Suzuki, T., Mori, M., Yoshimoto, Y., Takeuchi, T., and Yamada, K. (2016) An essential role for functional lysosomes in ferroptosis of cancer cells. *The Biochemical journal* **473**, 769-777

184. Xie, Y., Hou, W., Song, X., Yu, Y., Huang, J., Sun, X., Kang, R., and Tang, D. (2016) Ferroptosis: process and function. *Cell Death Differ* **23**, 369-379

185. Bogdan, A. R., Miyazawa, M., Hashimoto, K., and Tsuji, Y. (2016) Regulators of Iron Homeostasis: New Players in Metabolism, Cell Death, and Disease. *Trends in biochemical sciences* **41**, 274-286

186. Cao, J. Y., and Dixon, S. J. (2016) Mechanisms of ferroptosis. *Cellular and molecular life sciences : CMLS* **73**, 2195-2209

187. Conrad, M., Angeli, J. P., Vandenabeele, P., and Stockwell, B. R. (2016) Regulated necrosis: disease relevance and therapeutic opportunities. *Nat Rev Drug Discov* **15**, 348-366

188. Yang, W. S., Kim, K. J., Gaschler, M. M., Patel, M., Shchepinov, M. S., and Stockwell, B. R. (2016) Peroxidation of polyunsaturated fatty acids by

lipoxygenases drives ferroptosis. *Proc. Natl. Acad. Sci. U. S. A.* **113**, E4966-4975

189. Maccarrone, M., Melino, G., and Finazzi-Agro, A. (2001) Lipoxygenases and their involvement in programmed cell death. *Cell Death Differ* **8**, 776-784

190. Brutsch, S. H., Wang, C. C., Li, L., Stender, H., Neziroglu, N., Richter, C., Kuhn, H., and Borchert, A. (2015) Expression of inactive glutathione peroxidase 4 leads to embryonic lethality, and inactivation of the Alox15 gene does not rescue such knock-in mice. *Antioxidants & redox signaling* **22**, 281-293

191. Shi, Z. Z., Osei-Frimpong, J., Kala, G., Kala, S. V., Barrios, R. J., Habib, G. M., Lukin, D. J., Danney, C. M., Matzuk, M. M., and Lieberman, M. W. (2000) Glutathione synthesis is essential for mouse development but not for cell growth in culture. *Proc. Natl. Acad. Sci. U. S. A.* **97**, 5101-5106

192. Conrad, M., Friedmann Angeli, J. P., Proneth, B. . (2016) Glutathione peroxidase 4 and ferroptosis. in *Selenium. Its molecular biology and role in human health (4th ed.).* (Hatfield, D. L., Schweizer, U.,Tsuji, P. A., Gladyshev, V. N. ed.), 4th Ed., Springer. pp

193. Chen, L., Hambright, W. S., Na, R., and Ran, Q. (2015) Ablation of the Ferroptosis Inhibitor Glutathione Peroxidase 4 in Neurons Results in Rapid Motor Neuron Degeneration and Paralysis. *The Journal of biological chemistry* **290**, 28097-28106

194. Hambright, W. S., Fonseca, R. S., Chen, L., Na, R., and Ran, Q. (2017) Ablation of ferroptosis regulator glutathione peroxidase 4 in forebrain neurons promotes cognitive impairment and neurodegeneration. *Redox Biol* **12**, 8-17

195. Ueta, T., Inoue, T., Furukawa, T., Tamaki, Y., Nakagawa, Y., Imai, H., and Yanagi, Y. (2012) Glutathione peroxidase 4 is required for maturation of photoreceptor cells. *The Journal of biological chemistry* **287**, 7675-7682

196. Canli, O., Alankus, Y. B., Grootjans, S., Vegi, N., Hultner, L., Hoppe, P. S., Schroeder, T., Vandenabeele, P., Bornkamm, G. W., and Greten, F. R. (2016) Glutathione peroxidase 4 prevents necroptosis in mouse erythroid precursors. *Blood* **127**, 139-148

197. Brutsch, S. H., Rademacher, M., Roth, S. R., Muller, K., Eder, S., Viertel, D., Franz, C., Kuhn, H., and Borchert, A. (2016) Male Subfertility Induced by Heterozygous Expression of Catalytically Inactive Glutathione Peroxidase 4 Is Rescued in Vivo by Systemic Inactivation of the Alox15 Gene. *The Journal of biological chemistry* **291**, 23578-23588

198. Matsushita, M., Freigang, S., Schneider, C., Conrad, M., Bornkamm, G. W., and Kopf, M. (2015) T cell lipid peroxidation induces ferroptosis and prevents immunity to infection. *The Journal of experimental medicine* **212**, 555-568

199. Wortmann, M., Schneider, M., Pircher, J., Hellfritsch, J., Aichler, M., Vegi, N., Kolle, P., Kuhlencordt, P., Walch, A., Pohl, U., Bornkamm, G. W., Conrad, M., and Beck, H. (2013) Combined deficiency in glutathione peroxidase 4 and vitamin E causes multiorgan thrombus formation and early death in mice. *Circ Res* **113**, 408-417

200. Telorack, M., Meyer, M., Ingold, I., Conrad, M., Bloch, W., and Werner, S. (2016) A Glutathione-Nrf2-Thioredoxin Cross-Talk Ensures Keratinocyte Survival and Efficient Wound Repair. *PLoS Genet* **12**, e1005800

201. Bornkamm, G. W., Berens, C., Kuklik-Roos, C., Bechet, J. M., Laux, G., Bachl, J., Korndoerfer, M., Schlee, M., Holzel, M., Malamoussi, A., Chapman, R. D., Nimmerjahn, F., Mautner, J., Hillen, W., Bujard, H., and Feuillard, J. (2005) Stringent doxycycline-dependent control of gene activities using an episomal one-vector system. *Nucleic Acids Res* **33**, e137

202. Rodriguez, C. I., Buchholz, F., Galloway, J., Sequerra, R., Kasper, J., Ayala, R., Stewart, A. F., and Dymecki, S. M. (2000) High-efficiency deleter mice show that FLPe is an alternative to Cre-loxP. *Nat Genet* **25**, 139-140

203. Kagan, V. E., Tyurina, Y. Y., Tyurin, V. A., Mohammadyani, D., Angeli, J. P., Baranov, S. V., Klein-Seetharaman, J., Friedlander, R. M., Mallampalli, R. K.,

Conrad, M., and Bayir, H. (2015) Cardiolipin Signaling Mechanisms: Collapse of Asymmetry and Oxidation. *Antioxidants & redox signaling*

204. Parrinello, S., Samper, E., Krtolica, A., Goldstein, J., Melov, S., and Campisi, J. (2003) Oxygen sensitivity severely limits the replicative lifespan of murine fibroblasts. *Nature cell biology* **5**, 741-747

205. Gibson, D. G., Young, L., Chuang, R. Y., Venter, J. C., Hutchison, C. A., 3rd, and Smith, H. O. (2009) Enzymatic assembly of DNA molecules up to several hundred kilobases. *Nat Methods* **6**, 343-345

206. Peng, X., Mandal, P. K., Kaminskyy, V. O., Lindqvist, A., Conrad, M., and Arner, E. S. (2014) Sec-containing TrxR1 is essential for self-sufficiency of cells by control of glucose-derived H2O2. *Cell Death Dis* **5**, e1235

207. Poschmann, G., Seyfarth, K., Besong Agbo, D., Klafki, H. W., Rozman, J., Wurst, W., Wiltfang, J., Meyer, H. E., Klingenspor, M., and Stuhler, K. (2014) High-fat diet induced isoform changes of the Parkinson's disease protein DJ-1. *J Proteome Res* **13**, 2339-2351

208. Roveri, A., Maiorino, M., and Ursini, F. (1994) Enzymatic and immunological measurements of soluble and membrane-bound phospholipid-hydroperoxide glutathione peroxidase. *Methods Enzymol* **233**, 202-212

209. Tietze, F. (1969) Enzymic method for quantitative determination of nanogram amounts of total and oxidized glutathione: applications to mammalian blood and other tissues. *Anal Biochem* **27**, 502-522

210. Schmitt, S., Saathoff, F., Meissner, L., Schropp, E. M., Lichtmannegger, J., Schulz, S., Eberhagen, C., Borchard, S., Aichler, M., Adamski, J., Plesnila, N., Rothenfusser, S., Kroemer, G., and Zischka, H. (2013) A semi-automated method for isolating functionally intact mitochondria from cultured cells and tissue biopsies. *Anal Biochem* **443**, 66-74

211. Schmitt, S., Schulz, S., Schropp, E.-M., Eberhagen, C., Simmons, A., Beisker, W., Aichler, M., and Zischka, H. (2014) Why to compare absolute numbers of mitochondria. *Mitochondrion* **19**, 113-123

212. Schulz, S., Schmitt, S., Wimmer, R., Aichler, M., Eisenhofer, S., Lichtmannegger, J., Eberhagen, C., Artmann, R., Tookos, F., Walch, A., Krappmann, D., Brenner, C., Rust, C., and Zischka, H. (2013) Progressive stages of mitochondrial destruction caused by cell toxic bile salts. *Biochimica et biophysica acta* **1828**, 2121-2133

213. Suppmann S., P. B. C. a. B. A. (1999) Dynamics and effieciency in vivo of UGA-directed selenocysteine insertion at the ribosome. *The EMBO Journal* **18**, 2284-2293

214. Jiang, X., Lachance, M., and Rossignol, E. (2016) Involvement of cortical fast-spiking parvalbumin-positive basket cells in epilepsy. *Prog Brain Res* **226**, 81-126

215. Rossignol, E. (2011) Genetics and function of neocortical GABAergic interneurons in neurodevelopmental disorders. *Neural Plast* **2011**, 649325

216. Schwaller, B., Tetko, I. V., Tandon, P., Silveira, D. C., Vreugdenhil, M., Henzi, T., Potier, M. C., Celio, M. R., and Villa, A. E. (2004) Parvalbumin deficiency affects network properties resulting in increased susceptibility to epileptic seizures. *Molecular and cellular neurosciences* **25**, 650-663

217. Mihaly, A., Szente, M., Dubravcsik, Z., Boda, B., Kiraly, E., Nagy, T., and Domonkos, A. (1997) Parvalbumin- and calbindin-containing neurons express c-fos protein in primary and secondary (mirror) epileptic foci of the rat neocortex. *Brain Res* **761**, 135-145

218. Hitz, C., Wurst, W., and Kuhn, R. (2007) Conditional brain-specific knockdown of MAPK using Cre/loxP regulated RNA interference. *Nucleic Acids Res* **35**, e90

219. Klomsiri, C., Nelson, K. J., Bechtold, E., Soito, L., Johnson, L. C., Lowther, W. T., Ryu, S. E., King, S. B., Furdui, C. M., and Poole, L. B. (2010) Use of dimedone-based chemical probes for sulfenic acid detection evaluation of

conditions affecting probe incorporation into redox-sensitive proteins. *Methods Enzymol* **473**, 77-94

220. Ran, Q., Liang, H., Gu, M., Qi, W., Walter, C. A., Roberts, L. J., 2nd, Herman, B., Richardson, A., and Van Remmen, H. (2004) Transgenic mice overexpressing glutathione peroxidase 4 are protected against oxidative stress-induced apoptosis. *The Journal of biological chemistry* **279**, 55137-55146

221. Dranka, B. P., Benavides, G. A., Diers, A. R., Giordano, S., Zelickson, B. R., Reily, C., Zou, L., Chatham, J. C., Hill, B. G., Zhang, J., Landar, A., and Darley-Usmar, V. M. (2011) Assessing bioenergetic function in response to oxidative stress by metabolic profiling. *Free radical biology & medicine* **51**, 1621-1635

222. Castex, M. T., Arabo, A., Benard, M., Roy, V., Le Joncour, V., Prevost, G., Bonnet, J. J., Anouar, Y., and Falluel-Morel, A. (2016) Selenoprotein T Deficiency Leads to Neurodevelopmental Abnormalities and Hyperactive Behavior in Mice. *Mol Neurobiol* **53**, 5818-5832

223. Xu, X. M., Turanov, A. A., Carlson, B. A., Yoo, M. H., Everley, R. A., Nandakumar, R., Sorokina, I., Gygi, S. P., Gladyshev, V. N., and Hatfield, D. L. (2010) Targeted insertion of cysteine by decoding UGA codons with mammalian selenocysteine machinery. *Proc. Natl. Acad. Sci. U. S. A.* **107**, 21430-21434

224. Anestal, K., Prast-Nielsen, S., Cenas, N., and Arner, E. S. (2008) Cell death by SecTRAPs: thioredoxin reductase as a prooxidant killer of cells. *PLoS One* **3**, e1846

225. Conrad, M., Ingold, I., Buday, K., Kobayashi, S., and Angeli, J. P. (2015) ROS, thiols and thiol-regulating systems in male gametogenesis. *Biochimica et biophysica acta* **1850**, 1566-1574

226. Salmeen, A., Andersen, J. N., Myers, M. P., Meng, T. C., Hinks, J. A., Tonks, N. K., and Barford, D. (2003) Redox regulation of protein tyrosine phosphatase 1B involves a sulphenyl-amide intermediate. *Nature* **423**, 769-773

227. van Montfort, R. L., Congreve, M., Tisi, D., Carr, R., and Jhoti, H. (2003) Oxidation state of the active-site cysteine in protein tyrosine phosphatase 1B. *Nature* **423**, 773-777

228. Cox, A. G., Winterbourn, C. C., and Hampton, M. B. (2010) Measuring the redox state of cellular peroxiredoxins by immunoblotting. *Methods Enzymol* **474**, 51-66

229. Tahara, E. B., Navarete, F. D., and Kowaltowski, A. J. (2009) Tissue-, substrate-, and site-specific characteristics of mitochondrial reactive oxygen species generation. *Free radical biology & medicine* **46**, 1283-1297

230. Cole-Ezea, P., Swan, D., Shanley, D., and Hesketh, J. (2012) Glutathione peroxidase 4 has a major role in protecting mitochondria from oxidative damage and maintaining oxidative phosphorylation complexes in gut epithelial cells. *Free radical biology & medicine* **53**, 488-497

231. Liang, H., Van Remmen, H., Frohlich, V., Lechleiter, J., Richardson, A., and Ran, Q. (2007) Gpx4 protects mitochondrial ATP generation against oxidative damage. *Biochem Biophys Res Commun* **356**, 893-898

232. Shrimali, R. K., Irons, R. D., Carlson, B. A., Sano, Y., Gladyshev, V. N., Park, J. M., and Hatfield, D. L. (2008) Selenoproteins mediate T cell immunity through an antioxidant mechanism. *The Journal of biological chemistry* **283**, 20181-20185

233. Sherrer, R. L., Ho, J. M., and Soll, D. (2008) Divergence of selenocysteine tRNA recognition by archaeal and eukaryotic O-phosphoseryl-tRNASec kinase. *Nucleic Acids Res* **36**, 1871-1880

234. Hubert, N., Sturchler, C., Westhof, E., Carbon, P., and Krol, A. (1998) The 9/4 secondary structure of eukaryotic selenocysteine tRNA: more pieces of evidence. *RNA* **4**, 1029-1033

235. Bock, A., Forchhammer, K., Heider, J., and Baron, C. (1991) Selenoprotein synthesis: an expansion of the genetic code. *Trends in biochemical sciences* **16**, 463-467

236. Amberg, R., Mizutani, T., Wu, X. Q., and Gross, H. J. (1996) Selenocysteine synthesis in mammalia: an identity switch from tRNA(Ser) to tRNA(Sec). *J Mol Biol* **263**, 8-19

237. Sturchler-Pierrat, C., Hubert, N., Totsuka, T., Mizutani, T., Carbon, P., and Krol, A. (1995) Selenocysteylation in eukaryotes necessitates the uniquely long aminoacyl acceptor stem of selenocysteine tRNA(Sec). *The Journal of biological chemistry* **270**, 18570-18574

238. Juhling, F., Morl, M., Hartmann, R. K., Sprinzl, M., Stadler, P. F., and Putz, J. (2009) tRNAdb 2009: compilation of tRNA sequences and tRNA genes. *Nucleic Acids Res* **37**, D159-162

239. Wu, X. Q., and Gross, H. J. (1993) The long extra arms of human tRNA((Ser)Sec) and tRNA(Ser) function as major identify elements for serylation in an orientation-dependent, but not sequence-specific manner. *Nucleic Acids Res* **21**, 5589-5594

240. Ohama, T., Yang, D. C., and Hatfield, D. L. (1994) Selenocysteine tRNA and serine tRNA are aminoacylated by the same synthetase, but may manifest different identities with respect to the long extra arm. *Arch Biochem Biophys* **315**, 293-301

241. Kinney, J. W., Davis, C. N., Tabarean, I., Conti, B., Bartfai, T., and Behrens, M. M. (2006) A specific role for NR2A-containing NMDA receptors in the maintenance of parvalbumin and GAD67 immunoreactivity in cultured interneurons. *The Journal of neuroscience : the official journal of the Society for Neuroscience* **26**, 1604-1615

242. Behrens, M. M., Ali, S. S., Dao, D. N., Lucero, J., Shekhtman, G., Quick, K. L., and Dugan, L. L. (2007) Ketamine-induced loss of phenotype of fast-spiking interneurons is mediated by NADPH-oxidase. *Science* **318**, 1645-1647

243. Wang, X., Zhou, Z., Yang, C., Xu, J., and Yang, J. (2011) Nuclear factor-kappaB is involved in the phenotype loss of parvalbumin-interneurons in vitro. *Neuroreport* **22**, 264-268

244. Kann, O. (2016) The interneuron energy hypothesis: Implications for brain disease. *Neurobiol Dis* **90**, 75-85

245. Gulyas, A. I., Buzsaki, G., Freund, T. F., and Hirase, H. (2006) Populations of hippocampal inhibitory neurons express different levels of cytochrome c. *Eur J Neurosci* **23**, 2581-2594

246. Kageyama, G. H., and Wong-Riley, M. T. (1982) Histochemical localization of cytochrome oxidase in the hippocampus: correlation with specific neuronal types and afferent pathways. *Neuroscience* **7**, 2337-2361

247. Takacs, V. T., Szonyi, A., Freund, T. F., Nyiri, G., and Gulyas, A. I. (2015) Quantitative ultrastructural analysis of basket and axo-axonic cell terminals in the mouse hippocampus. *Brain Struct Funct* **220**, 919-940

248. Behrens, M. M., and Sejnowski, T. J. (2009) Does schizophrenia arise from oxidative dysregulation of parvalbumin-interneurons in the developing cortex? *Neuropharmacology* **57**, 193-200

249. Bitanihirwe, B. K., and Woo, T. U. (2011) Oxidative stress in schizophrenia: an integrated approach. *Neurosci Biobehav Rev* **35**, 878-893

250. Pitts, M. W., Raman, A. V., Hashimoto, A. C., Todorovic, C., Nichols, R. A., and Berry, M. J. (2012) Deletion of selenoprotein P results in impaired function of parvalbumin interneurons and alterations in fear learning and sensorimotor gating. *Neuroscience* **208**, 58-68

251. Burk, R. F., Hill, K. E., Olson, G. E., Weeber, E. J., Motley, A. K., Winfrey, V. P., and Austin, L. M. (2007) Deletion of apolipoprotein E receptor-2 in mice lowers brain selenium and causes severe neurological dysfunction and death when a

low-selenium diet is fed. *The Journal of neuroscience : the official journal of the Society for Neuroscience* **27**, 6207-6211

252. Schneider, M., Vogt Weisenhorn, D. M., Seiler, A., Bornkamm, G. W., Brielmeier, M., and Conrad, M. (2006) Embryonic expression profile of phospholipid hydroperoxide glutathione peroxidase. *Gene expression patterns : GEP* **6**, 489-494

253. Casanova, E., Fehsenfeld, S., Mantamadiotis, T., Lemberger, T., Greiner, E., Stewart, A. F., and Schutz, G. (2001) A CamKIIalpha iCre BAC allows brain-specific gene inactivation. *Genesis* **31**, 37-42

254. Gloster, A., Wu, W., Speelman, A., Weiss, S., Causing, C., Pozniak, C., Reynolds, B., Chang, E., Toma, J. G., and Miller, F. D. (1994) The T alpha 1 alpha-tubulin promoter specifies gene expression as a function of neuronal growth and regeneration in transgenic mice. *The Journal of neuroscience : the official journal of the Society for Neuroscience* **14**, 7319-7330

255. Downey, C. M., Horton, C. R., Carlson, B. A., Parsons, T. E., Hatfield, D. L., Hallgrimsson, B., and Jirik, F. R. (2009) Osteo-chondroprogenitor-specific deletion of the selenocysteine tRNA gene, Trsp, leads to chondronecrosis and abnormal skeletal development: a putative model for Kashin-Beck disease. *PLoS Genet* **5**, e1000616

256. Udan, R. S., Culver, J. C., and Dickinson, M. E. (2013) Understanding vascular development. *Wiley Interdiscip Rev Dev Biol* **2**, 327-346

257. Xie, J., Wu, T., Xu, K., Huang, I. K., Cleaver, O., and Huang, C. L. (2009) Endothelial-specific expression of WNK1 kinase is essential for angiogenesis and heart development in mice. *Am J Pathol* **175**, 1315-1327

258. Swartley, O. M., Foley, J. F., Livingston, D. P., 3rd, Cullen, J. M., and Elmore, S. A. (2016) Histology Atlas of the Developing Mouse Hepatobiliary Hemolymphatic Vascular System with Emphasis on Embryonic Days 11.5-18.5 and Early Postnatal Development. *Toxicol Pathol* **44**, 705-725

259. Folmes, C. D., and Terzic, A. (2014) Metabolic determinants of embryonic development and stem cell fate. *Reprod Fertil Dev* **27**, 82-88

260. Hom, J. R., Quintanilla, R. A., Hoffman, D. L., de Mesy Bentley, K. L., Molkentin, J. D., Sheu, S. S., and Porter, G. A., Jr. (2011) The permeability transition pore controls cardiac mitochondrial maturation and myocyte differentiation. *Dev Cell* **21**, 469-478

261. Aygun, C., Celik, F. C., Nural, M. S., Azak, E., Kucukoduk, S., Ogur, G., and Incesu, L. (2012) Simplified gyral pattern with cerebellar hypoplasia in Sedaghatian type spondylometaphyseal dysplasia: a clinical report and review of the literature. *Am J Med Genet A* **158A**, 1400-1405

262. Smith, A. C., Mears, A. J., Bunker, R., Ahmed, A., MacKenzie, M., Schwartzentruber, J. A., Beaulieu, C. L., Ferretti, E., Consortium, F. C., Majewski, J., Bulman, D. E., Celik, F. C., Boycott, K. M., and Graham, G. E. (2014) Mutations in the enzyme glutathione peroxidase 4 cause Sedaghatian-type spondylometaphyseal dysplasia. *Journal of medical genetics* **51**, 470-474

263. Doetschman, T. (2009) Influence of genetic background on genetically engineered mouse phenotypes. *Methods Mol Biol* **530**, 423-433

264. George, E. L., Georges-Labouesse, E. N., Patel-King, R. S., Rayburn, H., and Hynes, R. O. (1993) Defects in mesoderm, neural tube and vascular development in mouse embryos lacking fibronectin. *Development* **119**, 1079-1091

265. Baribault, H., Penner, J., Iozzo, R. V., and Wilson-Heiner, M. (1994) Colorectal hyperplasia and inflammation in keratin 8-deficient FVB/N mice. *Genes Dev* **8**, 2964-2973

266. Baribault, H., Price, J., Miyai, K., and Oshima, R. G. (1993) Mid-gestational lethality in mice lacking keratin 8. *Genes Dev* **7**, 1191-1202

267. Threadgill, D. W., Dlugosz, A. A., Hansen, L. A., Tennenbaum, T., Lichti, U., Yee, D., LaMantia, C., Mourton, T., Herrup, K., Harris, R. C., and et al. (1995)

Targeted disruption of mouse EGF receptor: effect of genetic background on mutant phenotype. *Science* **269**, 230-234

268. Rector, F. C., Jr. (1983) Sodium, bicarbonate, and chloride absorption by the proximal tubule. *Am J Physiol* **244**, F461-471

269. Niaudet, P. (1998) Mitochondrial disorders and the kidney. *Arch Dis Child* **78**, 387-390

270. Curthoys, N. P., and Moe, O. W. (2014) Proximal tubule function and response to acidosis. *Clin J Am Soc Nephrol* **9**, 1627-1638

271. Hulbert, A. J., Rana, T., and Couture, P. (2002) The acyl composition of mammalian phospholipids: an allometric analysis. *Comp Biochem Physiol B Biochem Mol Biol* **132**, 515-527

272. Vereb, G., Szollosi, J., Matko, J., Nagy, P., Farkas, T., Vigh, L., Matyus, L., Waldmann, T. A., and Damjanovich, S. (2003) Dynamic, yet structured: The cell membrane three decades after the Singer-Nicolson model. *Proc. Natl. Acad. Sci. U. S. A.* **100**, 8053-8058

273. Ikeda, M., Kihara, A., and Igarashi, Y. (2006) Lipid asymmetry of the eukaryotic plasma membrane: functions and related enzymes. *Biol Pharm Bull* **29**, 1542-1546

274. Lenoir, G., Williamson, P., and Holthuis, J. C. (2007) On the origin of lipid asymmetry: the flip side of ion transport. *Curr Opin Chem Biol* **11**, 654-661

275. Pamplona, R. (2008) Membrane phospholipids, lipoxidative damage and molecular integrity: a causal role in aging and longevity. *Biochimica et biophysica acta* **1777**, 1249-1262

276. Wallis, J. G., Watts, J. L., and Browse, J. (2002) Polyunsaturated fatty acid synthesis: what will they think of next? *Trends in biochemical sciences* **27**, 467

277. Haddad, L. S., Kelbert, L., and Hulbert, A. J. (2007) Extended longevity of queen honey bees compared to workers is associated with peroxidation-resistant membranes. *Exp Gerontol* **42**, 601-609

278. Shmookler Reis, R. J., Xu, L., Lee, H., Chae, M., Thaden, J. J., Bharill, P., Tazearslan, C., Siegel, E., Alla, R., Zimniak, P., and Ayyadevara, S. (2011) Modulation of lipid biosynthesis contributes to stress resistance and longevity of C. elegans mutants. *Aging (Albany NY)* **3**, 125-147

279. Grim, J. M., Hyndman, K. A., Kriska, T., Girotti, A. W., and Crockett, E. L. (2011) Relationship between oxidizable fatty acid content and level of antioxidant glutathione peroxidases in marine fish. *J. Exp. Biol.* **214**, 3751-3759

280. Dickinson, B. C., Peltier, J., Stone, D., Schaffer, D. V., and Chang, C. J. (2011) Nox2 redox signaling maintains essential cell populations in the brain. *Nature chemical biology* **7**, 106-112

281. Cossins, A. R., and Prosser, C. L. (1978) Evolutionary adaptation of membranes to temperature. *Proc. Natl. Acad. Sci. U. S. A.* **75**, 2040-2043

282. Che, R., Yuan, Y., Huang, S., and Zhang, A. (2014) Mitochondrial dysfunction in the pathophysiology of renal diseases. *Am J Physiol Renal Physiol* **306**, F367-378

283. Mix, H., Lobanov, A. V., and Gladyshev, V. N. (2007) SECIS elements in the coding regions of selenoprotein transcripts are functional in higher eukaryotes. *Nucleic Acids Res* **35**, 414-423

284. Salinas, G., Bonilla, M., Otero, L., Lobanov, A. V., Gladyshev, V.N. . (2016) Selenoproteins in Parasites. in *Selenium. Its molecular biology and role in human health (4th ed.).* (Hatfield, D. L., Schweizer, U.,Tsuji, P. A., Gladyshev, V. N. ed.), 4th Ed., Springer. pp

285. Mei, H., Thakur, A., Schwartz, J., and Lo Verde, P. T. (1996) Expression and characterization of glutathione peroxidase activity in the human blood fluke Schistosoma mansoni. *Infect Immun* **64**, 4299-4306

# 7    Appendix

**Amplification Primers:**    Forward:   `5'-GGATCCACTAGTAACGGCCGCCAGT-3'`
                             Reverse:   `5'-TCTAGAGCTAGCCTAGGCTCGAGAA-3'`

**Sequence as ordered:**

(sense strand, 5' - 3')

```
GGATCCACTAGTAACGGCCGCCAGTGTGCTGGAATTCGCCGCCACCATGGACTACAAGGACGACG
ACGACAAGGGCAGCGCCAGCGCTTGGAGCCACCCTCAGTTTGAGAAGGGCGGAGGCTCTGGCGGC
GGAAGTGGCGGAGGATCTTGGTCCCATCCCCAGTTCGAAAAGGGCGCCAGCTACCCCTACGACGT
GCCAGATTACGCCTGCGCCAGCAGGGACGATTGGAGATGCGCCAGATCCATGCACGAGTTCAGCG
CCAAGGACATCGACGGCCACATGGTGTGCCTGGACAAGTACAGAGGCTTCGTGTGCATCGTGACC
AACGTGGCCAGCCAGTGCGGCAAGACCGACGTGAACTACACCCAGCTGGTGGACCTGCACGCCAG
ATACGCTGAGTGCGGCCTGAGAATCCTGGCCTTCCCCATGCAACCAGTTCGGCAGACAGGAACCCG
GCAGCAACCAGGAAATCAAAGAGTTCGCCGCTGGCTACAACGTGAAGTTCGACATGTACAGCAAG
ATCTGCGTGAACGGCGACGACGCCCACCCCCTGTGGAAGTGGATGAAGGTGCAGCCCAAGGGCAG
AGGCATGCTGGGCAACGCCATCAAGTGGAACTTCACCAAGTTTCTGATCGACAAGAACGGCTGCG
TCGTGAAGAGATACGGCCCCATGGAAGAACCCCAAGTGATCGAGAAGGACCTGCCCTGCTACCTG
TGACTAGCCCTACAAGTGTGTGCCCCTACACCGAGCCCCCCTGCCCTGTGACCCCTGGAGCCTTC
CACCCCGGCACTCATGAAGGTCTGCCTGAAAACCAGCCTGCTGGTGGGGCAGTCCTGAGGACCTG
GCGTGCATCCCTGCCGGAGGAAGGTCCAGAGGCCTGTGGCCCTGGGCTCGAGCTTCACCCTGGCT
GCCTAATCTGAATTCGTCGACAAGCTTCTCGAGCCTAGGCTAGCTCTAGA
```

**Supplementary figure 1: FSH tagged *Gpx4* cDNA sequence.** The FLAG-Strep-Ha tagged *Gpx4* cDNA with a mutation of the Sec to Cys codon flanked by a B*stbI* and X*baI* restriction site was obtained as a GeneArt® String™ from Invitrogen. The cDNA sequence was synthesiszed as a codon-optimized sequence

**Supplementary Data on CD**:

**Video file**

Video showing *Gpx4$^{cys/cys}$* mice together with control littermates (of a mixed *129S6SvEvTac-C57BL/6J* genetic background). *Gpx4$^{cys/cys}$* mice at the age of 15 days suffered from severe spontaneous seizures when touched by the experimenter or littermates.

# 8    Curriculum vitae

**Irina Ingold geb. Kliewer**

| | |
|---|---|
| Title: | Master of Science (M.Sc.) |
| Place of birth: | Karaganda, Kazakhstan |
| Date of birth: | 28.08.1987 |
| Nationality: | German |
| Address: | Bertholdstrasse 20,D- 80809 Munich |
| Phone: | +491605511028 |
| E-Mail address: | Irina.ingold@outlook.de |

## Education

| | |
|---|---|
| June 2013 – dato | PhD student at the Institute of Developmental Genetics, Helmholtz Zentrum München |
| Oct. 2010 – March 2013 | Master degree course: Biology Wissenschaftszentrum Weihenstephan, Technical University Munich<br>Graduation: M.Sc. (1.4) |
| Oct. 2007 – August 2010 | Bachelor degree course: Biology Eberhard-Karls University Tübingen<br>Graduation: B.Sc. (1.8) |
| Sept. 1998 – June 2007 | Gymnasium bei St. Michael Schwäbisch Hal<br>Graduation: Abitur (2.2) |

## Work experience

| | |
|---|---|
| June 2013 – dato | PhD thesis at the Institute of Developmental Genetics, Helmholtz Zentrum München under the supervision of Dr. Marcus Conrad |
| August 2012 – March 2013 | Master thesis at the Institute of Developmental Genetics, Helmholtz Zentrum München under the supervision of Dr. Marcus Conrad |
| May 2012 – June 2012 | Internship at the clinical research group "Molecular Tumor Biology" at the Klinikum |

Rechts der Isar (Technical University Munich) under the supervision PD Dr. Janssen

| | |
|---|---|
| May 2011 – June 2011 | Internship at the Institute of Developmental Genetics, Helmholtz Center Munich under he supervision of Prof. Dr. Graw |
| April 2010 – August 2010 | Bachelor Thesis at the Institute of Tropical Medicine Eberhard-Karls University Tübingen under the supervision of Prof. Dr. Kuhn. |

## Publications

**Ingold I.**, Berndt, C., Schmitt S., Doll S., Poschmann G., Roveri A., Peng X., Porto Freitas F., Seibt T., Mehr L., Aichler M., Walch A., Lamp D., Jastroch M., Miyamoto S., Wurst W., Ursini F., Arnér E.S.J., Fradejas-Villar N., Schweizer U., Zischka H., Friedmann Angeli J.P., Conrad M. (2017): Selenium ulitlization by GPX4 isrequired to prevent hydroperoxide-induced ferroptosis. Cell 2018 Jan

Hassania B., Wiernicki B., **Ingold I.**, Qu F., Tyuirna Y., Bayir H., Abhari B., Friedmann Angeli J.P., Choi S., Meul E., Heyninck K., Declerck K., Chirumamilla, C., Lethela-Kakkonen M., Van Camp G., Krysko D., Ekert P., Fulda S., Conrad M., Kagan V., Van den Berghe W., Vandenabeele P, Van den Berghe T. (2017): Ferroptosis eradicates high risk-neuroblastoma by increasing the labile Fe(II) pool (submitted).

Doll S., Proneth B., Tyurina Y., Panzilius E., Kobayashi S., **Ingold I.**, Irmler M., Beckers J., Aichler M., Walch A., Prokisch H., Trümbach D., Füllekrug J., Scheel C., Wurst W., Schick J.A., Kagan V.E., Friedmann Angeli J.P., Conrad M.: Acsl4 Dictates Ferroptosis Sensitivity by Shaping Cellular Lipid Composition. Nat Chem Biol. 2017 Jan

Bradbury M., Kin S., Zhang L., Ma K., Rieman M., Chen F., **Ingold I.**, Conrad M., Turker M, Gao M., Jiang X., Monette S., Mohan P., Gonen M., Zanzonico P., Quinn T., Wiesner U., Overholtzer M.: Ultrasmall Nanoparticles Induce Ferroptosis of Nutrient-Deprived Cancer Cells and Suppress Tumor Growth. Nat Nanotechnol. 2016 Nov

Telorack M., Meyer M., **Ingold I.**, Conrad M., Bloch W., Werner S.: A Glutathione-Nrf2-Thioredoxin Cross-Talk Ensures Keratinocyte Survival and Efficient Wound Repair. PLoS Genet. 2016 Jan

Holzerova E., Danhauser K., Haack T.B., Kremer L.S., Melcher M., **Ingold I.**, Kobayashi S., Terrile C., Wolf P., Schaper J., Mayatepek E., Baertling F., Friedmann Angeli J.P., Conrad M., Strom T.M., Meitinger T., Prokisch H., Distelmaier F.: Human thioredoxin 2 deficiency impairs mitochondrial redox homeostasis and causes earlyonset neurodegeneration. Brain. 2016 Feb

**Ingold I.**, Aichler M., Yefremova E., Roveri A., Buday K., Doll S., Tasdemir A., Hoffard N., Wurst W., Walch A., Ursini F., Friedmann Angeli J.P., Conrad M.:

Expression of catalytically inactive form of glutathione peroxidase (Gpx) 4 confers a dominant negative effect in male fertility. J Biol Chem. 2015 Jun

Hellfritsch J., Kirsch J., Schneider M., Fluege T., Wortmann M., Frijhoff J., Dagnell M., Fey T., Esposito I., Kölle P., Pogoda K., Angeli J.P., **Ingold I.**, Kuhlencordt P, Östman A., Pohl U., Conrad M., Beck H.: Knockout of mitochondrial thioredoxin reductase stabilizes prolyl hydroxylase 2 and inhibits tumor growth and tumor-derived angiogenesis. Antioxid Redox Signal. 2015 Apr

Conrad M., **Ingold I.**, Buday K., Kobayashi S., Angeli J.P.: ROS, thiols and thiol-regulating systems in male gametogenesis. Biochim Biophys Acta. 2015 Aug

## Presentations

**Ingold I.**, Berndt C., Roveri A., Ursini F., Schmitt S., Jastroch M., Zischka H., Friedmann Angeli J.P., Conrad M. (2016). Selected speaker at the 3rd meeting of the study group redox biology of the German Society Biochemistry and Molecular Biology (GBM).

**Kliewer I.**, Friedmann Angeli J.P., Yefremova O., Giesert F., Wurst W., Roveri A., Ursini F., Conrad M. (2014). Selenothiol-mediated Gpx4 catalysis is dispensable for mammalian embryonic development but essential for neuronal survival and function. Poster presentation at the Gordon Research Conference Thiol-based Redoxregulations & Signaling.

# 9    Acknowledgements

This thesis has been a demanding, challenging and extensive work, but overall an instructive and great experience. The accomplishments of this work wouldn't have been possible without the help, support and encouragement of many people.

First of all I would like to thank my supervisor Dr. Marcus Conrad for great guidance and support throughout this work. I am very thankful to him for giving me the opportunity to stay in his lab and for sharing his passion for science and his broad scientific knowledge with me.

I want to thank my official supervisor Prof. Dr. Wolfgang Wurst, head of the Institute of Developmental Genetics, for giving me the opportunity to do my PhD in his institute and for his constructive comments throughout this work.

I am thankful to PD Dr. Hans Zischka for important suggestions and fruitful discussions not only at my annual thesis committee meetings.

I want to thank Dr. José Pedro Friedmann Angeli for his valuable suggestions and inspiring discussions. He always had an open ear to discuss problems and new ideas and encouraged me whenever I was doubtful.

I would like to thank Prof. Dr. Fulvio Ursini and Dr. Antonella Roveri from the University of Padova who helped me with GPX4 activity measurements.

I am very grateful to Dr. Carsten Berndt and Dr. Gereon Poschmann from the University of Düsseldorf who took great effort to analyze the redox state of GPX4 and provided the GPX4 mass spectrometry data presented in this work.

I am thankful to Adriane Tasdemir for her help with the *in vitro* fertilization assays and sperm quality measurements.

I owe gratitude to Sabine Schmitt for her great effort with the analysis of mitochondria and the valuable discussions we had.

I would like to thank Daniel Lamp and Dr. Martin Jastroch for their help with the Seahorse analysis.

## 10  Affidavit

I hereby declare that the dissertation titled „Interrogating the *in vivo* significance of selenium-based catalysis of GPX4 for mammalian development and survival" prepared under the guidance and supervision of Prof. Dr. Wolfgang Wurst, head of the chair of developmental genetics, and submitted to the degree-awarding institution Fakultät Wissenschaftszentrum Weihenstephan für Ernährung, Landnutzung und Umwelt of the Technical University of Munich is my own, original work undertaken in partial fulfillments of the requirements for the doctoral degree. I have made no use of sources, materials or assistance other than those specified in §6 (&) and (7), clause 2.

[ ] I have not employed the services of an organization that provides dissertations supervisors in return for paymaent or that fulfills, in whole or in part, the obligations incubement in me in connection with my dissertation.

[  ] I have not submitted the dissertation, either in the present or in a similar form, as part of another examination process.

The degree-awarding institution Fakultät Wissenschaftszentrum Weihenstephan für Ernährung, Landnutzung und Umwelt has approved prior publication oft he dissertation.

[  ] I have not yet been awarded the desired doctoral degree nor have I failed the last possible attempt to obtain the desired degree in a previous doctoral program.

I am familiar with the public available Regulations of the Award of Doctoral Degrees of the Technical University Municih, in particular §28 (invalidation of doctoral degree) and §29 (Revocation of doctoral degree). I am aware of the consequences of filling a false affidavit.

[  ] I agree,          [  ] I do not agree

that my personal data is stored in the TUM alumni database.

Munich,  _____

Irina Ingold